From astrophysics to astrobiology : significance of laboratory organic residues from photo-irradiation of cosmic ice analogs

Paola Modica

UNIVERSITÉ PARIS-SUD

ÉCOLE DOCTORALE 127 :
ASTRONOMIE ET ASTROPHYSIQUE D'ÎLE-DE-FRANCE

Laboratoire : Institut d'Astrophysique Spatiale

THÈSE DE DOCTORAT

PHYSIQUE

par

Paola MODICA

From astrophysics to astrobiology:

Significance of laboratory organic residues from photo-irradiation of cosmic ice analogs

Date de soutenance : 26/11/2014

Composition du jury :

Directeur de thèse :	Louis LE SERGEANT D'HENDECOURT	Directeur de recherche (IAS – CNRS - Université Paris-Sud)
Rapporteurs :	Hervé COTTIN	Professeur (LISA - Université Paris-Est)
	Murthy GUDIPATI	Principal Scientist (JPL - California Institute of Technology)
Examinateurs :	Guillaume PINEAU DES FORETS	Professeur (IAS - Université Paris-Sud)
	Matthieu GOUNELLE	Professeur (IMPMC - MNHN)
	Fathi MOUSSA	Professeur (LETIAM - Université Paris-Sud)
Membre invité :	Michel VISO	Responsable du programme Exobiologie (CNES)

Acknowledgments

During my PhD I received help, advice, and support from many people to whom I would like to show my greatest gratitude.

First of all I would like to express my special appreciation and thanks to my advisor Louis Le Sergeant d'Hendecourt for being such a remarkable mentor. His dynamism and confidence in obtained results were always encouraging me to perseverate. I would like to stress here his great spirit of sacrifice in accompanying me through this long scientific project until the day of my thesis defense and his constant concern in doing everything possible to make me feel at ease in my life in France, both emotionally and financially. As his last student, I hope having contributed to end in style his scientific mentoring activity.

Then I would like to thank all the members of the jury for letting my defense be a pleasant moment. In particular, I would like to offer my very sincere gratitude to the kind reviewers Professor Hervé Cottin and Doctor Murthy Gudipati for the time they have spent reading the manuscript and writing such detailed reports that were rich in useful remarks and suggestions. I feel really honored that both of them appreciated my work and contributed with enthusiasm in the complementation of the manuscript. I would also like to extend my thanks and appreciation to Professor Guillaume Pineau des Forêts for accepting the role of the jury president, Doctor Michel Viso for participating as jury guest member, Professor Fathi Moussa and Professor Matthieu Gounelle for finding the time in their schedule.

Most of the results in this thesis are the product of several collaborations. Therefore, it is a pleasure to extend my gratitude to Laurent Nahon and his staff at the DESIRS beamline of SOLEIL Synchrotron from whom I have greatly benefited during the course of two experimental campaigns. I am thankful to Uwe Meierhenrich for welcoming me several times in the ICN laboratory in Nice and for the useful discussions we had. I am extremely grateful to Cornelia Meinert for providing very accurate analysis of samples with GCxGC MS in the same laboratory and for her irreplaceable help on circular dichroism applications. I am really thankful to Zita Martins of Imperial College in London for sharing her expertise in meteorites and for performing

GC MS analysis of the “Paris” meteorite and the organic residues. Furthermore, I am very grateful to Denis Lesage of UPMC in Paris for his precious guide in the FT ICR analysis of organic samples and for his genuine interest in my work. I am also thankful to Roland Thissen for his warm welcoming at IPAG in Grenoble and his constructive criticism on FT ICR data interpretation.

Naturally, I wish to thank the entire “Astrochimie et Origines” team for all the help, useful advises, and suggestions. In particular, I acknowledge my gratitude to my colleague Sihane Merouane for the production of silicate analogs, Zahia Djouadi for her support in the experiments with silicates and for reading part of my manuscript, Emmanuel Dartois, Donia Baklouti, Rosario Brunetto who participated in many different occasions to the implementation of this thesis, Ivan Alata and Lisseth Gavilan for the really good time spent together talking about everything. I wish to thank the two engineers of the team, Obadias Mivumbi and Philippe Duret, for their admirable technical assistance, constant help and (last but not least) for providing an amusing and relaxed atmosphere at work. Undoubtedly, a very special mention goes to Pierre de Marcellus from whom I learned how to operate in the laboratory and whose thesis was my personal bible. He is a very caring person whose effectiveness and relaxed attitude was an exemplar to me. I am very grateful for his help in speeding my work and accurately reviewing my writing and, above all, I would like to heartily thank him for his invaluable support in the moments of frustration.

Certainly, I wish to take this opportunity to thank my friends and colleagues. First, I would like to express my appreciation from the deepest of the heart to Manale Noun for her selfless support and sacrifice at times of critical need during my oral presentation preparation. She is the nicest person imaginable and I owe her my eternal gratitude. Many thanks also to all my PhD colleagues that contributed to make these years more enjoyable: Vincent, Agnes, Lapo, Anna, JB, Andrea, Marco, Antoine… Moreover, a big thank to my friends out of academia for always being a major source of support when the circumstances were somewhat discouraging: (in casual order) Bernard, Natalia, Vladimiro, Michele, Pierre, Antoine, Cinzia, Giannis, Dmitri, Cecilia, Magda, Simona, Mariella, François, Marc, Maxim, Zuzana, Damien, Toni, Andreas...

Finally, I would like to thank my family for understanding and supporting me during these years far from home and for always showing how proud they are of me.

From astrophysics to astrobiology: Significance of laboratory organic residues from photo-irradiation of cosmic ice analogs

Abstract

Laboratory experiments have shown that ultraviolet photo-irradiation of astrophysical ice analogs and their following warm-up until room temperature lead to the formation of refractory organic residues. These residues consist of rich mixtures of organic compounds, including amino acids, which have a potential importance for prebiotic chemistry. They are considered as analogs of the organic refractory materials that are thought to be synthesized on dust grains in molecular clouds and/or in protoplanetary disks, as a product of the ice evolution, and that could be later accreted into comets and asteroids and eventually be delivered to the early Earth. Hence, the study of these analogs, produced under astrophysically relevant conditions, represents a valid tool to investigate the processes at work for the origin of complex organic molecules in the Solar System and, in particular, the possible introduction of enantiomeric excesses in chiral molecules.

This PhD work is devoted to the study of these laboratory organic residues, their characterization and the astrophysical applications of these results. We used different analytical techniques such as gas chromatography mass spectrometry (GC MS, classical and multidimensional), Fourier transform ion cyclotron resonance mass spectrometry (FT ICR MS), and infrared spectroscopy. We measured the enantiomeric excesses induced in five chiral amino acids by UV circularly polarized light (UV CPL) irradiation of our analogs and insert these results in a coherent astrophysical scenario for the origin of the enantiomeric excesses observed in meteoritic amino acids. We studied the amino acid content of the Paris meteorite and evidence some similarities with the distribution of the amino acids in our organic residues. We also produced more realistic analogs of interstellar grains, including a silicate surface, to test the potential effects of such a surface on the formation and nature of organic residues. Finally, we discuss the significance of these results in the astrophysical context and the possible relationship between astrochemistry and prebiotic chemistry.

De l'astrophysique à l'astrobiologie : L'intérêt des résidus organiques de laboratoire issus de la photo-irradiation d'analogues de glaces cosmiques

Résumé

Les expériences de laboratoire ont montré que la photo-irradiation ultraviolette d'analogues de glaces astrophysiques suivie de leur réchauffement à température ambiante mène à la formation de résidus organiques réfractaires. Ces résidus, solubles dans l'eau, consistent en un riche mélange de composés organiques incluant entre autres des acides aminés, molécules potentiellement importantes pour la chimie prébiotique. Ces résidus sont considérés comme des analogues de la matière organique réfractaire que l'on pense être synthétisée sur les grains de poussière dans les nuages moléculaires et/ou dans les disques protoplanétaires, produit de l'évolution des glaces, et qui pourra être accrétée plus tard en comètes ou en astéroïdes et finalement délivrée sur la Terre primitive. Ainsi, l'étude de ces analogues, produits dans des conditions astrophysiques pertinentes, représente un outil efficace pour explorer les processus à l'origine de la formation des molécules organiques complexes dans le Système Solaire et en particulier la possible introduction d'excès énantiomériques dans les molécules chirales.

Ce travail de thèse est consacré à l'étude de ces résidus organiques, leur caractérisation et les applications astrophysiques de ces résultats. Nous avons utilisé différentes techniques d'analyse comme la chromatographie en phase gazeuse couplée à la spectrométrie de masse (GC MS, classique et multidimensionnelle), la spectrométrie de masse par résonnance cyclotronique ionique à transformée de Fourier (FT ICR MS) ou encore la spectroscopie infrarouge. Nous avons mesuré les excès énantiomériques induits dans cinq acides aminés par irradiation de nos analogues avec de la lumière UV polarisée circulairement (UV CPL) et insérons nos résultats dans le cadre d'un scénario astrophysique cohérent pour expliquer l'origine des excès énantiomériques observés dans les acides aminés météoritiques. Nous avons étudié le contenu en acides aminés de la météorite de "Paris" et montré des similarités avec la distribution en acides aminés de nos résidus organiques. Nous avons également produit des analogues plus réalistes de grains interstellaires en incluant une surface silicatée, afin de tester l'effet potentiel de cette surface sur la formation et la nature des résidus organiques. Enfin, nous effectuons une discussion générale à propos de la pertinence de ces résultats dans le contexte astrophysique et soulignons le possible lien entre astrochimie et chimie prébiotique.

Contents

Foreword

Organic compounds and water are considered as prerequisites for life to emerge and evolve on the surface of a telluric planet such as the primitive Earth. Liquid water is required for life as we know it, since it participates as a solvent in the organization of biopolymers and as a chemical partner in most of the biochemical processes. Organic compounds are always involved in biochemistry; they include proteins, nucleic acids, carbohydrates and lipids which provide the structure of cells and perform many of the functions associated with life. These molecules are made from covalent combinations of only six elements called CHNOPS (for carbon, hydrogen, nitrogen, oxygen, phosphorus, and sulfur).

According to modern theories, life arose on the primitive Earth by a long process of prebiotic chemical evolution starting from organic precursors of proteins, nucleic acids and membranes which are essential for all living organisms. But from where did the original organic matter come? To answer this puzzling question, both endogenous and exogenous mechanisms have been proposed. Among the endogenous mechanisms, the most known example is certainly the pioneering Miller-Urey synthesis of amino acids and other organic compounds, from simple precursors, in experiments simulating the early Earth atmosphere (Miller 1953). These experiments were based on the assumption of a reducing primitive atmosphere dominated by CH_4. However, today it is thought that the primitive atmosphere was rather a weakly reducing one, even a neutral mixture of CO_2, N_2, and H_2O. In this case, the production of amino acids appears very limited.

The hypotheses of exogenous mechanisms propose the impact of a large number of comets, meteorites, and interstellar dust particles (IDPs) (Oró 1961), thought to have occurred approximately 4.1 to 3.8 billion years ago (Gomes et al. 2005), which would have supplied water and organic compounds to the early Earth. These compounds, perhaps in combination with other chemical compounds on the surface of Earth, may have been interacting under favorable conditions to form more and more complex compounds and eventually autocatalytic self-

replicant molecular entities. This hypothesis is one of the most widely accepted and it will be adopted in this thesis.

This scenario is supported by the detection of many different organic compounds in comets and, more significantly, in primitive meteorites such as the carbonaceous chondrites. In comets, astronomical observations have revealed the presence of a rich variety of organic compounds, and, in comet 81P/Wild 2, also amino acids (Elsila et al. 2009). Moreover, observations have shown that a remarkable similarity exists between cometary organic compounds and those observed in interstellar clouds. In the group of chondritic meteorites, known to include the most primitive meteorites, more than 80 different amino acids have been identified, especially in Murchison, Murray and Orgueil (e.g. Cronin 1976; Cronin & Pizzarello 1983). Other important prebiotic compounds such as fatty acids and purines have been detected as well (Stoks & Schwartz 1981). Moreover, and very interestingly, some meteoritic amino acids have been found in slight enantiomeric excess of the L-form, which has suggested that a chiral asymmetry in meteoritic amino acids may have influenced prebiotic processes toward the L-homochirality of amino acids on the primitive Earth.

All these findings support the idea of an extraterrestrial origin for organic compounds on Earth and, perhaps, an interstellar origin for part of the material found in comets and meteorites. Thus, in the context of the cosmic evolution, the sequence of events that led to the emergence of life on Earth seems to extend back through the origin of our Solar System, with the formation of small bodies, and through the rich chemistry of interstellar clouds, which is in turn connected to the death and birth of stars for the nucleosynthesis of the elements within their interiors.

Indeed part of the processes at the origin of the organic matter in the Solar System bodies seems to have occurred in the interstellar ices of the molecular cloud from which the solar nebula has originated. Interstellar ices are observed within collapsing molecular clouds that ultimately form stars, planets and “debris” that are asteroids and comets, the parent bodies of meteorites found on Earth. These ices are extremely abundant in terms of solid state molecular species and they dominate, often by orders of magnitude in abundance, gas phase species. Ices are mainly made of H, O, C, N and S, and share many similarities with cometary ices,

suggesting that they are part of the initial material out of which our Solar System has formed. These elements are the most cosmically abundant ones and are precisely those present in the ISM and in the molecular clouds from which the Solar System formed 4.556 billion years ago. Cosmically quite abundant, these elements are prone to react with themselves in the ISM to boost a chemistry that is essentially an organic one. This chemistry is governed by the cosmic abundances of the elements in harmony with their origin from the Big Bang and the nucleosynthesis in star generations prior to our Sun.

However, in the diffuse ISM, cosmic abundances are, surprisingly, not verified at all. When distant stars are observed, mainly in the UV and the blue part of the visible, the relative abundances of the elements, compared to the ones of the Sun, show that heavier elements are clearly missing from the gas phase, while others are only slightly depleted. O and C are moderately depleted; N, S and P basically not at all; and elements such as Si, Mg, Fe, Al, and Ca are considerably depleted by orders of magnitude. As proposed by Greenberg in a visionary article *(The interstellar depletion mystery, or where have all those atoms gone? 1974)*, these elements are trapped in the sub-micron solid particles dispersed through the ISM, the interstellar grains. These depletions are the result of condensation properties and cosmic abundances of the elements. As a consequence of that, the abundant and available CHNOPS are ready for a rich chemistry, whereas the underabundant and not available heavier elements (Si, Mg, Fe, Al, Ca…) are “definitely” locked in minerals constituting the refractory grains. Later, in the cold environments of molecular clouds, refractory grains will accrete the CHNOPS from the gas phase forming at their surfaces volatile structures called interstellar ice mantles (or simply ices). However, ice mantles and mineral grain cores will remain separated, apart from possible catalytic effects at their interface. Upon energetic processing and thermal evolution, these ices will drive an organic abiotic chemistry based on the same constituents used by biochemistry. Indeed ices may have an important role in the production of the building blocks of life.

The study of these interstellar ices is well documented and supported by numerous laboratory experiments aimed to simulate the physical and chemical conditions in which these ices form and evolve. Originally these experiments have been undertaken to interpret astronomical

infrared spectra, especially those from the ISO and Spitzer satellites, revealing soon to be a successful approach to decipher the interstellar ices composition. Since the end of the Seventies, the most abundant molecules present in the ices started to be discovered and quantified (H_2O, CH_3OH, CO_2, CH_3, NH_3, OCS, etc…) confirming that ices are indeed made by H, C, N, O, and S (the P is yet missing for the reason of its lower relative abundance). Thanks to the better knowledge of the composition of ices, more realistic ice mixtures started to be used in the laboratory to investigate the effects of energetic processing, such as UV photolysis and cosmic ion irradiation, in their evolution. After processing and gradual warm-up of the ice samples, it was observed that a refractory organic residue always remained at room temperature. From its characteristic color, this residue was named “yellow stuff”. The analysis of the yellow stuff became an independent and prolific field of research, in which, incidentally, the work presented in this thesis finds place. Since the first experiments, it was noted that the residue possesses some interesting properties such as a high water-solubility, a rich molecular variety, and a high molecular weight. Many different organic molecules started to be identified, some of them with a possible prebiotic interest, such as the amino acids (Bernstein et al. 2002; Muñoz Caro et al. 2002; Meinert et al. 2012).

Due to its characteristics and the formation under plausible astrophysical conditions, the residue has been suggested as an analog for the organic refractory material which is thought to be present on grains in molecular clouds and/or in protoplanetary discs as a product of ice evolution. We share the same idea and make of this assumption the starting point of the work presented in this thesis. We also consider the residue as a template for the study of the soluble organic matter extracted from chondritic meteorites. In our opinion, the studies on these analogs represent a valid tool to investigate the origin of organics, or a part of them, in the Solar System.

This thesis does not address specifically the field of prebiotic chemistry but rather that of astrochemistry, the chemistry which occurred in space and perhaps preceded prebiotic chemistry on the early Earth. Our work allows suggesting an astrophysical scenario in which molecular astrochemistry is in relationship with prebiotic chemistry. Our approach is an experimental one based on simulation experiments performed with our MICMOC experimental

set-up. This set-up allows the production of organic residues by UV photochemistry and warm-up of simple ice mixtures. The following analysis of these residues can be performed by means of different techniques, such as infrared spectroscopy, gas chromatography (classical and multidimensional) mass spectrometry, and Fourier transform ion cyclotron resonance mass spectrometry, which often require the collaboration with research groups of other laboratories. The analysis of the residue is not focused simply to its characterization, but it serves to extrapolate useful information with astrophysical applications. This empirical approach may allow obtaining surprising results in the way prebiotic chemistry may have been starting.

Reading the manuscript

In **chapter one,** the general astrophysical context in which the interstellar ices form and evolve, from the interstellar medium to the small bodies of the Solar System, is presented. At each one of the different steps during this evolution, the increasing molecular complexity is underlined. The chapter ends with a brief historical digression on the main simulation experiments on interstellar ice analogs, the same kind of experiments carried out in this thesis.

Chapter two is devoted to the description of our experimental set-up at IAS, MICMOC, and to the standard protocol used for producing the organic refractory residues that have been analyzed in the course of this work of thesis by various dedicated techniques.

Chapter three presents one of the central parts of the work of this thesis. It focuses on the emergence of enantiomeric excesses in amino acids by circularly polarized light irradiation of cosmic ice analogs. A complete ensemble of the results obtained during four experimental campaigns (Chiral-MICMOC experiments) at the SOLEIL synchrotron is presented. The results concern:

- The detection of 16 amino acids by multidimensional gas chromatography.
- The emergence of ee_L in alanine under different explored parameters (polarization state, photon energy, stage at which the sample are irradiated).

- The emergence of ee_L in five different amino acids at different polarization states at a fixed energy.

Based on the results and on astrophysical models, a coherent astrophysical scenario for the origin of the enantiomeric excesses observed in meteoritic amino acids is proposed.

In **Chapter four**, a high resolution method is used for the study of the residues, the Fourier transform ion cyclotron resonance mass spectrometry (FT ICR MS). Since this technique is new for our group, first the basic principles of the FT ICR MS are presented. Then the general aspects of the mass spectra obtained from the residues are described. Particular attention is given to the detection of HMT and HMT-based molecules and, tentatively, also to amino acids. The extreme complexity of the organic matter and the presence of high molecular weight compounds are evidenced.

In **Chapter five**, after an introduction on chondritic meteorites, the pristine CM Paris meteorite is presented. Then the amino acid content from the SOM of Paris meteorite, analyzed by gas chromatography mass spectrometry (GC MS), and their relative distribution are discussed in terms of primitiveness of Paris in comparison with other carbonaceous chondrites. The ee_L of some chiral amino acids, in particular isovaline, are discussed as well. Finally, the analysis of the amino acid content of our residues by the same analytical technique allows evidencing some similarities with primitive meteorites.

In **Chapter six,** more realistic simulation experiments allow obtaining residues on silicate films to verify for possible catalytic effects at the silicate surface. Then, one of these residues is extracted according to a procedure which mimics the classical meteoritic extraction of the SOM. This test is made in relation to a specific molecule, HMT, to check if it can be still detectable after this procedure, which appears not to be the case.

Finally, the **Conclusions** summarize the results and outline the perspectives of future researches. It proposes also a brief discussion of the relevance of this work in the field of prebiotic chemistry.

Chapter 1

Overview on the evolution of ices in space

Contents

1.1 The Interstellar Medium

The interstellar medium (ISM) consists of gas and dust distributed between the stars in galaxies and accounts for 20-30% of the mass of our own Galaxy (Ehrenfreund & Charnley 2000). The mass in the gas is much larger than that in the dust; by mass, 99% of the ISM is gas in any form, and only 1% is dust. The ISM is extremely dilute by terrestrial standards, reaching only 10^6 atomic nuclei cm^{-3} in the densest regions within the plane of the Galaxy where it is mainly concentrated in discrete structures such as interstellar clouds. These structures present a vast variety of shapes, sizes, densities, and temperatures.

As imposed by the cosmic abundances, the chemical composition of the gas, expressed in numbers of nuclei, is about 90% hydrogen, 9% helium, plus traces of heavier elements (O, C, N, Si, Mg, Fe…). This gas can exist in the form of single neutral atoms, radicals, simple molecules,

or ions depending on the different conditions of temperature, pressure, and the presence of radiation fields. All these different conditions lead to the description of the ISM as the coexistence and interaction of different components. According to the McKee & Ostriker (1977) model, the ISM is divided into three phases: the Cold Neutral Medium (CNM), often referred to as clouds; the Warm Ionized Medium (WIM) or Warm Neutral Medium (WNM), which is considered the boundary layer of the CNM; and the Hot Ionized Medium (HIM), which is referred to the coronal gas. These phases are thought to be in approximate pressure equilibrium with one another (Savage & Sembach 1996).

The CNM itself contains a variety of cloud types which covers a wide range of physical and chemical conditions. Conventionally, these clouds can be distinguished into three main types: diffuse, dense, and translucent (Spaans & Ehrenfreund 1999).

Diffuse clouds are dominated by H atoms but contain locally some molecular hydrogen (H_2); they typically present low densities (n_H~10-500 cm^{-3}) and low temperatures (30-100 K). Being the most tenuous clouds, they are fully exposed to ultraviolet radiation from stars which heat the gas and dissociate the molecules. Diffuse clouds can be observed in absorption, essentially in the UV and visible range, and in emission in the IR range.

Dense clouds (also called molecular, dark, or cold clouds) are the birthplace in which stars with their planetary systems form as a result of local gravitational collapses. These clouds are usually self-gravitating, and are most often observed by IR absorption and millimeter wavelength emission methods. Their densities are typically at least n_H~10^4 cm^{-3}, with temperatures around 10-30 K in the quiescent regions. In dense clouds, cold gas phase chemistry, mostly described by ion-molecule reactions with no activation energy barrier, can efficiently form simple species such as CO, N_2, O_2, C_2H_2, C_2H_4, HCN and simple carbon chains (Herbst 1995). Most of the more than 150 currently known interstellar molecules have been detected in such clouds (Irvine 1999; Herbst & van Dischoeck 2009) and, as we shall see later, the vast majority of these molecules pertain to organic species.

Translucent clouds constitute the bridge between the two previous types of clouds, since the gas may have an “onion-like” structure, with dense molecular clouds in the center, surrounded by translucent clouds, which are in turn surrounded by diffuse clouds. In translucent clouds some species, such as carbon, can be present into neutral atomic, ion or molecular form (mostly C_2 and CO). Simple molecules such as H_2, CH, CN and H_2CO are also observed (Magnani & Onello 1995; Rachford et al. 2002).

The classical distinction in different kind of clouds and different phases is a practical way to describe the multitude of environments existing in the ISM, however, all these environments are deeply connected and continuously interact with each other.

1.1.1 Dust grains

Dust grains represent the solid phase in the ISM consisting preferentially of small particles of heavy refractory elements such as silicates or carbon compounds. They are ubiquitously present in different environments and are constantly coupled with the gas phase, with which there is certainly interchange of materials (Greenberg 2002).

The main features of interstellar dust like size, shape, chemical composition, and amount can be determined by remote observations using telescopes on the ground, and more often in space, in a variety of wavelengths. The presence of dust grains in the ISM is deduced observationally by their interactions with the light of the stars via extinction (light blockage), in the visible and near-mid infrared, and emission, in the far-infrared and sub-millimeter. The presence of the dust is for example evidenced by the fact that it blocks the visible light from background stars, a phenomenon well illustrated in Fig. 1.1 by the dark cloud Horsehead Nebula.

Figure 1.1 - The Horsehead Nebula (Barnard 33). The darkness is mostly caused by the presence of dust particles which block the light from the background (http://en.wikipedia.org/wiki/Horsehead_Nebula).

The extinction is directly proportional to the amount of gas and dust present along the line of sight to the observed star. It is due to scattering and absorption by dust particles and is most effective when the wavelength of light roughly matches the particles size. An example of an extinction curve in the diffuse ISM is that observed in the direction to the star σ Sco with the characteristic UV absorption bump centered at ~4.6 μm^{-1} (Fig. 1.2). This figure evidences that each grain population component contributes to the average interstellar extinction, even if at present the specific carriers remain not completely identified being model dependent.

Since the extinction is wavelength-selective, from the shape of a typical extinction curve, it is possible to deduce that the particles responsible for the extinction are about 0.1 μm in size and those responsible for the bump and far ultraviolet are much smaller, between 0.01-0.001 μm (Greenberg 2002). Dust grain size distribution ranges from 0.001 to 0.5 μm, with ~10^4 atoms for the largest ones, and is classically a power law described originally in detail by Mathis et al. (1977) and progressively modified to take into account the continuous flow of new observations, particularly from infrared astronomical satellites (ISO and Spitzer) and from far-infrared and sub-millimeter satellites (Herschel and Planck).

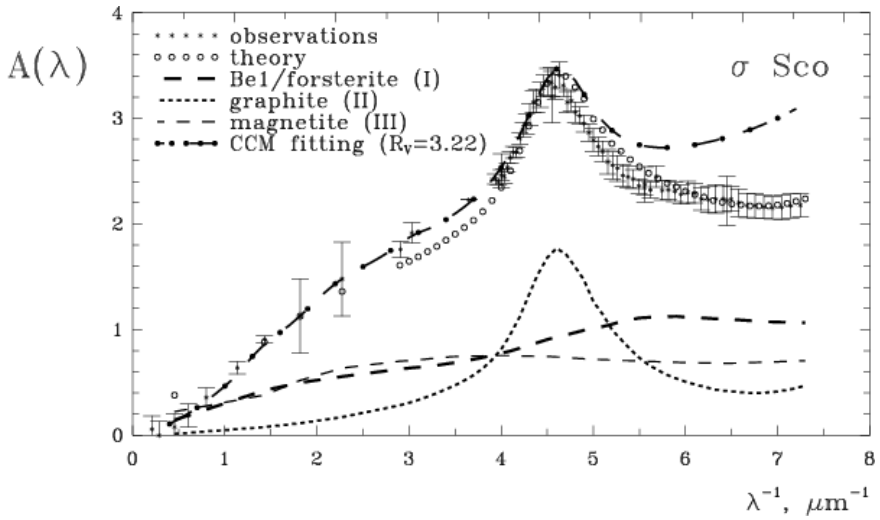

Figure 1.2 - Observed and calculated extinction in the direction to the star σ Sco. The contribution to the theoretical extinction from different grain population components is also shown (Voshchinnikov et al. 2006).

Observing a partial linear polarization of the starlight passing through dust grains (Hiltner 1949; Hall 1949), it was deduced that the particles are non-spherical and aligned by magnetic fields as very recently confirmed by Planck observations (e.g. Planck Collaboration 2014). However grains have been traditionally considered spherical or spheroidal because this simplification permits an easier study.

Most dust grains are formed in the cold atmospheres of dying stars like red giant stars or planetary nebula envelopes, following a complex process of nucleation and condensation; novae and supernovae are also sites of dust formation, albeit much less important in the total mass of the dust formed (Jones 2001; Draine 2003). These environments present the ideal conditions for dust formation: high densities (~10^9 cm^{-3}) coupled with cooling temperatures resulting from the adiabatic expansion of the gas down to the condensation temperatures of many heavy elements in the form of solids (2000-1000 K and less) (Henning 2003 and references therein).

The mechanism of the dust formation is not totally understood, but condensation sequences at equilibrium are generally used to describe the possible condensation pathways, in particular those concerning the presence of silicates. The results from these condensation sequences

largely depend on the C/O ratio of the envelopes that are expelled away from the stars. The CO molecule, strongly bound and thermodynamically stable, forms early in the expanding envelope at temperatures around 3000 K. It uses all the available C or O, whichever is the less abundant of these two species.

In a carbon-rich environment (initial C/O>1), if, after the formation of CO, there is some C leftover, then carbon-based dust chemistry will preferentially occur. The carbon in dust grains can be present as pure carbon in crystalline form, diamond and graphite, and/or in amorphous form. Diamonds are indeed observed in a very few objects (Guillois et al. 1999); graphite has never been confirmed but it has been a prime candidate for long (Gilman 1969) essentially because the presence of the UV bump was indeed predicted prior to its observation. Hydrocarbons are present in the form of hydrogenated amorphous carbon (Dartois & Muñoz Caro 2007), polycyclic aromatic hydrocarbons (PAHs) (Puget & Léger 1989; Tielens 2008), and aliphatic hydrocarbons (Chiar et al. 2000). Also present, but rare, are other very refractory carbonaceous compounds like carbides (SiC, TiC, Al_2C).

Conversely, in an oxygen-rich environment (initial C/O<1), if, after the formation of CO, O atoms are leftover, oxygen-rich silicate dust will form (Molster et al. 2002). The silicates expected are those formed with compounds with Fe and Mg since both of these elements are cosmically abundant. The principal forms of silicates are pyroxenes (e.g. enstatite ($MgSiO_3$) and ferrosilite ($FeSiO_3$)), and olivines (e.g. fayalite (Fe_2SiO_4) and forsterite (Mg_2SiO_4)) (Hanner & Bradley 2004), with on average 3-4 times more pyroxenes than olivines (Molster et al. 2002). Only a minor part of silicates is in the crystalline form, the preponderant part being amorphous, in particular in the diffuse medium (Kemper et al. 2001, 2004).

Once formed, dust grains are released into the interstellar medium by radiation pressure, stellar winds or in material thrown off by stellar explosions like supernovae (Dunne et al. 2003; Morgan & Edmunds 2003). Then the grains can be broken into smaller units by a combination of sputtering and grain-grain collisions, or grow by coagulation or by accretion of atoms and molecules onto their surfaces in the form of ice mantles, the subject of this thesis, when the grains enter in dense molecular clouds.

Interstellar depletions

The presence and composition of dust grains can be also inferred by the under-abundance (depletion) of heavy elements observed in the gas phase. Former observations from the mid 70's have been confirmed by the use of the Hubble Space Telescope (HST) combined with the Goddard High-Resolution Spectrograph (GHRS) (e.g. Cardelli et al. 1991). These observations have evidenced that in diffuse and moderately dense interstellar clouds, elements heavier than H and He are found to be depleted with respect to the ones in the solar photosphere (York 1980; Cardelli 1984; Hobbs et al. 1993), the usual reference for cosmic abundances. The amount of depletion is in good correlation with the condensation temperature of the elements being depleted (e.g. Welty et al.1995). Fig. 1.3 shows a plot of the depletion of elements relative to solar values as a function of the condensation temperature in an average dense interstellar cloud. Less severe depletions are found for warmer, more diffuse clouds.

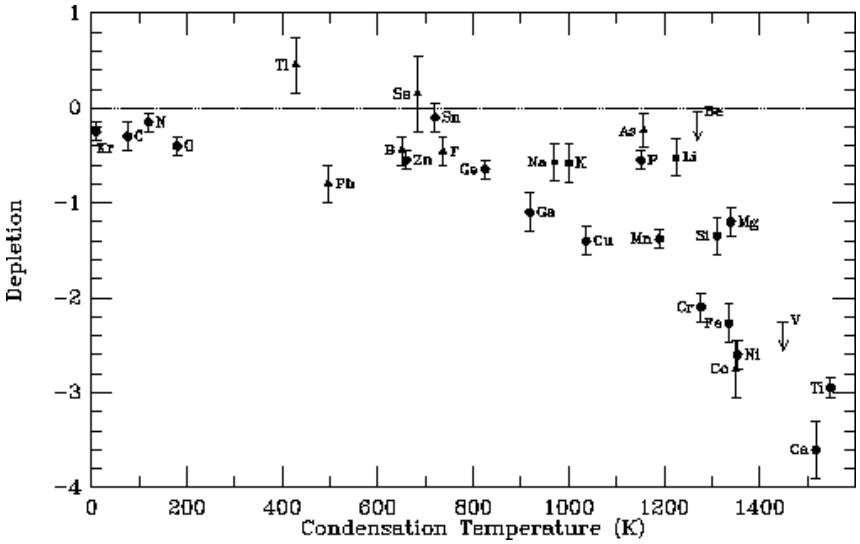

Figure 1.3 - Variation of interstellar depletion with condensation temperature for 30 elements in an average dense interstellar cloud (Welty et al. 1995).

As dust grains form in a cooling, expanding AGB star atmosphere, elements such as Ca, Ti, Co, Si, Mg, Fe, Al… with a high condensation temperature (>1000 K) condense first remaining locked in refractory grains, and will continue to be strongly depleted as the atmosphere cools

further down. Conversely, elements with lower condensation temperature and higher abundances (O, C, N, S…) condense out later, and thus are less depleted from the gas phase (see Ebel 2000; Henning 2003 and references therein). From the observation of the depletion patterns and the study of the products of stellar nucleosynthesis, it is possible to infer that missing “rocky forming” elements such as Mg, Fe, Si, Cr, Mn are incorporated in the solid phase into dust grains and do not participate in the gas phase chemistry.

Moreover, from the distribution of the elements in space (Table 1.1), the most condensable ones will impose the global mass gas-to-dust ratio (about 100:1) that can be found in the average ISM. The gas phase chemistry observed by radioastronomy shows the importance of the abundant elements having a low condensation temperature such as C, H, N, O, and S. They can actually react only between them, while heavier less abundant “rocky forming” elements are unavailable; as we will show later in this thesis, this is certainly a key point to start a rich organic chemistry that will lead to the formation of prebiotic molecules.

Table 1.1 – Abundances of the elements in space (Ehrenfreund et al. 2005).

Element	Relative number
H	1
He	7.5×10^{-3}
O	8.3×10^{-4}
C	4.0×10^{-4}
N	1.0×10^{-4}
Ne	0.8×10^{-4}
Mg	4.2×10^{-5}
Si	4.3×10^{-5}
S	1.7×10^{-5}
Fe	4.3×10^{-5}
Na	2.1×10^{-6}
P	3.0×10^{-7}

The interstellar dust cycle

Interstellar dust is not static in the ISM, but rather in continuous evolution through what is known as the interstellar dust cycle (Greenberg 1982) schematically depicted in Fig. 1.4. Dust particles are sequentially and repeatedly being cycled into and out of diffuse and molecular clouds, with each single cycle lasting about 10^8 years. During this cycling, dust particles experience various physical and chemical processes that modify their structure and/or composition.

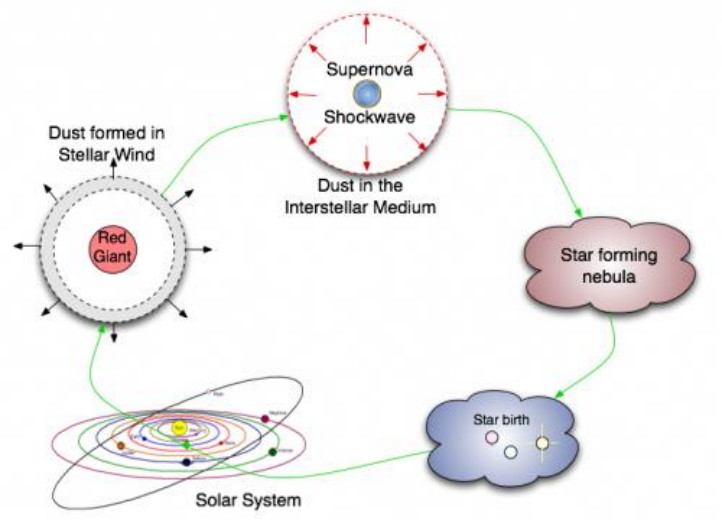

Figure 1.4 - Diagram of the interstellar dust cycle through different astrophysical environments (http://herschel.cf.ac.uk/science/infrared/dust).

Dust clumps in some portions of molecular clouds collapse under gravity, fragment, and form dense cores. These latter continue to collapse and start to turn into rotating disks. Most of the material in the core forms a star, and a much smaller part forms a planetary system (with comets, asteroids and IDPs as leftovers from planetary formation). At the end of its lifetime, the star replenishes the interstellar medium with dust ejected (e.g. in the AGB phase of red giants and supergiants and in supernova explosions). Dust in the ISM aggregates in diffuse and then in dense clouds under the effect of supernova shocks. The cycle of stellar birth, death and rebirth is replayed and in the meantime the dust grains are reprocessed, consumed by star and planet formation or become part of comets, asteroids and other minor bodies. According to Greenberg's model the grain may pass through a series of diffuse cloud/molecular cloud cycles. A typical grain anywhere in space undergoes at least 20 cycles but only one time out of 20 it is

incorporated into a star and destroyed. The other times, the grain gets ejected, and only the mantle is destroyed (Greenberg 1989).

1.1.2 Interstellar ice mantles

Dust grains are, by far, the primary sites of molecules formation acting as “catalyzers” and favoring chemical reactions at their surfaces. In dense molecular clouds, H atoms from the gas phase collide with the cold grain surfaces (~10 K) and are physically adsorbed; then these atoms diffuse on the surface and form H_2 molecules when they encounter each other (Hollenbach & Salpeter 1970, 1971). The formation of H_2 is indeed impossible in the gas phase as the molecule does not possess dipolar transitions to get rid of its huge formation energy (energy bond = 4.5 eV) and thus needs a third body to stabilize the newly formed molecule. Other gaseous species, in atomic, radical and molecular form (C, N, O, CO), accrete onto the surface of the refractory dust grains mostly via collisions (Sandford & Allamandola 1993) and weak van der Waals forces to form volatile van der Waals solids (d’Hendecourt & Dartois 2001) better known as ice mantles (Tielens & Hagen 1982; d’Hendecourt et al. 1985; Greenberg 1986; Whittet 1993; Tielens & Whittet 1997; Tielens & Charnley 1997). This is not the case in diffuse clouds where the higher temperatures and radiation field prevent mantle formation or favor constant destruction of growing mantles, as evidenced by the lack of observation of what is called the ice band at 3.1 micron in locally low extinction regions (Williams et al. 1992). In the interior of dense clouds, the accretion rate of the mantles is typically of one species per day, lasting for ~10^5 years before all the gas condense (Tielens & Allamandola 1987). Species with relatively low volatility accrete more readily than those with high volatility. Once on the grain, reactive species migrate until they encounter species with which they can react, typically by sticking together with the grain absorbing the excess energy (Greenberg 1986; Whittet 1993; Schmitt 1994). At the low temperatures of dense clouds, the chemistry occurs via reactions that are mostly exothermic and that have no potential barriers between reactants and products. Under normal terrestrial conditions the reactive species would be very short-lived, but the low temperatures allow some of them to persist, trapped in a cage of ices. The composition of the

first ices is expected to be dominated by hydrogenated atoms (H_2O, NH_4, CH_4…) since hydrogen is orders of magnitude more abundant than any of the heavier atoms. CO forms efficiently in the gas phase via ion-molecule reactions, and thus CO ice is explained by direct freeze-out of the molecular gas. Oxygenation of CO results in CO_2, while successive hydrogenations of CO through H_2CO produce formaldehyde and methanol (Watanabe et al. 2003). These first ice mantles, resulting of simple atom addition reactions, are thus expected to be dominated by water (H_2O), with significant amounts of H_2CO, N_2, CH_4, CO_2, H_2O_2, NH_3, and CO (Allen & Robinson 1977; Tielens & Hagen 1982; d'Hendecourt et al. 1985; Brown & Charnley 1990; Hasegawa et al. 1992). A possible path for ice chemistry is illustrated in Fig. 1.5. After their formation, ice mantles can continually be ejected into the ISM after several mechanisms such grain-grain collisions, desorptions induced by cosmic ion bombardment (Baratta et al. 1991) and UV photons (Westley et al. 1995; Leto & Baratta 2003; Öberg et al. 2009), and explosive exothermic reactions (d'Hendecourt et al. 1982; Garrod et al. 2008).

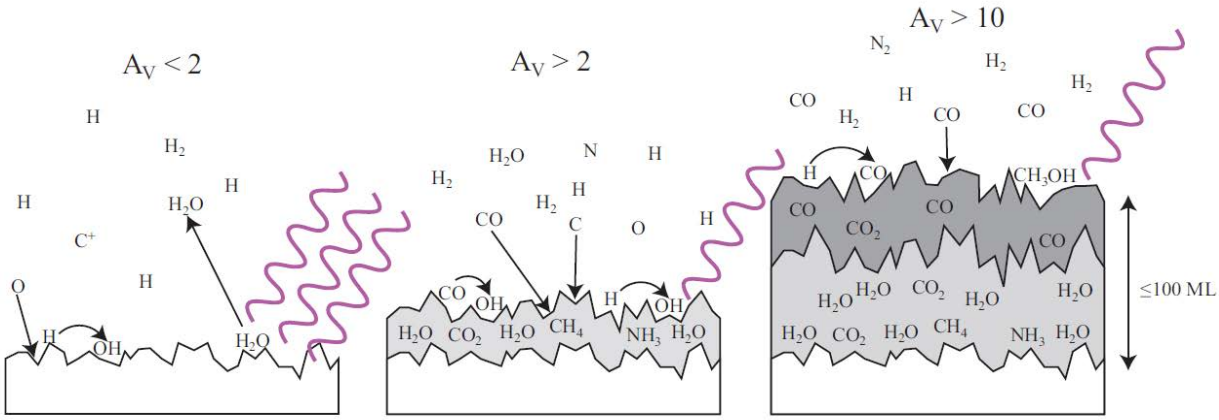

Figure 1.5 – Suggested scheme for ice accretion on grains and formation of the first simple molecules (from Öberg 2009).

Note that, as described later on in this thesis, the grain surfaces do not really act as catalyzers in a chemical sense, their role is to enhance the reaction rates (as a catalyst will do) only because they locally provide a medium of very high density (that of a solid) where a very complex chemistry can take place, contrary to what happens in the gas phase where two body

reactions between reactive species and various efficient destruction mechanisms do limit the complexity.

Ices can be directly detected in the infrared from absorption features superimposed to the background of the hot inner shell of dust spectra, according to the following mechanism. A star, situated in or behind a molecular cloud, produces a continuous infrared emission spectrum; as this radiation passes through a cloud, the molecules present in the ices, along the line of sight, absorb at their characteristic frequencies giving rise to a set of absorption features in the spectra. The infrared range between 2 and 30 μm is particularly suitable for the study of interstellar ices because it covers the portion of the spectrum where vibrational transitions of molecular bonds associated with the most abundant cosmic species fall.

The presence of ice mantles is well known since the advent of infrared spectroscopy in astronomy in the 70's. It was thanks to the OH broad infrared absorption at 3.1 μm that solid water was detected in the Orion BN-KL star forming region (Gillet & Forrest 1973). However, it was not before 1979 that laboratory simulations proved the amorphous nature of the interstellar ices by reproducing almost exactly the observed spectrum, a major advance at that time (Léger et al. 1979). Some years later, solid CO was identified from its 4.67 μm sharp spike and the associated wing in several protostellar sources (Lacy et al. 1984). The CO_2 was identified from the 15.2 μm band in IRAS-LRS spectra of three protostellar sources, an identification entirely based on laboratory data dedicated to reproduce interstellar ice analogs (d'Hendecourt & Jourdain de Muizon 1989). Numerous other molecules were then identified as components of ice mantles, such as CH_3OH (Grim 1991), CH_4 (Lacy et al. 1991), NH_3 (Lacy et al. 1998), OCS (Geballe et al. 1985), H_2CO (Schutte et al. 1996), etc. Today about 20 different features have been observed in ice mantles and assigned to their carrier molecule (Dartois 2005). The abundances of several of these molecules, relative to the water molecule, are given in Fig. 1.6. Water ice largely dominates the ices abundances; CO_2 and CO are also widely observed and display large abundances variations among different sources. CH_3OH can be dominant in some sources, becoming the second most abundant species after water ice, but also can be almost

absent in other sources. Species such as e.g. $HCOO^-$ (Schutte et al. 1999), $HCONH_2$, and H_2NCONH_2 (Raunier et al. 2004a) are also observed.

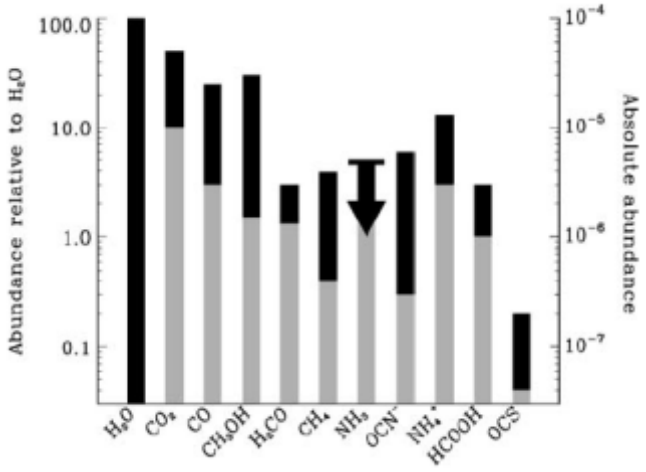

Figure 1.6 - Typical abundances of ice mantles components relative to H_2O. The black extension indicates variations of abundances from source to source (from Dartois 2005). Although NH_3 is given here only as an upper limit, more recent interpretations of Spitzer's data confirm the presence of high level of NH_3 in cosmic ices (Bottinelli et al. 2009).

Ices have been widely observed in a number of different infrared sources, from star forming regions to quiescent dense clouds, thanks to the Kuiper Airborne Observatory (KAO), the first infrared astronomical satellite (IRAS), then the Infrared Space Observatory (ISO), and the Spitzer Space Telescope. Note that, although observations are difficult within the Earth's atmosphere, large ground-based telescopes such as UKIRT (United Kingdom Infra-Red Telescope, located on Mauna Kea, Hawaii) or the VLT (Very Large Telescope, in the Atacama Desert of northern Chile) have also contributed to the understanding of the composition of the interstellar ices. A well-known example of interstellar ice spectra is shown in Fig. 1.7. This is the infrared spectrum towards the dust-embedded high mass young stellar object (YSO) W33A obtained with the ISO satellite from the Short Wavelength Spectrometer (SWS) (Gibb et al. 2000). This typical spectrum shows ice features including H_2O, CO, CO_2, CH_3OH, and CH_4, and amorphous silicate features. These latter come from the dust grain core and are always observed in the interstellar dust.

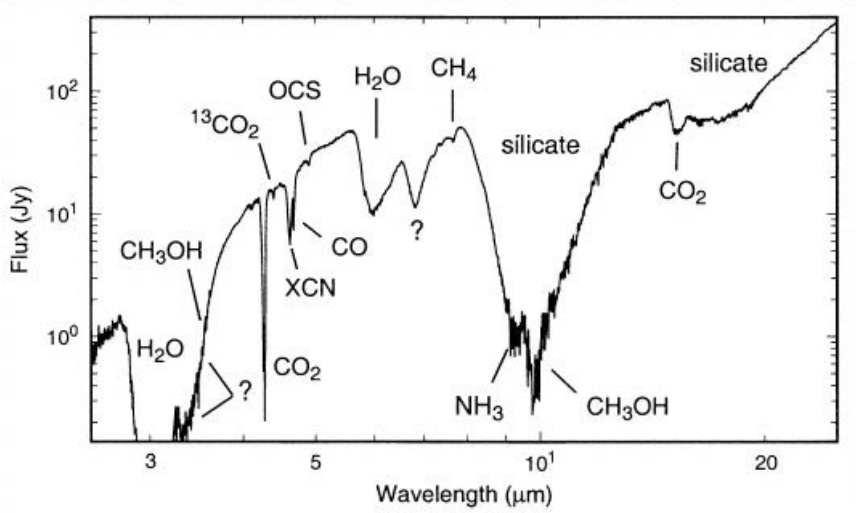

Figure 1.7 - 2.4-25 μm ISO SWS flux spectrum of the embedded protostar W33A showing the identified molecules. The H_2O absorption band is completely saturated (Gibb et al. 2000).

1.1.3 Interstellar molecules

A large fraction of interstellar molecules is incorporated in the solid state in refractory grains and ice mantles, however most of the known interstellar molecules are revealed in the gas phase only (Woon 2008). Gas phase molecules are free to rotate; this produces narrow and characteristic bands which fall in the radio and sub-millimeter portions of the spectrum. From these narrow bands a finer and more sensitive identification of molecules is possible with respect to the infrared ones. This explains the much larger number of interstellar molecular identifications in the gas phase.

The first interstellar molecules were discovered in the gas phase in the 1940s with the observation of CH, CH^+, and CN at optical wavelengths (McKellar, 1940; Adams 1941; Douglas & Herzberg 1941). At a later stage, many molecular detections such as NH_3, H_2CO were made at radio frequencies (Cheung et al. 1968; Snyder et al. 1969), but it was in the 1980s, with the development of new millimeter receiver technologies, that the study of interstellar molecules blossomed. As of today, more than 150 different interstellar molecules have been identified in the ISM, most of them in giant molecular clouds such as Sagittarius B2. The sources include

circumstellar envelopes around evolved stars, hot cores and corinos, outflows from young stars, etc. A list of the interstellar molecules detected in space in all the spectral domains is presented in Table 1.2. The molecules detected include light hydrides, ions, chain molecules, cyclic molecules, complex molecules, etc., many of them also common on Earth. One may note from this table that, as already discussed in this chapter, the observed gas phase chemistry is essentially made of the most abundant atoms and will favor organic chemistry. In this list the number of molecules decreases with the number of atoms, which is indeed not surprising. By interstellar standards, molecules containing six or more molecules are viewed as complex. With this definition, about one third of the molecules detected in space are complex and the more complex ones are those in the smaller relative concentrations. The largest organic molecule (13 atoms) that has been unambiguously identified is $HC_{11}N$ (Bell et al. 1997). Among these complex molecules, methanol (CH_3OH) is the only one detected unambiguously also in the solid state, while all the rest have been detected exclusively in the gas phase. This remark reflects the fact that absorption infrared features from molecules in the solid state are broad and cannot be assigned with as much certainty as narrow gas-phase features. Among the complex molecules detected, some of them are thought to be involved in processes useful for prebiotic chemistry on Earth. Molecules of this category have some structural elements in common with those found in living organisms. Of the interstellar prebiotic molecules, many were first detected toward Sgr B2(N-LMH). For example, the first interstellar sugar glycolaldehyde (Hollis et al. 2004), ethylene glycol (Hollis et al. 2002), acetamide (Hollis et al. 2006), and amino acetonitrile (Belloche et al. 2008), a direct precursor of the simplest amino acid, glycine. Furthermore there is a strong evidence for the presence of PAH (polycyclic aromatic hydrocarbons), large aromatic molecules containing up to 100 carbon atoms, although specific assignments to any peculiar molecule have not yet been possible (Léger & Puget 1984; Allamandola et al. 1989). Conversely, the detection of glycine, claimed by Kuan et al. (2003) remains still controversial.

In summary, many complex molecules are observed in the ISM (mainly in the gas phase) and some of them contain up to 13 atoms. Moreover, it is likely that many additional molecules exist both in the gas and in the ice phase. Unfortunately, in the ice phase the large complex molecules cannot be observed since line broadening and intermolecular reactions caused by

the solid environment leads to overlapping features that are dominated by the most abundant ice components. In the next section we will see how these complex molecules can be formed.

Table 1.2 - List of the interstellar molecules observed in the ISM (compiled by A. Wootten http://www.cv.nrao.edu/~awotten/allmols.html).

Diatomic	Triatomic	Four atoms	Five atoms	Six atoms	Seven atoms	Eight atoms
H_2	C_3	*c*-C_3H	C_5	C_5H	C_6H	CH_3C_3N
AlF	C_2H	*l*-C_3H	C_4H	*l*-H_2C_4	CH_2CHCN	$HCOOCH_3$
AlCl	C_2O	C_3N	C_4Si	C_2H_4	CH_3C_2H	CH_3COOH(?)
C_2	C_2S	C_3O	*l*-C_3H_2	CH_3CN	HC_5N	C_7H
CH	CH_2	C_3S	*c*-C_3H_2	CH_3NC	$HCOCH_3$	H_2C_6
CH^+	HCN	C_2H_2	CH_2CN	CH_3OH	NH_2CH_3	CH_2OHCHO
CN	HCO	CH_2D^+(?)	CH_4	CH_3SH	*c*-C_2H_4O	CH_2CHCHO
CO	HCO^+	HCCN	HC_3N	HC_3NH^+	CH_2CHOH	
CO^+	HCS^+	$HCNH^+$	HC_2NC	HC_2CHO		
CP	HOC^+	HNCO	HCOOH	NH_2CHO		
CSi	H_2O	HNCS	H_2CHN	C_5N		
HCl	H_2S	$HOCO^+$	H_2C_2O	HC_4N		
KCl	HNC	H_2CO	H_2NCN			
NH	HNO	H_2CN	HNC_3			
NO	MgCN	H_2CS	SiH_4			
NS	MgNC	H_3O^+	H_2COH^+			
NaCl	N_2H^+	NH_3				
OH	N_2O	SiC_3				
PN	NaCN	C_4	Nine atoms	Ten atoms	Eleven atoms	Twelve atoms	Thirteen atoms
SO	OCS		CH_3C_4H	CH_3C_5N(?)	HC_9N	$CH_3OC_2H_5$	$HC_{11}N$
SO^+	SO_2		CH_3CH_2CN	$(CH_3)_2CO$			
SiN	*c*-SiC_2		$(CH_3)_2O$	NH_2CH_2COOH			
SiO	CO_2		CH_3CH_2OH	CH_3CH_2CHO			
SiS	NH_2		HC_7N				
CS	H_3^+		C_8H				
HF	SiCN						
SH	AlNC						
FeO(?)	SiNC						

1.2 Energetic processing and thermal evolution of ices

Non-energetic reactions, such simple atom additions on grain surface, are necessary to initially form water-based ice mantles; however, additional energetic mechanisms appear to be necessary to further form molecules and, in particular, complex molecules. These mechanisms are often concomitant and include energetic processing by cosmic ion irradiation and UV photolysis, and thermal processing (Fig. 1.8).

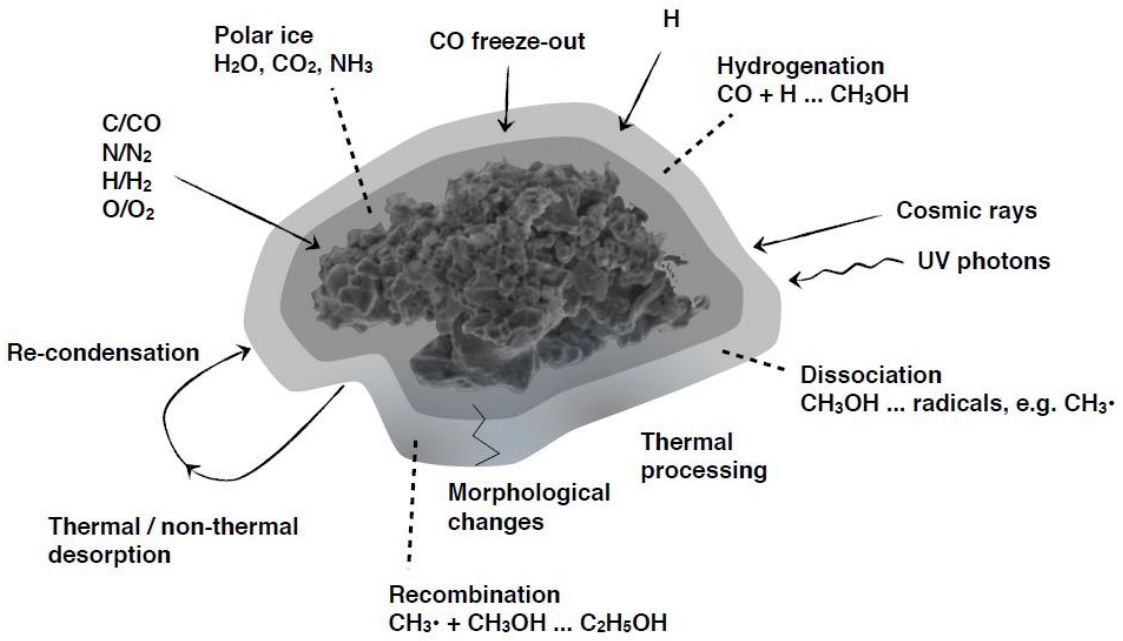

Figure 1.8 - Scheme of the different processes occurring on interstellar grains (from Guss 2013).

UV photons are widely present in space environments, and those with energy greater than ~4 eV can drive ice photochemistry. Indeed, ice photochemistry is now accepted to occur deeper into the dense clouds than thought earlier and at much lower energies than in the gas phase (Gudipati & Allamandola 2003). On the other hand, energetic UV photons produced by newly formed stars do not penetrate deeply into the surrounding molecular cloud and those from external stars affect only the outer edges of these clouds. However, internal young stars can be important sources of UV radiation especially during the T-Tauri phase. A high flux as 10^{12} photons cm^{-2} s^{-1} can penetrate the circumstellar disk and efficiently photolyze the ice. Moreover,

there is another internal source of UV photons that can affect the entire cloud, which is the decay process of the H_2 molecule after cosmic ion bombardment (Shen et al. 2004).

Cosmic ions are dominated by protons, mainly in the low MeV range, with an estimated flux value of 1 proton cm^{-2} s^{-1} in dense quiescent regions (Mennella et al. 2003). Cosmic ions penetrating the cloud lead to internal production of UV photons via a mechanism in which secondary electrons excite H_2, which then re-radiate photons when they decay. In dense clouds this internal UV flux is estimated to be 1.4-4.8 x 10^3 photons cm^{-2} s^{-1} with a typical energy of ~10 eV (Prasad & Tarafdar 1983; Mennella et al. 2003), much smaller than that one present in the diffuse ISM but strong enough to drive the photochemistry in the ices. This energy is released to the ice through a single photo-dissociation or photo-excitation event. As a consequence of these events, molecular bonds are broken, formed radicals diffuse through the ice and react with other molecules, giving rise to a rearrangement of the chemical structures and to the formation of new molecular species. In this way, a complex chemistry occurs. The energy dose from this internal UV source is thought to be similar in value to the energy contribution from the incoming cosmic ions. Moreover, this is the right dose of irradiation required to form new species in the ice preserving them from further irradiation that could led to their destruction. Recent studies suggest that the production of molecules, such as C_2H_5OH, $HCOOCH_3$ and CH_3OCH_3, relies on UV irradiation of interstellar ices (Öberg et al. 2009, Modica & Palumbo 2010).

Within the cloud, several circumstances such as the formation of a new star, stellar outflow winds, and shock waves can lead to warm-up of the ices. The gradual warm-up can promote the mobility of species, which diffuse through the ices and trigger new reactions. Some proposed reactions studied in the laboratory include polymerization to form polyoxymethylene (Schutte et al. 1993). Moreover, with the further increase of the temperature, the more volatile components of the ice mantle can sublimate while the more refractory organic material remains.

Evidences for energetic processing of ices arise from the analysis of the infrared spectra of observed sources. The interstellar 4.62 μm absorption band was discovered in the ground based spectrum of W33A (Lacy et al. 1984). Commonly referred to as the “XCN” feature (Gibb

et al. 2000), this band is observed in a large variety of objects (Soifer et al. 1979; Tegler et al. 1993, 1995; Demyk et al. 1998; Pendleton et al. 1999; Gibb et al. 2000; Keane et al. 2001; Whittet et al. 2001; Chiar et al. 2002; Spoon et al. 2003). The 4.62 μm absorption is now unambiguously attributed to OCN^- formed by UV photolysis or cosmic ion irradiation of NH_3 bearing ices, as supported by laboratory works (Palumbo et al. 2000; Bernstein et al. 2000; Hudson et al. 2001) and is considered as a key indicator of such processing. However, besides energetic processing, thermal evolution is also a possible formation alternative for the OCN^- (van Broekhuizen et al. 2004). The most probable counter ion of OCN^- is NH_4^+ (thus forming the ammonium cyanate salt) which is properly observed in evolved processed ices (Schutte & Khanna 2003). Another indication for energetic processing of interstellar ices is that of CO_2, a molecule detected for the first time by d'Hendecourt & Jourdain de Muizon (1989) by its 15.2 μm absorption in three distinct infrared sources with the IRAS telescope. Interestingly, this molecule was been predicted from laboratory experiments on UV photochemistry of ice mixtures of water and carbon monoxide, revealing the potentiality of this laboratory approach (d'Hendecourt et al. 1985, 1986; Allamandola 1988). Several attempts have been performed to detect the effects of UV photochemistry in space with some tentative successes, such as in NGC 7538-IRS9 where the 5 to 8 micron region may be interpreted by the presence of complex molecules such as urea, formamide and glycerol (Raunier et al. 2004). Some features, observed in the astronomical spectra, still remain not fully explained such as the 6.8 μm feature, attributed to NH_4^+ formed by UV photolysis of ice analogs (Shutte & Khanna 2003) but more likely due to multiple contributors (Boogert et al. 2008). However, the most emblematic spectroscopic signature which is considered the sign of interstellar ice processing is the series of absorption near 3.4 μm in the diffuse interstellar medium. These features have been attributed to the C-H stretching in aliphatic hydrocarbon chains carrying the CH_2 and CH_3 functional groups (Sandford et al. 1991; Pendleton et al. 1994). The correlation of these absorption features with those from different interstellar analogs (hydrogenated amorphous carbon, quenched carbonaceous condensate, and various organic residues including the ones described in this thesis) is remarkable. However, the best candidate material for the 3.4 μm feature is likely to be

hydrogenated amorphous carbon (Chiar et al. 2000; Pendleton & Allamandola 2002; Mennella et al. 2002).

Finally, the presence of organic refractory residues has long been postulated as a candidate for the carbon-rich components observed in interstellar dust at 3.1, 3.4, and 6 μm (Greenberg et al. 1995; Greenberg & Hage 1990; Pendleton et al. 1994; Whittet et al. 2001). This residue, that is expected to be rich in complex organics, is thought to be the result of ice energetic processing. As suggested by Gibb & Whittet (2002) this residue, which is not widespread in the diffuse interstellar medium, could in part contribute to the 6 μm band observed in YSOs. This hypothesis, well documented in the laboratory, is supported only by one observation of evolved ices in Mon R2 IRS3, the only observational evidence for organic refractory residues formation (Shutte & Khanna 2003). It is interesting to note how much these observations are biased because evolved ices can be tentatively observed only in evolved objects when the surrounding molecular cloud starts to dissipate. Finally, observations are quite limited in number as well as in performance. At this stage it is clear that a much more sensitive spaceborn telescope such as the JWST is needed.

1.2.1 Complex molecules in hot molecular cores

The formation of a new star has many effects on the chemistry of the surrounding material. One of the most extensively studied regions of star formation is the Orion molecular cloud (OMC-1), which contains a number of bright mid-infrared sources, thought to hold embedded protostars (Wynn-Williams et al. 1984). These sources, called hot molecular cores due to their high temperature ($T > 100$ K), are compact (< 0.1 pc) and massive ($10\text{-}10^3$ M_{sun}) condensations of gas and dust surrounding a protostar in the early phases of its evolution (Brown et al. 1988). The Orion hot core is one of the most studied objects of this type (Genzel & Stutzki 1989). The low-mass versions of the hot cores are known as hot corinos (Ceccarelli 2004). Hot cores and corinos are natural laboratories in which the most complex molecules of the interstellar medium can be observed and studied. In these regions grains experience thermal processing that lead

to molecular diffusion, structural changes, and subsequently to the complete sublimation of ices. Sublimation allows the molecular species previously formed in the solid state to be released into the gas phase, where they enrich the inventory of detected species and participate in new gas phase reactions. Because of the high temperature of the hot cores, many reactions can occur efficiently, including endothermic processes and exothermic processes with barriers. Hot cores are, in fact, particularly rich in complex organic molecules such as $HCOOCH_3$, HCOOH, CH_3OCH_3, and CH_2CHOH (Snyder et al. 2002; Hollis et al. 2000, 2002; Remijan et al. 2003; Kuan et al. 2003; Cazaux et al. 2003; Kuan et al. 2004; Bottinelli et al. 2004a, 2004b, 2007).The origin of these complex molecules was initially thought to be the rich gas phase chemistry of evaporated or sputtered species (e.g., Millar et al. 1991; Millar & Hatchell 1998; Herbst et al. 1977). However, recent experimental works have shown the inefficiency of gas phase reactions (Horn et al. 2004; Geppert et al. 2006) and that, according to models many of the observed molecules must be *primarily* produced in ices prior to evaporation (Charnley et al. 1995; Garrod & Herbst 2006; Wakelam et al. 2010). In particular, methyl formate ($HCOOCH_3$), a complex organic molecule widely observed toward numerous different sources, has been suggested to form in the solid state after ion irradiation of ice mantles containing methanol and carbon monoxide (Modica & Palumbo 2010), and released after sublimation into the gas phase, where it can be observed.

In summary, first generation complex molecules form in the ice as a consequence of UV/ion irradiation; they will eventually sublimate once the grain temperature rises above the ice sublimation temperature of ~100 K. Subsequent to ice sublimation, hot core gas phase chemistry between sublimated molecules can drive further complexity in second generation species (e.g., Millar et al. 1991; Charnley et al. 1992, 1995). However, after the formation of a new star and its planetary system, some material from interstellar or protostellar origin, could remain relatively unaltered in the colder edges of the disk. This material could be accreted into small bodies such as comets and asteroids, which are considered leftovers from the formation process of a planetary system. These small bodies are not subjected to extensive processing as the rest of the planetary system, as currently believed for the small bodies of our Solar System.

Therefore they may retain much of the original solar nebula materials, including first organic compounds.

1.3 Small Solar System bodies

Comets

Comets are icy objects of frozen gases, rocky materials, and large organic particles (Mumma 1997; Irvine et al. 2000). It is suggested that they formed from accretion of planetesimals in the colder parts of the protosolar nebula from a mixture of interstellar and nebular material (Irvine 1999, 2000; Ehrenfreund & Schutte 2000). Comets are the most volatile-rich objects of the Solar System and hence believed to be the least thermally processed material for the study of its formation (Delsemme 1982). After an observational campaign on comet Hale-Bopp, it was noted a remarkable similarity between the composition of cometary ices and hot cores (Bockelée-Morvan et al. 2000). This reinforced the idea that the processes at work in the interstellar medium, particularly in the dense molecular clouds, could play a major role in the formation of cometary ices. On the other hand, molecular cometary abundances can vary greatly among different comets (Bockelée-Morvan et al. 2004). This indicates that comets have different origins and that some cometary materials are the result of a certain degree of processing experienced in the interstellar cloud or in the protosolar disk.

There are two major reservoirs of comets: Kuiper Belt and Oort Cloud. Comets formed beyond Neptune constitute part of the Kuiper belt, a disc-shaped region extending from the orbit of Neptune (at 30 AU) to approximately 50 AU from the Sun. Comets from this region have a short period (less than 200 years) and low inclination on the ecliptic plane. Comets formed in the Jupiter-Neptune region have been subsequently ejected by gravitational interaction with the giant planets forming the Oort cloud, which is a vast, spherical shell of icy bodies surrounding the Solar System at 50000 AU from the Sun.

A number of missions such as Vega, Giotto, Galileo, Stardust, Deep Impact (in the recent past) and Rosetta (at the present day) have improved our knowledge on comets. Their mineral component shows the presence of silicates, both in the amorphous and crystalline form (Crovisier et al. 1997; Wooden et al. 1999). Their volatile component is dominated by water, followed by CO (1-30% w.r.t water) and CO_2 (5%), with trace amounts of other chemical species, some of them of interest for prebiotic chemistry such as CH_3OH, CH_4, NH_3, HCN, etc. (Bockeleée-Morvan et al. 2004). The in situ measurements of cometary grains have shown that they are mainly composed of solid organic matter made of carbon, hydrogen, oxygen and nitrogen atoms, thus they have been called ‘‘CHON grains’’ (Fomenkova 1999). Organic species identified in the more refractory organic material include PAH, highly branched aliphatic hydrocarbons, and unsaturated hydrocarbon chains (Kissel & Krueger 1987; Cottin et al. 1999; Fomenkova 1999). The amino acid glycine has been detected on the strewn dust of comet 81P/Wild-2 (Elsila et al. 2009). Hexamethylenetetramine (HMT), a molecule which is an important topic in Chapter 4 and 6 of this thesis, is suggested as a candidate component of the cometary organic material (Bernstein et al. 1995). Indeed, as proposed by Briani et al. (2013), cometary nuclei could contain a small fraction of HMT if materials have been slightly heated between 280 K (the temperature at which the molecule starts to form) and 400 K (the temperature at which it evaporates). Rosetta space mission on comet 67P/Churyumov–Gerasimenko (Fig. 1.9) will have the ability to search for direct evidence of cometary HMT as well for other important complex molecules.

Indeed, unprecedented advances in the knowledge of cometary nuclei composition are expected from the in situ measurements on this comet by the COSAC instrument (Goesmann et al. 2007). The COSAC instrument is a gas chromatograph coupled with a mass spectrometer designed to obtain information on the composition of volatile compounds and, in particular, on chiral molecules. The use of three different enantioselective chromatographic columns will ensure the separation of enantiomers in a wide range of chiral molecules, including amino acids, to search for clues on the origin of biomolecular homochirality on Earth (Meierhenrich et al. 2001). This goal is of fundamental interest in the context of the subject of Chapter 3 which deals with the induction of enantiomeric excesses in chiral amino acids.

At the time of this writing, after a long journey lasted ten years, five months and four days, Rosetta has finally arrived to the comet destination (Fig. 1.9) and started to identify the candidate sites to set down the Philae lander, planned in November 2014.

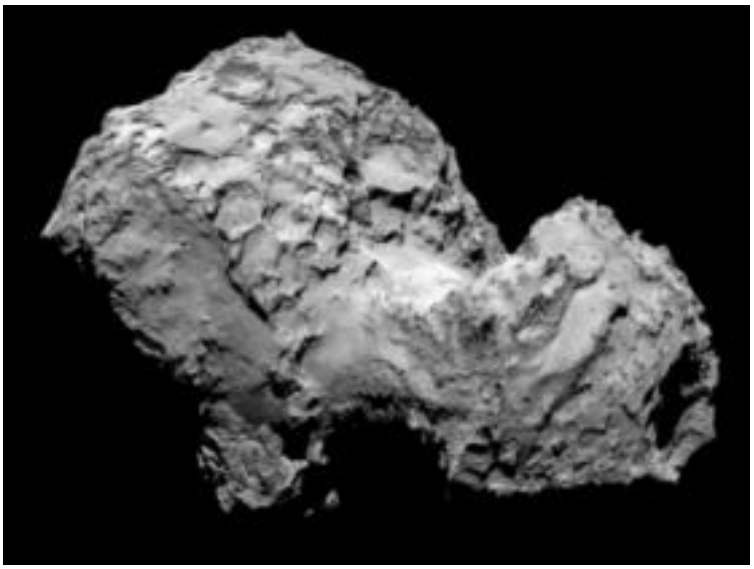

Figure 1.9 - Comet 67P/Churyumov–Gerasimenko showing a dusty crust covered of craters, as seen by the Rosetta spacecraft on 3 August 2014 from a distance of 285 km (credit ESA/Rosetta/MPS).

Asteroids

Asteroids are solid bodies that never got incorporated into the planets. The majority of known asteroids orbit within the asteroid belt between the orbits of Mars and Jupiter, which holds more than 200 asteroids larger than 100 kilometers in diameter.

Asteroids are thought to have a different origin from comets, having formed inside the orbit of Jupiter rather than in the outer Solar System as comets. It is thought that they formed as a consequence of the birth of Jupiter; the presence of this giant planet could prevent the other planetary bodies to form, causing the small objects in the gap between Mars and Jupiter to collide with each other and fragment into the asteroids seen today. However, the distinction

between asteroids and comets is not sharp. For example, extinct comets that have lost almost all of their volatile ices and dust may resemble small asteroids. The importance of asteroids, as well of comets, lies in the fact that they could have survived almost unchanged since the formation of the Solar System. This can be true for the small and non-differentiated asteroids which are good candidates for the study of the primitive Solar System.

Asteroids are classified according to their spectral features and composition (DeMeo et al. 2009). The composition of an asteroid in the asteroid belt depends on its distance from the Sun (Gradie & Tedesco 1982). Closer to the Sun, the majority of asteroids are principally made of silicate compound rocks. At the outer edges most of asteroids contain large quantities of carbon molecules. These ones are very similar in composition to the carbonaceous chondrite meteorites fallen on Earth. It is thought in fact that these meteorites are fragments produced during collisions between asteroids.

Interplanetary dust particles

Interplanetary dust particles (IDPs) are small grain (generally between 5 and 50 mm), constituted by smaller sub-grains of refractory materials (Fig. 1.10), in orbit around the Sun. The sources of interplanetary dust particles include at least: asteroid collisions, cometary activity and collisions in the inner Solar System (Backman 1997; Rietmeijer 2002). IDPs that reach the Earth's surface are called micrometeorites. The flux of micrometeorites to the Earth at the present day is estimated to be 2-6 x 10^7 kg/yr (Love & Brownlee 1993), while the flux of meteorites is estimated to be 2.9-7.3 x 10^3 kg/yr (Bland 2001). It can therefore be concluded that micrometeorites dominate the incoming mass flux of extraterrestrial materials to the Earth.

IDPs are collected by NASA aircrafts from the Earth's atmosphere. Their analysis reveals that they mainly consist of silicate grains coated by carbonaceous material and that the average carbon content is of 10-12%. Most of IDPs have a similar elemental composition with CI meteorites (Schramm et al. 1989) and some, such as the chondritic porous IDPs, are considered very primitive, meaning that they have never experience significant heating and hence thermal alteration (Bradley 2003).

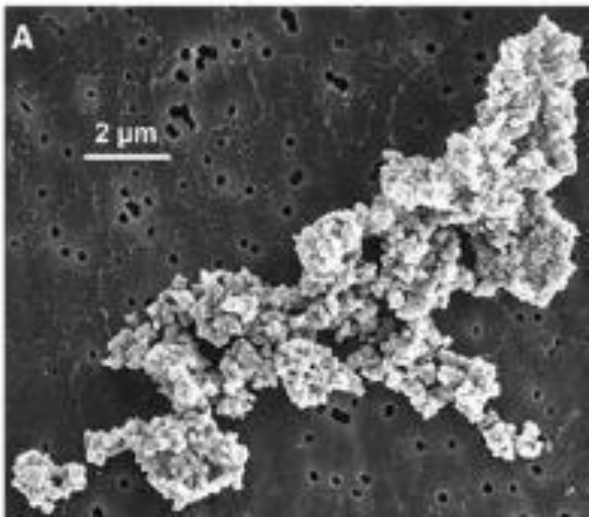

Figure 1.10 - A typical chondritic Interplanetary Dust Particle (IDP) (credit Lawrence Livermore National Laboratory).

1.3.1 Meteorites

Meteorites are solids that fall on Earth from the outer space and originate mainly from asteroids and comets and more rarely from the Moon and Mars. Meteorites are traditionally divided into three categories based on their composition: stony meteorites (composed of rocky material), iron meteorites (composed of metallic material), and stony–iron meteorites (composed of their mixtures).

Stony meteorites are then conventionally divided into two other categories: chondrites and achondrites. Chondrites are groups of meteorites that have undergone little changes since their parent bodies originally formed and are characterized by the presence of chondrules (Connolly 2005), spherical inclusions of about 1 mm in diameter consisting largely of the silicate minerals olivine and pyroxene, which are the oldest objects in our Solar System. Chondrules probably formed in the protoplanetary disk and were incorporated in asteroids. Because thermal metamorphism (alterations of the minerals in response to the increased temperature) suffered by asteroids generally destroys the chondrules, their presence in a meteorite is a sign of primitiveness. This group of meteorites includes the most primitive of all meteorites and for this

reason is particularly interesting for this thesis. Achondrites are groups of meteorites that have a complex origin involving melting and recrystallization on their parent body (Clayton & Mayeda 1996). Chondrites are divided into ordinary (O), enstatite (E), and carbonaceous (C) on the basis of their mineralogy, bulk chemical composition, and oxygen isotope compositions. Carbonaceous meteorites will be a subject of our study in this thesis, in relation with the organic matter originated from ice photo/thermo chemistry in our laboratory experiments, and thus will be more extensively treated in Chapter 5.

1.3.2 The exogenous organic delivery to Earth

The origin of life on Earth would have required the presence of liquid water and prebiotic organic compounds but also an environment from which prebiotic chemistry could really start and allow for the passage from non-living materials to the first primitive forms of life. The detection of organic molecules in comets, meteorites and IDPs has led to speculation that these objects may have brought the prebiotic organic compounds to Earth (Oró 1961; Greenberg 1986, Botta et al. 2002). Although this hypothesis is not, at the present time completely accepted and far from being proven, it remains however a perfect hypothesis in which our work takes place.

Evidence that a large number of collisional events occurred in our Solar System after its formation is given by the petrologic record of craters in the Moon (Chyba 1990). This suggests that in a short time interval, between 4.1 and 3.8 billion years ago, a cataclysmic event known as the Late Heavy Bombardment (LHB) occurred, approximately after 700 million years the planets formed (Gomes et al. 2005). Recent theories propose that the LHB was triggered by the rapid migration of the giant planets which caused asteroids to move to more eccentric orbits, collide each other, and impact the terrestrial planets (Gomes et al. 2005). During this short interval, a large number of comets, asteroids, and IDPs collided into Earth bringing their substantial organic content (Chyba & Sagan 1992; Pierazzo & Chyba 1999, Bailey 2006). It is interesting to note that life was already widespread 3.6 billion years ago, just after the end of the LHB (Schidlowski 1988). This rapid appearance of life on Earth constitutes a good argument in favor of the hypothesis according to which life may have originated from an extraterrestrial delivery of organic compounds. Moreover, experimental studies that simulate the physical

conditions in impact events in the laboratory indicate the survival of amino acids under these conditions (Blank et al. 2001). More generally, laboratory simulations are essential to study the formation of organic molecules in astrophysical environments and establish possible links with prebiotic molecules from which life started.

1.4 Laboratory simulations

Many laboratory works have been carried out to study the chemical and physical evolution of ices in astrophysical environments (e.g. Hagen et al.1979; Allamandola et al. 1988; Gerakines et al. 1995; Bernstein 1995; Strazzulla 1997; Hudson & Moore 2000; Bennett et al. 2007; Elsila 2007; Öberg et al. 2009). These works are often based on laboratory simulations which reproduce some astrophysical relevant parameters characterizing the ices and the environment in which they evolve. Infrared spectroscopy is used to compare the laboratory results with observational data.

In typical experiments, ice samples (cosmic ice analogs) are created under vacuum by condensation at low temperature (10-80 K) of gaseous mixtures representative of those observed in interstellar ices (e.g. H_2O, CH_3OH, NH_3, CO_2, CO…). Several processing mechanisms occurring in interstellar clouds can be simulated, such as the UV irradiation field (by using a microwave discharge lamp producing UV photons), or the cosmic ion bombardment (by using protons or heavier charged particles). It is verified that UV and ion irradiation have similar effects on ices (Gerakines et al. 2000; Baratta et al. 2002). In both cases the irradiation typically produces moderately complex species and volatiles in the ice sample, as observed spectroscopically. Later, the ice samples can be heated to simulate the thermal processing occurring when the temperature rises (e.g. in the inner parts of a circumstellar disk when a new star starts to form). During the warm-up, the species present became more reactive, volatiles sublimate while more refractory species remain. After the warm-up a pale yellow colored material, stable at room temperature, is left behind: the organic refractory residue (or “yellow stuff”). The characteristics of this residue, such as the composition and the degree of

complexity, and its possible astrophysical implications, sometimes connected with the origin of life, represents the subject of intensive studies started already more than 40 years ago.

The first studies on laboratory ultraviolet processing experiments on interstellar ice analogs were conceived by Greenberg in the early seventies (Greenberg et al. 1972). In Leiden, Greenberg and his collaborators developed an experimental system able to simulate interstellar ices in realistic conditions thanks to which they studied a variety of ice mixtures and produced the first samples of organic residues (Greenberg & Yencha 1973; Hagen 1979). This experimental approach proved soon to be robust and appropriate allowing, for example, the identification of water (Léger et al. 1979), the first molecule discovered in interstellar ices. Similarly, subsequent astrophysical discoveries have often required the support of the data obtained in this kind of experiments (Schutte 1999).

Moreover, the production of residues showed that photoprocessing can provide a path for the formation of large and complex molecules in space (Hagen et al. 1979). The first infrared analysis of residues showed the presence of functional groups such as amino groups (NH_2) and carboxyl groups (COOH) (Hagen et al. 1979), nitrile (CN) and carbonyl groups (C=O) (Allamandola et al. (1988), and hydroxyl group (OH) (Tielens 1989). The methyl (CH_3) and methylene (CH_2) group content was also shown with, in particular, a CH_2 predominance, thus implying the presence of long hydrocarbon chains in the residues (Allamandola et al. 1988).

Several molecules of the alcohol, amide, and carboxylic acid groups were detected by high performance liquid chromatography (HPLC) and gas chromatography coupled to mass spectrometry (GC-MS) (Agarwal et al. 1985). Hexamethylenetetramine (HMT, $C_6H_{12}N_4$), a heterocyclic organic compound with a cage-like structure, was detected by GC-MS for the first time (Briggs et al. 1992). Few years later, combining infrared spectroscopy, nuclear magnetic resonance spectroscopy and GC-MS, it was shown that HMT is indeed the main component of the residue (~60%), followed by esters, alcohols, and polyoxymethylene (POM) related compounds (20%), and then by ketones and amides (20%). Given its high abundance in laboratory residues, HMT is considered of great astrophysical interest, as it may be comprised in a large portion of interstellar grains, icy satellites, and the organic crust of comets. In 2004,

HMT and also a series of HMT based molecules (methyl-HMT, hydroxyl-HMT, amin-aldehyd-HMT, and methanyl-aldehyd-HMT) were detected by GC-MS (Muñoz Caro et al. 2004) on residues of different starting mixtures.

A wide variety of organic compounds, some of them with potentially prebiotic implications, is now reported to be present in the residues, mainly after acid hydrolysis, a technique largely used in analyzing meteoritic organic materials. These molecules include for example nucleobases (Nuevo et al. 2009), glycerol, urea, glycolic acid (Nuevo et al. 2010), and hydantoin (de Marcellus et al. 2011b). In particular, a class of molecules which deserves a great attention is that of amino acids, the building blocks of proteins. Indeed, the analysis of organic residues has been often focused on the search of amino acids for their prebiotic interest.

The first amino acid to be detected was glycine, the smallest of the 20 amino acids commonly found in proteins. It was found after acid hydrolysis of a residue obtained by photolysis of CO, NH_3, and H_2O (Briggs et al. 1992). Subsequently, several other amino acids such as alanine, β-alanine, and aminobutyric acid were found after hydrolysis of residues obtained by proton bombardment of propane, ammonia and water (Kasamatsu et al. 1997). These first detections were later confirmed in the same year thanks to two independent studies by isotopic labeling and after acid hydrolysis. Bernstein et al. (2002) detected glycine, alanine, and serine by irradiation of ice mixtures composed of H_2O, CH_3OH, NH_3, and HCN using HPLC and GC-MS. Muñoz Caro et al. (2002) detected 16 amino acids, 6 of them being proteinogenic, by irradiation of ice mixtures constituted by H_2O, CH_3OH, NH_3, CO, and CO_2 using GC-MS. As shown by Nuevo et al. (2007), it is possible to form amino acids whatever the nature of the carbon source (organic or “inorganic”) using for example an irradiated H_2O:CO_2:NH_3 mixture.

More recently, Meinert et al. (2012), using a sample produced in our group at IAS, identified 20 amino acids and 6 di-amino acids using a multidimensional GCxGC/TOF-MS instrument. Some of the di-amino acid identified (such as N-(2-aminoethyl)glycine) are the building blocks of peptide nucleic acid (PNA), considered by some authors as being part of the first genetic material, prior to the apparition of the RNA/DNA world (Wittung et al. 1994).

The presence of amino acids and other compounds with a potential prebiotic interest in the laboratory residue permits to make some predictions and speculations on the molecular species formed under astrophysical conditions. So far, amino acids have never been observed in the ISM. However, they are largely present in meteorites, such as in Murchison and Murray (Kvenvolden 1971; Engel & Macko 1997; Cronin & Pizzarello 1997, 1999). In particular, more than 80 different amino acids have been identified in Murchison and one of them, glycine, is also detected in comet 81P/Wild 2 (Elsila et al. 2009). The presence of amino acids in meteorites and comets supports the scenario of their exogenous delivery to the primitive Earth during the period of the heavy bombardment (Oró 1961; Chyba & Sagan 1992; Maurette 1998). However, a link between the meteoritic amino acids and the prebiotic molecules from which life started is far to be established.

Chapter 2

The MICMOC experiment at IAS

Contents

2.1 The experimental set-up MICMOC

The experimental set-up used at IAS to simulate the photo/thermochemical evolution of interstellar/circumstellar ice analogs is named MICMOC (Matière Interstellaire et Cométaire, Molécules Organiques Complexes) and it has been conceived and used by the Astrochimie et Origines team since 2003. This setup is specifically designed to produce routinely room temperature organic residues for different ex-situ chemical analytical methods. Moreover, it can be adapted to be temporarily mounted on the vacuum UV(VUV) DESIRS beamline at the SOLEIL synchrotron facility, as described in Chapter 3, to perform the Chiral-MICMOC experiments.

The main elements constituting the MICMOC device are the following:

- A stainless steel introduction line for gas mixtures preparation
- A cryostat and its vacuum chamber
- A microwave stimulated hydrogen flow discharge lamp for UV irradiation

- A Fourier transform infrared spectrometer
- A primary and secondary pump system
- An open flow liquid nitrogen (or helium) cooling system

The introduction line

The gas mixtures for our experiments contain water, methanol, and ammonia. They are prepared in a stainless steel introduction line (Fig 2.1). Different bottles are used for holding the individual gases: H_2O (triply distilled) vapor, CH_3OH (Sigma–Aldrich, 99.99% purity), $^{13}CH_3OH$ (Sigma–Aldrich, 99.99% purity), and NH_3 (Sigma–Aldrich, 99.5% purity). All the bottles are connected to the introduction line together with a mixing glass bottle (1.3 or 3 liters). The introduction line is evacuated by a turbo molecular pump up to ~10^{-6} mbar and remains at all times dynamically pumped when not used.

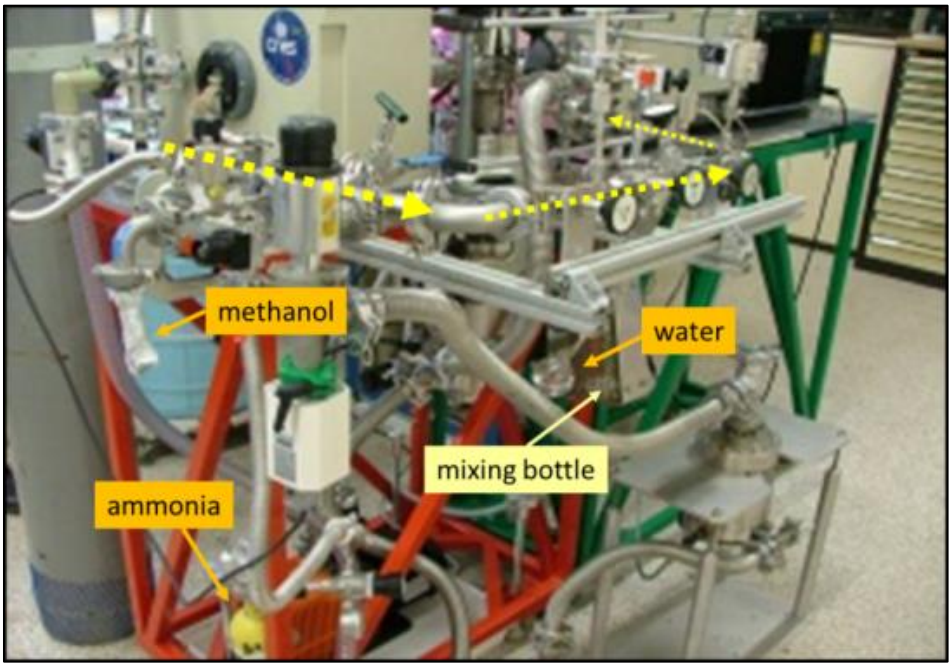

Figure 2.1 - The stainless steel introduction line where the gas mixtures are prepared. Dashed arrows evidence the path toward the vacuum chamber.

A gas mixture, prepared in the introduction line, is first stored in the mixing bottle, where it remains a few hours for proper mixing before being injected into the vacuum chamber. The flow of the mixture toward the vacuum chamber is regulated using a micrometric valve (203 Variable Leak Granville-Phillips) placed at the end of the line. The mixture is finally admitted into the vacuum chamber through an injection tube placed at the level of the window used for the deposition of the mixture itself.

The cryostat and the cooling system

The cryostat (Fig 2.2) is placed on top of a stainless steel high vacuum chamber evacuated by a primary dry pump (Alcatel ACP 15 G) coupled to a turbo molecular pump (Leybold Turbo Vac 361, 360 L/s) to a pressure of few 10^{-7} mbar. Inside the vacuum chamber, a substrate window, on the surface of which the gas mixtures can be deposited and irradiated, is placed in thermal contact with a cold finger (a copper block) thanks to the high thermal conductivity of indium seals.

An open liquid nitrogen cooling system is used to cool down the cryostat to about 80 K. This temperature is chosen for practical reasons; however the residues produced after irradiation of ices at ~80 K appear to be quite similar to those produced at more “interstellar” temperatures (10 – 15 K) (Muñoz Caro & Schutte 2003), essentially reflecting the fact that the residues themselves are always analyzed at room temperature (~300 K). The cooling system consists of a liquid nitrogen vacuum isolated transfer cane connected to a nitrogen dewar of 50 liters. The nitrogen circulation between the dewar and the upper part of the cryostat is assured by a dry vacuum pump. Alternatively, this system can work with liquid helium (4.2 K); however during this thesis we have always used liquid nitrogen. The temperature of the cold finger (and the substrate) can be measured and varied by a thermocouple and a small electric heater resistance connected to the cold finger. On top of the cold finger, a small reservoir of activated charcoal beads allows an efficient adsorption of residual gases present in the cryostat during the cooling down. This ensures final pressures in the 10^{-8} mbar range before starting the deposition/irradiation experiment.

The substrate is an infrared transparent window of 20 mm in diameter and 2 mm in thickness. It is generally a magnesium fluoride window (MgF_2) or, for some experiments, a potassium bromide (KBr) one. MgF_2 windows are preferred because they are not hygroscopic and can be reused after cleaning with methanol. Besides, the extraction procedure of the residues involves its dissolution in water, a method rather unpractical on KBr windows because they are water soluble. On the other hand, KBr windows have a natural transmission cut-off below 400 cm^{-1} and allow observing some infrared bands outside of the range covered by the MgF_2 windows, which have a cut-off around 970 cm^{-1}.

The position of the substrate is chosen to allow the introduction of the gaseous mixture, the UV irradiation, and the infrared transmission monitoring at the same moment during the experiment. Although the cryostat head is rotatable, our experiments never used this possibility in order to avoid possible air leaks in the chamber during rotation. The geometry of the deposition, UV irradiation and IR beam are thus fixed once for all.

Figure 2.2 - The cryostat is the heart of the MICMOC apparatus where the samples are produced. Several openings allow the connection to the infrared spectrometer (visible on the right), the introduction line, and the UV lamp.

The UV lamp

The UV photon source is a classical microwave stimulated hydrogen flow discharge lamp (Fig. 2.3). This lamp consists of a Pyrex tube filled by a continuous flow of molecular hydrogen (H_2) at a pressure of about 0.5 mbar. Ignition of the lamp is provided by a small electric discharge that initiates the ionization of H_2. It couples strongly with the microwave discharge producing a plasma from collisions with charged H_2 ions. Hydrogen molecules are dissociated and/or ionized after the absorption of the microwaves. When the excited species recombine, they emit photons of a characteristic energy, resulting in ultraviolet radiation mainly at 121.6 nm (Lyman α) but also at 160 nm and further. The pink color of the plasma is due to the combination of the specific transitions of the electrons between different energy levels. The lamp has a total flux of $2.2 \pm 0.7 \times 10^{14}$ photons $cm^{-2}s^{-1}$ at the sample position. It is interfaced with the vacuum chamber containing the sample through a UV transparent MgF_2 window. This window, as well the Pyrex tube, becomes easily dirty, partially blocking the UV passage. To prevent this inconvenient they are regularly renewed.

Figure 2.3 - The microwave-stimulated hydrogen flow discharge lamp provides the UV photon flux to irradiate the ice sample. The pink color is a characteristic of pure hydrogen plasma. The arrow indicates the direction toward the sample through the interface with the cryostat.

The Fourier transform infrared spectrometer

The infrared monitoring of the samples is made by a Fourier transform infrared (FT IR) spectrometer (Vector 22, Bruker). It works in the mid-infrared range between 7000 and 400 cm^{-1}. Its infrared source is a glowbar, a small silicon carbide element heated at ~ 1200 K emitting like a black body with a maximum intensity around 4000 cm^{-1}. The configuration of our system is adapted in such a way that the sample is placed outside the spectrometer along the infrared path between the interferometer and the detector (see de Marcellus 2010, PhD thesis). The detector is maintained under primary vacuum and the interferometer is purged by a continuous flux of dry N_2.

A typical Fourier transform spectrometer consists of two mirrors located at a right angle to each other and oriented perpendicularly, with a beam splitter placed at the vertex of the right angle. Radiation incident on the beam splitter from one of the two mirrors is divided into two parts, each of which propagates in two arms and is then reflected. The two beams are recombined and transmitted. When the position of one mirror is continuously varied, an interferogram is generated by the interferometer. The interferogram obtained is a record of the signal by the infrared detector as a function of the difference in the path for the two beams of the interferometer. A Fourier transform by the software OPUS turns the raw data into the final infrared spectrum. All the spectra are recorded with 2 cm^{-1} resolution.

2.2 Infrared spectroscopy

Infrared (IR) spectroscopy is a classical technique for functional group determination and structure interpretation of molecules. It is widely used in either organic and inorganic chemistry for the characterization of solid, liquid or gas samples. It has a large application range from small to large molecules; it requires a low amount of sample (even only a few μg), it presents a short measuring time (typically less than 15 minutes) and a relatively low cost. All these advantages make infrared spectroscopy a valuable non-destructive technique of investigation that allows some identification of new molecules formed in the final residue at room temperature. It is also the only direct method that allows a possible comparison with infrared

astronomical spectroscopic data, a characteristic which has been widely used in our group prior to 2003 (Dartois, PhD Thesis, 1998; Demyk, PhD Thesis, 2000). Moreover, in our case, it is a versatile means of controlling the experiments during all the phases from the initial gas mixture deposition to the final residue formation.

The covalent bonds of molecules can be seen as springs. The bonds vibrate at different frequencies, since they are of different strengths and have different masses attached to them. There can be different vibration modes such as symmetric stretches, asymmetric stretches (the highest energy vibrations) and lower energy vibration modes such as wagging/scissoring, and bending.

A molecule consisting of n atoms has a total of 3n degrees of freedom, corresponding to the Cartesian coordinates of each atom in the molecule. In a nonlinear molecule, 3 of these degrees are rotational, 3 are translational, and the remaining corresponds to fundamental vibrations; in a linear molecule, 2 degrees are rotational and 3 are translational. The net number of fundamental vibrations for nonlinear and linear molecules is therefore 3n-6 for nonlinear molecules and 3n-5 for linear molecules.

IR spectroscopy is sensitive to changes in dipole moment when the molecule vibrates. In order for a vibrational mode in a molecule to be "IR active", it must be associated with changes in the dipole moment during the vibration. Therefore, fully symmetrical molecules like O_2 and N_2 are not IR active and cannot be observed in the IR spectrum. Asymmetrical diatomic molecules, e.g. CO, absorb in the IR spectrum. More complex molecules have many bonds, and their vibrational spectra are correspondingly much more complex. Larger molecules are composed of many overlapping bands with the consequence that much information can be hidden under broad, featureless absorption bands.

When the frequency of an external IR source (such as that from a glowbar in an IR spectrometer), matches the vibrational frequency of a bond, resonant absorption occurs, while the remaining light is transmitted. The infrared spectrum is a plot the amount of transmitted light against the wavenumber (the inverse of the wavelength), which is proportional to the energy

and has the unit of reciprocal length cm^{-1}. The horizontal coordinate of the spectrum runs from high wavenumbers to low wavenumbers. The infrared spectral region is adjacent to the visible spectral region and extends from 0.78 μm to about 1000 μm. It can be further subdivided into the near-infrared region from 0.78 μm to 2.5 μm, the mid-infrared region from 2.5 μm to 50 μm and the far-infrared region from 50 μm to 1000 μm. The mid-infrared spectral range extending from 2.5 to 25 μm corresponds to 4000 to 400 cm^{-1} and represents the traditional range for vibrational spectroscopy.

The different vibrations result in an IR spectrum that is unique for each molecule because the ensemble of its single functional groups gives rise to characteristic bands both in terms of intensity and position. The approximate position of an infrared absorption band is determined by the vibrating masses and the type of bond (single, double, triple), the exact position by electron withdrawing or donating effects of the intra- and intermolecular environment and by coupling with other vibrations.

The stretching frequency of a bond can be approximated by Hooke's Law. In this approximation, two atoms and the connecting bond are treated as a simple harmonic oscillator composed of 2 masses (atoms) joined by a spring. According to Hooke's law, the vibration frequency of the spring is related to the mass and the force constant of the spring, *k*, by the following formula

$$\nu = \frac{1}{2\pi}\sqrt{\frac{k}{\mu}}$$

Where *k* is the force constant, *ν* is the frequency of the vibration, *μ* is the reduced mass defined as

$$\mu = \frac{m_1 m_2}{m_1 + m_2}$$

The infrared spectrum of a sample is recorded by passing a beam of infrared light through the sample. Examination of the transmitted light reveals how much energy is absorbed at each frequency (or wavelength). The fraction of incident light at a specified wavelength that passes through a sample is expressed in terms of transmittance *(T)*. In equation form,

$$T(\nu) = \frac{I_0}{I(\nu)}$$

where I_0 is the intensity of the incident radiation and I is the intensity of the radiation coming out of the sample.

We can also define the optical depth as

$$\tau(\nu) = ln\frac{I_0}{I(\nu)} = \sigma(\nu)nl = \sigma(\nu)N$$

where σ is the cross section (cm^2 $molecule^{-1}$), n is the number of molecules per volume unit traversed by the beam (cm^{-3}), and N is the column density (molecules cm^{-2}).

Transmittance *(T)* is related to absorbance *(A)* by the expression as *A=-log(T)* (Beer Lambert Law).

We can express N by the integral

$$N = \frac{\int_{\nu_1}^{\nu_2} \tau(\nu)d\nu}{\int_{\nu_1}^{\nu_2} \sigma(\nu)d\nu} = \frac{\int_{\nu_1}^{\nu_2} ln\frac{I_0}{I(\nu)}d\nu}{A}$$

Where A is the integrated band strength (cm $molecule^{-1}$) and where the numerator can be approximated by

$$\int_{\nu_1}^{\nu_2} ln\frac{I_0}{I(\nu)}d\nu \cong \tau_{max}\Delta\,\nu_{1/2}$$

2.3 The standard experiment

The experiments we describe here are directed only to the production of organic residue samples, the study of which is central to this thesis. All the samples are obtained from starting mixtures of the same composition and relative ratio to obtain as much as possible intercomparable results.

2.3.1 Preparation of the gaseous mixture

The first step in our experiments is the preparation of the gaseous mixture at room temperature. Different bottles connected to the introduction line are used for holding the individual components of the mixture. These components can be liquid or gaseous, however, only gases (vapors for liquids) are used. They are:

- Water, H_2O (liquid) purified thanks to a *Millipore Direct*-Q5 water purification system
- Methanol, CH_3OH (liquid), *Aldrich*, 99.9%
- Methanol, $^{13}CH_3OH$ (liquid), *Aldrich*, 99% ^{13}C
- Ammonia, NH_3 (gas), *Messer*, 99.98%

The gases are admitted one by one in a mixing bottle (3 or 1.3 liters capacity) in the order given by their increasing vapor pressure value (first water, then methanol, and finally ammonia). The composition of the gas mixture and the relative proportions between its components are controlled by their partial pressures in the introduction line. An absolute capacitance gauge (Baratron) allows measuring their partial pressures to better than 10% accuracy. The final mixture contains only three molecular species: H_2O, CH_3OH, and NH_3 (or H_2O, $^{13}CH_3OH$, and NH_3) approximately in the ratio of 2:1:1. About 45 mbar of total gaseous mixtures are prepared for each deposition/irradiation step. This pressure value can vary slightly with the variation of the room temperature. The gas mixture remains in the mixing bottle before being injected into the cold vacuum chamber for deposition for a couple of hours, the time necessary to cool down the system.

The second step of the experiments is the cooling-down to about 78 K of the cryostat, with the window substrate (MgF_2 or KBr) placed inside, thanks to the liquid nitrogen cooling system. During this step (1 or 2 hours) the pressure in the cryostat gradually diminishes reaching few 10^{-8} mbar. When this pressure is stabilized, the deposition/irradiation can start.

2.3.2 Deposition and irradiation

The gaseous mixture, previously prepared and stored in the mixing bottle, is admitted into the vacuum chamber by a micrometric valve and slowly deposited onto the cold substrate, where it condenses forming a solid ice sample. The irradiation takes place at the same time of the deposition and lasts two or three full days without interruptions and at constant temperature. Figure 2.4 shows a scheme of these processes and the formation of the ice sample on the cold substrate.

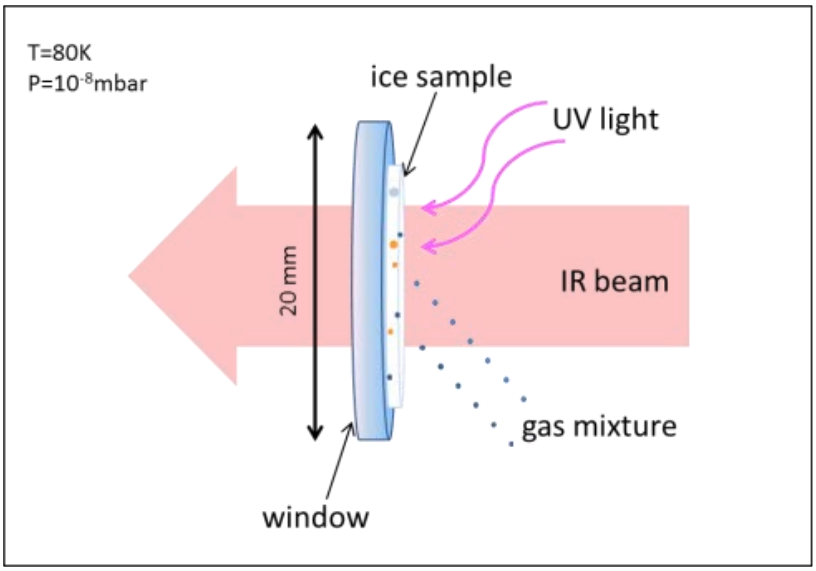

Figure 2.4 - Scheme of the deposition of a H_2O:CH_3OH:NH_3 =2:1:1 gas mixture on a cold window and the simultaneous UV irradiation. The infrared beam is used to monitor the formation and evolution of the sample. The window is placed inside the cryostat in thermal contact with a cold finger (80 K) under vacuum (10^{-8} mbar).

The deposition rate can be controlled with good approximation by checking the diminishing of pressure in the introduction line. An average of 0.5 mbar of gases per hour is deposited. Ice samples are irradiated with a constant photon dose of roughly one photon per deposited molecule, thus an energy of ~10 eV per molecule. The formation rate of the ice sample and the effects of photochemistry are monitored by Fourier-Transform Infrared Spectroscopy taking one spectrum per hour (or even less). In general, several days are necessary to obtain a sensible amount of residue. A shorter deposition time would not be enough to form an appreciable

amount of final residue, while a longer deposition time could cause the ice film to be too heavy and collapse under gravity, as already occurred during some experiments. Two or three days are then the good compromise to obtain enough material. Anyway, the length of a given experiment may be also limited by the amount of liquid nitrogen in the dewar.

After the simultaneous deposition and irradiation step, the ice is slowly warmed-up simply stopping the cooling system. This is the softest way to reach the room temperature. Normally 30-35 hours are necessary. During this phase, radicals diffuse reacting and forming more complex molecules; the volatiles sublimate while non-volatiles species remain on the surface of the window. The formation of the organic residue is gradual during the warm-up. At temperatures around 170 K the refractory residue starts to be visible as evidenced by spectra. During this step most of the bands decreases implying they are due to volatiles, largely present in the ice. In the meantime other bands arise. This is the case of the bands at 1007 and 1235 cm^{-1}. These bands are due to the formation of hexametylenetetramine (HMT, $C_6H_{12}N_4$) a molecule that will be later discussed in this thesis. Generally, the residue is kept in the cryostat two full days to be sure most of the volatiles have sublimated and the possible reactions have taken place. When the residue is stable, a last spectrum of the residue is taken.

When a thick sample is needed, a multilayer (2 or 3 layers) residue is made. In this case, the window covered by the first layer of residue is kept in the cryostat under a dynamic vacuum and a new gaseous mixture is prepared. The cryostat is cooled down and when the temperature reaches ~80 K, the new mixture is introduced in the cryostat and a second cycle of deposition/irradiation followed by warming-up is performed. Thus, the final residue consists of two (or more) layers of residues one over the other.

Once the residue is ready (single or multilayer), the cryostat is brought to atmospheric pressure under dry clean nitrogen. Then the window covered by the residue can be extracted by the cryostat and recovered. Figure 2.5 shows a typical single layer residue on its window viewed through the microscope (X60). The residue appears in the form of tiny droplets of a vivid yellow color which tend to merge on the surface of the window.

During the recovering step, the sample is inevitably exposed to the atmospheric air but care is used to reduce this time as much as possible (generally less than 15 minutes). Since this step is particularly delicate, large attention is used to handle the window. The procedure of recovering is made in a clean environment in a horizontal laminar flow cabinet.

Figure 2.5 – Two images of an organic refractory residue, after recovering at room temperature, captured through the microscope (target: 1 cm, magnification: X60) in a clean room at IAS. The residue appears in the form of tiny droplets of a vivid yellow color on the surface of the MgF_2 window.

Once recovered, the window is sealed in a special sample holder, designed by us, under an inert argon atmosphere (~1 atm) to prevent any alteration of the organic residue. The sample holder is then stored at 4 ºC until further analyses of the residue. The sample holders (Fig. 2.6) are small, easy to carry and particularly safe for transport the samples from our laboratory to others. Note that, as evidenced by previous work (de Marcellus et al. 2011; Nuevo et al. 2010), this method of conservation of the samples allows analyses to be carried out many months after the experiment.

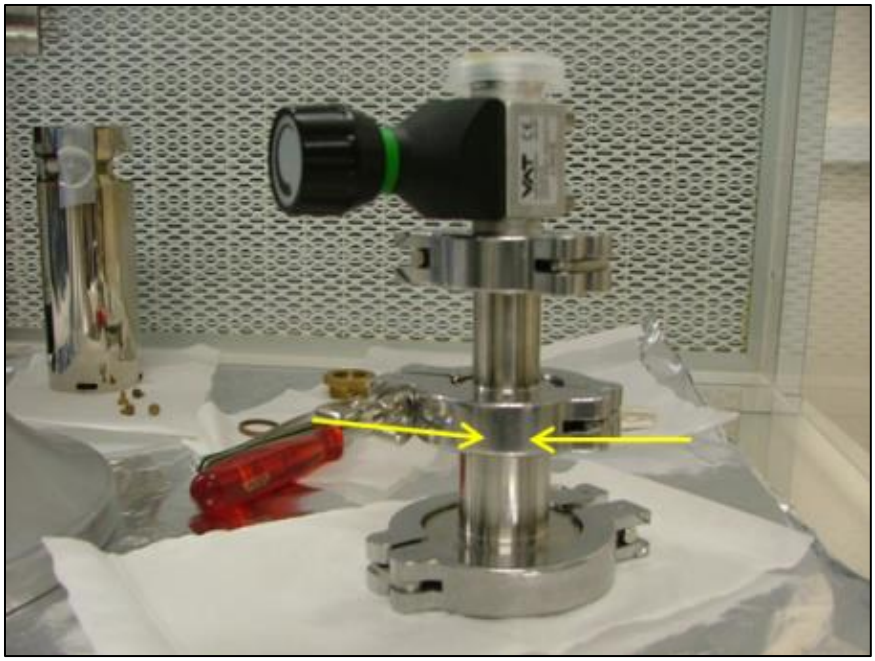

Figure 2.6 – A sealed sample holder to safely store the window covered by the residue before analysis. The arrows indicate the horizontal position of the window inside the sample holder.

2.4 Infrared analysis of interstellar/circumstellar analogs

2.4.1 Infrared ice spectra before irradiation

The individual components used for the gaseous mixture are: water (H_2O), methanol (CH_3OH), and ammonia (NH_3) in the ratio of 2:1:1. H_2O is the main source for oxygen, CH_3OH the source of carbon, and NH_3 the source of nitrogen. The mixture is not proposed to mimic the multicomponents ice mixtures present in space with their ratio, but it reflects qualitatively the most abundant species observed in interstellar ices.

The IR spectra of the pure individual components of our standard mixture are shown in Fig 2.7, while the ensemble of the three components (standard mixture) is shown in Fig. 2.8. We can note that the resulting spectrum is not a simple superposition of its three components. However we can clearly assign the main bands to their respective responsible species.

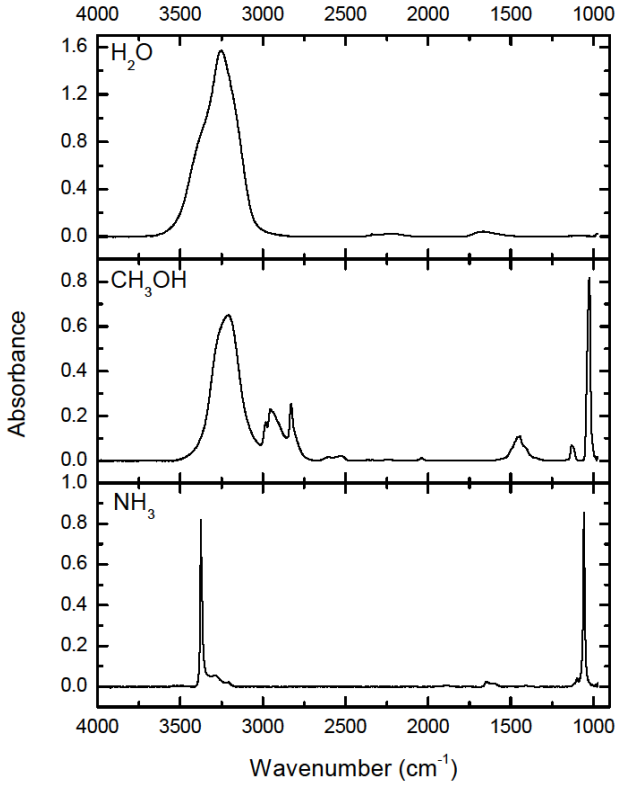

Figure 2.7 - Infrared spectra of the individual components of an ice mixture at 80 K: water (top), methanol (middle), and ammonia (bottom) in the 4000-900 cm^{-1} range.

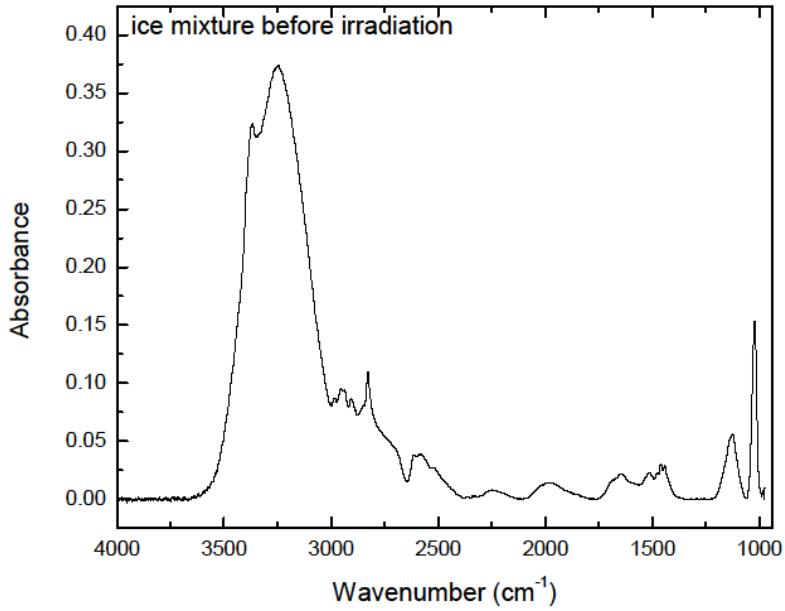

Figure 2.8 - Infrared spectrum of a H_2O:CH_3OH:NH_3 =2:1:1 ice mixture at 80 K before irradiation.

2.4.2 Infrared spectra of an irradiated thin ice film

In a standard experiment focused on the production of a final residue, during the gaseous mixture deposition, the ice sample condensing on the window is simultaneously irradiated with a UV flux without any interruption. Here, instead, with the aim to better understand the evolution of the ice, we want to show the effects of the irradiation on a thin ice layer deposited without irradiation and after gradually irradiated. An ice mixture made of H_2O, CH_3OH, and NH_3 in the ratio of 2:1:1 is deposited without irradiation for only 30 minutes. After this short time, a thin film of ice is already formed on the surface of the window, as evidenced by the spectrum shown in Fig. 2.9. Because of its thinness, this film can be efficiently irradiated in its depth, considering that the penetration power of the UV light through the ice is 100-200 nm from the surface. At a later stage and without further deposition, the ice film is irradiated by UV light in four distinct steps at increasing time intervals of 3, 7, 20, and 60 minutes respectively. At the end of each irradiation step a spectrum is taken. The progressive and cumulative irradiation steps are then of 3, 10, 30, and 90 minutes respectively. The first new bands start to be clearly visible after 10 minutes and are the band at 2135 cm^{-1}, 1725 cm^{-1}, and 992 cm^{-1}. As the irradiation progresses, other new bands appear. At the end of 90 minutes of irradiation, about 20 different bands, strong and weak, are visible. Figure 2.9 shows the spectrum after 90 cumulative minutes of irradiation compared to the one before irradiation. Figure 2.10 is an enlargement of the 2400-1250 cm^{-1} range where the spectrum as deposited and the four spectra at cumulative irradiation steps are shown. As noticeable from this figure, some bands are gradually destroyed during the photolysis, such as the methanol band at 1982 cm^{-1}, while new bands not present in the spectrum before irradiation appear; this is the case for the band at 2341, 2167, 1720, and 1388 cm^{-1}. The appearance of these new bands testifies for the formation of new species such as CO_2 (carbon dioxide), OCN^- (cyanate ion), CO (carbon monoxide), $HCO^{\bullet}$ (formyl radical), H_2CO (formaldehyde), NH_2CHO (formamide), HCOOH (formic acid), and CH_4 (methane). Even a small band due to $^{13}CO_2$ is visible, given that methanol used to make the starting gaseous mixture is not pure at 100% and always contain small amount of ^{13}C. Traces of photolyzed $^{13}CH_3OH$ could give rise to species containing ^{13}C as in this case. Table 2.1 lists the main new bands observed during the photolysis (de Marcellus 2010, PhD thesis).

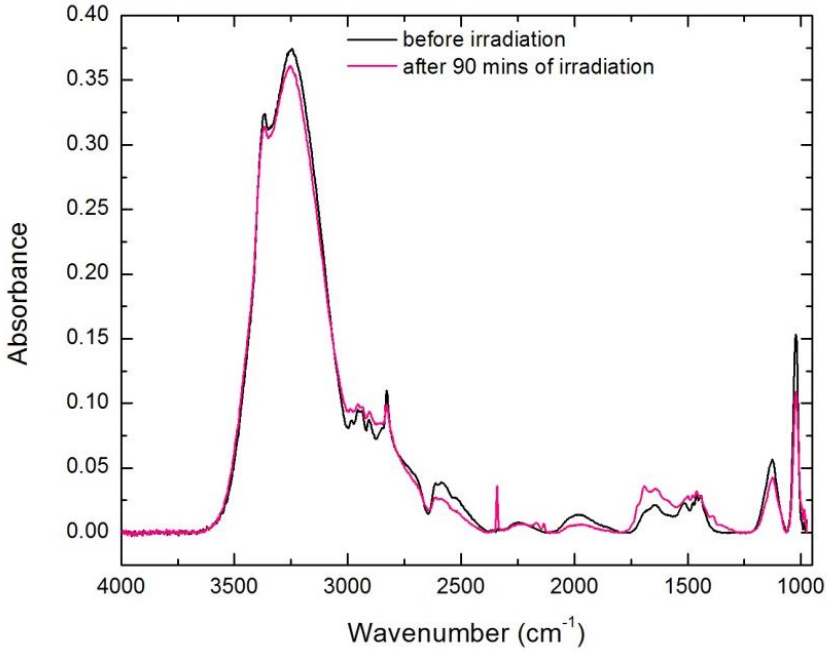

Figure 2.9 - Infrared spectra in the range between 4000 and 950 cm^{-1} of a $H_2O:CH_3OH:NH_3$ ice mixture before irradiation and after 90 minutes of irradiation.

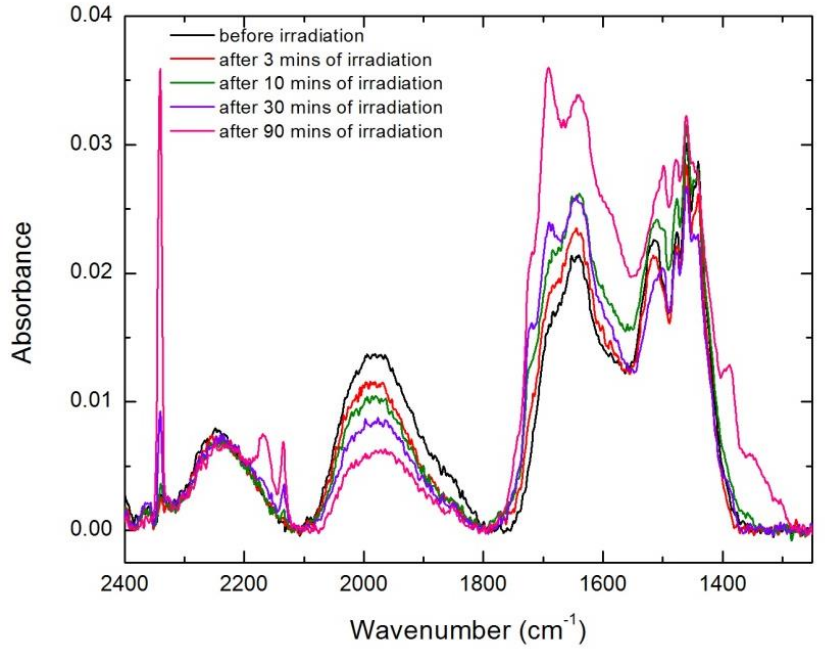

Figure 2.10 - Infrared spectra in the range between 2400 and 1200 cm^{-1} of a $H_2O:CH_3OH:NH_3$ ice mixture before irradiation and after four irradiation steps.

Table 2.1 - Main infrared bands observed during the UV photolysis of a H_2O:CH_3OH:NH_3 = 2:1:1 ice mixture along with the associated molecule and vibrational mode.

Band position cm^{-1}	Molecule (mode)
3000-2800	carbonaceous chains (CH_2 /CH_3 stretch)
2341	CO_2 (C=O stretch)
2167	OCN^- (C≡N stretch)
1849	$HCO^{\bullet}$
1720	H_2CO (C=O stretch)
1691	NH_2CHO (C=O stretch)
1588	$HCOO^-$
1388	HCOOH (C-H bend)
1351	$HCOO^-$? CH_3CHO?
1304	CH_4 (C-H def)

2.4.3 Infrared analysis of a typical residue

The final spectra of the residues made from a given starting mixture and fixed ratios of the components are globally similar and reproducible (see de Marcellus 2010, PhD thesis). Figure 2.11 shows the infrared spectrum of a typical residue at room temperature obtained from a H_2O:CH_3OH:NH_3 starting mixture in the ratio of 2:1:1. The spectrum is dominated by the presence of a broad feature ranging from 3600 to 3000 cm^{-1} (O-H and N-H stretching) ascribed to carboxylic acids, amines and alcohols; a strong double peaked band due to CH_2 and CH_3 stretching in aliphatic chains, three strong features in the region from 1700 to 1500 cm^{-1} assigned to esters and amides, and numerous sharp features in the region of the fingerprints such as the 1236 and 1007 cm^{-1} (C-N stretching) that are ascribed to HMT (the most abundant molecule in the residue). Table 2.2 lists these bands along with their assignments and molecular functions (Muñoz Caro & Schutte 2003; Muñoz Caro & Dartois 2009; Bernstein et al. 1995).

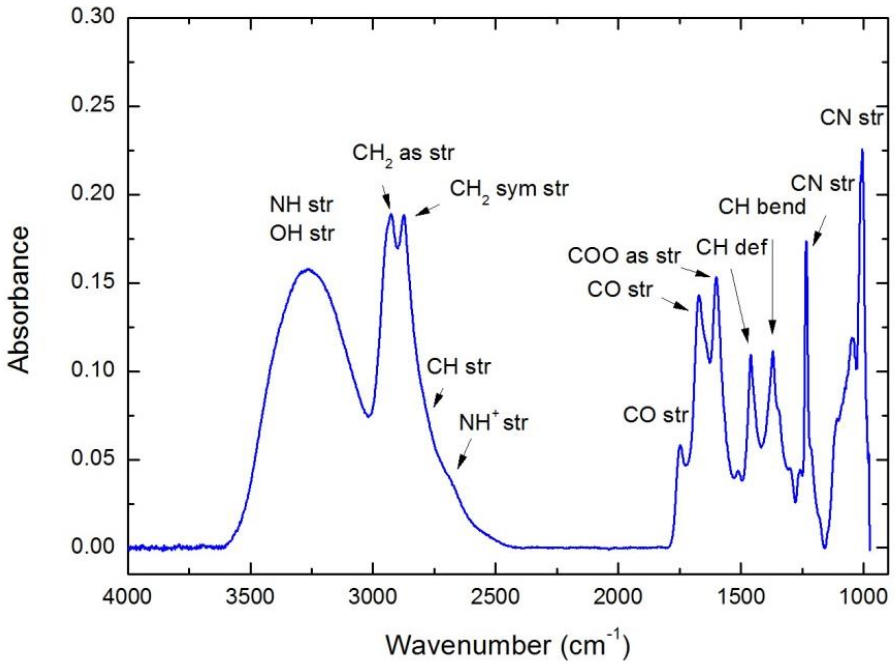

Figure 2.11 - Infrared spectrum of a typical residue at room temperature with the band assignments.

Table 2.2 - Identifications of the bands in a typical residue with band position, carrier and vibration mode.

Band position cm^{-1}	Carrier	Vibration mode
3265	carboxylic acids, amines, alcohols	O-H str, N-H str
2926	aliphatic chains	CH_2 as str, CH_3 as str
2872	aliphatic chains, HMT	CH_2 sym str, CH_3 sym str
2790	amines	C-H str
2687	amines hydrohalides, NH_2^+	$N-H^+$ str
1746	esters	C=O str
1672	primary amides	C=O str
1646	primary amides	NH def, CN str
1600	$R-COO^-$	COO^- asym str
1460	NH_4^+, HMT	CH def, N-H bend
1369	HMT	C-H bend
1235	HMT	C-N str
1048	alcohols	CCO str
1006	HMT	C-N str

Chapter 3

Asymmetric UV photochemistry of cosmic ice analogs: induction of enantiomeric excesses in amino acids

---

Contents

The content of this chapter is published in *The Astrophysical Journal* (Modica et al. 2014).

The discovery of meteoritic amino acids with enantiomeric excesses of the L-form (ee_L) has suggested that extraterrestrial organic materials may have contributed to prebiotic chemistry and directed the initial occurrence of the ee_L that further led to the homochirality of amino acids on Earth. A proposed mechanism for the origin of ee_L in meteorites involves an asymmetric photochemistry of extraterrestrial ices by UV circularly polarized light (CPL). We have performed the asymmetric synthesis of amino acids on *achiral* extraterrestrial ice analogs by UV CPL, investigating the chiral asymmetry transfer at two different evolutionary stages at which the analogs were irradiated (regular ices and/or organic residues) and at two different photon

energies (6.6 and 10.2 eV). We identify 16 distinct amino acids and we precisely measure the L-enantiomeric excesses using enantioselective GC×GC-TOFMS technique in five of them: α-alanine, 2,3-diaminopropionic acid, 2-aminobutyric acid, valine, and norvaline, with values ranging between $ee_L = -0.20 \pm 0.14$ % to $ee_L = -2.06 \pm 0.34$ %. The sign of the induced ee_L depends on the helicity as well on the energy of CPL, but not on the evolutionary stage of the samples and is the same for all the five considered amino acids. Our results support an astrophysical scenario in which the Solar System was formed in a high-mass star-forming region where icy grains were irradiated during the protoplanetary phase by an external source of CPL of a given helicity and a dominant energy, inducing a stereo-specific photochemistry.

3.1 Introduction

One of the salient problems in prebiotic chemistry concerns the origin of chiral asymmetry in prebiotic materials that may have stereo-controlled the emergence of homochirality in biological molecules such as amino acids and sugars. These molecules are chiral, i.e., they can exist in two forms chemically equivalent, the L- and D-enantiomers, which are non-superimposable three-dimensional mirror images of each other. Although the two forms have equivalent physico-chemical properties, living organisms use only L-enantiomers of amino acids in proteins, and only D-enantiomers of sugars in RNA and DNA, a property known as homochirality.

Several mechanisms have been proposed to explain the origin of homochirality (see Bonner 1991 for a review). One of them involves an asymmetric photochemistry of the molecules present in space by circularly polarized light (CPL), followed by the delivery of the enantioenriched photoproducts to Earth by comets and meteorites. This scenario was first suggested by Rubenstein et al. (1983) and further developed by Bonner & Rubenstein (1987), Bonner (1991), Greenberg et al. (1994), Bailey et al. (1998), Cerf & Jorissen (2000), Bailey (2001), Hough et al. (2001).

Several experimental results support the hypothesis of an extraterrestrial origin of organic molecules, including chiral ones and, in particular, amino acids. In the laboratory, simulations of

photo- and thermo-chemistry of interstellar ices lead to the formation of complex semi-refractory and water soluble organic residues, known to contain a large variety of identified organic compounds and many others still to be discovered (Agarwal et al. 1985; Briggs et al. 1992; Bernstein et al. 1995; Muñoz Caro & Schutte 2003; Nuevo et al. 2010; de Marcellus et al. 2011b; Danger et al. 2013). These residues are often considered as analogs of the primitive organic material thought to be present in interstellar/circumstellar grains, mostly at the late stage of molecular clouds, prior to planetary disks formation, and then incorporated into comets and asteroids, where they may experience some further chemical evolution. Among the organic molecules that have been detected in organic residues, numerous amino acids have been reported, generally after acid hydrolysis of larger macromolecular structures (Bernstein et al. 2002; Muñoz-Caro et al. 2002; Nuevo et al. 2008; Meinert et al. 2012a). Note that the hydrolysis step is widely used in the meteoritical community because it allows the identification of bound amino acids in meteorites. For laboratory residues, Nuevo et al. (2008) showed that amino acids detected as free ones (without hydrolysis) and bound ones (hydrolyzed) remain qualitatively similar, a trend confirmed very recently in amino acids detected in Paris meteorite (Martins et al. 2013, 2015).

Amino acids or amino acid precursors are thus present in extraterrestrial environments, as evidenced by the identification of over 80 different amino acids in carbonaceous meteorites, mainly in Murchison and Murray (Kvenvolden et al. 1970; Sephton 2002). The majority of amino acids have been found to be racemic (i.e. equal amounts of L- and D-enantiomers), but when non-racemic, the detected enantiomeric excesses have generally been measured to be of the L-form (Engel & Nagy 1982; Cronin & Pizzarello 1997; Glavin & Dworkin 2009; Glavin et al. 2012), which is the same form used by living organisms for proteinogenic amino acids. These findings represent a good argument in favor of the idea of an extraterrestrial origin for complex organic compounds on primitive Earth; they also suggest that a chiral asymmetry in meteoritic amino acids or amino acid precursors may have influenced prebiotic processes toward homochirality on the primitive Earth (Engel & Macko 1997; Cronin & Pizzarello 1997; Glavin et al. 2012). The mechanisms involved in the synthesis of amino acids in space (Elsila et al. 2007)

and more precisely in the asymmetric mechanisms which led to their enantioselective enrichment (de Marcellus et al. 2011a) have been a subject of considerable discussion (see Evans et al. 2012 for a review). Abiotic syntheses of amino acids in the absence of any asymmetric agent would be expected to produce racemic mixtures. Therefore, an enantiomeric selection process is required at some stage of their synthesis in given astronomical environments.

CPL irradiation as a chiral agent has long been proven to be an efficient mechanism capable of producing measurable enantiomeric excesses in racemic samples (Kuhn & Braun 1929; Balavoine et al. 1974) including amino acids (Norden 1977; Flores et al. 1977) by asymmetric photoprocesses (photochemical reactions proceeding at different rates for the two enantiomers of a given chiral molecule) or via asymmetric CPL-induced photoionization in the gas phase (Tia et al. 2013). The observation of CPL in astronomical sources, such as the reflection nebulae OMC-1 (Bailey et al. 1998; Fukue et al. 2010) and NGC 6334 (Menard 2000; Kwon et al. 2013), provided a further support for an extraterrestrial scenario.

Recently, our group experimentally tested this scenario (de Marcellus et al. 2011a). We showed that a small but significant L-enantiomeric excess (ee_L) up to −1.34% can be induced in alanine recovered from the organic residue formed after irradiation by UV CPL at 6.64 eV of a mixture of *initially achiral* interstellar/circumstellar ice analogs (H_2O, NH_3, and CH_3OH). The two CPL helicities induced ee_L of opposite signs, whereas linearly polarized light (LPL) did not induce any ee_L, as indeed expected. This study was limited to only one amino acid (alanine, the simplest chiral proteinogenic one) and to a single photon energy (6.64 eV). Since the work has left several open questions, we decided to continue the investigation of the effects of CPL in three following experimental campaigns in which we explored several parameters: the two helicities of the CPL, two different stages at which the samples were irradiated by CPL (ice and residue), two different photon energies, and two qualitative amounts of residues produced.

Herein we report the results obtained during the ensemble of our four experimental campaigns. We first present the 16 amino acids detected in our samples. We then focus on the

measurements of the ee_L induced in five of them by CPL irradiation. Our goal is to investigate the origin of chiral asymmetry in prebiotic materials in order to suggest a coherent astrophysical scenario for the origin of organics in primitive Solar System objects.

3.2 Experiments

The experimental set-up has been already described elsewhere (Nuevo et al. 2007; de Marcellus et al. 2011a). In brief, it consists in a high vacuum chamber operating at a pressure lower than 10^{-7} mbar, interfaced with a Fourier-Transform Infrared (FTIR) spectrometer. Inside the vacuum chamber, a substrate composed of MgF_2, transparent in the IR range, is placed in thermal contact with a cold finger whose temperature can be modified. A micrometric valve is used to admit a gas mixture into the chamber, where it freezes onto the cold substrate at 77 K, forming a solid ice sample.

This set-up was adapted to be temporarily mounted on the vacuum UV(VUV) DESIRS beamline (Nahon et al. 2012) at the SOLEIL synchrotron facility (France). During the deposition of the mixture, the ice sample was simultaneously irradiated by an intense VUV light beam produced by a variable-polarization undulator generating tailored quasi-perfect VUV CPL of any chosen helicity, i.e. right (R) and left (L), as well as LPL. This radiation, as transmitted by the zeroth order of the monochromator, possesses a 7 % broadband spectrum (typically 0.7 eV around 10 eV) with an integrated flux of about 1 to 2 × 10^{15} photons s^{-1} at the sample position. High harmonics of the undulator were filtered-off by use of an Ar or Xe-filled gas filter. The deposition and formation rate of the ice samples as well as the effects of photochemistry were monitored in-situ by IR spectroscopy.

We have performed four different experimental campaigns at the SOLEIL synchrotron, during which a total of 14 samples of organic residues have been produced. Each residue has been obtained by UV/VUV irradiation of an initially achiral ice mixture (77 K) of H_2O:$^{13}CH_3OH$:NH_3 in the ratio of ~ 2:1:1, qualitatively representative of the interstellar/circumstellar ices, considering our experimental constraints. Methanol was labeled with ^{13}C in order to exclude any terrestrial

contamination that may occur during the experiments, through the manipulation of the samples, or during the following analyses that need to use several solvents and derivatization agents. At the end of deposition/irradiation, each ice sample has been gradually warmed (1 K min^{-1}) to room temperature to allow diffusion of radical species and subsequent recombination. Note that during this process the volatiles, by far the largest amount of sample (99.9% at least), sublimate and are carried out by the dynamic pumping system.

Once at room temperature, a semi-refractory solid residue remains on the window as recorded through infrared spectroscopy (see for example Muñoz Caro & Schutte 2003). Some residues obtained have been further irradiated by CPL. At the end of each experiment the residues have been immediately recovered under nitrogen flushing, stored in special home-made stainless steel sample holders and kept under argon at atmospheric pressure until their analysis. Since these can occur many weeks/months later, the samples are stored at low temperature in a commercial refrigerator (2 °C).

The experiments have been performed at 6.6 eV and 10.2 eV, primarily because these energies are astrophysically relevant (Robitaille et al. 2006), and secondly because the CD spectra of alanine and other α-hydrogenated amino acids show intense active transitions around 6.7 eV (Meierhenrich et al. 2005, 2008, 2010; Meinert et al. 2012b) and, in the case of alanine and valine, around 10 eV (Kaneko et al. 2009; Tanaka et al. 2010).

Four parameters influencing the asymmetric formation of amino acids were explored during the different campaigns:

- The polarization of the irradiation light: R (right) CPL, L (left) CPL, and LPL.
- The stage at which the sample is irradiated by CPL: ice only, residue only, ice and residue.
- The photon energy: 6.6 eV and 10.2 eV.
- The qualitative amount of the produced residue: small (<100 µg) and large (>100 µg).

3.2.1 Experimental campaigns

First campaign (09/2009)

In the first series of experiments, the *in situ* asymmetric synthesis of amino acids from achiral interstellar ice analogs triggered by CPL was studied (de Marcellus et al. 2011a). Two samples were irradiated by L and R CPL, respectively; a third sample was irradiated by LPL. The photon energy of CPL was selected to be 6.6 eV. In the three cases the samples were irradiated during the ice stage (at 77 K) as well as further, after the warm-up phase, at the residue stage (~ 300 K).

Second campaign (07/2010)

In order to investigate whether the photon-to-matter chirality transfer takes place preferentially or exclusively during the irradiation of the ice itself or the irradiation of the residue itself, three samples were prepared. R CPL irradiation was used onto two distinct samples at two different stages: *i)* in the ice and *ii)* in the residue (previously irradiated by LPL at the ice stage). A third sample was irradiated by LPL only during the ice stage. Because of stringent beamtime constraints, these experiments were limited to the irradiation by CPL of only R helicity and could not be completed by irradiation of a sample by the opposite L helicity. As in the previous campaign, the photon energy of CPL was selected to be 6.6 eV.

Third campaign (12/2011)

The photon energy was fixed at 10.2 eV. A complete series of five different experiments was performed at conditions which allowed investigating the effects of the irradiation by the two CPL helicities (R and L) together with the stage (ice or residue) at which the samples were irradiated by CPL; one sample was irradiated by LPL at the ice stage. The amount of residues produced was small (<100 μg) and comparable to that obtained during the previous series of experiments.

Fourth campaign (11/2012)

In the last series of experiments, three samples of increased quantity of organic residues (>100 µg), compared to the ones of the former experimental campaigns, were produced (see next section). The increase in the amount of organic material formed was supposed to improve the complexity of the produced amino acids as well as the quality of the subsequent chemical analysis. The residues have been produced at the Institut d'Astrophysique Spatiale (IAS, Orsay) by VUV unpolarized light (UPL) from a classical H_2 UV lamp. The amount of obtained residue is linked to the integrated photon dose. Consequently, IAS-made samples, which are not dependent on highly constrained beamline time, do contain more material than SOLEIL-made ones. Two of these samples were then transported to SOLEIL synchrotron were one was irradiated with L CPL, while the other was irradiated with R CPL. The photon energy of CPL was maintained at 10.2 eV, which corresponds to the maximum output of a classical H_2 UV lamp (Jenniskens et al. 1993; Chen et al. 2014). A third sample was irradiated with UPL at IAS with the same integrated photon dose (and roughly same energy) than the one of CPL used for the two previous samples.

3.2.2 Preparation of residue-enlarged samples

Three residue-enlarged samples (>100 µg) of organic residues were prepared at IAS by irradiation of H_2O:$^{13}CH_3OH$:NH_3 (2:1:1) ice mixtures using VUV unpolarized light (UPL) at about 10.2 eV. Since the UV beam footprint at IAS is much larger than the one of the DESIRS beamline at SOLEIL, a thin (0.2 mm) circular copper mask (20 mm in diameter) with two rectangular openings (4 x 9 mm each, corresponding to the size of the UV beam at SOLEIL) was put on each MgF_2 window at the beginning of the sample preparation at IAS (see Fig. 3.1). The gaseous mixture was simultaneously deposited and irradiated through the two rectangular openings directly on the surface of the window. The rest of the window surface was sheltered by the copper. The IR beam could pass through the openings and allowed monitoring the evolution of the ice sample by absorption spectroscopy. This geometry allowed doubling the amount of samples that was then irradiated by UV-CPL at SOLEIL. After 2 days of simultaneous

deposition and irradiation by VUV UPL, the ice was allowed to gently warm-up to room temperature for about 30 hours (0.1 K min^{-1}). Once at room temperature, the typical IR spectrum of an organic residue was observed. With the aim to further increase the thickness of the residue produced, the window with this first layer of residue was left in the vacuum chamber; it was cooled down to 77 K and undergone two more subsequent cycles of deposition/irradiation followed by warming-up. Each sample was irradiated for about 150 hours in total. Following this procedure, three residue-enlarged samples were produced.

Once ready, two of them were transported to the SOLEIL synchrotron facility and placed in a vacuum chamber at the end of the UV/VUV DESIRS beamline. They were put together on a movable system which permitted aligning precisely the VUV CPL beam (4 x 9 mm) on each single rectangular spot without opening the chamber. The two spots on the same window were successively irradiated with CPL of the same helicity (L or R) for 16 hours. The third sample was further irradiated with VUV UPL at IAS for about 30 hours to assure the same integrated photon dose. At the end of the irradiation, the copper masks were carefully removed. Two well visible rectangular spots of yellow organic residues were observed on each of the three windows.

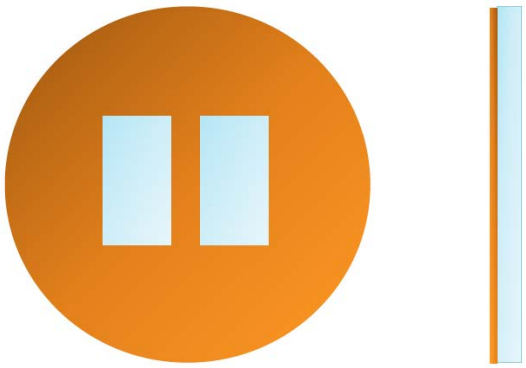

Figure 3.1 - Schematic front and side view of a single MgF_2 window covered by a copper mask with two rectangular openings.

3.2.3 Analytical procedure

The following analytical procedure was performed by Dr Cornelia Meinert at the Institut de Chimie de Nice (ICN) in Nice University.

CPL-, LPL- and UPL-irradiated samples were all extracted from their MgF_2 windows with 4 × 50 µL MilliQ water (4ppb TOC) followed by 2-4 × 50 µL of 0.1 M HCl and transferred into conical reaction vials (1 mL V-Vial®, Wheaton) under a class II biological safety cabinet. After evaporation to dryness, the extracted samples were hydrolyzed each with 300 µL 6 M HCl at 110 °C for 24 h. Following hydrolysis, the samples were again evaporated to dryness, and pure water was repeatedly added and evaporated until a pH of about 6 was obtained.

For derivatization, the samples were dissolved in 50 µL of 0.1 M HCl, and 25 µL of a 2,2,3,3,4,4,4-heptafluoro-1-butanol/pyridine mixture (3:1, *v*/*v*) was added followed by 5 µL of ethyl chloroformate. Vials were capped tightly and shaken vigorously for 10 seconds to form *N*-ethoxycarbonyl heptafluorobutyl ester (ECHFBE) derivatives. Subsequently, 20 µL of chloroform were added and the vials shaken again for extraction of the amino acid ECHFBE derivatives into the organic phase. The organic phases were withdrawn and transferred into 1 mL GC vials equipped with 100-µL inserts for enantioselective GC×GC analyses.

The GC×GC Pegasus IV D system is equipped with a time-of-flight mass spectrometer operated at a storage rate of 200 Hz, with a 50−400 amu mass range and a detector voltage of 1.8 kV. Data were processed using the LECO Corp ChromaTOFTM software. The column set generally consisted of a Varian-Chrompack Chirasil-D-Val primary column (24.85 m × 0.25 mm ID, 0.08 µm film thickness) modulator-coupled to a DB Wax secondary column (1.4 m × 0.1 mm ID, 0.1 µm film thickness). For the last measurement campaign of the residue-enlarged samples, two Press-Tight® connected Varian-Chrompack Chirasil-L-Val columns (49.2 m × 0.25 mm inner diameter, 0.12 µm film thickness) in the first dimension modulator-coupled to a DB Wax secondary column (1.4 m

× 0.1 mm inner diameter, 0.1 µm film thickness) were applied. Helium was used as carrier gas at a constant flow of $\bar{u}$ = 1 mL min^{-1}. Sample volumes of 1 or 2 µL were injected in the splitless mode at an injector temperature of 230 °C.

Various temperature programs were applied to allow for optimal resolution of individual amino acid enantiomers. Generally, the primary oven was operated as follows: 40 °C for 1 min, warm up to 80 °C with 10 °C min^{-1} and holding for 3 or 10 min, to finally heat up to 180 °C with 2 °C min^{-1} and a hold time of 15 to 25 min. The secondary oven used a temperature program of 60 °C for 1 min, 10 °C min^{-1}, 100 °C for 3 or 10 min, 2 °C min^{-1}, 150 °C, and 4 °C min^{-1}, 210 °C for 25 to 35 min. The modulation period was adjusted between 2.5 and 5 seconds. The samples were alternately injected 6–14 times in order to accurately determine ee_L values with reliable statistical error bars.

Volume peak integration for both enantiomers was performed using software-based calculations, taking into account possible modulation-induced errors. Potential ^{12}C-contamination from biological and/or laboratory sources was investigated by analyzing several blank samples during each measurement campaign under identical irradiation and analytical conditions. The identification of amino acids in the interstellar/circumstellar ice analogs was confirmed by comparison with external standards of amino acids that have identical retention times and shifted mass spectra due to ^{12}C composition.

3.3 Results

3.3.1 Distribution of identified amino acids

Several ^{13}C amino acids (chiral and achiral) have been identified by comparison with external ^{12}C standards thanks to their identical retention times and their properly shifted mass fragments. Enantioselective GC×GC-TOFMS analyses, furthermore, allowed for baseline-resolving most of the identified chiral amino acids. In particular, the three residue-enlarged samples of the fourth experimental campaign considerably increased the number of identified amino acids.

Table 3.1 lists the 24 amino acids, including the enantiomers, identified along with their ^{13}C mass fragments as well as the corresponding ^{12}C mass fragments of the external standards. Note that the ^{13}C-mass spectrometric fingerprint confirms the genuine nature of the detected amino acids in the experiments. Retention times from the primary and secondary column (first and second dimension) are given in minutes and seconds, respectively. Amino acids are listed from the simplest one, the non-chiral glycine (2 carbon atoms), to the most complex ones, in our case D- and L-proline, D- and L-valine, D- and L-norvaline (5 carbon atoms). Some of these amino acids are proteinogenic, such as glycine, α-L-alanine, L-serine, L-aspartic acid, L-valine, and L-proline, thus of biological relevance. Note that D- and L-valine have been identified here for the first time in extraterrestrial residue analogs. α-L- and α-D-alanine are the simplest (3 carbon atoms) and most abundant chiral amino acids identified.

The abundances decrease with increasing number of carbon atoms, as expected for abiotic compound syntheses, a characteristic already observed in similar residues (Meinert et al. 2012a) and in meteoritic organic material (Meierhenrich et al. 2004). Alanine has already been identified in meteorites where it presents an ee_L of 1.2% (Cronin & Pizzarello 1999). The enantiomers of alanine have been resolved and identified in all of the samples. Other enantiomers such as L- and D-DAP have been detected and resolved in most of the samples but their low quantities did not allow for reliable determination of their ee_L.

Table 3.1 - Amino acids identified in the organic residues after circularly polarized light irradiation. Due to the ^{13}C isotopic labelling of the $^{13}CH_3OH$ reactant, the amino acid analytes are composed of ^{13}C isotopes. The corresponding external standards show identical retention times, their mass spectra, however, show ^{12}C isotopic signatures. The observed mass shift between ^{13}C amino acids in the sample and ^{12}C amino acids in the standard allows us to exclude amino acid contamination.

C		Compound	MS-fragmentation ^{13}C sample	MS-fragmentation ^{12}C standard	R_{t1} [min]	R_{t2} [sec]
2	**1**	Glycine	257, **103**, 57	256, **102**, 56	32.67	0.77
3	**2**	Sarcosine	272, 228, **118**, 90	270, **116**, 88	30.07	3.00
	3	*N*-Methyl-D,L-alanine	287, **133**, 105, 61	284, **130**, 102, 58	17.53	2.81
	4	α-D-Alanine	272, **118**, 72	270, **116**, 70	30.07	3.00
	5	α-L-Alanine	272, **118**, 72	270, **116**, 70	30.80	2.89
	6	β-Alanine	346, 317, 301, 273, 244, 147, 117, **103**, **101**, 73, 57	343, 314, 298, 270, 242, 144, 115, **102**, **98**, 70, 56	35.06	3.86
	7	D-Serine	317, 258, 206, 131, **116**, 103, 88, 62	314, 256, 204, 129, **114**, 101, 86, 60	52.86	3.37
	8	L-Serine	317, 258, 206, 131, **116**, 103, 88, 62	314, 256, 204, 129, **114**, 101, 86, 60	53.13	3.34
	9	D-2,3-Diaminopropionic acid	316, 258, 205, 159, **103**, 87	313, 256, 203, 157, 129, **102**, 85	67.46	3.77
	10	L-2,3-Diaminopropionic acid	316, 258, 205, 159, **103**, 87	313, 256, 203, 157, 129, **102**, 85	68.19	3.34
4	**11**	*N*-Ethylglycine	287, 273, 257, 244, **133**, 105, 89, 61	284, 270, 256, 242, **130**, 102, 86, 58	19.27	1.60
	12	D-2-Aminobutyric acid	287, 258, **133**, 87, 61	284, 256, **130**, 84, 58	33.13	2.69
	13	L-2-Aminobutyric acid	287, 258, **133**, 87, 61	284, 256, **130**, 84, 58	33.87	2.54
	14	D,L-3-Aminoisobutyric acid	259, 162, 132, 116, **103**, 87	256, 158, 129, 112, **102**, 84	35.40	3.06
	15	D-3-Aminobutyric acid	288, 273, 244, 229, 161, 132, **118**	284, 270, 242, 227, 158, **116**	36.20	2.88
	16	L-3-Aminobutyric acid	288, 273, 244, 229, 161, 132, **118**	284, 270, 242, 227, 158, **116**	36.40	2.83
	17	4-Aminobutyric acid	288, 273, 244, 214, 160, 104, **88**, 58	284, 158, 129, 102, 86, **84**, 56	45.60	2.90
	18	D-Aspartic acid	345, 299, 273, 255, 229, 145, 101, **73**, 57	342, 296, 270, 254, 228, 142, 98, **70**, 56	47.26	3.03
	19	L-Aspartic acid	345, 299, 273, 255, 229, 145, 101, **73**, 57	342, 296, 270, 254, 228, 142, 98, **70**, 56	47.41	3.01
5	**20**	D,L-Proline	300, 259, **146**, 118, 101, 74	296, **142**, 114, 98, 70	35.39	3.15

21	D-Valine	302, 258, **148**, 131, 120, 103, 76, 59	298, 256, **144**, 129, 116, 101, 98, 72, 55	33.53	2.39
22	L-Valine	302, 258, **148**, 131, 120, 103, 76, 59	298, 256, **144**, 129, 116, 101, 98, 72, 55	34.13	2.29
23	D-Norvaline	302, 258, **148**, 76, 59	298, 256, **144**, 72, 55	37.33	2.38
24	L-Norvaline	302, 258, **148**, 76, 59	298, 256, **144**, 72, 55	38.06	2.29

3.3.2 Enantiomeric excesses in alanine

The L-enantiomeric excess (ee_L = $(A_L-A_D)/(A_L+A_D)$ where A is the peak area) in alanine has been precisely measured by peak volume quantification in all 14 samples of organic residues obtained in the course of the four distinct experimental campaigns. Table 3.2 shows the measured ee_L values accompanied by their experimental 3σ error bars as a function of the photon energy, the stage at which the samples were irradiated by CPL, and the helicity of CPL or the polarization state used. The amount of material available has permitted several independent gas chromatographic analyses (up to 10) for each sample, necessary for the statistical error evaluation. Induced ee_L are low (on the order of 1-2%) but significant and in accordance with the low optical yields involved in asymmetric photoprocesses mediated by CPL (Flores et al. 1977; Norden 1977). Note that comparing absolute values of ee_L from different campaigns is difficult because of differences in the experimental conditions, such as the photon flux per deposited molecules, and in the concentration of the extracted samples. We therefore limit our discussion in the following on the sign of the induced ee_L only.

As can be noted from Table 3.2, the values of the induced ee_L switch in sign as the helicity of CPL switches between R and L. This behavior is observed in *all* the samples irradiated by CPL and expected from chiral molecules placed in a chiral field, such as CPL. This confirms that the observed ee_L are indeed due to CPL irradiation only. The first experiments (de Marcellus et al. 2011a) performed at 6.6 eV showed that the sign of the ee_L induced in alanine followed the helicity of the incident light. Our further investigations reinforce these results and stress the effect of CPL irradiation as a plausible process in inducing ee_L in initially achiral and/or racemic samples.

Table 3.2 - L-enantiomeric excess (ee_L), determined by enantioselective GC×GC-TOFMS, measured in ^{13}C alanine. Each value is obtained from a distinct sample of initially achiral circumstellar analog as function of helicity, photon energy, and stage of CPL irradiation.

Experimental campaign	Energy (eV)	CPL[a] irradiation stage	R CPL ee_L [%][d]	L CPL ee_L [%]	LPL[b]/UPL[c] ee_L [%]
1st	6.6	ice + residue	-1.34 ± [e] 0.40	0.71 ± 0.30	-0.04[b] ± 0.42
2nd	6.6	ice	-0.51 ± 0.21	-	0.30[b] ± 0.26
2nd	6.6	residue	-0.74 ± 0.34	-	
3rd	10.2	ice	1.30 ± 0.45	-0.76 ± 0.29	0.00[b] ± 0.96
3rd	10.2	residue	0.72 ± 0.26	-0.82 ± 0.33	
4th	10.2	residue	1.04 ± 0.39	-0.34 ± 0.24	0.46[c] ± 0.36

[a] Circularly polarized light. [b] Linearly polarized light. [c] Unpolarized light using a microwave-stimulated hydrogen flow discharge lamp. [d] $ee_L = (A_L-A_D)/(A_L+A_D)$ where A is the peak area. [e] ± gives the standard deviation at 3σ over *n* injections.

Irradiation of samples using LPL or UPL is supposed to lead to an ee_L equal to zero. However, the peak integration for the determination of the ee_L is affected by some experimental systematic uncertainties, mainly due to chromatographic peak tailing. This explains why in some case the ee_L values are not centered on zero.

The switching in sign with the energy is likely due to the energy-dependence of asymmetric photochemical reactions. Indeed, recently reported circular dichroism (CD) and anisotropy spectra of amorphous solid state alanine enantiomers in the VUV region revealed two intense CD bands but with opposite sign at about 6.6 eV (Meierhenrich et al. 2010; Meinert et al. 2012) and at about 10.2 eV (Tanaka et al. 2010).

The energy-dependence of inducible ee_L has been experimentally evidenced by Meinert et al. (2014) on racemic amorphous solid state alanine thin films irradiated by CPL at 6.19 and 6.74 eV. In that case the switching in sign of the ee_L could be predicted from the recorded anisotropy spectra of enantiopure alanine which possesses two intense CD bands of opposite signs at these given photon energies. However, these results refer to pure alanine, whereas our results refer to alanine released after acid hydrolysis from amino acid precursors in macromolecular structures. This difference has to be taken into account because the environment in which amino acids are formed is expected to influence their response to CPL-mediated photoprocesses.

Another remarkable result of our experiments is that the ee_L have been induced in all the samples irradiated by CPL, *independently from the stage* at which the irradiation was performed (ice, residue, or the combination of both). These experimental data demonstrate for the first time that both the sign and the qualitative value of the induced ee_L do not depend on the degree of polymerization of interstellar/circumstellar ice analogs.

These effects are due to the CPL properties. CPL is a true chiral field capable of performing asymmetric photochemistry (Barron 1994). In the case of the irradiation of the ices, a two-step photochemical process can be suggested.

1) Initially CPL acts on achiral molecules (H_2O, $^{13}CH_3OH$, NH_3) to form the first chiral photo-products such as ions, radicals, and/or small molecules that exhibit a stereogenic center. These chiral photo-products present a racemic distribution since achiral molecules are not sensitive to chiroptical effect and therefore cannot lead to any stereo-specific reactions; this same effect can be induced by photochemical processes due to ordinary unpolarized light.

2) After the formation of chiral racemic photo-products, the preferential selection of one of the alanine enantiomers and/or its precursor may occur by asymmetric photochemical processes such as CD-driven asymmetric photolysis, as suggested by the ee_L strong photon-energy dependence that we observe. Such an effect discriminates asymmetric photochemistry from ordinary photochemistry (Rau 2004).

Interestingly, the results show that CPL can effectively induce ee_L in alanine in samples at low temperatures (77 K) even if one must take into consideration that the analytical procedure requires that the samples are warmed to room temperature prior to extraction and subsequent analysis. The recombination reactions while warming-up the ices without any further irradiation, however, do not influence the enantiomeric enrichment: the irradiated samples appear to have clearly kept the memory of the chiral field footprint used for its photoprocessing.

In the case of the asymmetric irradiation of the residue only, CPL acts directly on racemic mixtures of chiral (and achiral) molecules, given that the complex organic residue statistically contains chiral molecules. Similarly to the previous case, asymmetric photoprocesses are capable of discriminating between optical isomers leading to an asymmetric enrichment of one of the alanine enantiomers.

Figure 3.2 shows the quality of the data as well as the dependence of the sign of the ee_L on the helicity and the energy of CPL and, at the same time, the non-dependence on the stage at which the irradiation is performed. It can be noticed that the error bars (3σ) accompanying the data are rather large in some cases, particularly for the samples of the third campaign (samples irradiated at 10.2 eV in the residue only and in the ice only stage). This can partly be explained by a slight contamination of terrestrial amino acids (hence alanine), shown by the presence of ^{12}C fragments in the mass spectra. Alanine is a proteinogenic amino acid widespread in the biosphere, being the second most abundant amino acid after leucine in human proteins. In order to provide accurate ^{13}C-based quantitative results, it became therefore necessary to exclude any natural introduced ^{13}C contributions from the samples. The correction was performed by measuring the peak area of ^{13}C and ^{12}C mass fragments and their ratio from an external ^{12}C alanine standard after acid hydrolysis and derivatization. This instrument-dependent $^{13}C/^{12}C$ ratio was later used in the calculation of the ee_L of ^{13}C alanine to correct for any natural occurring ^{13}C alanine in the samples of the third experimental campaign. The LPL sample of the third measurement campaign showed the highest ^{12}C contamination as well as highest amino acid concentrations that caused insufficient enantioseparation and hence large statistical error bars.

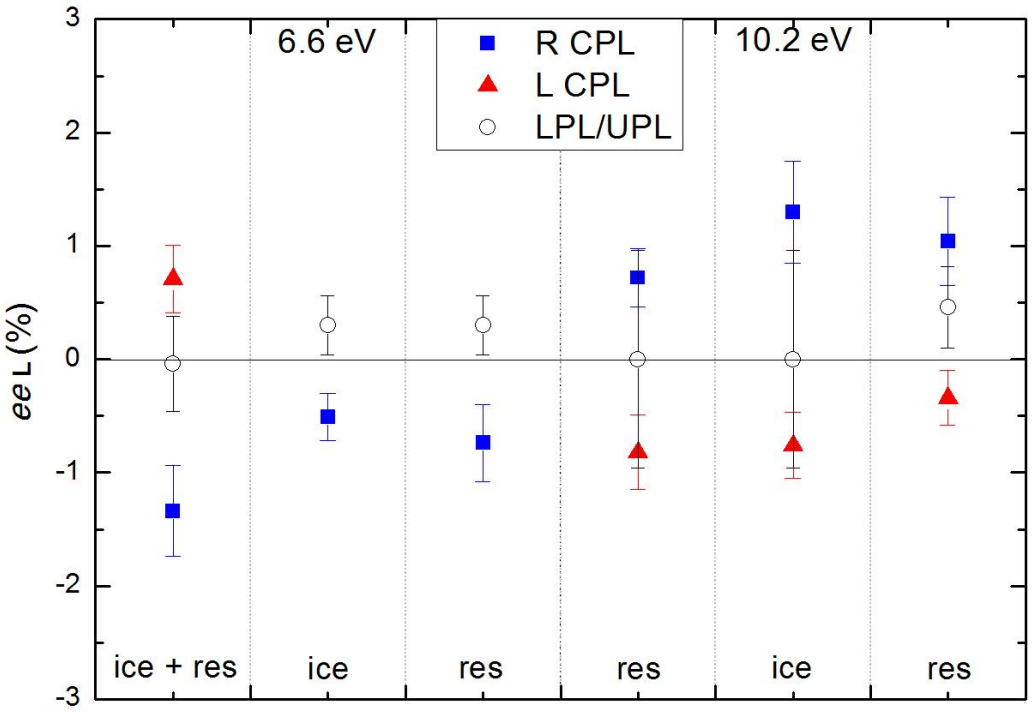

Figure 3.2 - L-enantiomeric excess (ee_L), determined by enantioselective GC×GC-TOFMS, measured in ^{13}C alanine. Experimental values are obtained from samples of initially achiral circumstellar analogs at different stages of CPL irradiation (ice and residue, ice only, residue only), at 6.6 and 10.2 eV. Blue squares refer to ee_L induced by R CPL, red triangles refer to ee_L induced by L CPL, white circles refer to ee_L measured after linearly polarized light (LPL) or unpolarised light (UPL).

3.3.3 Enantiomeric excesses in five different amino acids

Among the list of identified amino acids, five pairs of enantiomers of chiral amino acids were present in sufficient concentration in the residue-enlarged samples of the fourth measurement campaign to allow for their ee_L determination: α-alanine (Ala), 2,3-diaminopropionic acid (2,3-DAP), 2-aminobutyric acid (2-Aba), valine (Val), and norvaline (Norval). Alanine and valine are proteinogenic, while 2-aminobutyric acid, norvaline, and 2,3-diaminopropionic acid are non proteinogenic.

Figure 3.3 shows the multidimensional enantioselective gas chromatograms relative to the pairs of eluting L- and D-enantiomers of these five amino acids in the three light polarization states explored (L CPL, UPL, R CPL). As can be noted, each peak is properly resolved owing to the high separation power of this technique.

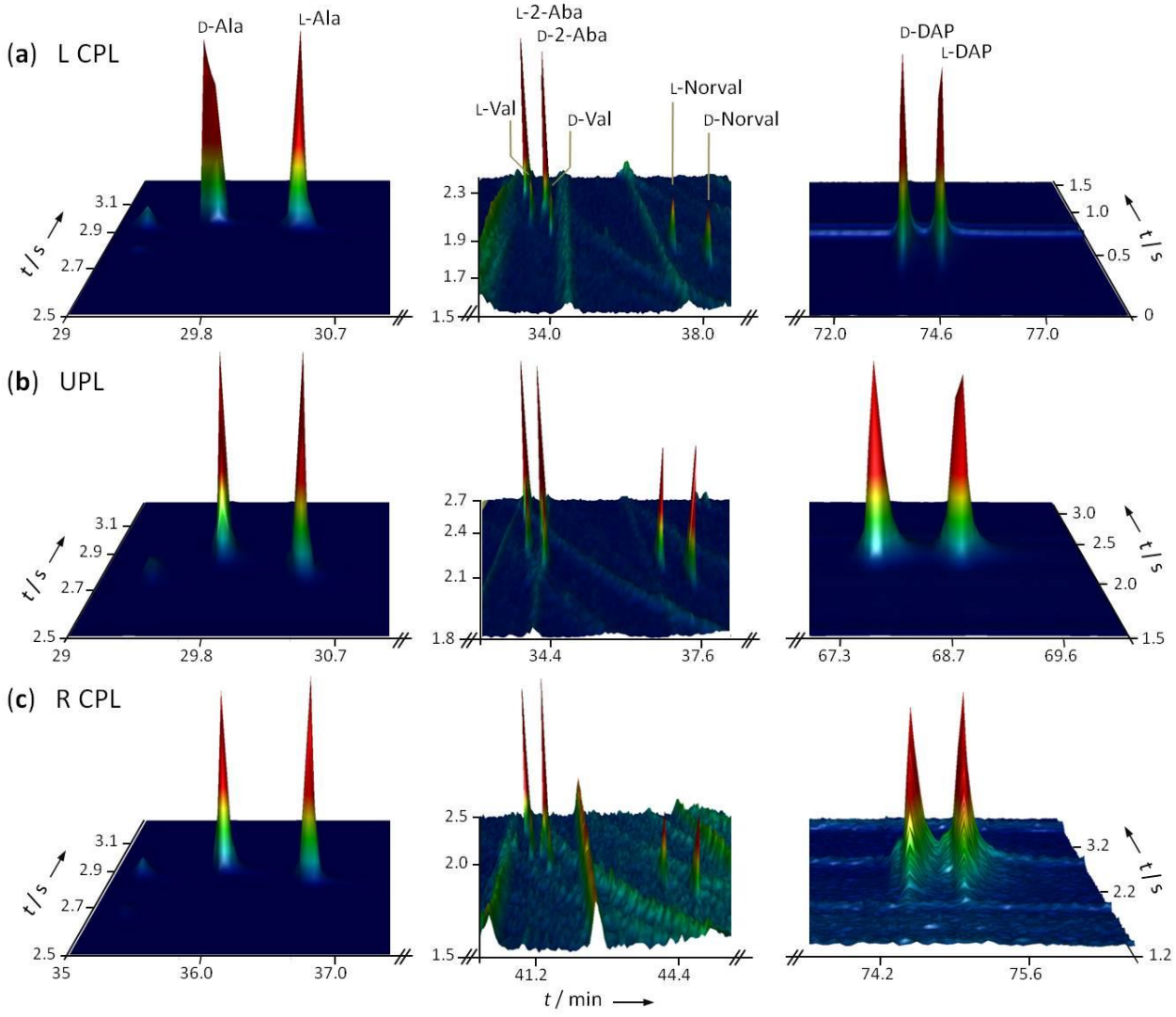

Figure 3.3 - Multidimensional enantioselective gas chromatographic resolution of ^{13}C enantiomers of alanine (Ala), 2-aminobutyric acid (2-Aba), valine (Val), norvaline (Norval), and 2,3-diaminopropionic acid (DAP) produced by 10.2 eV UV photoirradiation with (a) L CPL, (b) UPL, and (c) R CPL.

The ee_L in the five considered amino acids have been precisely measured by peak volume quantification in the three residue-enlarged samples. Figure 3.4 shows the results for each amino acid and their respective error bars as a function of the light polarization state explored (R CPL, L CPL, UPL) at 10.2 eV. The sign of the induced ee_L switches as the helicity of CPL switches between R and L. This behavior, already observed in the case of alanine, is adopted by *all* the five different amino acids here considered. The sign of the induced ee_L is indeed constantly positive in the five cases in which R CPL is used and constantly negative in the five cases in which L CPL is used. This evidences that the induced ee_L are due to CPL-mediated asymmetric processes leading to a chiroptical photon-to-matter chirality transfer.

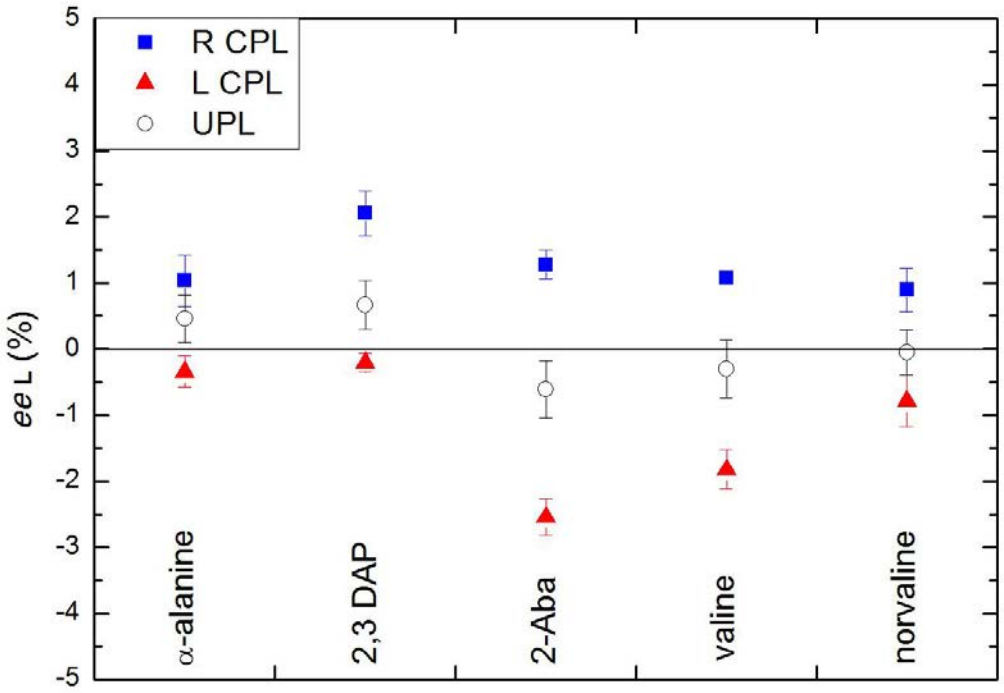

Figure 3.4 - L-enantiomeric excess (ee_L), determined by enantioselective GC×GC-TOFMS, measured in five different amino acids labeled with ^{13}C. Experimental values are obtained from three residue-enlarged samples of initially achiral circumstellar analogs at the stage of residue irradiated by CPL at 10.2 eV. Blue squares refer to ee_L induced by R CPL, red triangles refer to ee_L induced by L CPL, and white circles refer to ee_L measured after unpolarised light (UPL). The ee_L are of the same sign in all five amino acids for a given helicity of CPL.

Table 3.3 shows the measured ee_L values in each amino acid together with their error bar values as function of the light polarization state (R CPL, L CPL, and UPL) at 10.2 eV. The values range between ee_L = −0.20% ± 0.14 % (in the case of 2,3-diaminopropionic acid irradiated by L CPL) and ee_L = −2.54% ± 0.28 % (in the case of 2-aminobutyric acid irradiated by L CPL). The error bars are calculated on the number of injections (up to 7) and are given as 3σ, indicating a confidence level larger than 99.7%. It is noted that the ee_L in valine could be determined precisely only in one of the injections of the sample irradiated by R CPL. Consequently, no statistical error bar is given for this measurement; nevertheless, we have decided to show this value for completeness of the results.

Table 3.3 - L-enantiomeric excess (ee_L), determined by enantioselective GC×GC-TOFMS, measured in five different amino acids. Experimental values are obtained from three residue-enlarged samples of initially achiral circumstellar analogs irradiated by CPL at the stage of residue at photon energy of 10.2 eV, as function of helicity.

Amino acid	R CPL[a] ee_L [%][c] (n)[d]	L CPL ee_L [%] (n)	UPL[b] ee_L [%] (n)
α-Alanine	1.04 ± 0.39[e] (6)	-0.34 ± 0.24 (6)	0.46 ± 0.36 (7)
2,3-Diaminopropionic acid	2.06 ± 0.34 (5)	-0.20 ± 0.14 (4)	0.67 ± 0.36 (7)
2-Aminobutyric acid	1.28 ± 0.22 (5)	-2.54 ± 0.28 (6)	-0.61 ± 0.43 (6)
Valine	1.08 (1)	-1.82 ± 0.30 (6)	-0.30 ± 0.44 (6)
Norvaline	0.90 ± 0.33 (3)	-0.78 ± 0.39 (6)	-0.05 ± 0.34 (7)

[a] Circularly polarized light. [b] Unpolarized light using a microwave-stimulated hydrogen flow discharge lamp. [c] $ee_L = (A_L-A_D)/(A_L+A_D)$ where A is the peak area. [d] Number of replicate analyses. [e] ± gives the standard deviation at 3σ over n injections.

The fact that the induced ee_L values are of the same sign in *all five amino acids* for a given helicity of CPL could be explained by the CD and anisotropy spectra of these amino acids at 10.2 eV but, to the best of our knowledge, these data are available for alanine and valine only (Kaneko et al. 2009; Tanaka et al. 2010). Interestingly, both amino acids show indeed a similar CD spectrum at about 10.2 eV. However, the initial molecules irradiated through our protocol might only be precursors of the amino acids, for which the CD spectra are not only unknown but inaccessible without a complete modeling of the photoreaction network – a scope that is beyond the goal of this chapter.

3.4 Astrophysical implications

Our simulation experiments are relevant to the outer solar nebula, where icy grains could have been irradiated by an external source of VUV CPL. The best candidates as CPL sources are reflection nebulae in star-forming regions associated with a dominant high-mass young stellar object (YSO). High degrees of CPL have been observed in the near-IR in reflection nebulae such as OMC-1, at levels of 17% (Bailey et al. 1998; Chrysostomou et al. 2000; Buschermohle et al. 2005; Fukue et al. 2010) and more recently in NGC 6334, at levels of 22% (Menard et al. 2000; Kwon et al. 2013). Such high degrees of CPL could originate from two main mechanisms:

- Scattering of light by non-spherical grains aligned by magnetic fields (Chrysostomou et al. 2000; Gledhill & McCall 2000).
- Dichroic extinction of light which has been previously linearly polarized by scattering on aligned non-spherical grains (Martin 1978; Lucas et al. 2005; Kwon et al. 2013).

OMC-1 and NGC 6334 are active sites of star-forming regions which present high dust obscuration for direct observation of UV CPL. However, detailed models for aligned grains with small axis ratios have shown that CPL can also be present in the UV range with similar high levels than those observed in the IR one (Bailey et al. 1998).

These CPL regions present a quadrupolar-shape pattern of polarization where each quadrant *of a single handedness* covers a wide area (Buschermole et al. 2005; Fukue et al. 2009).

Indeed, the extent of CPL in OMC-1 is about 0.4 pc (Fukue et al. 2010) while in NGC 6334 it is about 0.65 pc (Kwon et al. 2013), which are hundreds of times the size of most forming planetary systems, including ours. If our Solar System formed in a similar star forming region, it may have been irradiated by CPL of a single handedness. Most low-mass stars like our Sun are indeed believed to be born alongside high-mass stars, as it is observed in the case of OMC-1, where high- and low-mass stars are forming together (Miller & Scalo 1978; Hillenbrand 1997). The hypothesis that our Solar System formed in a high-mass star-forming region is supported by the presence of short half-life radionuclides such as ^{60}Fe and ^{26}Al in primitive meteorites (Hester et al. 2004; Mostefaoui et al. 2005; Gounelle & Meynet 2012).

During the early phases of our protoplanetary disk evolution, icy grains driven by disk instabilities, moved along radial and vertical motions to be accreted onto the young Sun. However, part of them did not experience this fate. Ciesla & Sandford (2012) have modeled the path of these surviving grains through the disk, showing that they could have been exposed to substantial external UV irradiation (~50 photons per ice molecule) during a lifetime of 10^6 years. Under these conditions, this irradiation may well have been circularly polarized and with a single helicity. The dense protoplanetary environment could have offered the ideal location for grains to be shielded by the direct unpolarized UV irradiation of the young Sun, avoiding a possible destruction of enantioenriched material (Bailey 2001). The main amount of CPL would have been received outward and at high latitude in the disk, where lower densities prevented the flux to be too strongly attenuated compared to the midplane. The episodic exposures to this increased photon flux would have triggered the double effect of asymmetrically photoprocessing and heating the ices. These processes may have converted at least 5% of the ices into organic compounds (Ciesla & Sandford 2012) including chiral molecules such as amino acids and/or their precursors. Photo- and thermo-chemistry in ices is well known to generate reactive ions and radicals which subsequently react with other molecular species present in the ices to form more complex molecules (d'Hendecourt et al. 1982, 1985, 1986; Elsila et al. 2007) finally producing complex macromolecular structures containing amino acid precursors. Although the exact structure of these macromolecules of large molecular weight is

still unknown (Takano et al. 2007; Danger et al. 2013), amino acids and their precursors embedded in such networks are thought to be more stable than free amino acids against further irradiation in space (Takano et al. 2004) as well as against any possible racemization processes.

Along with the synthesis of interstellar/circumstellar organic compounds, the asymmetric photoreactions triggered by CPL may have simultaneously induced an ee_L in any chiral molecule. As suggested by our current results, this action could have occurred both at the stage in which grains were covered by ices and/or the stage in which they were already covered by a refractory residue of organic compounds, thus maximizing the possibility to accumulate a significant ee_L before the accretion into larger grains, planetesimals and finally comets and asteroids. To date, however, no chiral molecule has been identified in the ISM, but this is an observational bias because radioastronomy observations are limited to rather simple molecules. The fact that we successfully measured ee_L in the case CPL irradiation occurred during the ice stage only demonstrates that chiral molecules are indeed formed in the ices in our laboratory analogs. These chiral molecules should then be present in the bulk of the ice mantles of interstellar/circumstellar grains, since UV photochemistry is a common phenomenon in extraterrestrial environments. They are likely the precursors of the amino acids detected later in the organic residues. This hypothesis is reinforced by the measurement of ee_L of the same sign after irradiation with CPL at the residue stage only. The identification of these chiral precursors is of importance for understanding the interstellar/circumstellar chemistry in more detail, followed by their exploration in favorable interstellar environments such as hot molecular cores where complex molecules are observed in the gas phase (Cazaux et al. 2003; Bottinelli et al. 2007; Belloche et al. 2013).

A further important aspect evidenced by our results is the dependence of the sign of the ee_L with the energy of incident CPL. In space this effect could lead to a competition in the sign of the enantioselected amino acids. Natural sources of CPL are spectrally broad-band and the CPL produced is expected to be absorbed in multiple circular dichroic bands of amino acids, possibly of opposite signs. However, the spectrum of the actual broad-band CPL in star-forming

regions should yield a non-zero effective CD coefficient ($\Delta\varepsilon$) to overcome the rare event in which the integral of the concerned CD bands would equal to zero (Buchardt 1974) according to the Kuhn-Condon rule (Kuhn 1930; Condon 1937).

Regarding the pertinence to asymmetric photoprocesses, we point out our choice to consider the VUV spectral range at higher energies (10.2 eV) than those typically considered so far, with a cut-off around 6.19 eV (Bailey et al. 1998). A similar cut-off in the spectrum would favor most normal stars (Bailey et al. 1998) excluding the more massive ones, which are indeed the only ones associated with high degrees of CPL. A specific example is given by the high-mass YSO (IRc2) at the center of the CPL region in OMC-1 with a mass of 25 M_{sun} (Genzel & Stutzki 1989). On the contrary, low-mass YSOs are not associated with high levels of CPL, probably because their magnetic fields are too weak to efficiently align the grains (Chrysostomou et al. 2007). Moreover, according to the model of Robitaille et al. (2006), YSOs of higher masses (~20 M_{sun}) do present Spectral Energy Distribution (SED) favouring high energy photons at the earliest stages of their evolution. Over the time this emission becomes dominant and its maximum is moving to higher energies. At the Stage II of the protostellar evolution, which is associated with the presence of an optically thick disk and an infalling envelope, the emission is peaked around 10-11 eV.

If we consider 10-11 eV as the dominant energy in the SED of an YSO at the Stage II associated with a CPL region, we expect a higher efficiency of asymmetric photoreactions near this energy due to the higher number of photons available. This may lead to a non-zero enantioselection in chiral precursors even in case of broad-band CPL absorbed in multiple CD bands of opposite sign and equal magnitude. However, the dominant energy changes at different evolutionary stages. It is therefore important to first consider a definite evolutionary stage of an YSO, well characterized by its SED. Afterwards the anisotropy spectra (Evans et al. 2013) of different chiral precursors can be weighted with this SED, recalling that these anisotropy spectra are so far largely unknown as discussed above.

A number of amino acids have been identified in chondritic meteorites, both proteinogenic and non-proteinogenic ones (Engel & Nagy 1982; Cronin & Pizzarello 1997; Pizzarello & Cronin 2000; Pizzarello et al. 2003). Several of them such as alanine, isovaline, and α-methyl norvaline have been found to be enantiomerically enriched – all of them in the L-enantiomer. Enantiomeric excess in α-hydrogenated amino acids are small (less than 2%) and comparable to the ee_L induced in our experiments. However, higher ee_L (up to 18.5%) have been reported for α-dialkyl amino acids in Murchison and Murray meteorites (Glavin & Dworkin 2009). These ee_L cannot be explained solely by the influence of CPL and the authors suggested that aqueous alteration within the parent body (subsequent to the melting of ices from short-lived radionuclides heating) could have amplified a small initial ee_L of these amino acids. Thus, post-accretion would affect the distribution of amino acids in primitive meteorites as well as their initial ee_L, a trend which is actually observed (Glavin & Dworkin 2009; Martins et al. 2013, 2015). Subsequent autocatalytic processes during the early evolutionary stages of prebiotic chemistry on Earth could have amplified these initial ee_L to much larger values. Such processes are susceptible to approach homochirality, as experimentally shown by Soai et al. (1995) and Shibata et al. (1998). They include some chiral amino acids with small starting ee_L (around 1%). However, the intimate mechanisms involve specific reaction pathways not necessarily applicable to a prebiotic scenario. Actually, in our experiments, we simulate organic materials in their pre-accretional form, i.e., on the individual grains, but no post-accretional processes are considered. Amplification phenomena, starting from initial pre-accretional conditions should be the subject of further experimentation.

As evidenced by Meinert et al. 2012b, some proteinogenic amino acids like alanine, valine, serine, and proline have similar anisotropy spectra (in sign and magnitude) at 6.19 eV. Although the CD spectra of the precursors remain unknown, this observation favors the model in which CPL of a given energy and helicity can select the same handedness in proteinogenic amino acids under circumstellar conditions.

Our results indeed show that CPL of a given helicity at the more astrophysical relevant energy of 10.2 eV (Robitaille et al. 2006) is capable of inducing ee_L of the same sign in all the five

amino acids investigated, both proteinogenic and non proteinogenic. This result indicates that under the hypothesis of a well-defined dominant irradiation energy and a given helicity in our Solar System, CPL could have preferentially favored the L-enantiomer simultaneously in proteinogenic and non proteinogenic amino acids acting either directly on them or on their precursors by asymmetric photochemistry, in coherence with the ee_L findings from meteoritic matter analysis.

3.5 Conclusions

We have experimentally investigated the effects of VUV-CPL irradiation on extraterrestrial ice analogs at different evolutionary stages: *(i)* in the ice stage only, *(ii)* in the organic residue only, *(iii)* both in the ice and in the residue. After the asymmetric irradiation of the analogs at 6.6 and 10.2 eV, a total of 16 chiral and achiral amino acids have been detected in the organic residues. Among the chiral amino acids, alanine shows statistically significant ee_L in all analyzed residues. Such enantiomeric enrichments are induced independently on the evolutionary stage of the circumstellar ice/residue analogs. The sign of the induced ee_L depends on the helicity (R or L) as well as the energy of the CPL, suggesting that the chiroptical process leading to this enantio-specific reaction is CD-driven. The detection of ee_L after irradiating only the ice samples with CPL demonstrates the formation of chiral precursors of amino acids within the ice analogs, which should indeed be present in interstellar/circumstellar ices.

For the first time a precise measurement of ee_L is reported for five different amino acids in such asymmetrically photoprocessed ice analogs: α-alanine, 2,3-diaminopropionic acid, 2-aminobutyric acid, valine, and norvaline. The measured ee_L in these amino acids are of the same sign after CPL irradiation at 10.2 eV, for each given helicity. This supports the hypothesis that CPL in space could have introduced an initial chiral bias into prebiotic molecules, such as amino acids, with the same handedness. The enantiomeric purities induced are low but consistent with ee_L values found for α-hydrogenated amino acids in several meteorites. Note, however, that post-accretion and/or aqueous alteration within the parent bodies, that may alter initially induced ee_L, were not simulated here.

Our results support an astrophysical scenario in which the Solar System formed in a high-mass star-forming region where it was irradiated during the protoplanetary phase by an external source of CPL of a given handedness and a dominant energy defined by the SED of the massive star. In such an environment, the grains, on which absolute asymmetric molecular synthesis results in the formation and accumulation of a chiral bias in key biomolecular compounds, would have accreted to comets and asteroids. These bodies would have shielded their enantioenriched organic content until their delivery to the early Earth during or just after the late heavy bombardment. Autocatalytic processes during the early evolutionary stages of life could have amplified the initially small ee_L to reach the homochiral state found in all living matter on Earth today (Shibata et al. 1998).

Further investigations will have to include the detection of additional α-hydrogenated and α-dialkyl amino acid enantiomers (Meinert & Meierhenrich 2014) – ideally the same enantioenriched molecules that are found in meteorites as well as the measurement of their anisotropy spectra at 10.2 eV. Similar experiments considering homochiral biomolecules of different handedness (e.g. sugars) should also be undertaken. Finally a refinement of our proposed astrophysical scenario has to be considered after the *in-situ* measurements of comet 67P/Churyumov-Gerasimenko by the COSAC instrument (Thiemann et al. 2001; Thiemann & Meierhenrich 2001) onboard the European space mission Rosetta planned for November 2014 (Goesmann et al. 2007).

Chapter 4

Analysis of laboratory organic residues by FT ICR mass spectrometry

Contents

In this chapter, we present the analysis of our laboratory organic residues by Fourier transform ion cyclotron resonance mass spectrometry (FT ICR MS), which is a very high mass resolution technique. The analyses have been performed with a direct involvement in the frame of a TGE (Très Grand Equipement) project thanks to a collaboration with D. Lesage at the Institut Parisien de Chimie Moléculaire (UPMC, Université Pierre et Marie Curie, Paris). A further collaboration with R. Thissen (IPAG, Institut de Planétologie et d'Astrophysique de Grenoble) has also permitted a preliminary statistical analysis of the data formerly acquired by FT ICR MS.

Previous analyses on equivalent laboratory organic residues produced by our group at IAS have been realized in collaboration with the PIIM (Physique des Interactions Ioniques et Moléculaires) team in Marseille and the IPAG team in Grenoble using a different high resolution technique, the Orbitrap mass spectrometer instrument, and significant results have been obtained about the high molecular complexity of our samples (Danger et al. 2013). Inspired by this approach, we explored the possibilities of the FT ICR MS, a promising technique which is known to offer a better mass resolution and mass accuracy than Orbitrap mass spectrometry.

This chapter describes the basic principles of FT ICR mass spectrometry and shows a qualitative analysis and a description of mass spectra obtained from our laboratory residues. No previous chemical treatment is performed on the samples, such as acid hydrolysis or derivatization, in order to preserve the molecular structure of the residues unaltered. Due to the complexity of this molecular structure, we focus on the search for specific molecules such as HMT, HMT-based molecules and amino acids because they may represent a link between evolved ices in the final stages of molecular clouds and the origin of the organic matter in our Solar System, as we will see in the next chapters of this thesis where amino acids and HMT will be searched for in the Paris meteorite. In this chapter, first the analyses are done by visual examination of spectra. Then we try a global statistical approach of the data extracted from the mass spectra using algorithm calculations from dedicated software developed at IPAG (Orthous-Daunay 2011, PhD thesis). Since in our analysis we follow the general approach used by Danger et al. (2013) with the Orbitrap MS instrument, we can often compare our results obtained by FT ICR MS with those obtained by Orbitrap MS.

Future works of our group envisage a comparison between laboratory organic residues and pristine meteoritic organic matter using this high resolution technique which has been already applied to studies on meteorites (Schmitt-Kopplin et al. 2010). Since the soluble organic matter extracted from meteorites is expected to be much more complex than laboratory organic residues, the study presented in this chapter represents the first part of a more extensive work in which the pristine Paris meteorite will also be analyzed.

4.1 FT ICR mass spectrometer

Fourier transform ion cyclotron resonance (FT ICR) is a type of mass spectrometer that can be used to determine the mass-to-charge ratio (m/z) of ions with very high mass resolution and high mass accuracy (Amster 1996; Marshall et al. 1998). It is a powerful tool to determine the composition of complex mixtures and in particular to study large macromolecules, even without previous separation of the mixtures. These characteristics, together with the important property

of very low sample consumption, make this instrument well adapted for the analysis of complex organic residues of small amounts as it is the case for our samples.

4.1.1 Instrument description

In our study, a hybrid quadrupole Fourier transform ion cyclotron resonance (hQh-FT/ICR) mass spectrometer (Solarix, BrukerDaltonics, Bremen, Germany) equipped with an actively shielded 7 Tesla magnet was used for accurate mass-to-charge ratio (m/z) measurements (Fig. 4.1). It consists mainly of an electrospray ESI ion source associated to ion funnel geometry, a linear quadrupole (Q) ion guide to select and/or transfer the ions, and an ion cyclotron resonance (ICR) analyzer cell. The instrument is called hybrid because it combines two different m/z separation devices, a linear quadrupole and a FT ICR. The electrospray source is separated from the ICR cell by several stages of differential pumping which drop the pressure from atmosphere (at the ESI source inlet) to ultra-high vacuum (10^{-10} mbar in the ICR cell region).

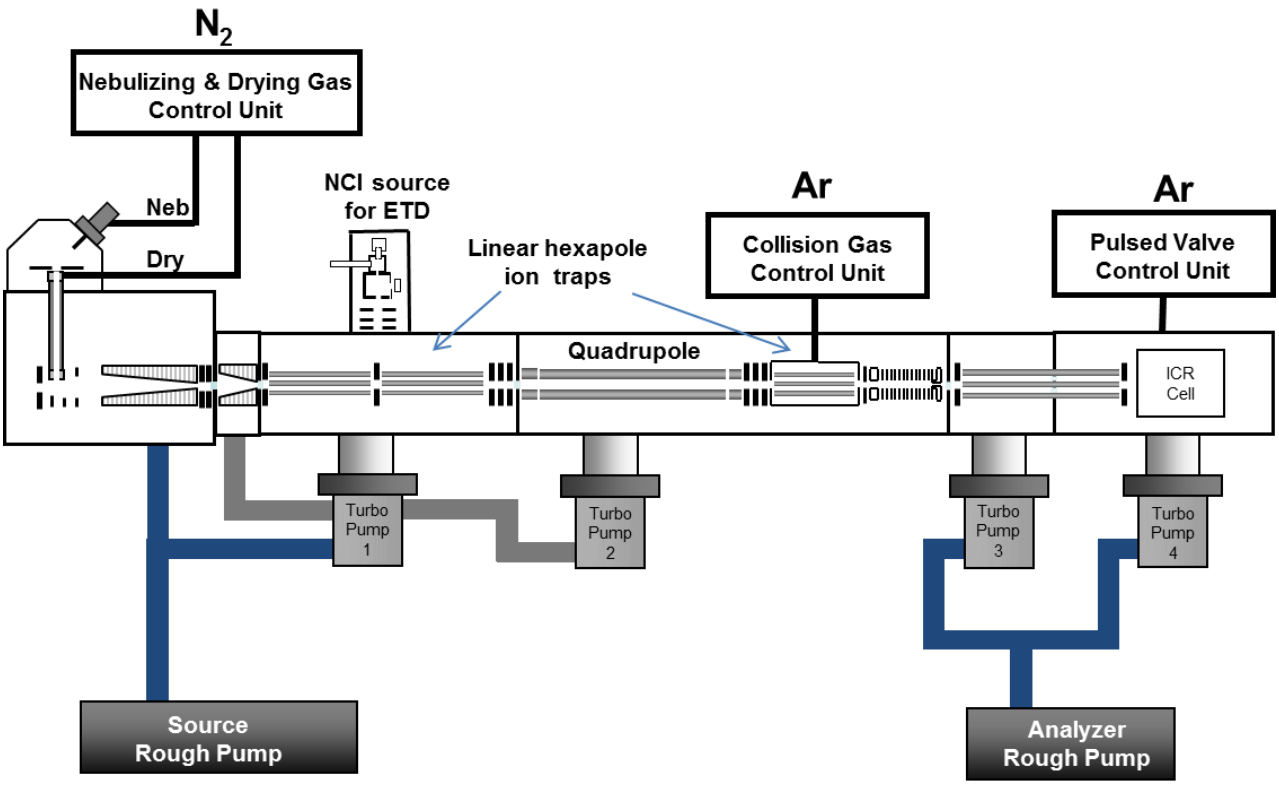

Figure 4.1 - Schematic view of the hybrid quadrupole FT ICR MS 7 Tesla Solarix Bruker Daltonix (from the SolariX user's guide).

Ion source

The ion source is an electrospray ionization (ESI) source. The ESI source is based on an extremely soft ionization technique which permits the desorbed ions from liquid analytes to be analyzed. It is suitable in producing ions also from macromolecules because it overcomes the tendency of these molecules to fragment when ionized (Hendrickson & Emmett 1999).

The analytes are infused in the electrospray ion source at atmospheric pressure at a flow rate of 120 Lh^{-1}. First, the liquid is forced through a capillary tube to which a high voltage of 4000 V is applied: small charged droplets are then generated (see Fig. 4.2). The evaporation of the solvent leads to a reduction of the multiply charged droplets. This process is enhanced through the use of a dry and warm N_2 nebulizing gas. When the magnitude of the charges repulsion is sufficient to overcome the surface tension holding the droplets, desolvated ions in the gas phase are formed. Molecules possessing various sites capable of protonation or deprotonation (addition or removal of a proton, respectively) can be evaporated as quasi-molecular ions, $[M+zH]^{z+}$ or $[M-zH]^{z-}$ in positive and negative ESI mode, respectively. Generally, at low m/z ratios, only singly charged ions (z=1) are observed.

Voltages applied in the desolvation zone are the following: capillary voltage 4200 V (3500 V in negative mode) capillary exit 200 V (-200V), funnel voltage 150 V (-150 V), skimmer 8 V (-6 V). Other parameters are: drying nitrogen flow rate 2 Lm^{-1}(3 Lm^{-1}), drying nitrogen temperature 200 °C, nebulizer nitrogen flow rate 0.5 bar (1 bar).

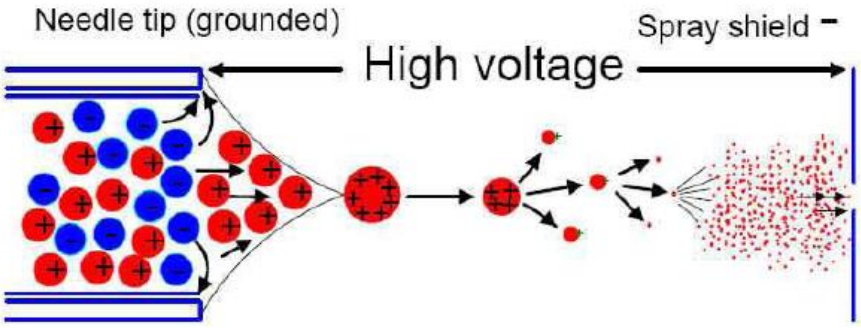

Figure 4.2 - Ion generation process from a liquid analyte (from the Bruker SolariX user's guide).

Linear quadrupole analyzer

The linear quadrupole analyzer consists in a set of four parallel rods which applies a varying voltage and radiofrequency potential. As the field changes, ions respond by undergoing complex trajectories. Depending on the applied voltage and radiofrequencies, only ions of a certain m/z ratio will have stable trajectories and pass through the analyzer. All other ions will be lost by collision with the rods. The quadrupole can work in radio frequency mode (RF-only), which permits to transfer ions of large mass ranges, or can act as a filter where a precursor ion of interest may be selected to be then decomposed for structural analysis in the following hexapole by collision-induced dissociation (CID) mechanisms.

ICR cell

The generated ions are accumulated in the linear collision cell for 0.5 s and then isolated in a cylindrical ICR cell (Fig. 4.3). The ICR cell (Caravatti & Allemann 1991) is the heart of the instrument and is located inside a spatially uniform superconducting magnetic field (7 Tesla). It is cooled by liquid helium at 3.9 K and equipped with opposing pairs of plates which have the different functions of trapping, exciting, and detecting the ions.

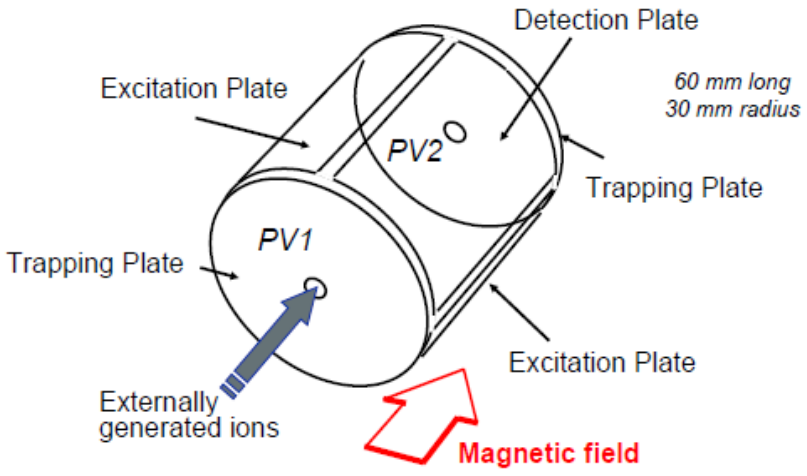

Figure 4.3 - Scheme of the ICR cell (from the Bruker SolariX user's guide).

In the analyzer, cell ions describe a complex three-dimensional movement due the combination of three forms of motion: trapping motion, magnetron motion, and cyclotron motion. The trapping motion is the oscillating motion in the electric field between trapping plates; the magnetron motion arises from the combination of the magnetic and electric field; the cyclotron motion is the stable cyclic motion in a plane perpendicularly to the magnetic field. The frequencies of the trapping and magnetron motion can be generally neglected with respect to that one of the ion cyclotron motion for small size ions. Therefore the FT ICR mass spectrometer can be described as based on the cyclotron motion.

4.1.2 Basic principles

Cyclotron motion of ions in the ICR cell

In a magnetic field B, ions of charge z and velocity v experience the Lorentz force F_L, perpendicular to both the ions velocity and the magnetic field lines:

$$\boldsymbol{F_L = zv \times B} \tag{4.1}$$

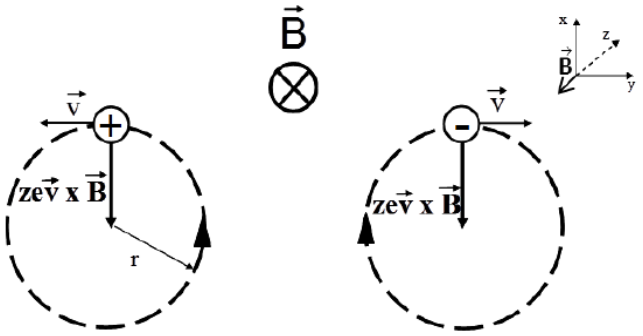

Figure 4.4 - Lorentz force acting on charged particles moving perpendicular to the magnetic field (adapted from Marshall & Grosshans 1991).

The Lorentz force is directed inward and is counterbalanced by the centrifugal force F_c, which is directed outward

$$F_c = \frac{m v_{xy}^2}{r} \tag{4.2}$$

(Where m = ion mass, v_{xy} =ion velocity in the x-y plane, r = orbital radius)

By equating equations (4.1) and (4.2) and introducing the frequency component ν_C via the angular velocity

$$\omega = \frac{v_{xy}}{r} = 2\pi\nu_c \tag{4.3}$$

the so called cyclotron equation (4.4) is obtained:

$$\nu_c = \frac{zB}{2\pi m} \tag{4.4}$$

The cyclotron equation describes the relationship between the ions mass-to-charge ratio m/z and the cyclotron frequency ν_C. Each ion of a certain m/z is thus characterized by its typical cyclotron frequency ν_C which depends only upon the ion's charge *z*, its mass *m*, and the constant magnetic field *B*. Because ν_C is inversely proportional to m/z, the smaller the mass-to-charge ratio, the higher the corresponding cyclotron frequency.

Signal generation

When ions start their cyclotron motion, they are not in phase and are statistically distributed at different radii in the ICR cell. Ions with the same m/z have the same cyclotron frequency but different velocity v_{xy} in the plane and different orbital radius. To obtain a measurable signal, the ions must be excited to a larger cyclotron radius by an oscillating electric field parallel to the magnetic field. When the excitation field is removed, the ions of the same m/z are rotating at their cyclotron frequency in phase (as a "packet" of ions) at their final radius. Ions induce a charge (detected as an image-current) on a pair of detection plates as the packets of ions pass close to them (Fig. 4.5).

In the case of a circular orbit, this image-current oscillates at the ion's resonant frequency. It can be amplified and digitized using 128 k to 4000 k data points, depending on the expected resolution, resulting in the varying recording time domain. The image signal of ions with different m/z can thus be separated, detected, and analyzed by way of the different cyclotron frequencies. It has to be noted that the measured frequency is not strictly identical to the cyclotron frequency because the magnetron frequency reduces the cyclotron frequency;

however this contribution can be neglected for ions with low m/z. The useful signal is extracted from data by performing a Fourier transform, which converts the signal from the time-domain to the corresponding frequency-domain and provides the final mass spectrum.

All mass spectra and collision activation spectra are acquired with Solarix control (version 1.5 BrukerDaltonics) in broadband mode from m/z 75 to m/z 5000 in different m/z domains. The ESI mass spectra are calibrated from Tuning Mix (ESI) file.

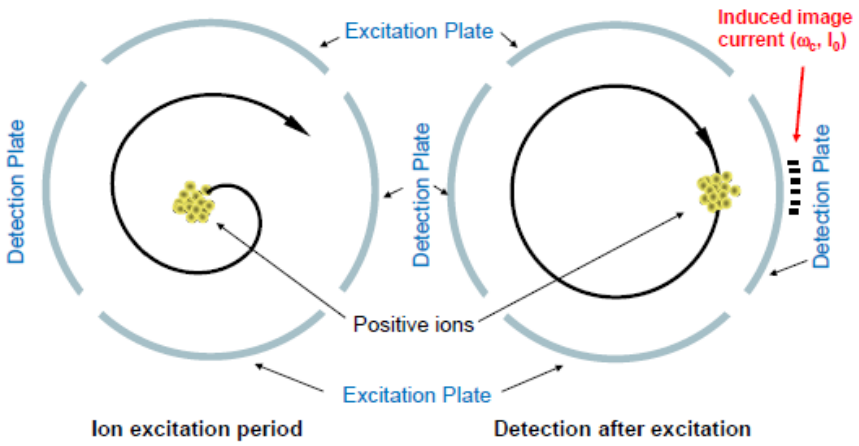

Figure 4.5 - Excitation of the ions in the ICR cell (from the Bruker SolariX user's guide).

Definitions

Here we give some useful definitions of the terms that will be used in the following. The ion exact mass is the theoretical ion mass, that is the calculated mass obtained by adding up algebraically the known exact (rest) masses of each constituent atom, taking into account also the exact mass of the proton added (in positive ESI mode) or removed (in negative ESI mode). Atomic exact masses are monoisotopic and refer to the most abundant naturally occurring stable isotopes. Hence, in the case of isotopic elements such as those of hydrogen, carbon, oxygen, and nitrogen, the exact mass of these atoms refers to the mass of ^{1}H, ^{12}C, ^{16}O, and ^{14}N, respectively. When ^{13}C atoms are present in an ion (for example in the case of a ^{13}C labeled sample), the mass of this latter isotope is used. Table 4.1 summarizes the exact atomic masses

for the elements of interest used in the calculation of the ion exact masses. The nominal mass of an ion is instead calculated using the nominal mass (integer mass) of the most abundant isotope of each element. For simplicity reasons, we will use the ion nominal masses in some cases when high accuracy is not essential.

Table 4.1 - Values of the atomic exact masses for the element of interest used in the calculations of the ion exact masses.

Element	Symbol	Nominal mass	Exact mass
^{1}Hydrogen	H	1	1.0078250
^{12}Carbon	^{12}C	12	12.0000000
^{13}Carbon	^{13}C	13	13.0033548
^{16}Oxygen	^{16}O	16	15.9949146
^{14}Nitrogen	^{14}N	14	14.0030740
Charged particle			
Proton	H^{+}	1	1.0072766

The accurate mass is the experimentally measured mass value. All the accurate masses in the following are reported with 5 decimals (if not differently specified) and accompanied with their error.

The difference between the exact mass and the accurate mass is the mass error, which is expressed in parts per million (ppm).

$$\text{Mass error} = (\text{exact mass} - \text{accurate mass}) / (\text{exact mass}) \times 10^{6}$$

The mass error refers to the accuracy of the measurement and is the most important parameter in establishing the compound identity. In the following, the mass errors are rounded to one decimal place.

Another important parameter which characterizes the mass measurements is the mass resolution:

$$\text{Mass resolution} = (\text{ion mass}) / (\text{mass peak width})$$

It varies with $(m/z)^{-1}$, implying lower resolution at higher masses. Mass resolution refers to the precision of the measurement and is important for the detection of ions of very similar mass, a circumstance often occurring in complex mixtures.

4.2 Mass spectra description

Sample preparation

We have prepared two residues in our laboratory at IAS, both obtained following the standard procedure of photo- and thermo-processing of simple starting mixtures composed of water, methanol and ammonia. One residue was obtained from H_2O:CH_3OH:NH_3 in the ratio of 2:1:1 (hereafter the ^{12}C residue) and the other one, isotopically labeled with ^{13}C, was obtained from H_2O:$^{13}CH_3OH$:NH_3 in the ratio of 2:1:1 (hereafter the ^{13}C residue). These residues are basically similar to those prepared by our group and analyzed by an LTQ-orbitrap-XL instrument (Danger et al. 2013). In the following, we will often refer to these Orbitrap results for comparison.

Each sample was extracted with 20 μl of ultrapure water and the recovered solution mixed in the ratio of 1:100 with a binary solvent composed of equal amounts of CH_3CN and H_2O. Before running the analyte solutions, the appropriate blank solutions containing the solvent only (CH_3CN and H_2O) were acquired with the same experimental conditions chosen for the analyte. About 30 μl of solution was used to acquire each spectrum, which corresponds to about 1/50 of the total analyte solution available. This permitted to acquire mass spectra at different experimental conditions (ionization mode, m/z range, calibration) for a same sample and to repeat measurements when needed. A wide mass-to-charge range from m/z 70 to m/z 5000 was explored. Calibration was optimized in three main ranges: low m/z (m/z<200), medium m/z (200<m/z<2000), and high m/z (m/z>2000). Both negative and positive ESI modes were exploited.

4.2.1 Analysis at low and medium mass-to-ratio range

General overview of spectra

The ^{12}C residue was analyzed by the FT ICR mass spectrometer in positive ESI (electrospray ionization) mode. A multitude of well-resolved peaks are observed within a wide mass range between m/z 70 and 300 (low to medium mass range) at a signal-to-noise ratio higher than 4 and at a resolution of about 200000 at m/z 400. In Fig. 4.6, panel *a*, we present an overview of the spectrum obtained in the m/z 130-220 range which will be further analyzed in more details in the next sections of this chapter. Panel *b* and *c* of the same figure show subsequent zooms of the same spectrum and allow appreciating its high resolution.

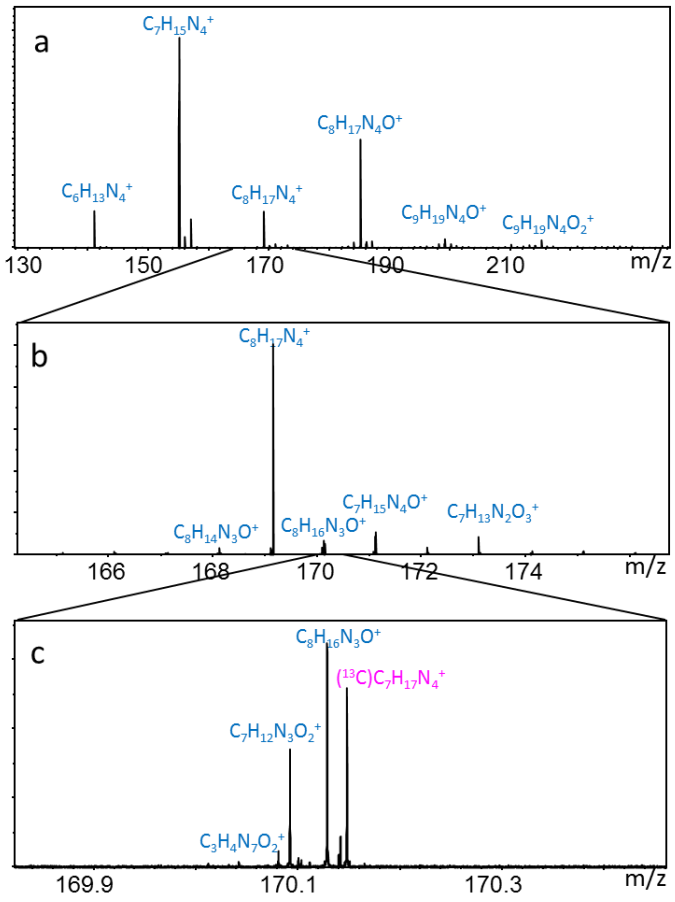

Figure 4.6 - ESI mass spectra in positive mode of the ^{12}C residue in the m/z 130-220 range (panel a) and subsequent zooms in the m/z 167-174 range (panel b) and m/z 170.00-170.20 range (panel c). Individual peaks are resolved also in narrow m/z ranges.

The spectrum is dominated by the intense peaks at the nominal m/z 141, 155, 169, and 185, and in addition it shows the presence of many other peaks. The two progressive enlargements on narrower mass ranges permit to visualize the presence of further peaks of lesser intensity near the peak at m/z 169 (panel *b*) and near the peak at m/z 170 (panel *c*). Ion empirical formulas are attributed to the main peaks by using the Compass DataAnalysis software version 4.0 by comparison of the accurate masses with the exact masses expected. It can be noted that peaks having a m/z ratio very close to others can be resolved as individual peaks and that even the presence of naturally occurring ^{13}C atoms can be appreciated. For example the $(^{13}C)C_7H_{17}N_4^+$ ion peak visible in panel *c* is identified as belonging to the isotopic pattern of the $C_8H_{17}N_4^+$ intense ion peak present in panel *b*. This identification is based on the intensity of the ^{13}C-bearing ion peak with respect to the ^{12}C-bearing one, in good agreement with the statistical natural occurrence of ^{13}C atoms in an ion containing 8 carbon atoms. A comparison with the blank spectrum (not shown) under the same experimental conditions and at the same intensities reveals that the observed peaks are due to the residue and are not contaminants present in the solvent or in the ESI ion source.

A spectrum in the range between m/z 190 and 300 has been recorded after the experimental conditions have been optimized to favor the transfer of medium mass ions (Fig. 4.7). The presence of intense peaks at each nominal mass indicates that the residue contains a very high variety of compounds (panel *a*). The peak richness observed is similar, although to a lesser extent, to that observed in the Murchison meteorite soluble organic matter (Schmitt-Kopplin et al. 2010) and is a feature of abiotic synthesis due, in our case, to the photo- and thermo-processing of the sample. It can be noted that the peak intensity distribution follows a repetitive and almost regular wave structure across the considered range. This feature is due to the circumstance under which when C, H, N, and O atoms combine together to form molecular species; some assemblies are chemically favored and thus statistically more frequent than others. A comparison with the solvent blank spectrum (panel *b*) at the same intensities clearly shows that the peaks observed are largely due to the residue and that the presence of *repetitive structures* is an exclusive characteristic of the residue.

Because of the richness and complexity of the spectrum and, in particular, the fact that the number of possible chemical formulas increases exponentially with mass, we could not assign univocal chemical formulas to peaks starting from about m/z 220. We thus limit our work mainly to the range between m/z 70 and 220 which can be more easily explored and interpreted.

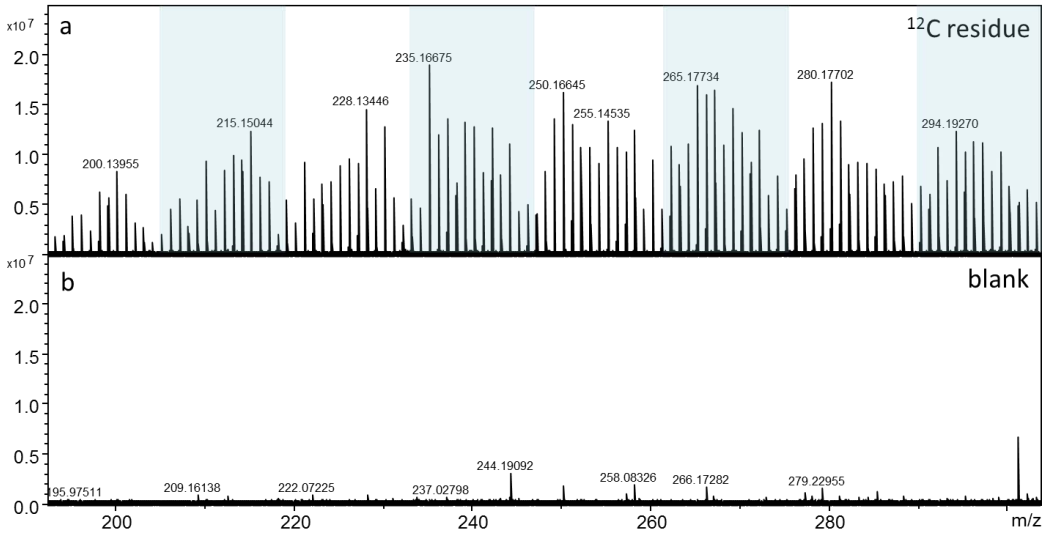

Figure 4.7 - ESI mass spectra of the ^{12}C residue (panel a) and the corresponding blank (panel b) in the m/z 190-300 range. Alternation of blue and white boxes in panel a evidences the repetitive patterns of peaks.

Search of HMT and HMT based molecules

Among the numerous peaks observed in the mass spectra shown above, we focused to peaks in the low mass range where we searched for signals from known molecules such as HMT (hexamethylenetetramine) and HMT-based species.

HMT ($(CH_2)_6N_4$) is a heterocyclic organic compound with a cage-like structure, which has been reported in residues as the most abundant species (Briggs 1992; Bernstein et al. 1995; Cottin 2001; Muñoz Caro & Schutte 2003; Vinogradoff et al. 2011). HMT-based molecules have been reported for the first time by Muñoz Caro et al. 2004 by GC MS and include: methyl HMT

($C_6H_{11}N_4$-CH_3), hydroxy-HMT ($C_6H_{11}N_4$-OH), methanyl-HMT ($C_6H_{11}N_4$-CH_2OH), amin-aldehyd-HMT ($C_6H_{11}N_4$-NH-CHO) and methanyl-aldehyd-HMT ($C_6H_{11}N_4$-CHO). These detections have been later confirmed with high resolution techniques by Orbitrap on residues made by our group at IAS and sent for analysis at the PIIM in Marseille (Danger et al. 2013). In this latter study HMT-C_2H_5O was also reported. HMT-based molecules are suggested to form by substitution of a HMT H atom by a side group (Muñoz Caro et al. 2004). Since HMT in residues forms only around room temperature (Muñoz Caro & Schutte 2003; Vinogradof et al. 2013), HMT-based species are thought to form not directly by HMT, but from its precursors formed during the photoirradiation of ices. Indeed, photoirradiation at low temperature (80 K) is capable of breaking chemical bonds and generating different radicals which, after gradual warming (300 K) and further reactions, can result in different species such as those of the same family of HMT.

Figure 4.8 illustrates the chemical structure suggested for a specific HMT-based molecule, amin-aldehyd-hexamethylenetetramine. Each vertex in the cage structure corresponds to a CH_2 group, with the exception of the vertex in which the side group is attached. In this vertex, one of the two hydrogens of the CH_2 group is replaced by the side group. The remaining hydrogen is explicit whereas the carbon atom is implicit.

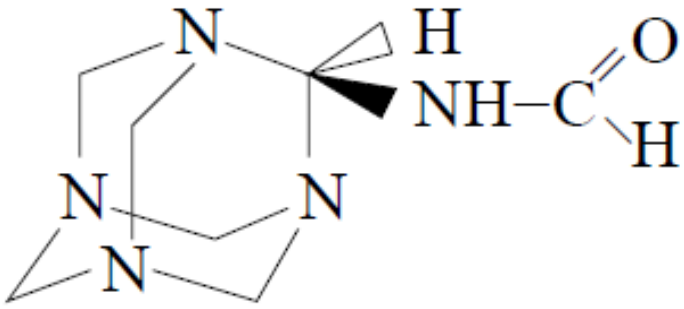

Figure 4.8 - Representation of amin-aldehyd-hexamethylenetetramine (Muñoz Caro et al. 2004).

Here we report on the identification of HMT and several HMT-based molecules realized by means of a careful inspection of mass spectra of the ^{12}C and the ^{13}C residues and their mutual

comparison starting from data available in the literature (Muñoz Caro et al. 2004; Danger et al. 2013).

The following method is used for the identifications. Each peak in the ^{12}C spectrum thought to be assigned to a HMT-based molecule is matched to a peak in the ^{13}C spectrum on the basis of the number of carbon atoms contained in its carrier. For example, HMT after proton positive ionization (HMT-H$^+$) has a theoretical exact mass of m/z 141.11347, which corresponds to the $C_6H_{13}N_4^+$ ion. A peak is indeed observed at the accurate mass of m/z 141.11329 (as shown in Fig. 4.9, panel *a*). The high mass accuracy of this measurement (-1.3 ppm) permits to be largely confident about this identification. On the other side, in the spectrum of the ^{13}C labeled residue, the search of a peak properly shifted in m/z (whose assigned empirical formula contains six ^{13}C atoms at the place of six ^{12}C atoms) leads to the peak at m/z 147.13369 (0.6 ppm) which thus can be confidently attributed to ^{13}C HMT-H$^+$. The two corresponding blanks (not shown) associated with the spectra of the samples do not display any peak at the same position of the observed matching peaks, allowing excluding any contamination contribution.

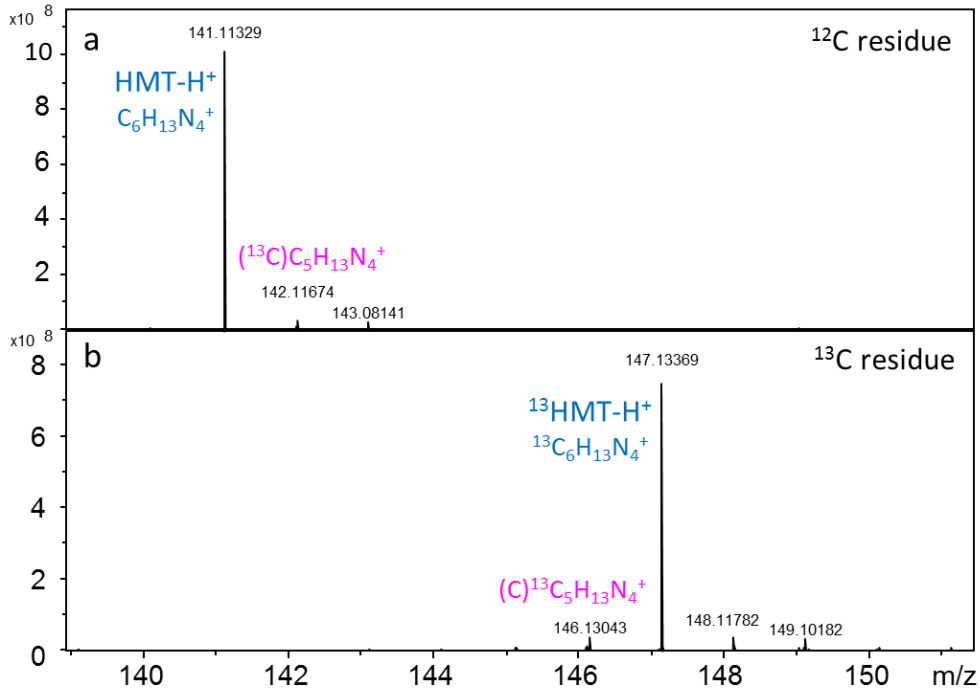

Figure 4.9 - Comparison between ESI mass spectra of the ^{12}C residue (panel a) and the ^{13}C residue (panel b) showing the detection of HMT-H$^+$ and ^{13}HMT-H$^+$, respectively.

Note that the ion at m/z 142.11674 in panel *a* is due to the presence of naturally occurring ^{13}C atoms in the methanol used in the starting mixture. This peak corresponds to a HMT-H^+ ion where one carbon out of the six is replaced by a ^{13}C atom, that is $(^{13}C)C_5H_{13}N_4^+$. Similarly, but related to a different origin, the ion at m/z 146.13043 in panel *b* has an associated formula of $(C)^{13}C_5H_{13}N_4^+$ in which one atom out of the six ^{13}C is replaced by one ^{12}C. The presence of this atom does not seem related to an external possible contamination during the sample preparation, but rather to a not complete isotopic labeling of the ^{13}C methanol used in the starting mixture. The purity of ^{13}C methanol is in fact 99% (Aldrich) and the low intensity of this peak with respect to its corresponding monoisotopic peak is consistent with this interpretation.

The method described above can be equally used to search for protonated HMT-based molecules for which we will consider only detections with mass accuracy within 2 ppm. The mass range between m/z 140 and 220 is explored (Fig. 4.10) and empirical formulas attributed to the most intense peaks present in the spectrum of the ^{12}C residue (panel *a*) and the ^{13}C residue (panel *b*).

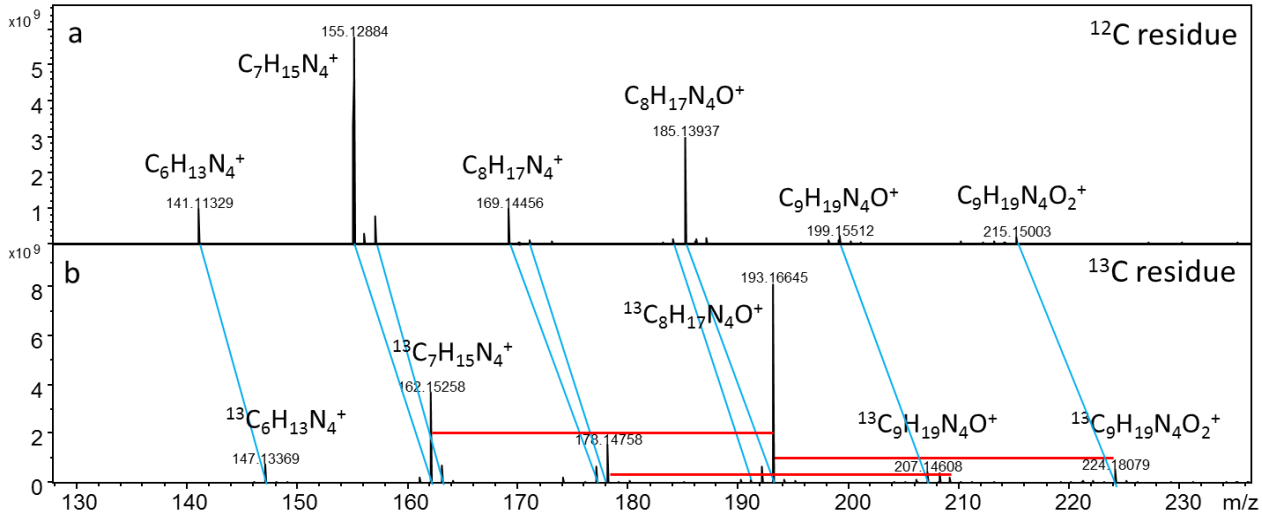

Figure 4.10 - Comparison between ESI mass spectra of the ^{12}C residue (panel a) and the ^{13}C residue (panel b) in the m/z 130-230 mass range. Pairs of matching peaks between the two spectra are evidenced by blue connecting segments. In panel b, peaks spaced by 31 nominal masses ($^{13}CH_2O$) are evidenced by red horizontal segments.

The proper m/z shifts observed between pairs of matching peaks in the two spectra highlight the equivalence of the two ion empirical formulas and serve as a crosswise identification between each one of the two counterparts. It can be noted that, in general, similar intensity ratios are observed between corresponding peaks of the two spectra. This is related to the fact the same ionization and ion transfer conditions were applied in both cases, and indirectly proves that the two samples are chemically equivalent. The peaks at m/z 162.15258, 193.16645, and 224.18079 in the ^{13}C residue spectrum (panel *b*) are equally spaced of 31 nominal mass apart (30 nominal mass in the ^{12}C residue spectrum for the respective matching peaks). This characteristic is due to the presence of oxymethylene repeated subunits ($^{13}CH_2O$) added by polymerization of the smaller molecule responsible for the ion peak at m/z 162.14258. The exact mass of the $^{13}CH_2O$ subunit is 31.01392, which permits an easy identification of this class of polymers in the mass spectrum. In a similar way, the ion peak at m/z 209 is obtained by addition of $^{13}CH_2O$ to the smaller ion which gives rise to the ion peak at m/z 178.14758.

HMT and four of its based molecules have already been reported by Danger et al. 2013. We confirm all these detections in our samples and compare their mass measurement accuracy with respect to the ones obtained with the Orbitrap. In general, for the same set of ions, the detections with Orbitrap are accurate at levels better than 5 ppm, whereas the detections with FT ICR are accurate at levels better than 2 ppm, as shown in Table 4.2. Therefore we can affirm that the higher mass accuracy provided by FT ICR allows improving the quality of the measurements reported.

Table 4.2 - Comparison between the experimental m/z of ions of the HMT family determined by Orbitrap and FT ICR along with their theoretical exact m/z. Errors (δ) are given in ppm.

Empirical Ion Formula $[M+H]^+$	Theoretical m/z	Orbitrap Experimental m/z (δ)	FT ICR Experimental m/z (δ)
$C_6H_{13}N_4^+$	141.11347	141.1128 (5)	141.11329 (1.3)
$C_7H_{15}N_4^+$	155.12912	155.1286 (3)	155.12884 (1.8)
$C_8H_{17}N_4^+$	169.14477	169.1442 (3)	169.14456 (1.3)
$C_7H_{15}N_4O^+$	171.12404	171.1234 (4)	171.12388 (0.9)
$C_8H_{17}N_4O^+$	185.13969	185.1391 (3)	185.13937 (1.7)

The entire set of our identifications of HMT-based molecules includes 10 ions which are listed in Table 4.3. Several of these identifications are based on known ions, already detected by Muñoz Caro et al. 2004 and/or Danger et al. 2013. Besides these identifications, new peaks can be tentatively ascribed to HMT-based molecules as suggested by their m/z ratio and their most reliable empirical formula. These new detections refer to the peaks at m/z 201.13444, 215.15003, and 279.20395 for which we propose the structures illustrated in the last column of Table 4.3. In the structures of the carriers, the notation HMT' indicates the molecule of HMT in which an H atom is missing, that is $C_6H_{11}N_4$.

Table 4.3 - Identifications of HMT-based molecules in ^{12}C and ^{13}C residues alongside their empirical and possible structure formula.

Empirical ion Formula	m/z in ^{12}C residue	m/z in ^{13}C residue	Carrier structure $[M+H]^+$
$C_6H_{13}N_4^+$	141.11329	147.13369	HMT + H^+
$C_7H_{15}N_4^+$	155.12884	162.15258	HMT'-CH_3 + H^+
$C_6H_{13}N_4O^+$	157.10819	163.12864	HMT'-OH + H^+
$C_8H_{17}N_4^+$	169.14456	177.17177	HMT'-C_2H_5 + H^+
$C_7H_{15}N_4O^+$	171.12388	178.14758	HMT'-CH_2OH + H^+
$C_7H_{14}N_5O^+$	184.11911	191.14311	HMT'-NH + CHO + H^+
$C_8H_{17}N_4O^+$	185.13937	193.16645	HMT'-CH_3 + CH_2O + H^+
$C_8H_{15}N_4O_2^+$	199.11877	207.14608	HMT'-CHO + CH_2O + H^+
$C_8H_{17}N_4O_2^+$	201.13444	209.16181	HMT'-CH_2OH + CH_2O + H^+
$C_9H_{19}N_4O_2^+$	215.15003	224.18079	HMT'-CH_3 + CH_2O + CH_2O + H^+
$C_{12}H_{23}N_8^+$	279.20395	291.24543	2HMT' + H^+

Figure 4.11 illustrates the detection of the ion at m/z 201.13444, which we potentially assign to HMT'-CH_2OH CH_2O H^+, and that of its ^{13}C counterpart at m/z 209.16181.

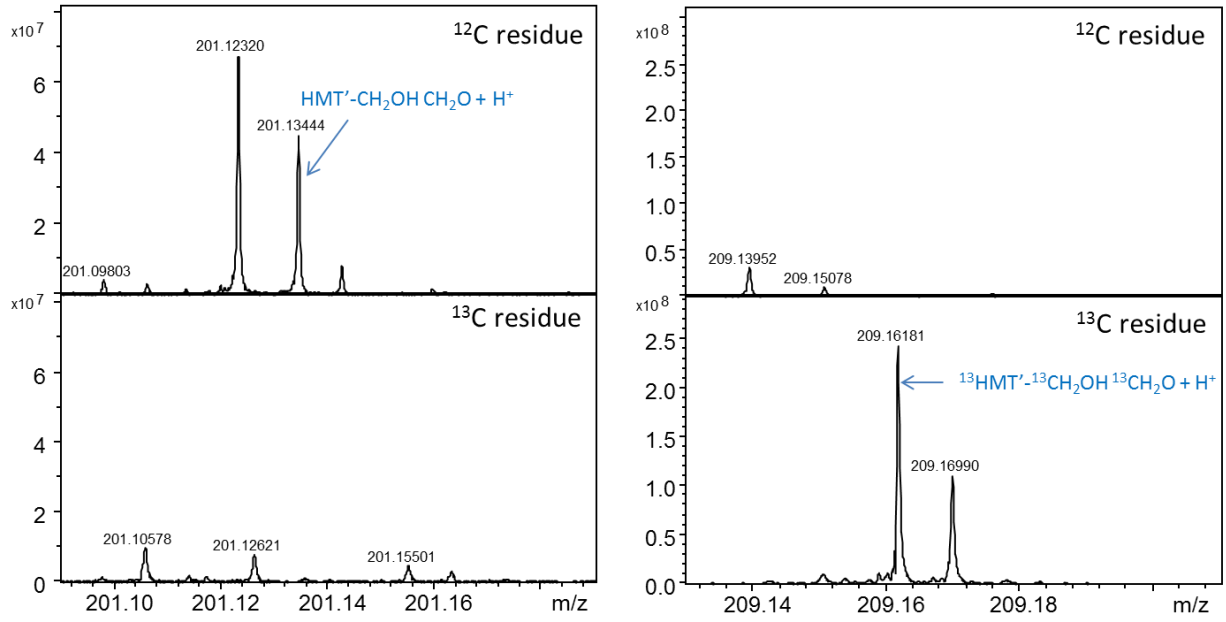

Figure 4.11 - Identification of a new potential HMT-based molecule in the ^{12}C residue (left box, upper panel) and in the ^{13}C residue (right box, bottom panel) mass spectra.

The structure of the ions at m/z 201.13444 and 215.15003 contains the groups CH_2OH and CH_3 respectively, and both contain the CH_2O group. These groups are rather common among the other HMT-based molecules and in general among the carriers of the most intense peaks observed. The presence of the repeated CH_2O subunits, as already outlined, suggests that the formation mechanism for these molecules could be the polymerization of smaller molecules by addition of repeated subunits through relatively simple radical reactions.

The ion at m/z 279.20395 is potentially assigned to the dimer of HMT, consisting of two HMT monomers joined together by a covalent bond (Fig. 4.12). In order to form this chemical entity, two HMT molecules, each one with a missing hydrogen atom, should bond together. The identification of the ^{13}C counterpart at m/z 291.24543 is however difficult and not reliable as the rest of our identifications because of peak deformation. For this measurement the mass accuracy is only 3.0 ppm. Further identifications of HMT-based molecules at higher m/z ratios

are unfortunately prevented by the presence of instrumental artifacts in the spectra which deform the profile of some peaks.

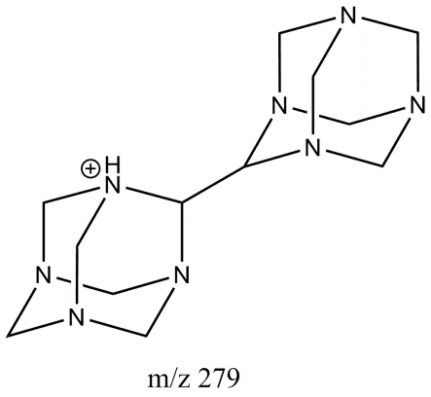

Figure 4.12 - Suggested structure for the HMT dimer ion ($C_{12}H_{23}N_8^+$) containing two HMT monomers.

Spectra in negative ionization mode

The molecules listed in Table 4.3 are only detected in positive ESI mode. Their search in the mass spectra obtained in the negative ESI mode gave systematically a negative result. This is not surprising because these molecules do not carry proton donors such as acidic protons in their structure.

In the negative mode proton donors such as carboxylic acids and phenols are ionized, while in the positive mode proton acceptors such as amine and amides are ionized. The two ionization modes are thus often complementary. This phenomenon is illustrated in Fig. 4.13 which displays two mass spectra obtained from the same residue in the same m/z range but with the two opposite ionization modes. The main peaks observed in the two cases are clearly different as can be noted by their m/z ratio; moreover, their mass defects are different, which implies different elemental compositions. In one of the next sections, we will explore the spectrum in negative mode searching for amino acids, whose structure can discriminate between the positive and the negative ionization mode.

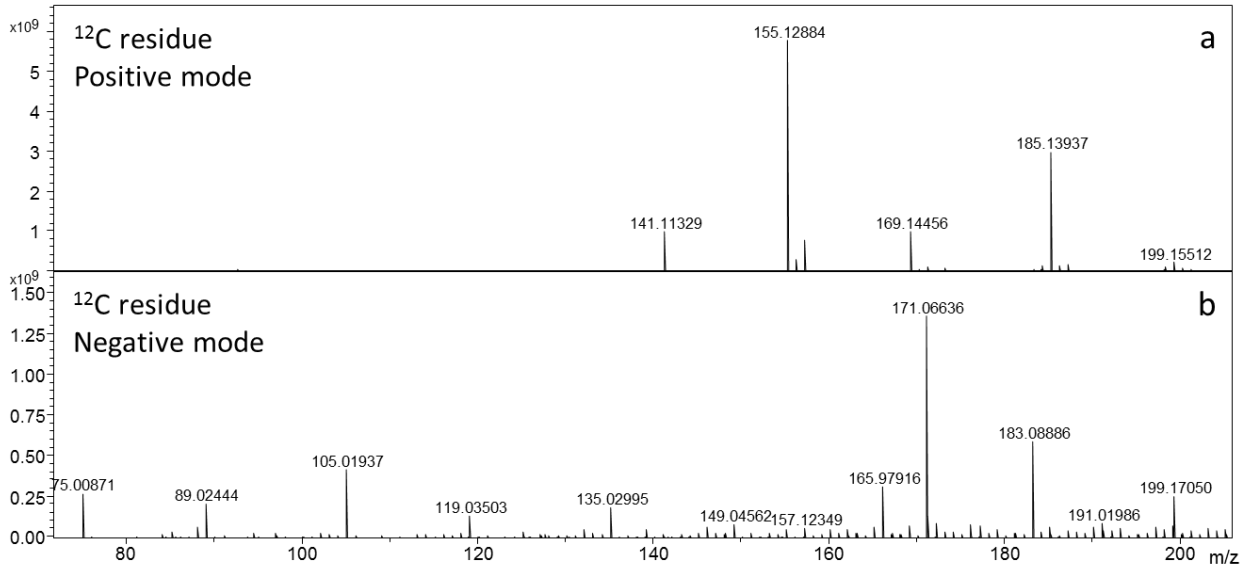

Figure 4.13 - FT ICR spectra of the ^{12}C residue in positive ESI mode (panel a) and in negative ESI mode (panel b). The two ionization modes generate different sets of ions.

Ion fragmentation

Among the most intense ions listed in Table 4.3, six of them were chosen to obtain structural information by means of their fragmentation patterns. The ions were first individually selected and isolated in the linear quadruple, and were then processed by collision-induced dissociation (CID) into the collision cell or by sustained off-resonance irradiation (SORI) CID into the ICR cell. CID is a mechanism by which the selected ions are accelerated and allowed colliding with neutral argon molecules. The collisions result in bond cleavage and fragmentation of the precursor ion into smaller fragment ions, which can then be analyzed in the ICR cell. The SORI CID consists in collision-induced dissociation of accelerated ions directly in the ICR cell for excited ions that have a cyclotron frequency close to the frequency of the excitation field. Despite this latter mechanism generally allows finer m/z isolation, it gave results of lesser quality with respect to CID in terms of number of peaks observed. We will thus only show fragmentation patterns obtained by CID.

The CID fragmentation pattern of the HMT-H⁺ ion is shown in Fig. 4.14. By observing the main peaks of this fragmentation pattern, we can deduce that the precursor ion (m/z 141.11318) loses a neutral group with the exact mass of 43.04220 (C_2H_5N) and a neutral group with the exact mass of 29.02655 (CH_3N), which in turn loses a group with the exact mass of 27.01090 (CHN). The loss of these three fragments produces the intense peaks observed at m/z 85.07591, 98.07109, 112.08671. The further loss of a CHN group from the m/z 98.07109 ion produces the small peak at m/z 71.06025. This mechanism is depicted in Fig. 4.16 where the use of segments of different colors corresponds to the different neutral groups involved in the cleavage.

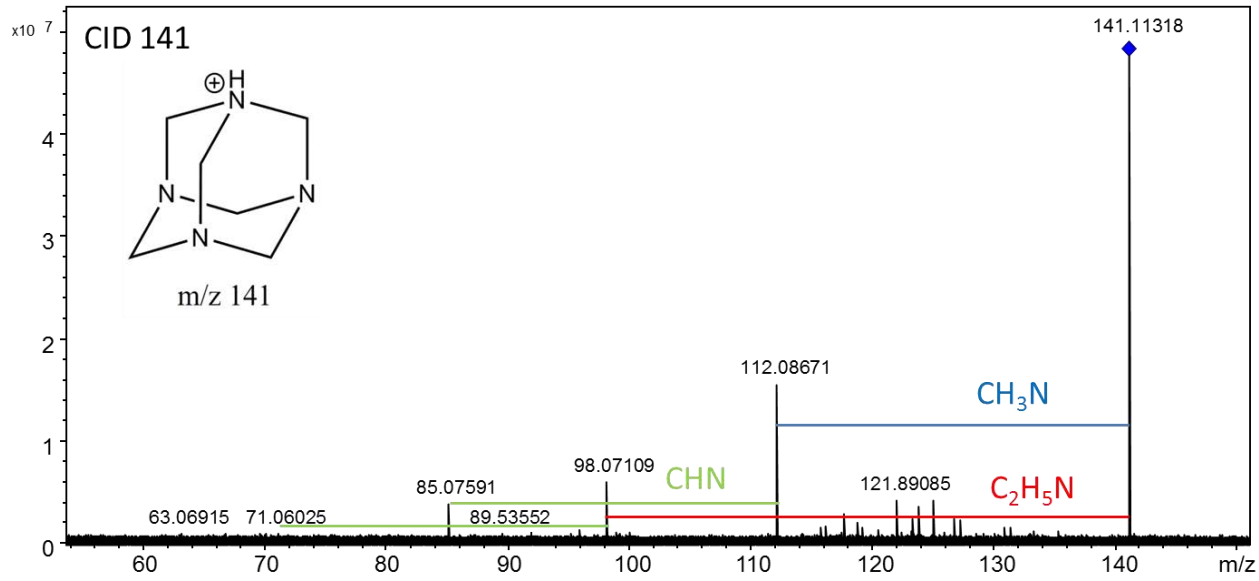

Figure 4.14 - CID fragmentation pattern of the HMT-H⁺ ion. The precursor ion (m/z 141) is indicated by a rhombus. The colored segments indicate the neutral fragments lost after cleavage of the precursor ion.

The peaks observed after CID fragmentation of the HMT-H⁺ ion isolated in our residue are all present in the fragmentation pattern of a pure external HMT standard shown in Danger et al. (2013). This confirms the correctness of our detection. Table 4.4 lists the ion fragments of the HMT standard and HMT detected in our residue. Four fragment peaks from the residue match properly with the main ones from the standard, whereas the peak at m/z 69 is not observed in our case likely because it is of a very low intensity.

Table 4.4 - Comparison between the ion fragments of the HMT standard and the residue ones. Among the 5 most intense peaks observed for the standard, 4 of them are present in our residue.

Parent ion m/z	Ion fragment formula	Theoretical m/z	Standard m/z	Residue m/z
141.1128	$C_5H_{10}N_3^+$	112.08692	112.0864	112.08671
	$C_4H_8N_3^+$	98.07127	98.0707	98.07109
	$C_4H_9N_2^+$	85.07602	85.0755	85.07591
	$C_3H_7N_2^+$	71.06037	71.0599	71.06025
	$C_3H_5N_2^+$	69.04472	69.0443	-

In Fig. 4.15 we propose a mechanism to account for the formation of the m/z 112 ion starting from the m/z 141 precursor ion. This formation implies the cleavage of three C-N covalent bonds. Two of these cleavages can be easily induced by the subsequent positive charge carried by two nitrogen atoms. The cleavage of the third bond needs the transfer of an H atom in the form of a hydride H^-.

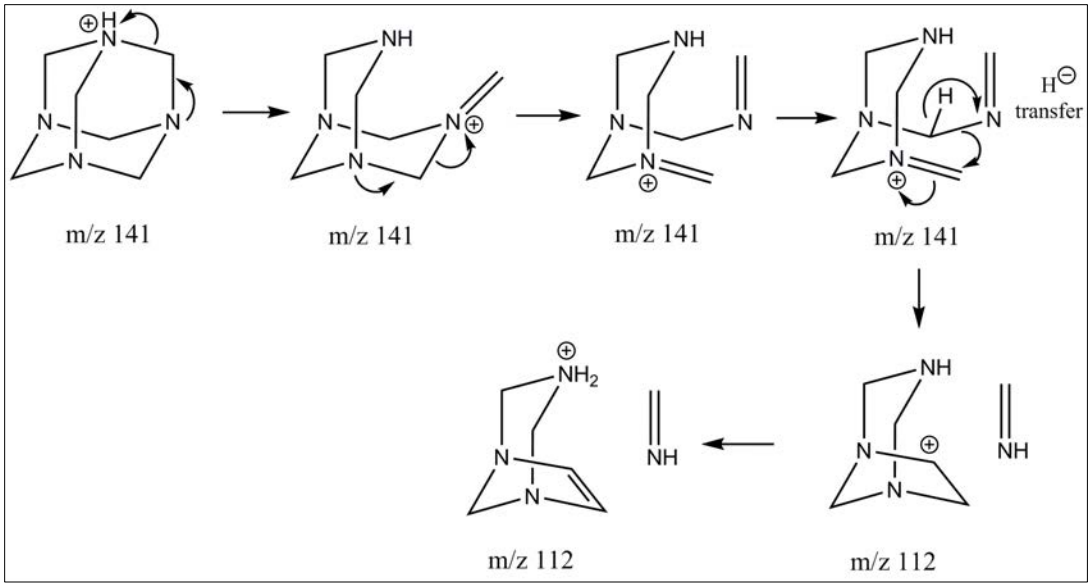

Figure 4.15 - Proposed mechanisms for the formation of the m/z 112 ion after CID fragmentation starting from the m/z 141 ion.

In the same way as for the m/z 141 ion, the CID fragmentation patterns of the individual positive ions at the nominal m/z 155, 185, 199, 201, and 215 were obtained after isolation and then examined to confirm the belonging of these ions to the HMT family (Fig. 4.16).

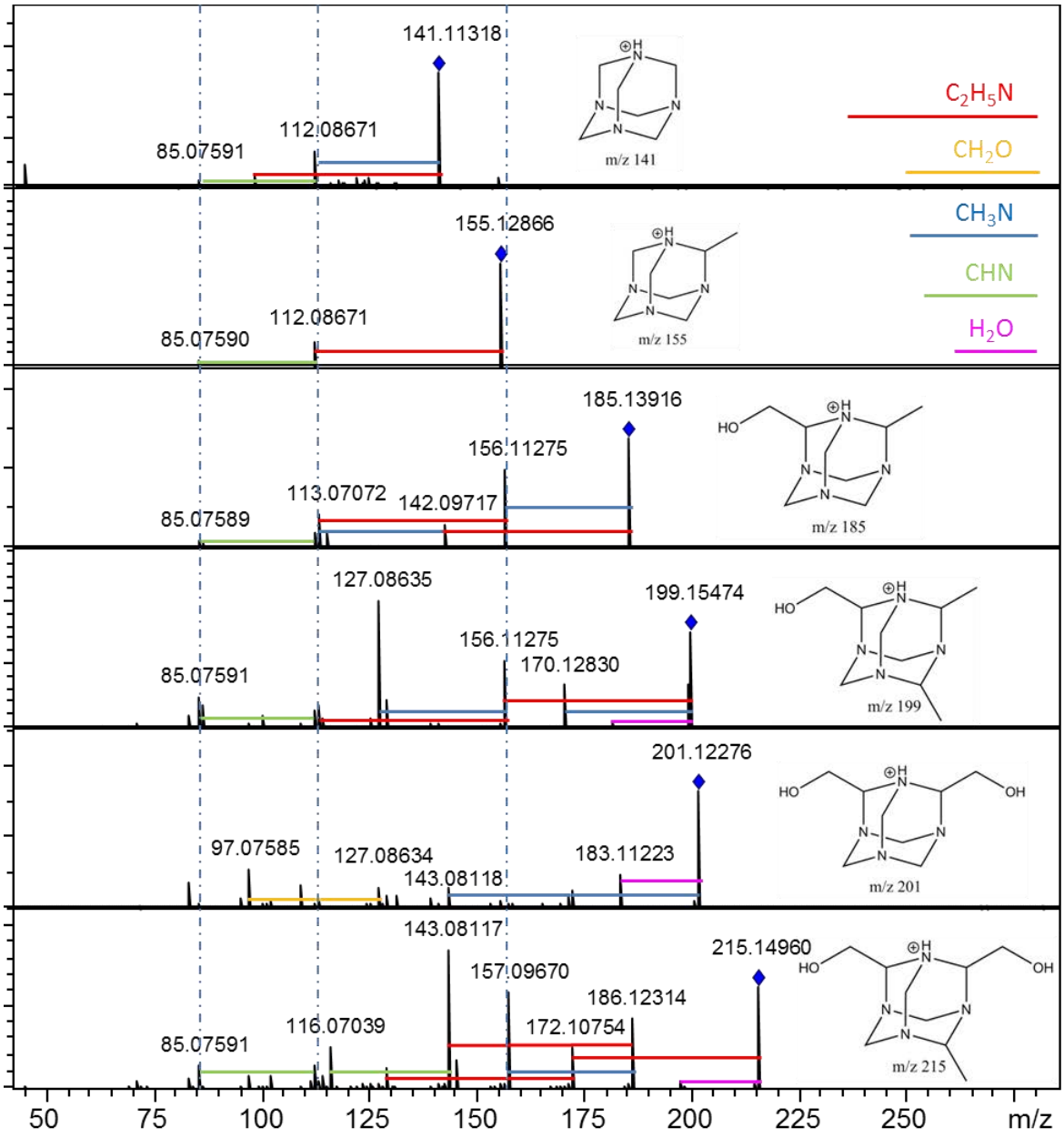

Figure 4.16 - CID fragmentation patterns for HMT ion and possible HMT-based ions from the ^{12}C residue. The precursor ion peaks are marked with a rhombus and their possible structure is shown in a graphical representation. Segments of the same color refer to the loss of the same functional group.

All these fragmentation patterns show the presence of several peaks in common. The peaks at m/z 85 and m/z 112 are present in all the fragmentation patterns here considered; the peak at m/z 113 is present in the fragmentation pattern of all the HMT-based ions except the HMT-H^+ ion itself; moreover, the peak at m/z 156 is present only in fragmentation patterns of the largest ions. This evidence, even if not sufficient alone, already suggests that all these ions share a similar structure and are related to HMT-H^+. Moreover, the precursor ions show similar cleavages, observed by the loss of the same functional groups (C_2H_5N, CH_3N, CHN, CH_2O). This behavior is a sign indicating that all these ions share a similar structure which then cleaves in similar ways. We can also note that the loss of the group CH_2O is observed in the fragmentation pattern of the precursor ions at m/z 185, 199, 201, and 215. This confirms the presence of the group CH_2O in their structure, as correctly suggested in Table 4.3.

Search for free amino acids

In laboratory organic residues, amino acids are in general detected by GC-MS after acid hydrolysis and derivatization techniques. Acid hydrolysis breaks peptidic bonds from amino acid polymers, releasing the individual constituting amino acids, while derivatization is used to obtain favorable chromatographic properties for their detection as well as a better peak separation. The main difference between the detection with and without acid hydrolysis is in the abundance of the detected amino acids, since acid hydrolysis can enhance it by a factor of up to 10 (Nuevo et al. 2008). Furthermore, the distribution of the different amino acids seems to change after acid hydrolysis, favoring the simplest ones as the most abundant (Nuevo et al. 2008).

However, free amino acids are also present in residues and here we will search for them in our non-hydrolyzed residues by examination of the mass spectra. For this purpose, we consider the spectra of the ^{12}C and ^{13}C residue in the low mass range between m/z 70 and m/z 200, both in positive and in negative ESI mode, where we search for peaks that can be attributed to amino acids among the ones already detected in similar residues by liquid chromatography (Nuevo et al. 2007, 2008) and GCxGC MS (Meinert et al. 2012; Modica et al. 2014). The spectrum in ESI negative mode of the ^{13}C residue and the corresponding blank is shown in Fig. 4.17.

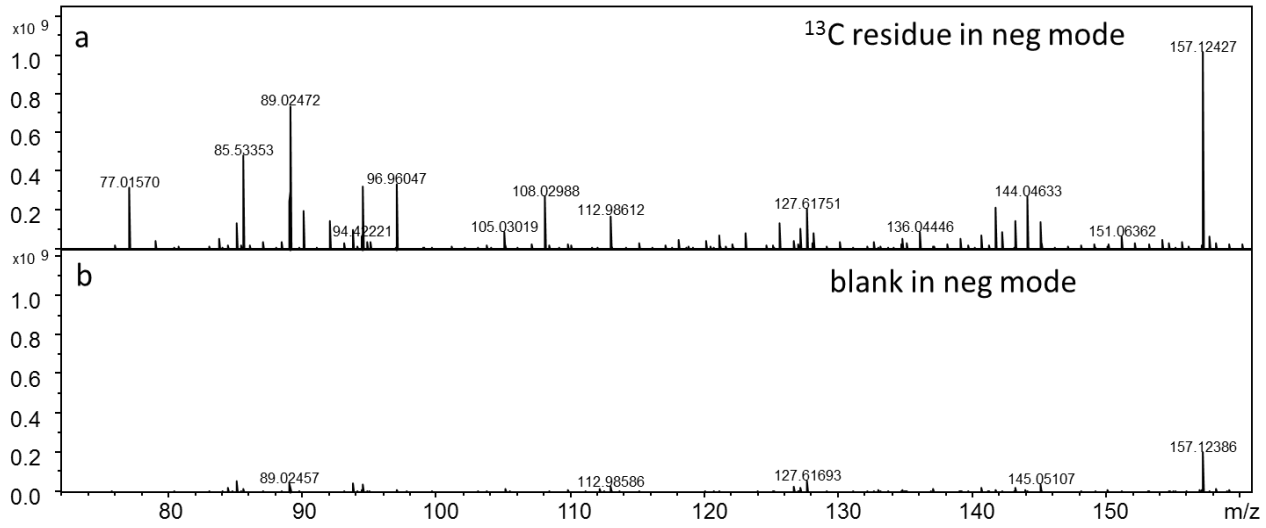

Figure 4.17 - ESI mass spectra of the ^{13}C residue obtained in negative mode (panel a) and its corresponding blank in the mass range between m/z 70 and 160.

The very low mass range until m/z 90 turns out to be poor of peaks because experimental conditions cannot be optimized for small ions. Basically, these ions are lost during their transfer toward the ICR cell, mainly in the hexapole ion traps and in the linear quadrupole one, so they cannot reach the ICR cell to be detected. Over m/z 95, the spectra are slightly richer in peaks, even if not intense, and permit to detect several of them for which the attribution of the empirical formulas of the searched amino acids is unequivocally possible with sufficient accuracy.

Table 4.5 lists 13 detections along with the corresponding m/z values, which are rounded to four decimal places for simplicity reasons. In the last column, we give only one or two examples of the possible assignments, knowing that numerous other possibilities exist (not only amino acids) as can be verified from the NIST (National Institute for Science and Technology) database. Among the 13 peaks, five of them are detected in the negative mode only and one in the positive mode only. A more favorable response to the negative ionization mode is indeed expected for amino acids because their carboxylic functional group is a proton donor. The detections have mass accuracy within a 2 ppm range, except for the ^{13}C residue analyzed in

negative mode (mass accuracy in general within a 6 ppm range). It can be noted that all these latter errors are of the same sign (negative) and approximately of the same magnitude (5 ppm). The reason is that a not optimal calibration in this mass range did produce a peak shift to the right of the spectra, introducing a systematic error in the peak position of about -5 ppm. However, even considering this problem, FT ICR provides higher mass accuracy than the Orbitrap instrument for a similar set of detections.

Note that, naturally, the same formula can be assigned to multiple isomers for which it is impossible to discern unambiguously their specific structure without further investigations. For example the ion $C_4H_{10}NO_2^+$, whose detection is shown in Fig. 4.18 in both ^{12}C and ^{13}C residue in the positive ESI mode, has a formula that corresponds to several possible compounds such as N-ethylglycine, aminobutyric acid, N-methyl alanine and so on. In order to unambiguously identify this ion, a comparison between its fragmentation pattern and the various individual pure standards should be necessary. This comparison is not possible in this work because the peak is not intense enough to allow for an efficient fragmentation; the same problem occurs for the other peaks attributed to isomers. However, more appropriate gas chromatographic techniques are available for these identifications, but this is not our goal in this chapter. Indeed, GC-MS or better GCxGC-MS, much more sensitive, do allow the identification of the precise amino acids that are given in the table. Moreover the GC-MS method will allow for reporting absolute quantities as well as the relative amino acids distribution. This information is essential if one wants to couple analytical results of sophisticated instruments with significant astrophysical and astrobiological (if any) applications. This was already suggested by our results in Chapter 3 but will appear very clear in Chapter 5. Here we wish only to show the ability of the FT ICR technique in attributing the empirical formulas to a large number of peaks with high accuracy.

Table 4.5 - Tentative identification of amino acids in ^{12}C and ^{13}C residues in positive and negative ESI mode. The m/z values are rounded to four decimal places. Errors are expressed in ppm between parentheses.

Empirical formula [M]	m/z Pos mode (δ ppm)		m/z Neg mode (δ ppm)		Possible amino acid
	^{12}C	^{13}C	^{12}C	^{13}C	
$C_2H_5NO_2$	-	-	74.0247 (0.7)	76.0316 (-2.1)	Glycine
$C_3H_7NO_2$	-	-	88.0403 (0.9)	91.0508 (-3.6)	Alanine Sarcosine
$C_4H_9NO_2$	104.0706 (0.5)	108.0841 (-0.8)	-	106.0699 (-4.4)	Aminobutyric acid N-Methyl alanine
$C_5H_7NO_3$	-	-	128.0354 (0.4)	133.0529 (-5.9)	Pyroglutamic acid
$C_5H_9NO_2$	116.0705 (0.6)	121.0875 (-0.9)	114.0562 (-1.0)	119.0735 (-5.4)	Proline
$C_5H_{11}NO_2$	118.0862 (0.6)	123.1031 (-0.3)	-	121.0891 (-4.8)	Valine Norvaline 5 Aminovaleric acid
$C_4H_9NO_3$	-	-	118.0508 (1.6)	122.0650 (-5.4)	Threonine
$C_4H_{10}N_2O_2$	119.0814 (0.4)	123.0951 (-1.0)	-	-	N(2 aminoethyl) glycine 2,4-diaminobutyric acid
$C_5H_9NO_3$	132.0655 (0.4)	137.0825 (-1.5)	130.0510 (-0.4)	135.0686 (-6.0)	Hydroxyproline
$C_4H_7NO_4$	-	-	132.0303 (-0.5)	136.0445 (-6.0)	Aspartic acid
$C_5H_{10}N_2O_3$	147.0763 (0.8)	152.0934 (-1.6)	145.0619 (-0.5)	150.0796 (-6.5)	Glutamine
$C_6H_9N_3O_2$	156.0766 (0.8)	162.0972 (-1.7)	154.0623 (-0.5)	160.0833 (-5.8)	Histidine
$C_9H_{11}NO_2$	166.0862 (0.5)	-	-	173.1024 (-3.0)	Phenylalanine

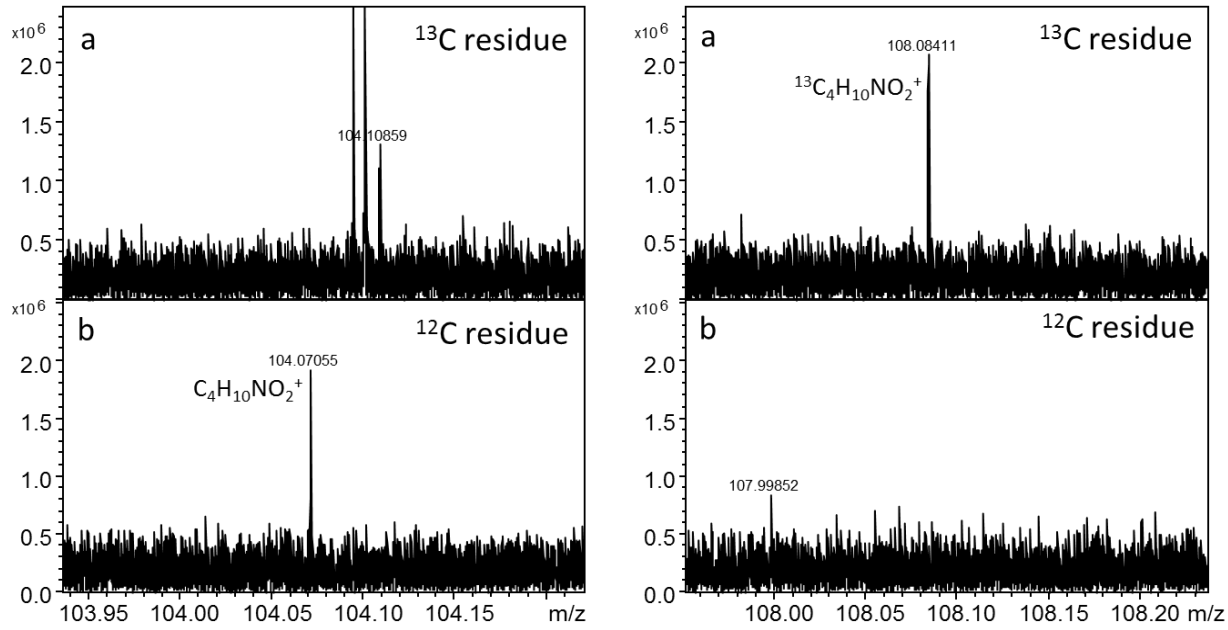

Figure 4.18 - Detections of the ion $C_4H_{10}NO_2^+$ in the ^{12}C residue (left box, panel b) and the corresponding $^{13}C_4H_{10}NO_2^+$ in the ^{13}C residue (right box, panel a). Multiple assignments are possible for this ion.

4.2.2 Analysis in the high mass-to-charge ratio range

The detection of macromolecules in laboratory residues represents an important target because of the possibility to form similar large molecules on cold grains and their following potential prebiotic implications. In Modica et al. 2012, we reported on the presence of macromolecules with masses up to 2600 amu using previous results obtained from MALDI-TOF technique by de Marcellus (2010, PhD Thesis), and the largest macromolecules reported so far have masses up to 4000 amu (Danger et al. 2013).

With the aim of searching for high mass molecules, we recorded a spectrum of the ^{12}C residue in the positive mode between m/z 1000 and 5000 (see Fig. 4.19). At these high masses, the peaks cannot be individually resolved. Moreover, the mass spectral resolution is here intentionally lowered as a compromise to increase the signal-to-noise ratio. Due to the large amount of mass spectral information, the spectrum appears as a very dense and rich ensemble of peaks which covers the whole mass range. The peak intensity distribution is asymmetric with

a large ridge around m/z 2000-2500; on the right, some repetitive patterns are present until m/z 3500 and peaks persist at least until m/z 5000. In this latter part of the spectrum the signal is rather noisy, but the comparison with the blank suggests that most of the peaks are indeed due to the residue. Moreover, a zoom in a narrow range around m/z 2500 (inset box in Fig. 4.19) shows the presence of peaks at half nominal m/z [M+0.5], clearly not present in the blank, implying the presence of double charged ions and therefore indirectly confirming the presence of ions with masses of about 5000 amu. These are the highest masses found in a laboratory residue. In the insert, the low mass resolution causes the peaks to merge and serves to better appreciate this feature, which is observed only in narrow m/z ranges. This result is interesting because, from an astrophysical point of view, macromolecules are thought to be more stable than small ones in space. The spectrum in negative mode also shows a similar distribution but with different peaks. Unfortunately the spectrum (not shown) is highly contaminated by impurities present in the solvent.

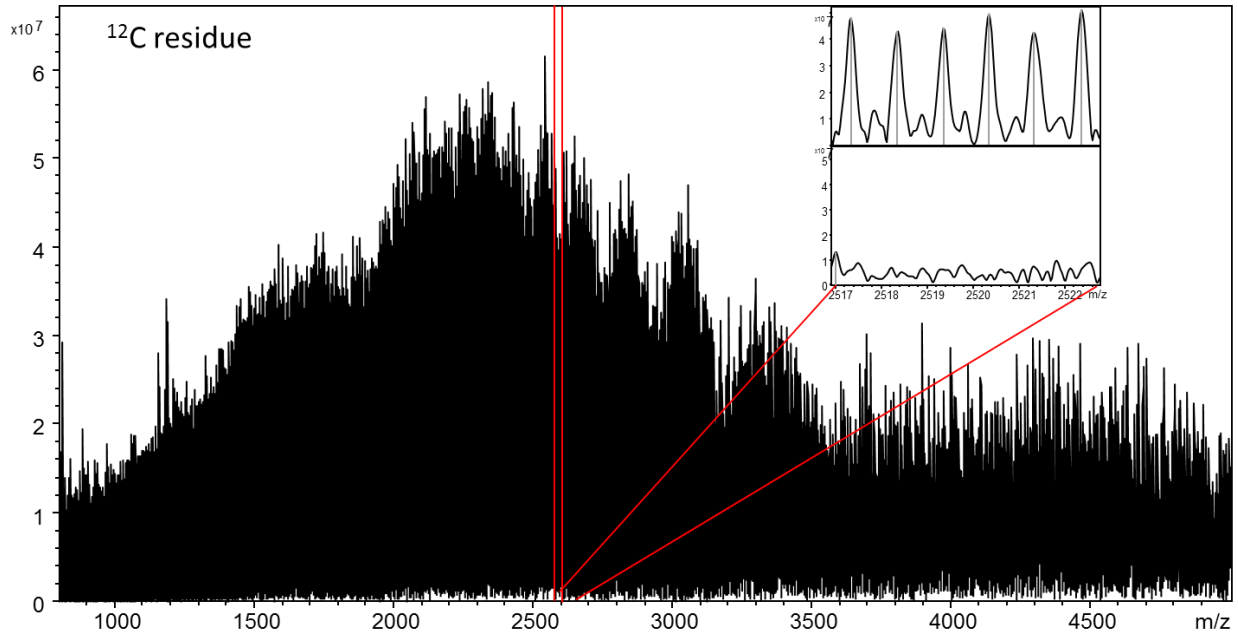

Figure 4.19 - Positive ESI FT ICR mass spectrum of the ^{12}C residue in the mass range between m/z 800-5000. The inset box is a zoom of the spectrum in the narrow mass range between m/z 250-252 showing the presence of peaks at every m/z and less intense peaks at half m/z. The corresponding blank is shown in the bottom of the box.

The reduction in the peak intensity observed before m/z 2000 seems to be related to a phenomenon of signal intensity discrimination against lower mass ions, rather than a real distribution. It is likely the result of the tuning which has been optimized to favor the transfer of high mass-to-charge ions. The smaller molecules, even if ionized in the source, are often lost during their transfer through the ion funnels, the quadrupole or in the collision cell. Therefore, the reason of their minor intensity could be the suppression of the signal due to the transfer technique which favors larger ions.

MALDI TOF analyses

In order to check our initial hypothesis of a discrimination against small molecules, a spectrum of the same sample was acquired with a different technique, Matrix-Assisted Laser Desorption/Ionization (MALDI), using a BrukerAutoflex III instrument in the same laboratory at the Institut Parisien de Chimie Moléculaire (UPMC, Université Pierre et Marie Curie, Paris).

First, we briefly report the basic principles of this technique. MALDI is a technique for protein/peptide characterization and polymer analysis. It allows the desorption of high molecular weight compounds such as organic macromolecules as intact ions. In MALDI-MS analysis, the analyte is first co-crystallized with a larger excess of a matrix compound, after which laser irradiation of this matrix-analyte preparation allows desorption of the matrix as a hot plume which carries the analyte into the gas phase (Fig. 4.20). The matrix plays a key role by strongly absorbing the laser beam energy and causing, indirectly, the analyte to vaporize. The matrix also serves as a proton donor and acceptor, acting to ionize the analyte in both positive and negative ionization modes, respectively. A TOF analyzer is used with this MALDI ionization source.

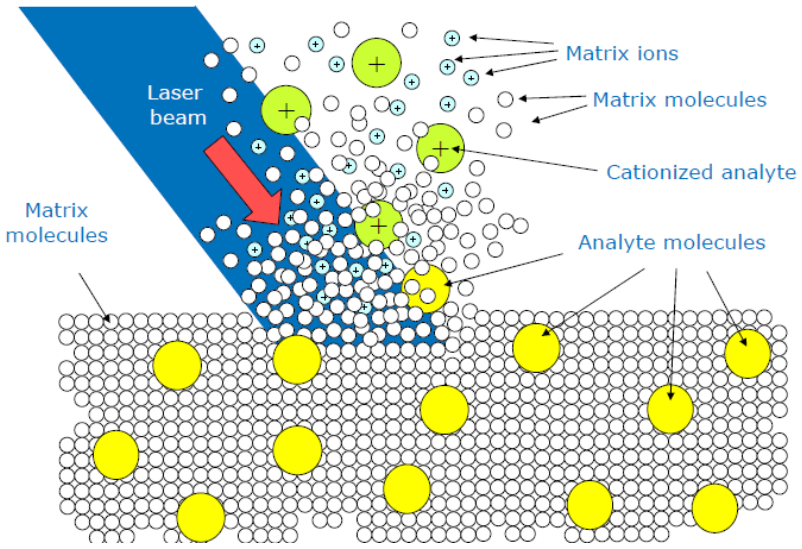

Figure 4.20 - Schematic diagram of MALDI ion source (from Bruker SolariX user's guide).

We tested two different kinds of matrix, DHB (2,5-dihydroxybenzoic acid) and HCCA (α-cyano-4-hydroxycinnamic acid) in positive and in negative ionization modes. Both matrices are used for peptides, they seem thus well-adapted for our residues. In particular, the DHB is used also for nucleotides, oligonucleotides, and oligosaccharides; the HCCA is used also for lipids and nucleotides.

After the analysis, similar results were obtained with the two matrices in terms of peak intensity distribution, confirming a similar general trend. However, with the HCCA matrix we observed more peaks at higher mass-to-charge ratios, meaning that this matrix slightly favors desorption and ionization of larger molecules with respect to the DHB matrix. Therefore, we will show a spectrum obtained with the HCCA matrix in the negative mode only.

As shown in Fig. 4.21, the peaks have a regular power-law distribution with a long right tail. Weak but significant signals are present until about m/z 4000. The spectrum is recorded until m/z 10000 but signals at these high mass ranges are too weak to be considered real. This statistical distribution shows that the spectrum is dominated by relatively low m/z peaks and that higher m/z peaks are present with decreasing intensities, as indeed it is reasonable to expect because large molecules should be statistically less abundant. This result is achieved because

MALDI technique does not discriminate excessively in mass as the FT ICR does. Finally, the intense individual peaks, out of the main regular distribution, are due to the matrix and solvent contribution which are mainly present until m/z 1100. The inset box in Fig. 4.21 is an enlargement of the spectrum at the lower masses to better show this contribution.

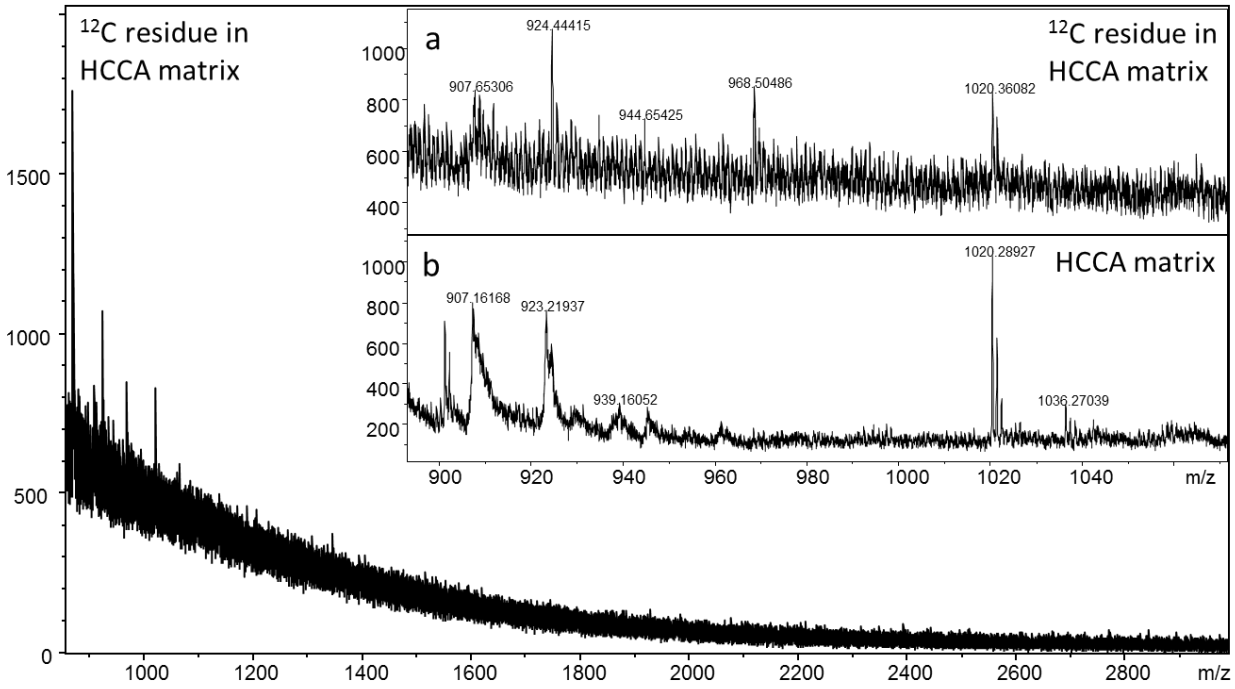

Figure 4.21 - MALDI spectrum of the ^{12}C residue obtained in negative mode with the assistance of HCCA matrix in the m/z 850-3000 range. The inset box is a zoom in the m/z 850-1070 range showing the residue spectrum with the HCCA matrix and solvent (panel a) and the HCCA matrix and solvent spectrum (panel b).

4.3 Mass defect versus mass diagrams

The intrinsic complexity of our residues leads to a large amount of mass spectral information that cannot be fully explored by simple visual inspection of the spectra. Such approach is valid when we limit ourselves to an investigation on specific molecules or class of molecules, as we have shown previously, but of course it cannot be used for a global and complete analysis of the residues.

Due to the difficulty of this task, we believe it is opportune to test an analytical approach that considers the global and non-targeted investigation of complex mass spectra by automated software tools based on statistical methods. This approach has been used successfully on FT ICR and FT Orbitrap complex mass spectra acquired on soluble organic matter of meteoritic samples (Schmitt-Kopplin et al. 2010; Orthous-Daunay 2011, PhD thesis).

In order to test this new approach, raw data were extracted from our spectra, converted to txt data and then processed thanks to the implemented software Attributor in collaboration with Roland Thissen at IPAG (Institut de Planétologie et d'Astrophysique) in Grenoble.

These data were represented by the MDvM (mass defect versus mass) diagrams, a kind of representation whose further explanations can be found in Orthous-Daunay 2011, PhD thesis. This representation allows visualizing complex mass spectra in a specific two dimensions fashion, which permits to obtain instructive information on the elements present in the samples even without any prior knowledge or assumption on the elements making the samples.

In this kind of diagrams the mass defect is plotted as a function of the measured mass-to-charge ratio (m/z) for ions observed in a mass spectrum. The mass defect is defined by the difference between the measured m/z value and its closest integer; it is therefore a decimal number ranging between -0.5 and 0.5. For instance, HMT-H^+ has a measured m/z of 141.11329 and its closest integer is 141; therefore the mass defect of this ion is 0.11329. In a MDvM diagram HMT-H^+ is represented by a point with the coordinates 141.11329, 0.11329. Its peak intensity can be qualitatively indicated by the color of the point in a color scale. In the same way, each ion peak present in a mass spectrum will correspond to only one point on this diagram.

The interest of this representation is that points corresponding to chemically related ions will align on specific directions from which chemical information can be obtained.

We selected two mass spectra obtained by FT ICR MS in positive ESI mode, one for the residue in ^{12}C and one for the residue in ^{13}C. From the raw data of these spectra we realized two MDvM diagrams which are displayed in Fig. 4.22. In both diagrams we can observe that points are arranged in a dense cloud. This cloud occupies a specific zone of the diagram because of the elements constituting the ions, in our case H, O, C, and N. In the presence of other elements, other zones would have been covered. Moreover, the defined overall orientation of the clouds (given by the respective average slopes) is due to the presence of ^{12}C or ^{13}C, respectively. It can be noted that the points are regularly distributed according to geometrical patterns in which some vertical repeated "packets" of the same width are visible. This regularity, which can be better appreciated in the ^{13}C residue, recalls the presence of the wave structures observed in Fig. 4.7 and is due to chemically related ions with a polymeric structure of different lengths. These structures are caused by different linear combination of the masses of the elements H, O, C and N that are chemically possible.

Finally, in Fig. 4.22, all points whose position falls out of the clouds are due to instrumental artifacts or impurities (as confirmed by the blanks). On the other hand, not all the points inside the clouds represent genuine signals from the residues.

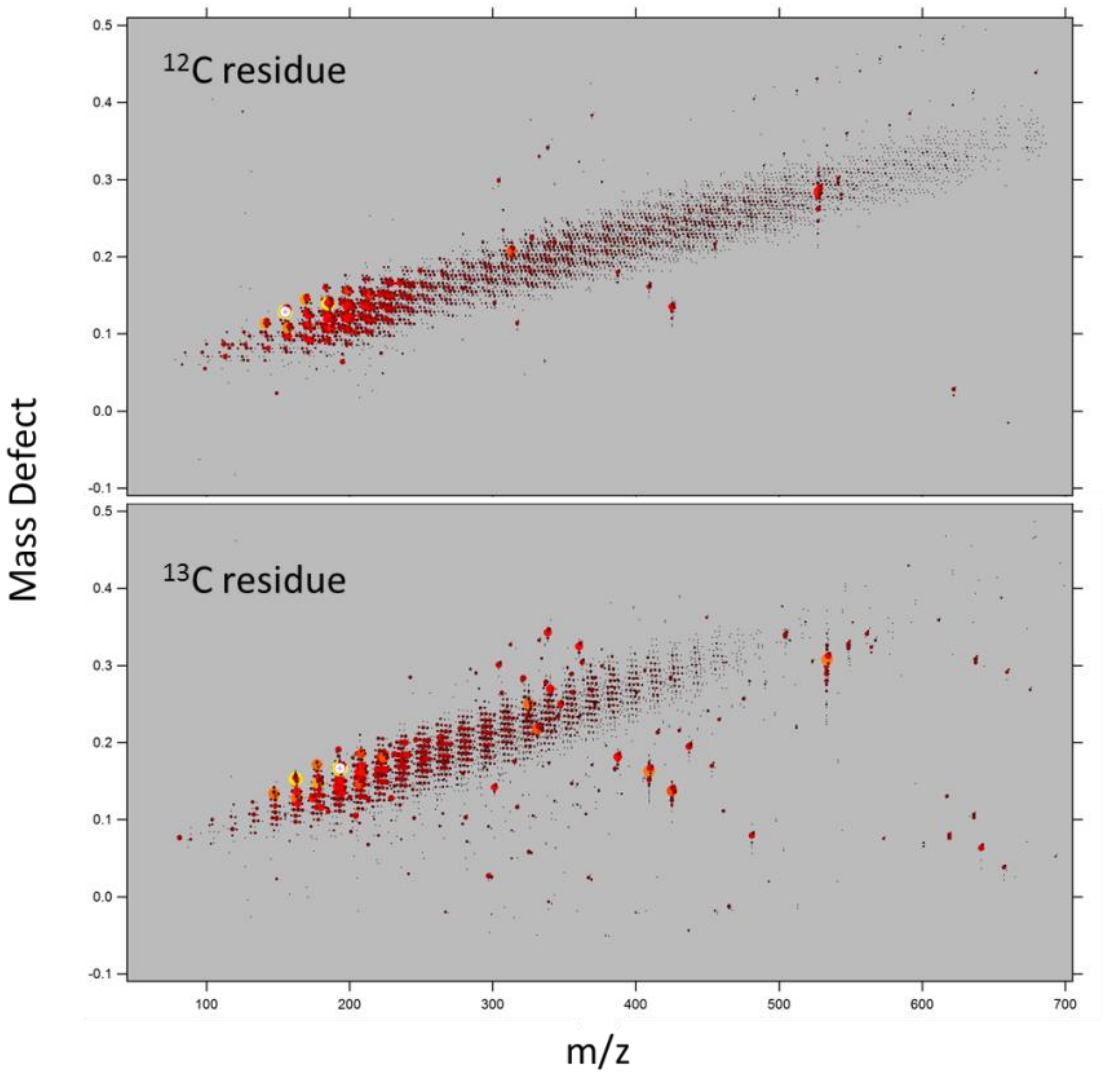

Figure 4.22 - MDvM diagrams corresponding to the ^{12}C (top box) and ^{13}C (bottom box) residues in positive ESI mode at low and medium masses.

In order to reduce as much as possible the undesired signals, data were processed with the software Attributor to discard the signals from instrumental artifacts, noise, and pollutions. The application of this filtering procedure was feasible only in the case of the ^{13}C residue because of its better conditions of calibration. Unexpectedly, this procedure revealed the presence of numerous “ghost” peaks that can be considered as instrumental artifacts due to system non-ideality or distortions in the detection system. They manifested in the mass spectra as side-

shifted peaks preceding real peaks of the residues and harmonic peaks with decreasing intensity, present on both sides of the most intense real peaks. These problems, known to occur in typical ICR analysis, are difficult to avoid and unfortunately the software processing with Attributor could not eliminate them. After the data treatment, the number of points in the MDvM diagrams are considerably reduced (Fig. 4.23). They better represent the chemically significant species only, but the persistence of the above mentioned problems does not allow us to proceed with further studies, which could be planned in the future but are well beyond the investigations of this PhD thesis.

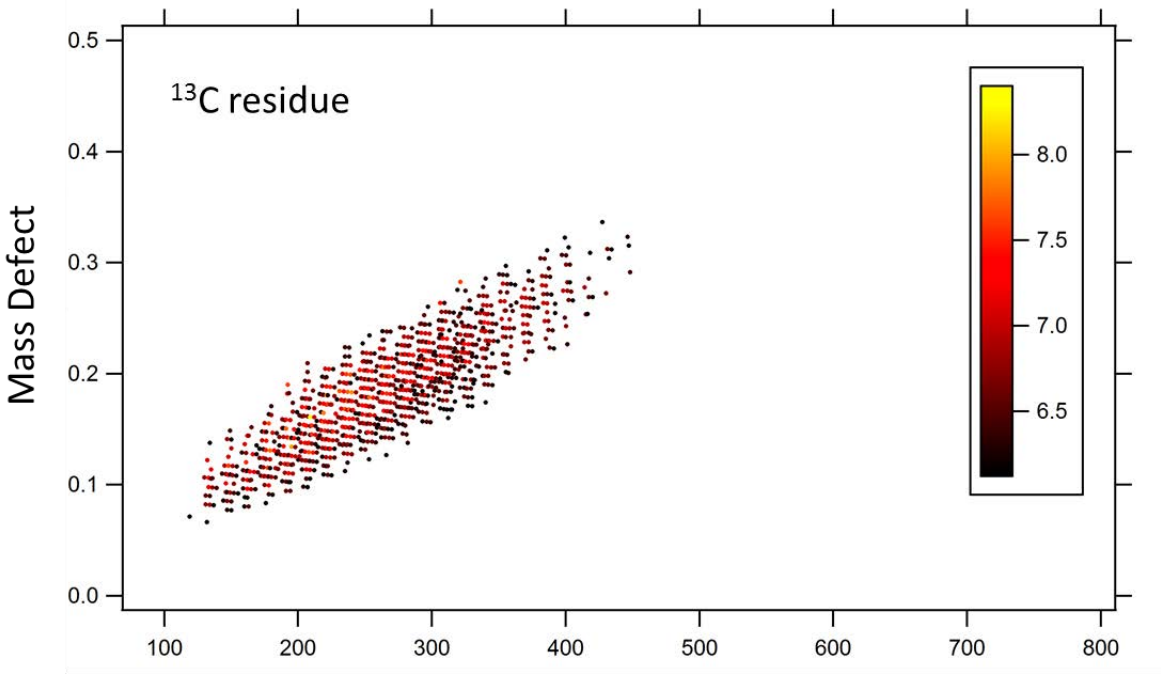

Figure 4.23 - MDvD diagram for the ^{13}C residue after partial removing of the undesired signals. The different colors represent the intensity of the corresponding peak.

In order to fight the occurrence of “ghost” peaks in FT ICR MS, there are several known ways. One is based on optimizing the hardware by designing an “ideal” detection system, which however is virtually impossible. Another one is based on software processing to remove the ghost peaks in the final mass spectra, which however could eliminate also important information. A further non-conventional way is based on a deconvolution procedure which is able to identify and eliminate ghost peaks directly in the frequency spectrum following the patent

deposited by Misharin & Zubarev (2012). In the next future, the more appropriate of these solutions will be applied to the FT ICR system. Once the problem is solved, new and better data could be acquired first on residues and then on Paris meteoritic soluble organic matter, a material expected to provide much complex FT ICR spectra. Data of higher quality for both samples could generate MDvM diagrams constituted of chemically significant points. From them, important information on the composition of the molecules present could be obtained and also permit their comparison. For this work we plan to use similar methods used to characterize Murchison (Schmitt-Kopplin et al. 2010) and Renazzo meteoritic soluble organic matter (Orthous-Daunay 2011, PhD Thesis).

4.4 Conclusions

In this work, we used the FT ICR mass spectrometry to analyze our laboratory residues produced by the UV irradiation of simple mixtures made from only three starting components (H_2O, CH_3OH, NH_3) in the form of ices, followed by warm-up. FT ICR analysis has shown the extreme complexity and the high diversity of the molecular content of the final organic residues, confirming the efficiency of photo- and thermo-chemistry in the synthesis of a high variety of complex organic molecules. Among these molecules, which have a polymeric structure, we have searched for HMT and HMT based molecules. We confirmed their identification by means of the fragmentation patterns and proposed the identification of three additional members of the same HMT family, including the possible covalent dimer of HMT. We also searched for free amino acids, already detected by other methods in similar residues, and reported the tentative identification of 13 peaks although from this method only, it is not possible to distinguish between the different isomers. We observed a decreasing distribution of molecules from low to high molecular masses (by MALDI MS) and deduced that molecules of up to 5000 amu should be also present (by FT ICR MS). Finally, we attempted a different approach based on statistical tools which unfortunately did not turn out applicable to our current data on residues. Therefore, we could not compare the residue data with the meteoritic ones. This comparison will be done in the next chapter, focusing on amino acids where we use a classical method (GC-MS), widely employed for this kind of analysis.

Chapter 5

The amino acid content in the Paris meteorite and in laboratory residues

Contents

In this chapter, after an introduction to carbonaceous chondrites, we present the Paris meteorites, a CM chondrite reported to be the least aqueously altered meteorite of its class. We analyze the amino acid content of this meteorite by gas chromatography mass spectrometry (GC MS) and discuss their distribution in the perspective of a low degree of aqueous alteration, comparing our results with those present in the literature for other CM chondrites. Glavin & Dworkin (2009) have suggested a correlation between the degree of aqueous alteration and the L-enantiomeric excess (ee_L) of isovaline found in several meteorites, with the lower ee_L found in the less aqueously altered meteorites. We measure the ee_L for several chiral amino acids and, in the specific case of isovaline, we compare these ee_L values with values present in the literature

to check if this correlation can be supported. In the second part of this work, following the same gas chromatographic techniques, we analyze the amino acid content of two laboratory residues and evidence their similarities with the results reported for Paris and other pristine meteorites.

This work is realized in collaboration with Dr Zita Martins (Department of Earth Science & Engineering, Imperial College, London). Part of this work is the object of a paper (Martins et al. 2015) which is accepted for publication in *Meteoritics & Planetary Science*.

5.1 Carbonaceous chondrites

5.1.1 Classification

Carbonaceous chondrites are primitive and undifferentiated meteorites whose parent bodies formed during, or shortly after, the birth of the Solar System (Allègre et al. 1995). They contain significant amounts of carbon, a characteristic that contributes to a generally dark appearance.

According to their compositions, carbonaceous chondrites are divided in seven different groups: CI, CM, CR, CO, CV, CK, and CH. The first letter refers to the group, the second one to a prominent meteorite in the group (e.g. in CI, C stands for carbonaceous, I stands for Ivuna), apart for the CH (H stands for high metal). Additionally, there are a few carbonaceous chondrites that cannot be classified according to their chemical and mineralogical composition, the ungrouped chondrites (e.g. the Antarctic meteorite LEW85332).

Several groups of carbonaceous chondrites, notably the CM and CI groups, contain high percentages of carbon. Carbon is present in different forms, including graphite (0.005%), diamonds (0.04%), carbonates (0.2%), and organic matter (2%) (Sephton 2002). The chemical composition of carbonaceous chondrites matches the elemental chemistry of the Sun more closely than any other class of chondrites, a characteristic particularly noticeable in the CI group (Ringwood 1979). The presence of volatile organic compounds and water indicates that they have not undergone significant heating (>200°C) since they formed. Another characteristic is the presence of hydrous minerals that were formed at low temperature by liquid water from original anhydrous minerals.

In their parent body, chondrites experienced different degrees of processing due to aqueous alteration and thermal metamorphism. Aqueous alteration is the transformation of the original minerals into new assemblages caused by reactions at low temperature with liquid water. These minerals are phyllosilicates, which can be associated to carbonates, sulphates, oxides or secondary sulphurs (Zolensky & McSween 1988; Brearley 2005). Thermal metamorphism is the modification of the minerals after the increased temperature caused by radioactive decay of short-lived nuclides such as ^{26}Al or ^{60}Fe (McSween et al. 1988).

Chondrites can be classified into groups according to their chemical composition (primary characteristic) and also by their degree of processing (secondary characteristic) which includes aqueous alteration (petrographic types 1 and 2) and thermal metamorphism (petrographic types 3 through 6) (Fig. 5.1). Type 3 is thought to represent the most pristine materials. Combined with the degree of processing, carbonaceous chondrites are classified as CM1 or CM2, CR1 and CR2, and so on.

CM chondrites exhibit a number of changes in textures, petrographic characteristics and mineralogy with increasing degrees of aqueous alteration. In order to take into account this variability, which correlates with progressive alteration, a new classification scheme for CM chondrites introduces petrologic subtypes ranging from 2.6 (for the least aqueously altered CM chondrites examined) to 2.0 (for highly altered chondrites) (Rubin et al. 2007). The subtype 2.0 of this new classification includes all chondrites previously classified as CM1.

Two additional sources of alteration can affect the meteorites: shock metamorphism and weathering. Shock metamorphism is a measure of the degree of fracturing of the matrix, due to collisions in space; weathering is a measure of terrestrial alterations which can affect metals and silicates.

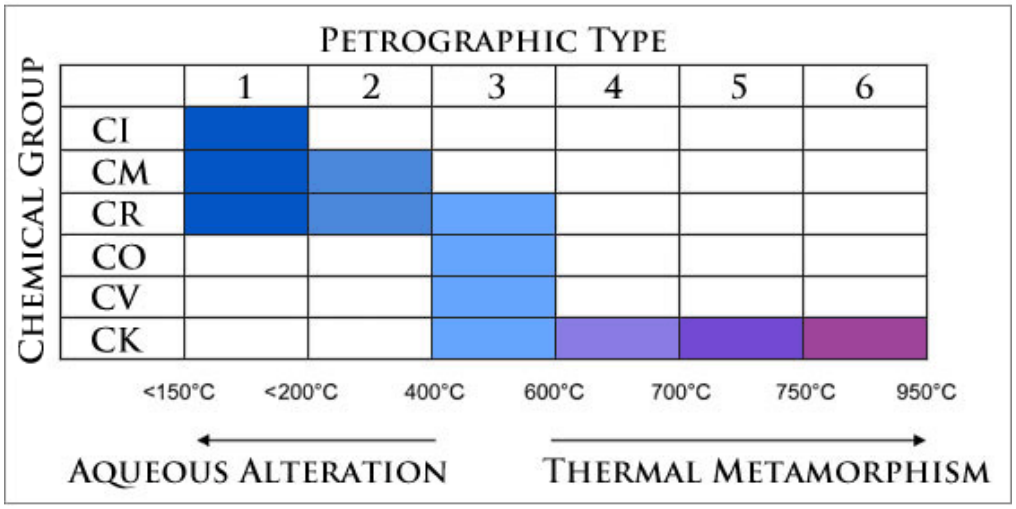

Figure 5.1 - Classification of carbonaceous chondrites based on their chemical type and degree of processing (petrologic type). Colored boxes show currently known carbonaceous chondrites. Darker blue colors represent more aqueous alteration and redder colors represent increased thermal metamorphism. Temperatures corresponding to different petrographic types are also indicated (adapted from Sephton 2002).

5.1.2 Organic matter content

Any organic compounds contained in carbonaceous chondrites represent a perfect example of molecules formed without biochemistry, being antecedent to the first biochemical processes arisen on Earth.

Carbonaceous chondrites contain up to 2% of organic carbon (Sephton 2002; Botta & Bada 2002), divided in soluble and insoluble fraction.

- The soluble fraction constitutes about 30% of the organic carbon; it can be isolated by treating the meteorite sample with common organic solvents of different polarities, mainly water and methanol. It is also called “SOM” for soluble organic matter.
- The insoluble fraction, which constitutes the remaining 70%, is composed of macromolecular material (Cody & Alexander 2005) that can be isolated after removing

silicates and carbonates (inorganic carbon) by pyrolysis at 500 °C with hydrochloric acid and hydrofluoric acid, respectively. It is also called “IOM” for insoluble organic matter.

Only the soluble fraction will be considered and analyzed in this thesis because our laboratory organic residues are also almost totally soluble in water and methanol and show some possible similarities with meteoritic SOM in their structure and, more importantly, in their composition.

Carbonaceous chondrites have a rich organic inventory. Organic compounds that have been identified include: carboxylic acids (e.g. Lawless & Yuen 1979; Yuen et al. 1984), amino acids (e.g. Cronin & Pizzarello 1983; Cronin et al. 1988; Cronin & Chang 1993), diamino acids (Meierhenrich et al. 2004), aliphatic and aromatic hydrocarbons (Kvenvolden et al. 1970; Pering & Ponnaperuma 1971; Hahn et al. 1988; Sephton et al. 1998) amines and amides (e.g. Jungclaus et al. 1976); alcohols (e.g. Jungclaus et al. 1976), aldehydes and ketones (Cronin & Chang 1993), sulphonic and phosphonic acids (Cooper et al. 1992).

The most extensively studied meteorites for organic compounds include the CM Murchison (fell in 1969 in Australia), the CM2 Murray (1950, USA), the CI Orgueil (1864, France), and the C2 ungrouped Tagish Lake (2000, Canada). In particular, the fall of Murchison provided a huge amount of sample (approximatively 100 kg) in a good state of preservation (Oró 1971).

Amino acids in carbonaceous chondrites

Amino acids are the first class of compounds possibly related to the origin of life that were unambiguously identified and quantified in Murchison just after its fall (Kvenvolden et al. 1970). Today, among the distinct groups of carbonaceous chondrites, five of them (CI, CM, CR, CO, CV) have been reported to contain extraterrestrial amino acids (Burton et al. 2012). More than 80 amino acids, ranging from two to nine carbon atoms, have been identified in carbonaceous meteorites, most of them in the CM Murchison (Cronin et al. 1988; Cronin & Chang 1993). Only few of these amino acids such as glycine, alanine, aspartic acid, glutamic acid, valine, leucine, isoleucine, and proline are the same as those used by living organisms as constituents of

proteins (α-amino acids). A few others, including β-alanine, α-amino-isobutyric acid (α-AIB), isovaline, have a restricted biological occurrence on the Earth, e.g. as components of bacterial cell walls. All the others are found only in meteorites; they can exist on Earth, but only after laboratory synthesis.

The observation of so many amino acids rare or unknown in the terrestrial biosphere is a strong argument for their extraterrestrial origin. Moreover, the presence of racemic chiral amino acids, the enrichment in heavy isotopes of hydrogen, carbon and nitrogen, and their complete structural diversity are powerful criteria for determining their extraterrestrial origin (e.g. Cronin et al. 1993).

The total amino acid abundances are the highest in the most primitive (least altered) CR2 and CR3 chondrites (Martins et al. 2006) and seem significantly lower in the more aqueously altered CI, CM, and CR type 1 chondrites (Glavin et al. 2010) as well as in thermally altered CO and CV chondrites (Burton et al. 2012). Moreover, the CM and CR carbonaceous chondrites contain predominantly α-amino acids, while CI, CO, CV carbonaceous chondrites contain high abundances of γ- and δ-amino acids (Glavin et al. 2010; Burton et al. 2012). Every possible isomeric form of a certain amino acid is present in meteorites with the abundances tending to decrease as the carbon number increases (Cronin & Pizzarello 1986). Additional characteristic includes the predominance in abundance of branched carbon chain isomers over straight ones (Sephton & Botta 2008). Diamino acids have also been detected in the Murchison meteorite (Meierhenrich et al. 2004).

5.1.3 The Paris meteorite

The Paris meteorite is a fresh stone weighing 1.3 kg and covered with a very black shiny fusion crust. It belonged to Jacques Corré, who purchased a box lot of African statuettes in 2001 in an auction in the Hotel-Drouot in Paris. He discovered a black stone hidden in the box and kept it for 7 years. The stone was later identified as a meteorite by G. Cornen of the University of

Nantes. In 2008, this meteorite was then acquired by the Muséum National d'Histoire Naturelle (MNHN, Paris) and officially named “Paris” (Hewins et al. 2014).

Based on the fresh black fusion crust and its Na/K ratio, it was suggested that Paris is an observed fall collected immediately after and was not exposed to rain (Haack et al. 2012; Hewins et al. 2014). The Paris meteorite shows almost no signs of terrestrial weathering (Bourot-Denise et al. 2010; Zanda et al. 2010, 2011) or shock, given that chondrules are perfectly spherical. Analyses of the petrography, oxygen isotopic distribution, and bulk, elementary and organic composition of a few fragments are in agreement with a CM chondrite assignment (Bourot-Denise et al. 2010; Zanda et al. 2011). A CH_2/CH_3 ratio of 2.2 ± 0.2 obtained by infrared spectroscopy is also in good agreement with that of the CM meteorite Murchison (Merouane et al. 2012). The carbonaceous matrix is not as abundant as in other CM meteorites (71% in the low matrix-rich Murchison) and constitutes about 66% of the volume (Bourot-Denise et al. 2010). Paris is composed of two different lithologies, one less aqueously altered (about 40%) and one more altered (the remaining 60%) (Zanda et al. 2010, 2011).

Figure 5.2 - The CM chondrite Paris showing its fresh black fusion crust (credit MNHN).

Blanchard et al. (2011) suggested that Paris is one of the least altered CM chondrites on the hydrothermal scale designated by Rubin et al. (2007), being a CM2.7 or CM2.8. In particular, a significant contribution of FeNi metal in the matrix confirms that Paris has experienced much less aqueous alteration than other CM chondrites (Caillet Komorowski et al. 2011; Cournede et al. 2011). Moreover, its aromatic component, metal and sulphide compositions, and petrographic relationships suggest that only low temperature metamorphism occurred in the meteorite parent body after accretion (Bourot-Denise et al. 2010; Caillet Komorowski et al. 2011; Kimura et al. 2011; Merouane et al. 2012). Therefore, on the basis of the thermal metamorphism experienced, Blanchard (2011) proposed Paris to be a CM2.7/2.8 A/B chondrites, the A/B letters referring to low thermal metamorphism. The recent comparison between the IR spectra of some micron-sized fragments of Paris and the spectra from solid-state materials in molecular clouds points to a rather primitive origin for the organic matter in this meteorite (Merouane et al. 2012).

5.2 Analytical procedures

Analyses were performed by Dr. Zita Martins at the Faculty of Engineering, Department of Earth Science & Engineering, Imperial College (London).

Chemicals and tools

All chemicals (>99% purity) were purchased from Sigma-Aldrich, except the AG® 50W-X8 cation exchange resin (100-200 mesh, from Bio-Rad), ammonium hydroxide (28–30 wt%, puriss. p.a., from Acros Organics), D- and L-isovaline standards (>99% purity, from Acros Organics), trifluorocetic anhydride/isopropanol (TFAA-IPA) derivatization kit (from Alltech), sodium hydroxide (>99% purity, from Boom) and hydrochloric acid (37%, ≤5 ppm extractable organic substances, from Boom). All glassware and sample handling tools were wrapped in aluminium foil, and then heated in an oven at 500 °C for 3 hours.

Sample preparation

Two interior chips without fusion crust of the Paris meteorite (199.8 mg for sample 1 and 102.9 mg for sample 2) were provided by the Muséum National d'Histoire Naturelle (MNHN), Paris,

France. A sample of serpentinite (hydrated magnesium silicate) provided by the Natural History Museum Bern, was heated to 500°C for 3 hours, subjected to the same experimental procedure as the meteorite samples and used as a procedural blank. The two fragments of Paris and the sample of serpentinite were separately crushed and homogenized into powder using new ceramic mortars and pestles in a laminar flow cabinet.

5.2.1 Amino acid extraction and derivatization

The two powder samples of the Paris meteorite and the two powder samples of serpentine control blank were analyzed using the optimized procedure for extracting, derivatizing and analyzing amino acids in meteorites (Kvenvolden et al. 1970; Tsugita et al. 1987; Keil & Kirchman 1991; Glavin et al. 1999, Martins et al. 2007; Martins et al. 2013). Each one of the powdered samples was placed inside a Pyrex test tube together with 1 ml of HPLC grade water, flame sealed and heated for 24 hours at 100 °C. One of two equal parts of the water supernatants of each sample was subjected to a 6 M HCl acid vapor hydrolysis (150 °C for 3 h). The non-hydrolyzed fraction (containing only the free amino acids) and the acid-hydrolyzed fraction (containing the free plus the bound amino acids) hot-water extracts were desalted on a cation exchange resin and the amino acids eluted with 5 ml of 2 M ammonium hydroxide. The eluates were dried under vacuum and derivatized with TFAA-IPA.

The hydrolyzed and non-hydrolyzed fractions of sample 1 of the meteorite and one of the serpentine blank controls were analyzed by GC-MS (Agilent 7673 series injector, Agilent 6890 series GC equipped with an Agilent 5973 inert mass selective detector; MS quad set to 150 °C, MS source to 230 °C, and injection port and the MSD transfer line set to 220 ºC). Separation of the D, L-amino acid enantiomers was achieved using a Chirasil-L-Val column (50 m x 0.25 mm ID x 16 µm film thickness) from Alltech, except for the D- and L-isovaline enantiomers, which could not be separated under these chromatographic conditions. Helium was used as carrier gas with a flow of 1 ml/min. The oven program was held for 5 mins at 65 ºC, increased by 2 ºC/min to 80 ºC and held for 5 mins, increased to 100 ºC by 1 ºC/min, increased to 200 ºC by 2 ºC/min and held for 10 mins, and finally increased by 10 ºC/min to 220 ºC and held for 5 mins.

Separation of the D, L-isovaline amino acid enantiomers was achieved by using a Chirasil-Dex CB column (25 m x 0.25 mm, 0.25 μm thickness) from Varian, on the hydrolyzed fraction of sample 2 of the Paris meteorite and on the second serpentine blank control sample, according to the method of Pizzarello et al. (2008). Separation of these two amino acid enantiomers was obtained by using a Perkin Elmer Clarus SQ8S MS and a Clarus 580 GC, with a helium flow of 0.6 ml/min. The oven program was held for 7 mins at 65 ºC, increased by 2 ºC/min to 85 ºC, increased to 200 ºC by 4 ºC/min, and held for 90 mins. The elution times of the derivatized isovaline enantiomers on the Chirasil-Dex CB column were established to be L-isovaline followed by D-isovaline by running individual isovaline pure (D and L) standards.

The amino acids were identified by comparison of the retention times and the mass fragmentation pattern with known amino acids standard mixtures. Single ions were used to identify and quantify the amino acid content of the meteoritic sample and are shown in the Appendix (Table 1). Amino acids were quantified by peak area integration of the corresponding ion fragment after background level correction using the serpentine blank.

5.3 Results and discussion

5.3.1 Amino acid content in the Paris meteorite

We have obtained the amino acid content of both the non-hydrolyzed and acid-hydrolyzed hot water extracts of Paris sample 1. The corresponding selected ion GC-MS chromatograms are shown in Fig. 5.3 and Fig. 5.4, the identification of the peaks is given in the Appendix (Table 1). The serpentine blank does not display any amino acid above the detection limit of the GC-MS (10 pg of amino acids) and is shown in the Appendix (Fig. 1).

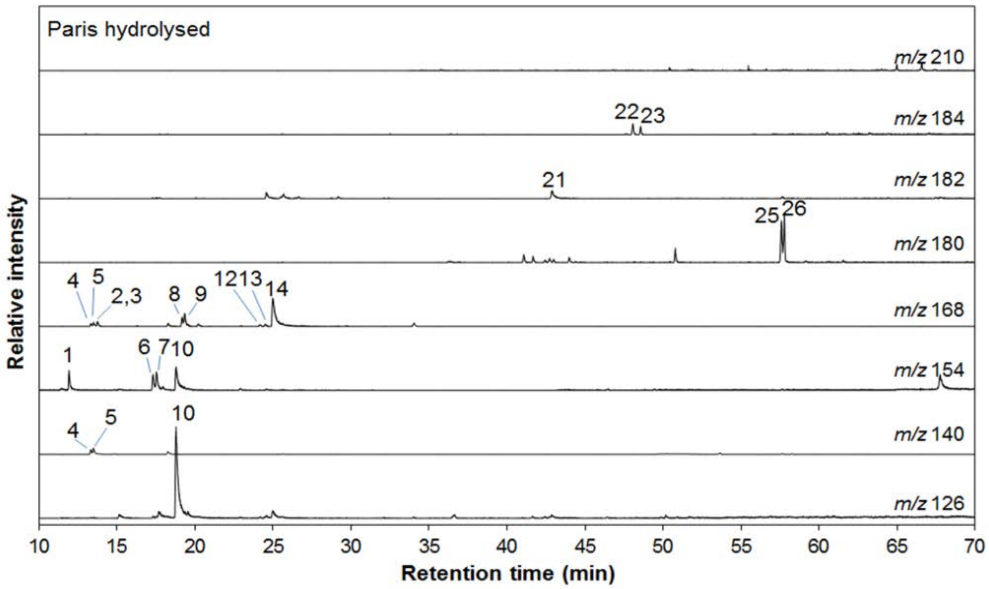

Figure 5.3 - The 10 to 70 min region of the single ion GC-MS traces of the derivatized and hydrolyzed hot-water extracts of the Paris meteorite (from Martins et al. 2015). The identification of the peaks is given in the Appendix (Table 1).

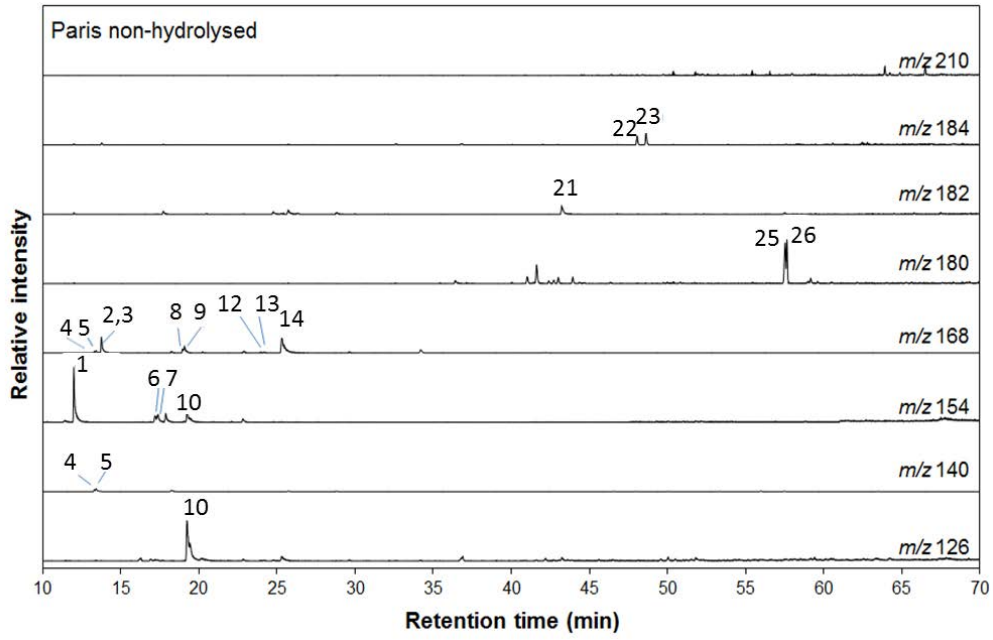

Figure 5.4 - The 10 to 70 min region of the single ion GC-MS traces of the derivatized non-hydrolyzed hot-water extracts of the Paris meteorite (from Martins et al. 2015). The identification of the peaks is given in the Appendix (Table 1).

The abundances of the amino acids of the non-hydrolyzed and acid-hydrolyzed fractions of sample 1 are displayed in Table 5.1. The associated errors are based on the standard deviation of the average value of eight to nine separate measurements. Optically pure α-ABA standards were not available for enantiomeric identification. Therefore, the order of elution of D-α-ABA and L-α-ABA is only tentatively assigned, considering that when using a Chirasil-L-Val column the D-enantiomer of all other amino acids elutes first followed by the L-enantiomer. Quantifications for the separated D-α-ABA and L-α-ABA are indicated in italic between parentheses in Table 5.1.

The non-hydrolyzed fraction of the Paris meteorite has a total amino acid abundance (free amino acids) of 7060 parts-per-billion (ppb), while the hydrolyzed fraction has a total amino acid abundance (free and bound amino acids) of 15760 ppb (abundances are rounded to the tens place). Thus, the percentage of free amino acids in the hydrolyzed fraction corresponds to 45% of the total (free and bound) amino acid abundance. This is a typical value for CM chondrites in which free amino acids contribute with 40% to 50% of the total amino acid abundance (Shimoyama & Ogasawara 2002; Glavin et al. 2006, 2011; Botta et al. 2007). The most abundant amino acids in both fractions are α-amino acids (mainly linear and dicarboxylic), followed by β-amino acids and γ-amino acids. Linear α-amino acids are the most abundant fraction of α-amino acids and include glycine, L-alanine, D-alanine, L,D-α-ABA (α-amino-*n*-butyric acid), L-norvaline, and D-norvaline. The amino acids D-norleucine, L-norleucine, D-leucine, L-leucine, D-β-ABA, L-β-ABA, D,L-β-AIB and EACA are not detected above the detection limit of the GC-MS. It has to be noted that the comparison between the non-hydrolyzed and the hydrolyzed fraction shows that the hydrolysis protocol *does not affect* the composition and relative abundances of the detected amino acids.

Table 5.1 - Individual and total amino acid abundances (in ppb) in the non-hydrolyzed and hydrolyzed fractions of Paris meteorite measured by GC-MS in sample 1 (from Martins et al. 2015).

Amino acid	Non-hydrolyzed fraction	Hydrolyzed fraction
Linear α-amino acids	*$R\text{-}CH(NH_2)\text{-}COOH$*	
Glycine	3380 ± 146	8252 ± 369
D-Alanine	296 ± 8	710 ± 32
L-Alanine	433 ± 43	961 ± 46
D,L-α-ABA	121 ± 4	306 ± 7
(D-α-ABA)	*(58 ± 3)*	*(145 ± 14)*
(L-α-ABA)	*(63 ± 4)*	*(161 ± 4)*
D-Norvaline	<30	155 ± 3
L-Norvaline	<50	178 ± 6
2-methyl α-amino acids	*$R\text{-}C(CH_3)(NH_2)\text{-}COOH$*	
α-AIB	87 ± 6	312 ± 10
D,L-Isovaline	26 ± 2	117 ± 4
Other branched α-amino acids	*$R\text{-}CH(CH_3)\text{-}(R)CH(NH_2)\text{-}COOH$*	
D-Valine	218 ± 8	574 ± 14
L-Valine	226 ± 28	614 ± 23
Non-α-amino acids	*$R\text{-}CH_2(NH_2)\text{-}R\text{-}COOH$*	
β-Alanine	620 ± 28	1250 ± 152
γ-ABA	126 ± 10	185 ± 23
Dicarboxylic α-amino acids	*$HOOC\text{-}R\text{-}CH(NH_2)\text{-}R\text{-}COOH$*	
D-Aspartic acid	89 ± 4	135 ± 5
L-Aspartic acid	120 ± 7	199 ± 5
D-Glutamic acid	600 ± 48	828 ± 54
L-Glutamic acid	720 ± 45	981 ± 80
Total abundance	**7060**	**15760**

We have plotted in Fig. 5.5 the linear α-amino acid abundances versus increasing carbon number from glycine (C2) to norleucine (C6), for several CM chondrites (whenever data were available). These include the CM2.7/2.8 chondrite Paris (this study, hydrothermal classification proposed by Bourot-Denise et al. 2010), the CM2.5 Murchison, the CM2.4/2.5 Murray, the CM2.4 Y-791198, the CM2.2 Nogoya, the CM2 LON 94192, and the CM2.0 MET 01070 and SCO 06043 (Ehrenfreund et al. 2001a; Botta et al. 2002; Shimoyama & Ogasawara 2002; Rubin et al. 2007; Glavin et al. 2011). Norleucine was not detected above the detection limit of the GC-

MS in Paris. All these considered CMs (Paris included) follow the same trend, with decreasing amino acid concentrations with increasing carbon number from glycine (C2) to norleucine (C6).

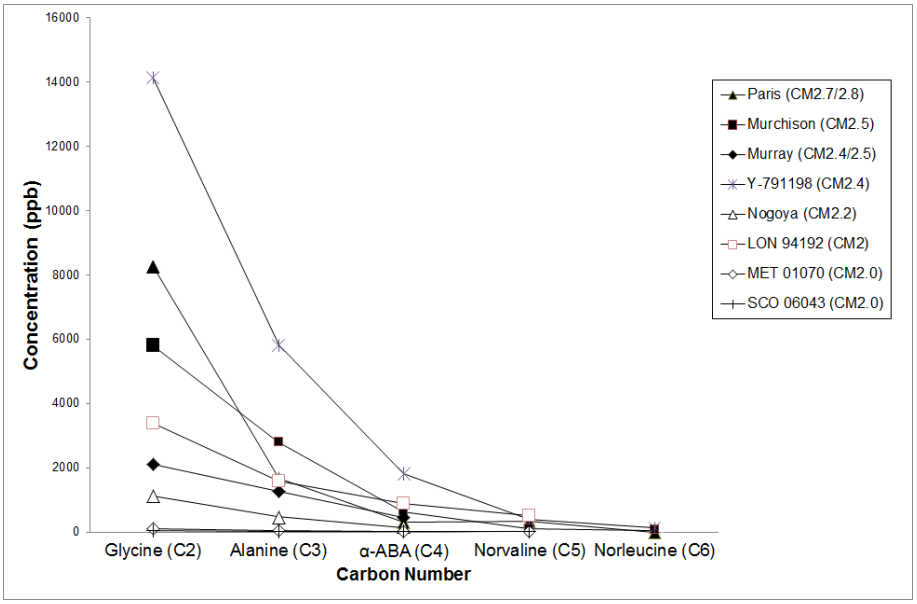

Figure 5.5 - Plot of linear α-amino acid concentrations (in ppb) versus carbon number for the CM chondrites Y-791198 (asterisk), Paris (black triangle), Murchison (black square), Murray (black diamond), Nogoya (white triangle), LON 94102 (white square), MET 01070 (white diamond), and SCO 06043 (line).

Formation of meteoritic amino acids

The precise mechanisms for the formation of amino acids, as well as other complex organic molecules found in meteorites are not well understood. Moreover, it is not clear if these molecules formed within the meteoritic parent bodies or in the materials from which the parent bodies originated. It has been suggested that amino acids formed within meteoritic parent bodies (Peltzer & Bada 1978; Peltzer et al. 1984; Cronin & Chang 1993; Cronin et al. 1995; Ehrenfreund et al. 2001a) via the Strecker synthesis, a reaction in liquid water between hydrogen cyanide (HCN), ammonia (NH_3), and an aldehyde (RCHO). However, the Strecker synthesis cannot explain the formation of beta amino acids and, in this case, a Michael addition synthesis has to be invoked (Ehrenfreund et al. 2001a; Glavin & Dworkin 2009). Moreover, the Strecker synthesis cannot explain the isotopic enrichments of amino acids in Murchison and

other CM2 carbonaceous chondrites, which strongly suggest an interstellar heritage for these compounds (Pizzarello et al. 1991, 1994; Pizzarello & Huang 2005).

These inconsistencies lead to questions about other potential mechanisms of formation for meteoritic amino acids. As shown by laboratory simulations, UV photochemistry in ices is well known to generate reactive ions and radicals (d'Hendecourt et al. 1982, 1986; Elsila et al. 2007). These species are thought to diffuse and react with neighboring molecules, allowing for the formation of molecules originally not present in the ices. Subsequent recombination reactions, favored by thermo-processes, lead to the final formation of organic residues. These residues contain a long list of organic molecules, including numerous amino acids (Bernstein et al. 2002; Muñoz Caro et al. 2002; Nuevo et al. 2008; Meinert et al. 2012; Modica et al. 2014), and also macromolecules (Danger et al. 2013), the precise structure of which being still unknown. Subsequent acid hydrolysis of the macromolecules favors the release of amino acids from peptidic bond cleavages, as evidenced by Nuevo et al. (2008) and Meinert et al. (2012).

These observations suggest that these amino acids have originally been part of polymeric molecules of higher molecular masses (Takano et al. 2007) and released as free amino acids and diamino acids after the acid hydrolysis. It is important to underline the significant abundance and diversity of amino acids (α, β, γ, and δ amino acids and L and D enantiomers) and diamino acids found in the hydrolyzed residues (Meinert et al. 2012), similarly to what found in meteoritic amino acids in which every possible structural and optical isomers are present. Moreover, it is interesting to note the presence of free amino acids, detected without hydrolysis (Nuevo et al. 2008). This is similar to what is reported in analyses of meteoritic materials where the absolute abundance of amino acids is enhanced by acid hydrolysis (Cronin 1976). In our analyses of Paris, for example, acid hydrolysis increases the amount of free amino acids by a factor 2.

A possible formation mechanism for complex organic molecules in space, included amino acids, considers a process in which these molecules formed in molecular clouds and/or in the solar nebula from UV irradiation and thermo-processing of icy grains. Recently, Ciesla & Sandford (2012) investigated the production of organics within the solar nebula. They modeled the paths of icy grains through the protoplanetary disk in environments exposed to UV irradiation and

thermal warming, in the same conditions shown to produce organics in laboratory experiments. They state that the solar nebula represented an ideal environment to form complex organic molecules, where at least ~5% of the mass of ices could be converted to organics, and predict that amino acids would also be formed in this global process.

In support of this hypothesis, Elsila et al. (2007) observed that amino acid formation in photo- and thermo-chemistry of ice analogs occurs via multiple pathways, some major and many minor others existing as well. For example, although HCN appears to be necessary for the major pathway, amino acids such as glycine may still be formed in the absence of HCN. The pathways observed do not match mechanistic predictions such as a Strecker-type synthesis (Bernstein et al. 2002) or specific radical-radical mechanisms (Woon 2002). The observation of multiple pathways suggests that the formation of amino acids in ice analogs is not rigidly dependent on a precise ice composition, but may occur under a variety of conditions. In the astrophysical context, these conditions could be met within dense molecular clouds or at the edge of protostars. If amino acids do form in a variety of presolar ices, they may contribute to the inventory of compounds detected in Murchison and other carbonaceous meteorites.

Amino acid distribution

Aqueous alteration on the meteorite parent body of CM chondrites was an important alteration process for their mineral, isotopic and volatile contents (Clayton & Mayeda 1984; Tomeoka & Buseck 1985; Zolensky & McSween 1988; Browning et al. 1996; Palmer & Lauretta 2011). Moreover, the degree of aqueous alteration in the meteorite parent body seems to have influenced the relative distribution of amino acids in carbonaceous chondrites (Glavin et al. 2006; 2011; Martins et al. 2007).

In order to further investigate the influence of aqueous alteration on the amino acid abundance and distribution on CM chondrites, we have plotted in Fig. 5.6 the relative abundances for the 4-carbon α-amino acids (α-ABA and α-AIB), β-amino acids (β-ABA and β-AIB), and γ-amino acids (γ-ABA) for CM chondrites with different degrees of aqueous alteration, according to the hydrothermal scale designated by Rubin et al. (2007), and for which the amino acid composition

is fully available. These include the CM2.7/2.8 Paris (hydrothermal classification proposed by Bourot-Denise et al. 2010), the CM2.5 Murchison, the CM2.4/2.5 Murray, the CM2.4 Y-791198, the CM2.2 Nogoya, the CM2.0 MET 01070, and the CM2.0 SCO 06043 (this study; Ehrenfreund et al. 2001a; Botta et al. 2002; Shimoyama & Ogasawara 2002; Glavin et al. 2011). The least altered CM chondrites are on the left of the plot, while the most altered are on the right. There is no clear linear trend between the relative amino acid abundances and the increasing aqueous alteration for each of the individual 4-carbon α-, β-, and γ-amino acid sets. However, it can be noted that the least and medium aqueously altered CMs (i.e. Paris, Murchison, Murray and Y-791198) have much higher relative abundances of 4-carbon α-amino acids than β- and γ-amino acids when compared to the most aqueously ones (i.e. Nogoya, MET 01070, and SCO 06043). In particular, Paris has one of the highest relative abundance of 4-carbon α-amino acids in CM chondrites (0.77), only comparable to Y-791198 (0.81). Moreover, in Paris the 4-carbon β-amino acids are absent (they were not detected above the detection limit of the GC-MS).

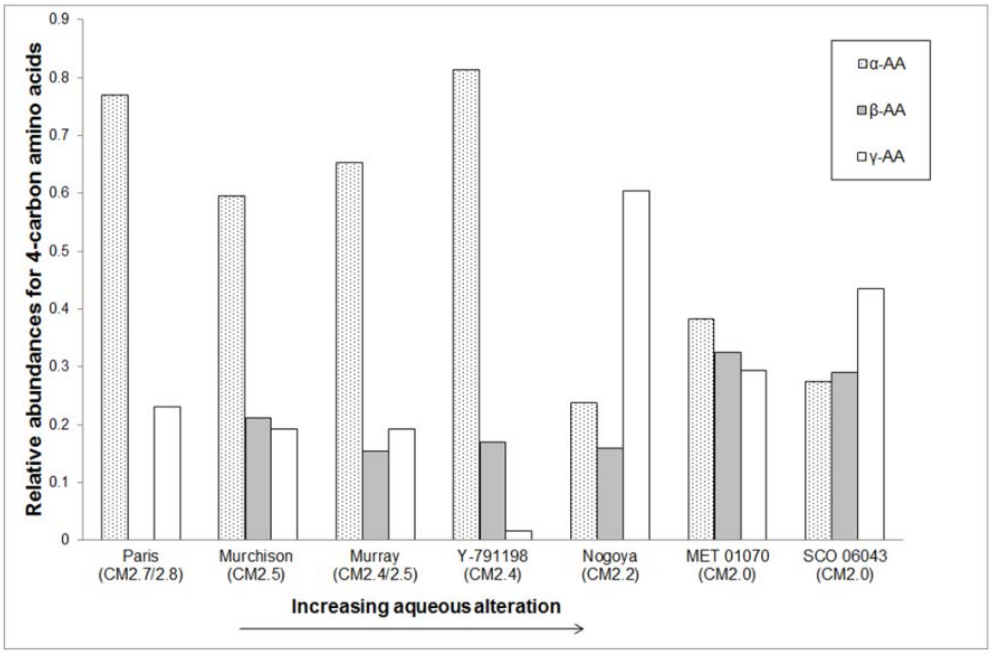

Figure 5.6 - Relative abundances (total = α- plus β- plus γ-amino acids) for the 4-carbon amino acid content of α- (dots), β- (grey) and γ- (white) amino acids for CM chondrites with different degrees of aqueous alteration according to the hydrothermal scale designated by Rubin et al. (2007) (from Martins et al. 2015).

The low relative abundance of α-amino acids in Nogoya, MET 01070, and SCO 06043 may be an indication of the decomposition of these amino acids due to extensive aqueous alteration in the meteorite parent body (Botta et al. 2007; Martins et al. 2007). Moreover, extensive aqueous alteration may also result in hydrolysis of lactams, yielding β- and γ-amino acids (Cooper & Cronin 1995) which would explain the higher relative abundances of β- and γ-amino acids in these three meteorites.

Glavin et al. (2006, 2011) observed an increase of the relative abundance of the amino acid β-alanine with increasing aqueous alteration. Extensive aqueous alteration seems in fact to favor the synthesis of β-amino acids (in particular β-alanine) in the parent body of CM chondrites. In order to verify if our data for Paris follow this trend, we plotted in Fig. 5.7 the relative abundances of β-alanine/glycine, α-AIB/glycine, and β-alanine/α-AIB for CM chondrites with different degrees of aqueous alteration. It can be noted that Paris, the least aqueously altered CM chondrite analyzed to date, has a ratio of β-alanine/glycine of 0.15 ± 0.02 which is the smallest observed in CM chondrites. This value is perfectly in agreement with the trend observed by Glavin et al. (2006, 2011).

The same general trend seems to be also valid for the relative abundance of β-alanine/α-AIB for several of these CM chondrites. However, Paris is the exception to the rule with its high β-alanine/α-AIB ratio (4.0 ± 0.5). Paris has in fact a low abundance of α-AIB when compared to other CM chondrites. Finally, in relation to the relative abundance of α-AIB/glycine, we did not observe any trend with aqueous alteration, as already verified for other CMs (Botta et al. 2007).

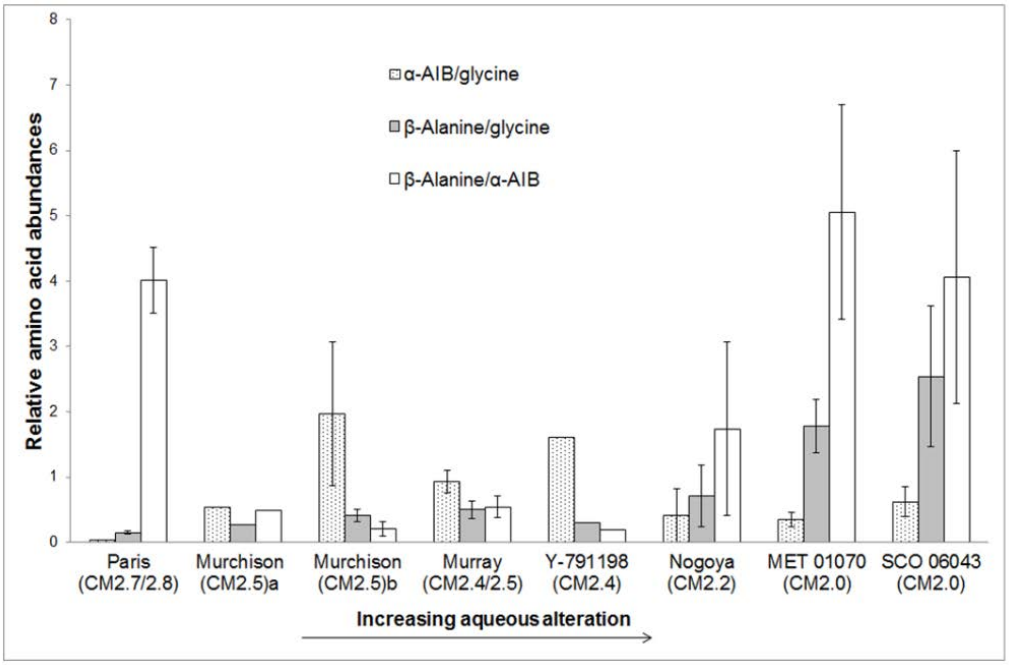

Figure 5.7 - Relative abundances of α-AIB/glycine (dots), β-alanine/glycine (grey) and β-alanine/α-AIB (white) for CM chondrites with different degrees of aqueous alteration according to the hydrothermal scale designated by Rubin et al. (2007) (from Martins et al. 2015).

5.3.2 Enantiomeric measurements in chiral amino acids

Insight into the extra-terrestrial nature of the amino acids present in Paris can be provided by examining the asymmetry between the D- and L-enantiomeric abundances for the chiral amino acids detected in the hydrolyzed fraction of sample 1: aspartic acid, glutamic acid, alanine, valine, norvaline, and α-ABA; all except norvaline and α-ABA being typical proteinogenic amino acids.

From the gas chromatograms, we deduced the abundances of each D and L enantiomers since the peak areas are proportional to the amount of material present. Then, we measured the L-enantiomeric excesses (ee_L) and the corresponding amino acid enantiomeric ratios (D/L) with the uncertainties (1 sigma) obtained by standard error propagation from data in Table 5.1. Preliminary results are presented without any previous correction in Table 5.2.

Table 5.2 - Amino acid enantiomeric ratios (D/L) and corresponding L-enantiomeric excess (ee_L) for chiral amino acids detected in Paris meteorite (sample 1).

Amino Acid	D/L	ee_L (%)
Aspartic acid	0.68 ± 0.03	19.1 ± 2.1
Glutamic acid	0.84 ± 0.09	8.4 ± 5.3
Alanine	0.74 ± 0.05	15.0 ± 3.4
Valine	0.93 ± 0.04	3.4 ± 2.3
Norvaline	0.87 ± 0.03	6.9 ± 2.0
α-ABA	0.90 ± 0.09	5.2 ± 4.8

We can note that aspartic acid, alanine, and norvaline present high ee_L ranging from 6.9 ± 2.0 % (for norvaline) to 19.1 ± 2.1% (for aspartic acid) which suggest that these amino acids are non-racemic. Glutamic acid, valine, and α-ABA present moderately high ee_L ranging from 3.4 ± 2.3 % (for valine) to 8.4 ± 5.3 % (for glutamic acid). The errors accompanying the data are comparable to those typically obtained with similar techniques (Glavin & Dworkin 2009; Burton et al. 2012).

Most of these amino acids have been already found as non-racemic in other CM chondritic meteorites. Glavin et al. (2012) found small D/L ratios (i.e. smaller than 0.4) for aspartic and glutamic acids in the C2 Tagish Lake chondrite, with carbon isotope measurements of D- and L-aspartic acid falling well outside of the terrestrial range and indicating that the measured L-enantio-enrichment was indeed indigenous to the meteorite. Cronin & Pizzarello (1999) in Murchison found alanine with an ee_L of 1.2% and valine with an ee_L of 2.2%.

From our analysis, the ee_L found suggest the presence of positive ee_L in several chiral amino acids, but caution has to be used for a rigorous interpretation. Two main sources of errors could affect the measurements: possible contaminations and intrinsic effects of the chiral column. Both of them could have introduced an apparent imbalance between the D and L enantiomers leading

to an overestimate of the L proteinogenic enantiomers (in the case of a terrestrial contamination) or indifferently of one or the other enantiomer (in the case of systematic effects of the column).

Possible contaminations

The best way to evaluate the indigenous or terrestrial source of the amino acids would be to measure the compound-specific stable isotope ratios of carbon, hydrogen, and/or nitrogen. However, we were unable to produce isotopic measurements of the amino acids in Paris due to the limited meteoritic sample available for this kind of analysis.

Regarding possible contaminations from the analytical protocol, we can affirm that the serpentine control blank does not contain any detectable amino acids; therefore, if a contamination occured, it has not originated during the extraction procedure. On the other hand, for genuine terrestrial contaminations, Paris shows almost no signs of terrestrial weathering (Bourot-Denise et al. 2010; Zanda et al. 2010, 2011), and recent analysis of the Na/K ratio suggests that it was collected immediately after its fall and not exposed to rain (Haack et al. 2012; Hewins et al. 2014), which significantly minimizes the percolation of the landing site soil through the meteorite. It is also important to report the presence of norvaline, α-AIB and isovaline which are rare in the terrestrial biosphere but common in other CM2 meteorites (Kotra et al. 1979; Shimoyama et al. 1979a, 1979b, 1985; Pizzarello & Cronin 2000; Ehrenfreund et al. 2001a; Shimoyama & Ogasawara 2002; Glavin et al. 2006, 2011; Botta et al. 2002). The presence of these non proteinogenic amino acids testifies for the extraterrestrial origin of the material analyzed. In particular, the concentrations (for L+D enantiomers) of α-AIB (312 ppb) are comparable to those of other C4 amino acids, such as α–ABA (306 ppb) and aspartic acid (334 ppb). Aspartic acid is a proteinogenic amino acid but is not anomalously abundant.

Considering all these arguments, although contamination issues for proteinogenic amino acids cannot be firmly excluded, we consider that possible contaminations are minimal for this well-preserved meteorite.

Intrinsic effects of the column

The problem of intrinsic effects of the column is more delicate and needs a rigorous approach, as discussed in Nuevo et al. 2006. The D and L peak areas in the chromatograms are proportional to the concentration of the compounds, but proportionality constants are different for each different amino acid, even for the two enantiomers of a same amino acid. This is due to their different interactions with the stationary phase in the chiral column. As a consequence, a racemic amino acid will display an apparent ee_L value different from zero, while a non-racemic amino acid will display an ee_L shifted value (toward positive or negative values). In both cases, the problems arise from a non-well definition of the zero on the ee_L scale. This could compromise the interpretation of (very) small ee_L, but may not affect too much the high ee_L. This source of errors can be identified and corrected by using optically pure racemic standards. At the time of this writing, however, we could not perform this correction.

For the moment, we consider these ee_L values as preliminary results and we reserve the possibility to correct them in the next future. Nevertheless, we can still give a general evaluation of these results. Assuming negligible any possible contamination (natural and due to the laboratory protocol), if we consider the sign of the ee_L (which is constantly positive) and the highest ee_L values, the results suggest the presence of general positive amino acid ee_L mainly for aspartic acid, alanine, and norvaline.

The origin of the ee_L in meteoritic amino acids

One promising mechanism that may explain the origin of the observed ee_L in different meteoritic amino acids, experimentally explored in this thesis (Chapter 3), is the asymmetric photoprocessing of amino acids or their precursors by UV circularly polarized light (UV CPL) in space (Bonner & Rubenstein 1987; Bailey et al. 1998; Lucas et al. 2005). In support of this hypothesis, non-racemic alanine (ee_L up to -1.34 ± 0.40%) has been obtained in laboratory from UV CPL photoprocessing of *initially achiral* interstellar/circumstellar ice analogs, with the two CPL helicities (R and L) inducing ee_L of opposite signs (de Marcellus et al. 2011) whereas UV

LPL (Linearly Polarized Light) did not induce any ee_L. As discussed in Chapter 3 (Modica et al. 2014), these results have been recently confirmed and extended to a total of five chiral proteinogenic and non-proteinogenic amino acids (among which alanine and valine) in similar experiments with UV CPL. All the five considered amino acids are found non-racemic with ee_L of the same sign induced by each given CPL helicity, and of opposite sign in relation to the two different helicities. Taking into account these and other results, a plausible astrophysical scenario for the origin of the amino acid enantiomeric excess in meteorites has been proposed in Chapter 3. It is important to underline here that UV CPL irradiation of ices would play the same role than UV irradiation in generating reactive ions and radicals leading then to the formation of organic molecules including amino acids. Thus, not only UV CPL would have a major role in the formation of amino acids, but it would also induce in them a stereo-specific photochemistry.

The question of isovaline

Isovaline is a non-proteinogenic amino acid which is rare on Earth, although it may be found, mainly in the D-configuration, in fungal peptides (Keller et al. 1990; Bruckner et al. 2009). It has been detected in the two enantiomeric configurations (L and D) in several carbonaceous chondrites such as Murray, Orgueil, SCO 06043, and Murchison and has been extensively discussed by several authors (Cronin & Pizzarello 1997; 1999; Pizzarello & Cronin 2000; Pizzarello et al. 2003, 2008, 2012; Glavin & Dworkin 2009; Glavin et al. 2011).

Significant differences are observed in its enantiomeric measurements within different chondritic meteorites, and within different fragments of the same Murchison chondrite. In certain meteorites such as the CM2.3 LON 94102, the CR2 EET 92042, the CR3 QUE 99177, and in some fragments of the CM2.5 Murchison, isovaline is found to be racemic *in the limit of the experimental errors*. In other chondritic meteorites such as the CI1 Orgueil, the CM2.0 SCO 06043, in other fragments of the CM2.5 Murchison, the CM2.4/2.5 Murray, and the CR2 GRA 95229, isovaline is found to be clearly non-racemic with ee_L up to 18.5 ± 2.6% (Pizzarello et al. 2003, 2008; Glavin & Dworkin 2009). These large ee_L are unlikely due to terrestrial contaminations of meteoritic samples because, as already mentioned, isovaline is rare on Earth;

on the other hand, an abiotic synthesis of isovaline (or other amino acids), in the absence of any asymmetric field or chiral asymmetric molecular precursors, should produce only racemic mixtures of L- and D-enantiomers.

The origin of non-racemic meteoritic isovaline may be consistent with UV CPL photoprocessing of ices in space, provided however, that a secondary mechanism for amplification of the low initial ee_L from asymmetric photoprocessing is invoked to explain the much larger ee_L observed in some CM meteorites. Isovaline (or any other amino acid) could be synthesized from precursors which can be chiral and thus be able to interact asymmetrically with UV CPL. On the other hand, UV-CPL could form chiral precursors of amino acids even from initially achiral mixtures, as indeed demonstrated by our group (de Marcellus et al. 2011; Modica et al. 2014). However, the nature of these precursors remains unknown. Isovaline has unfortunately not been reported yet in this kind of experiments but its isomers valine and norvaline have been indeed found with slight enantiomeric excesses up to −1.82 ± 0.30% (in the case of valine) (Modica et al. 2014).

Pizzarello et al. (2003) have noted a possible correlation between the isovaline ee_L found in individual fragments of Murchison and the relative abundance of hydrous silicate minerals, suggesting that aqueous alteration may have played a role, leading to the large isovaline ee_L in this meteorite. More explicitly, Glavin & Dworkin (2009) have shown that a correlation does exist between the large ee_L in isovaline and the increasing degree of aqueous alteration within different CI, CM, and CR chondritic meteorites.

Indeed, large enantiomeric excess may be obtained from a slight initial ee_L, such as the one produced by UV CPL, which can be amplified under aqueous conditions (Soai et al. 1995; Shibata et al. 1998; Mathew et al. 2004). Therefore, amplification of a slight initial ee_L by aqueous alteration in the meteorite parent body has been suggested as a secondary mechanism to explain the large isovaline ee_L observed (Glavin & Dworkin 2009). Isovaline, as the other α-dialkyl amino acids, is resistant to racemization under aqueous conditions (Pollock et al. 1975); therefore, its enantiomeric imbalance should not have been canceled from the time of its

formation. Our results on Paris, the least aqueously altered CM chondrite analyzed to date, present an opportunity to verify if the isovaline ee_L is in agreement with a low degree of aqueous alteration, as expected from the correlation observed by Glavin & Dworkin (2009).

Isovaline was detected in sample 1, but the D and L enantiomers could not been individually separated with the chromatographic techniques used for the others amino acids. We then used another sample (sample 2), accurately selected by Brigitte Zanda of the MNHN (Paris) from the less altered lithology of Paris meteorite, and performed the analysis with optimized chromatographic conditions (Chirasil-Dex CB column) that enabled the separation of these two enantiomers.

Since the crucial importance of an accurate determination of this ee_L value, we used a racemic isovaline standard which served the purpose of correcting the ee_L preliminary value. The racemic isovaline standard was carried through the same analytical procedure used for sample 2. The selected ion GC-MS chromatograms of the D- and L-isovaline enantiomers present in Paris (sample 2) and the standard are shown in Fig. 5.8. The mass spectra for the peaks assigned to the L-isovaline in Paris and the L-isovaline in the standard are also shown. The same fragmentation pattern is observed in both the mass spectra, excluding the coelution of any potential contaminants. The abundances of the separated D- and L-isovaline enantiomers present in the acid-hydrolyzed fraction of the Paris meteorite are 220 ± 16 for D-isovaline and 221 ± 7 for L-isovaline, respectively. A preliminary (non-corrected) isovaline ee_L value of 0.2 ± 4.0% was found. In the case of the racemic standard, an ee_L value of 1.8 ± 1.4 % was found. As already mentioned, the reason of the apparent ee_L different from zero for this optically pure racemic standard is almost certainly linked to the intrinsic effects of the column. We used this value to re-define the zero in the ee_L isovaline scale of meteoritic isovaline. The corrected isovaline ee_L value corresponds to -1.6 ± 4.2 % (ee_L corrected = ee_L non-corrected - ee_L standard). Unfortunately, after the correction, we could not distinguish between the racemic or non-racemic nature of isovaline in Paris *because of the large uncertainty of the measurements.* From this result, we can only exclude the presence of moderate to large excess of the L-enantiomer in isovaline.

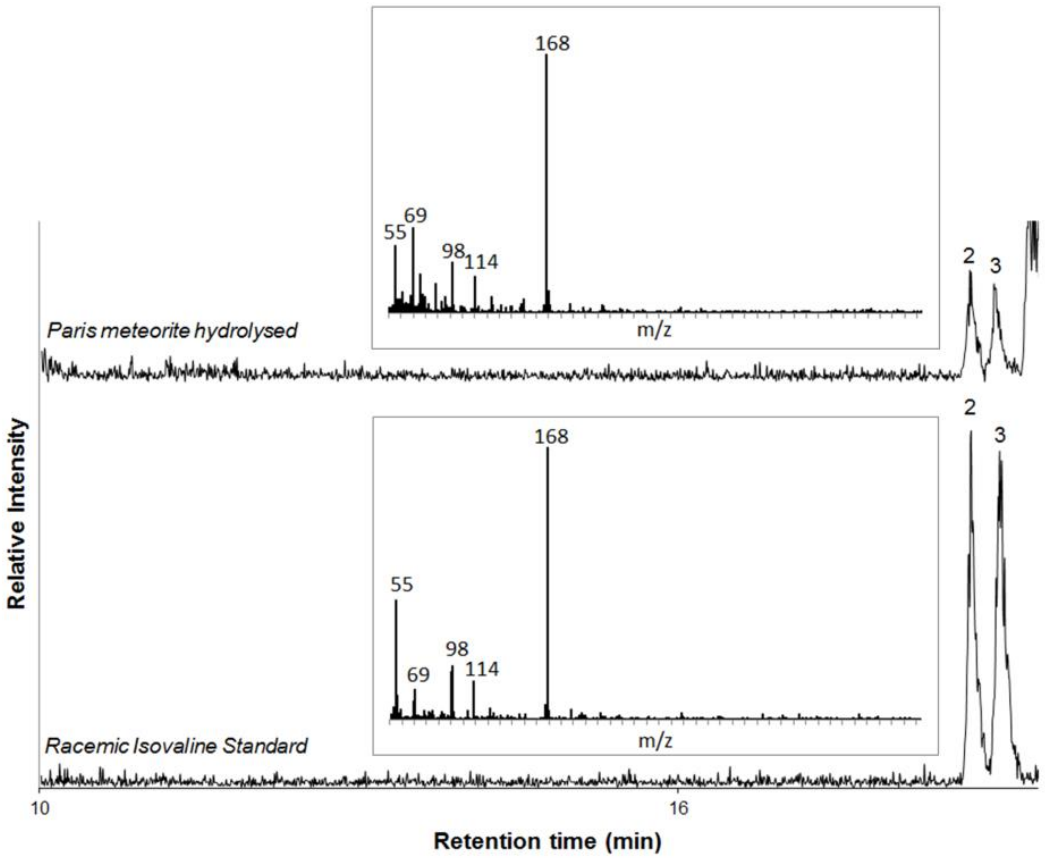

Figure 5.8 - The single ion GC-MS traces (m/z 168) of the racemic D- and L-isovaline standard mixture (bottom) and D- and L-isovaline in the hydrolyzed extracts of Paris meteorite (sample 2, top). Peak number 2 corresponds to L-isovaline and peak number 3 corresponds to D-isovaline. The insets show the GC-MS mass spectra for the peak assigned to the L-isovaline in both samples (from Martins et al. 2015).

Glavin & Dworkin (2009) have shown that a correlation does exist between the ee_L in isovaline and the degree of aqueous alteration within different CI, CM and CR chondritic meteorites, with the more altered ones showing the highest ee_L values (up to 18.5 ± 2.6% for the CM2.5 Murchison), followed by the moderately altered ones showing medium ee_L (e.g. 3.3 ± 1.8% for the CM2 LEW 90500), to end with the least altered ones (e.g. 0.3 ± 2.1% for CR3 QUE 99177), where isovaline is considered racemic in the limit of the experimental error. This correlation is further supported by the high ee_L found in the altered CM2.0 SCO (16.5 ± 6.1%, Glavin et al. 2011) and CM2.4/2.5 Murray (6%, no associated error was provided) (Pizzarello et al. 2003). The large range of ee_L values found in distinct fragments of Murchison, from 0 to 15.2 ± 0.2%

(Pizzarello et al. 2003), also supports this correlation, being possibly explained by the different degree of aqueous alteration characterizing different lithologies in a same meteorite.

The ee_L= -1.6 ± 4.2 % obtained for Paris seems comparable to those found for the Antarctic CR3 QUE 99177 (0.3 ± 2.1%) and CR2 EET 92042 (-1.0 ± 4.3%) chondrites (Glavin & Dworkin 2009), which are reported to be pristine meteorites, thus having experienced almost no aqueous alteration. Our results on Paris, the least aqueously altered CM chondrite, support the correlation found by Glavin & Dworkin (2009). Unfortunately, the large error bars accompanying the isovaline ee_L value in CR3 QUE 99177 and CR2 EET 92042 chondrites, similarly to Paris, cannot allow appreciating the presence of possible very small ee_L. We note that if a very small isovaline ee_L is present in a pristine meteorite, it could be precisely measured only with a very sensitive technique, such as the multidimensional GCxCC TOF MS, the one we used in performing the experiments described in Chapter 3 where small excesses were measured together with small and accurate error bars. This measurement may then allow supporting the hypothesis of an initial isovaline ee_L due to UV-CPL irradiation of ices before incorporation of the materials in planetesimals or any parent body of meteorites.

5.3.3 Amino acid content in laboratory organic residues

In order to establish possible links between the organic matter produced by UV irradiation in icy grains prior to their accretion in planetesimals and the soluble organic matter (SOM) in primitive meteorites, we made use of our laboratory organic residues, considered as analogs for the organic matter synthesized on cold grains, and compared the amino acid content and distribution in residues, in Paris (this study), and in other CM chondrites (data from literature). The comparison with less altered CM chondrites, and in particular with Paris, is appropriate because of the non-altered nature of the residues, whose composition may then be considered very close to that of very primitive and minimally altered meteorites.

With the aim of such comparison, we prepared at IAS two equivalent organic residues (named residues 1 and 2) from the standard procedure of photo- and thermo-processing of initial ice mixtures of H_2O:CH_3OH:NH_3, as described in Chapter 2. In addition, two distinct blanks were also prepared, one obtained by deposition of the ice mixture without irradiation, followed by warm-up and recovery at room temperature and one by irradiation of the MgF_2 window only, without any mixture deposition, followed by warm-up and recovery at room temperature. For the blank preparation, we respected the same time schedule used for the residue (~70 hours of irradiation time, ~30 hours of warm-up). This allowed taking into account possible sources of contamination occurring during the sample preparation (manipulation of the windows, gas mixtures preparation, deposition, irradiation, and recovery procedures of the samples).

Once ready, we brought the 4 samples (2 residues + 2 blanks), safely kept in argon filled vessels, to the laboratory of Dr. Zita Martins to analyze them. All the samples were extracted with 50 µL of ultrapure water and then carried through the same protocol of hydrolysis, derivatization and gas chromatography-mass spectrometry (GC-MS) analyses used for the organic matter present in Paris and previously described in this chapter. The gas chromatograms obtained for the two residues are shown in Fig. 5.9 and Fig. 5.10, respectively; as expected, the two blanks do not contain any peak due to amino acids and are shown in the Appendix (Fig. 2).

In both samples, we detected glycine, D- and L-alanine, β-alanine, and D,L-α-ABA. The abundances of these amino acids are expressed in absolute values (nanograms) and shown in Table 5.3.

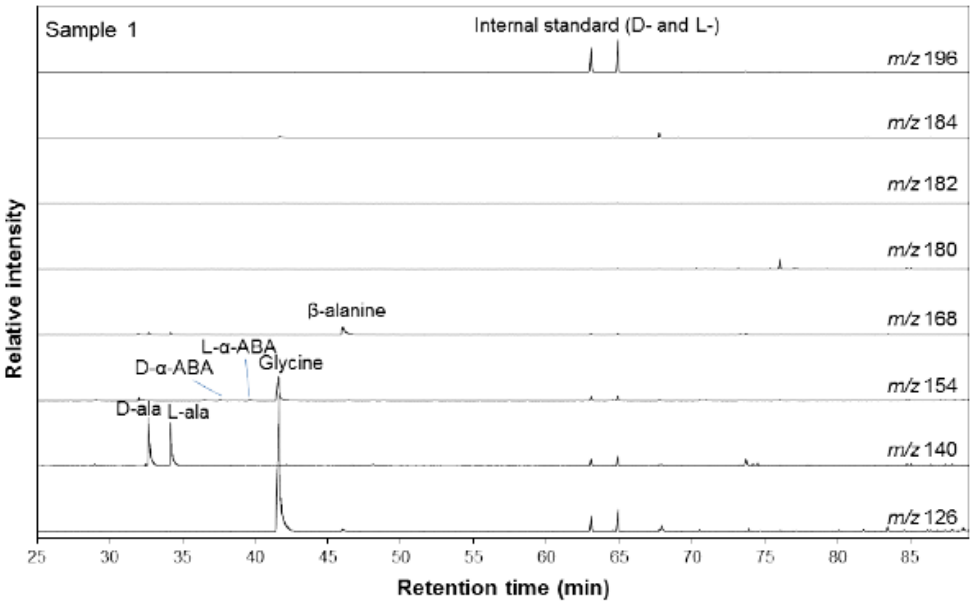

Figure 5.9 - Gas chromatograms showing the detection of D-alanine, L-alanine, glycine, D-α-ABA, L-α-ABA, and β-alanine in residue 1 (sample 1).

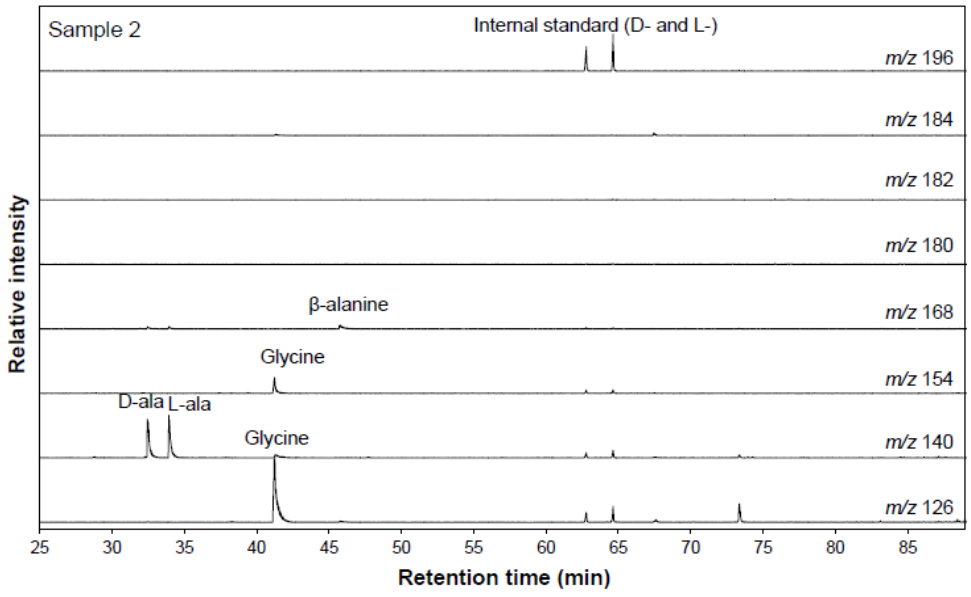

Figure 5.10 - Gas chromatograms showing the detection of D-alanine, L-alanine, glycine, and β-alanine in residue 2 (sample 2).

Table 5.3 - Amino acids detected in residue 1 and residue 2 along with their abundances in nanograms.

Amino acid	Abundance (ng) in residue 1	Abundance (ng) in residue 2
Glycine	1034 ± 28	249 ± 19
D-alanine	246 ± 16	109 ± 8
L-alanine	221 ± 9	107 ± 9
β-alanine	136 ± 5	37 ± 3
D,L α-ABA	71	<36

We observe that in both residues, glycine is by far the most abundant amino acid, followed by D- and L-alanine and then by β-alanine; D,L α-ABA is the less abundant among the detected amino acid; for residue 2, only upper limits are given. Results between residue 1 and residue 2 agree well in terms of amino acid distribution even if the absolute abundances are higher in residue 1 for all the amino acids considered. These differences can be explained by the variability of some parameters during the sample preparation, such as the deposition rate of the mixture and the flux of the UV lamp, which are difficult to maintain strictly constant over a long time. However, these differences in the absolute amounts do not limit the interpretation of the results.

Alanine enantiomers were well separated and their individual abundances could be measured in both residues. D-alanine presents higher abundances than L-alanine, a result mainly noticeable in residue 1. This needs to be clarified since it could be incorrectly interpreted as the presence of an enantiomeric excess of the D form. We remind that these samples have been produced using a classical UV lamp generating unpolarized light, thus without any source of asymmetry; therefore, only racemic amino acids are expected in the residues. The racemic nature of amino acids using UV LPL (linearly polarized) and UV UPL (unpolarized light) has been largely demonstrated by our team on similar samples analyzed by a much more sensitive method for measurements of small enantiomeric excesses with GCxGC-MS (see Chapter 3, and de Marcellus et al. 2011). The apparent D enantiomeric excess observed in alanine from Table 5.3 is likely due to the intrinsic effects of the chiral column. To overcome these effects, we used a

racemic standard of alanine ($ee_{L\ stand}$ = -2.47 ± 0.77) and correct the preliminary ee_L alanine values. After the correction the ee_L values in alanine are -2.80 ± 4.71 for residue 1 and 1.48 ± 6.28 for residue 2, respectively. Alanine can thus be considered as racemic within the (unavoidably large) experimental error in both residues, confirming what was indeed expected.

When comparing the two residues with Paris, we note that the list of amino acids detected in the residues (4 amino acids) is much shorter than that in Paris (11 amino acids) and limited to α and β amino acids only. This is not surprising because the degree of complexity of the residues produced in the laboratory is expected to be lower than the meteoritic samples; it has in fact a simpler composition being made only of C, H, O, and N. However, the detection of only 4 amino acids does not mean that these are the only amino acids present in our residues, as the number of detections depends on the specific technique used and its ability to assess the chemical constituents of a sample. In other words, the classical GC-MS method is much less sensitive than the multidimensional GCxGC-TOF MS one.

Even with the restricted number of amino acids detected, some similarities between residues and Paris samples can be evidenced. Firstly, the amino acid distribution is analogous to that of Paris and other CM chondrites (section 5.3.1 of this chapter) with the simplest amino acids as the most abundant and abundances tending to decrease as the number of carbon atoms increases (glycine (2C)>D,L α-alanine (3C)> D,L α-ABA (4C)). Unfortunately, no 5C amino acids were detected in the residues for a more comprehensive comparison; however, the initial decreasing trend is already clearly observed and in line with what previously discussed in this chapter (see Fig. 5.5). This characteristic, already observed in residues produced by our group (Nuevo et al. 2008; Meinert et al. 2012; Modica et al. 2014), is a signature of an abiotic synthesis of these molecules.

For a quantitative comparison, we considered the ratio β-alanine/glycine for residue 1 (0.13 ± 0.01) and residue 2 (0.15 ± 0.02). Firstly, we can observe that these two values are largely consistent between them, indicating that this ratio is reproducible. Secondly, these values are perfectly comparable to that of Paris (0.15 ± 0.02), indicating a strong resemblance between laboratory residues and this primitive meteorite. We chose the value obtained for residue 1 (the

lowest between the two) and compared it to that of the same set of CM chondrites with different degree of aqueous alteration already considered (Fig. 5.11). Since we consider the residue as an analog of the organic material that forms on grains before accretion in planetesimals and before any aqueous alteration by liquid water, we placed the β-alanine/glycine value for residue 1 at the extreme left of the figure, in a position which ideally indicates no aqueous alteration on the x-scale. Indeed, the residue, after production, has never been exposed to water and thus to any degree of aqueous alteration. The increasing trend of β-alanine/glycine observed in the ensemble of residue and several CM chondrites with increasing aqueous alteration can be considered as one of the indications which may contribute to the validation of the astrophysical pertinence of our laboratory simulations. This kind of indications may help to establish links between the formation pathways of complex organic molecules, in particular amino acids, by photo- and thermo- processing of icy grains and soluble organic material in primitive meteorites.

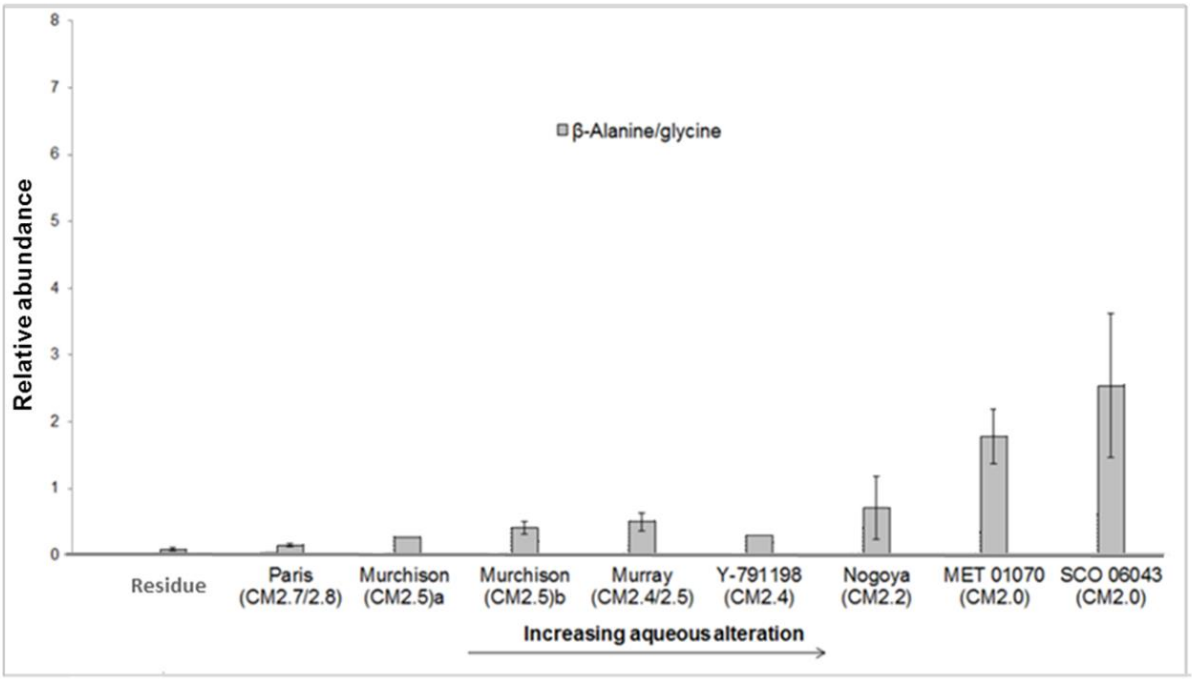

Figure 5.11 - Relative abundance of β-alanine/glycine for residue 1 and CM chondrites with different degrees of aqueous alteration. The β-alanine/glycine value for residue 1 ideally indicates no aqueous alteration. This figure is obtained by a modification of Fig. 5.7.

Another sign for lack of aqueous alteration would be the comparison between α, β , and γ amino acids as we have already done for the comparison illustrated in Fig. 5.7 of section 5.3.1. Since the analysis by classical GC-MS could not provide an adequate number of amino acids of the different classes α, β, and γ for the analysis of their distribution, we considered the list of amino acids detected in a similar laboratory residue (hereafter residue 3) produced in a previous work in our group at IAS by Pierre de Marcellus during his PhD thesis. Residue 3 has been obtained from an initial ice mixture of H_2O:$^{13}CH_3OH$:NH_3, (similarly to residue 1 and 2), but as a multilayered thick residue. In this residue, 26 different amino acids have been detected and relative abundances (to glycine) obtained thanks to the enhanced sensitivity of the multidimensional gas chromatography technique and the large amount of residue (Meinert et al. 2012, Supporting Information, Table S1). As a matter of fact, expecting the great chemical complexity of the residues produced by photo/thermo-chemistry, we have decided since long to work on quite similar analogs in order to be able to reach coherent conclusions, owing to the difficulty to produce significant amounts of residues.

Among the amino acids detected in residue 3, we considered a set of 4-carbon α-amino acids (α-ABA), β-amino acids (β-ABA and β-AIB) and γ-amino acids (γ-ABA) and calculated their relative abundance with respect to the total amino acid abundances (α- plus β- plus γ-amino acids) in the same way we have done for Paris. In Table 5.4 we report the relative abundances of the considered 4-carbon α-amino acids with respect to glycine (**ϕ** gly= 100), as in Meinert et al. 2012.

Table 5.4 - Abundances relative to glycine for the set of 4 carbon α, β, γ-amino acids in residue 3 (from Meinert et al. 2012).

Amino acid	**Abundance in residue 3 (ϕx100/ ϕ gly)**
α-ABA	0.73
β-ABA	0.02
γ-ABA	0.17
β-AIB	0.23

In Fig. 5.12, we thus modified Fig. 5.6 adding the relative abundances of α, β, and γ-amino acids obtained for residue 3 and compared the values between residue 3 and CM chondrites with different degrees of aqueous alteration. The values for residue 3 nicely fit the trend already drawn by those for the CM chondrites with increasing aqueous alteration. In particular, the α-value (0.64) is comparable to those of the less aqueously altered CM chondrites Paris, Murchison, Murray and Y-791198. The β-value (0.21) is in the average between the other β-values, with no trend observed among the different meteorites with increasing aqueous alteration. Finally, the γ-value (0.15) is low and comparable again to that of the less aqueously altered CM chondrites Paris, Murchison, Murray, and Y-791198. These results thus show a strong similarity between the relative abundances of the same kind of amino acids in the laboratory residues and those in primitive meteorites and can be considered as a further important indication to validate our experimental approach.

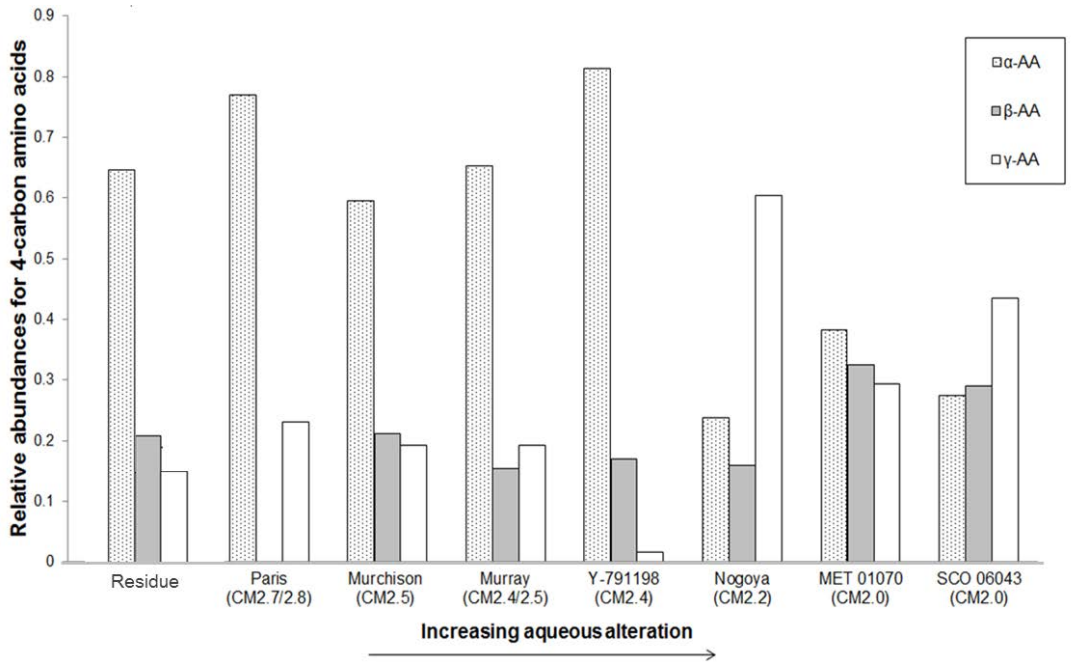

Figure 5.12 - Relative abundances (total = α- plus β- plus γ-amino acids) for the 4-carbon amino acid content of α- (dots), β- (grey) and γ- (white) amino acids for residue 3 (from Meinert et al. 2012) and CM chondrites with different degrees of aqueous alteration. This figure is obtained by a modification of Fig. 5.6.

5.4 Conclusions

We have obtained and analyzed for the first time the amino acid content of the Paris meteorite, which is reported to be the least aqueously altered CM chondrite analyzed to date. The analysis shows that free amino acids constitute about 45% of the total amino acids. The α-amino acids are the most abundant, followed by the β and γ-amino acids; moreover the abundances of the individual amino acids decrease with the increasing number of carbon atoms in their molecular structure. The same distribution is observed between the hydrolyzed and the non-hydrolyzed fraction of the organic extracts, indicating that the hydrolysis protocol does not affect the composition and relative abundances of the detected amino acids.

When comparing Paris to other CM chondrites, the distribution of α, β and γ-amino acids and, in particular, the very low β-alanine/glycine ratio is in agreement with a low degree of aqueous alteration. Preliminary enantiomeric measurements for aspartic acid, alanine, and norvaline suggest the presence of L-enantiomeric excesses; enantiomeric measurements for isovaline are in agreement with what found in meteorites having experienced almost no aqueous alteration and where isovaline is considered racemic, although the large uncertainty of these measurements.

In order to compare laboratory and meteoritic organic materials, we produced and analyzed two laboratory residues following the same protocol of hydrolysis, derivatization and gas chromatography-mass spectrometry used for Paris. We detected 4 amino acids: glycine, D- and L-alanine, β-alanine, and D,L α-ABA with decreasing abundances with increasing number of carbon atoms. From enantiomeric measurements, alanine is found racemic, as expected. Abundances of amino acids from a third equivalent residue previously produced by our group and analyzed with a more sensitive gas chromatographic technique (GCxGC-TOFMS) were also considered. The distribution of α, β and γ-amino acids is in accordance with that of the less aqueously altered CM chondrites. In particular, the ratio β-alanine/glycine is the same of that for Paris, the lowest ever measured in CM chondrites.

The similarities observed between amino acids in laboratory residues and in meteoritic materials can be considered as indications which can contribute to the validation of the astrophysical pertinence of our laboratory simulations. This kind of indications helps to establish a link between the formation of complex organic molecules, in particular amino acids, by photo- and thermo-processing of icy grains and soluble organic material in primitive meteorites.

The next and last chapter of this thesis will focus on further similarities between our residues and the Paris meteorite regarding only infrared spectroscopy, a non-destructive method which is also the only one connected to astronomical observations.

Chapter 6

Laboratory simulations using silicate surfaces

Contents

Interstellar grains are mainly formed by condensation in the atmospheres of late-type stars, which eject a significant fraction of their outer envelope into the ISM (Henning 2003). Silicate grains are produced in the envelopes of oxygen-rich asymptotic giant branch (AGB) stars, red supergiants, and, to a lesser extent, supernovae (Tielens 2005). They are made of highly refractory elements (mainly Si, Mg, Fe, Al, Ca…) which cannot extensively participate in the gas phase chemistry. In dense molecular clouds, silicate grains will start to condense volatiles (atoms, radicals, molecules) to form icy mantles. Thus, refractory silicate grains do precede the icy mantles formation, according to the simple model of core-mantles grains suggested by Greenberg (1973). Moreover, cosmic abundances of volatile species impose that the icy mantles constitute an important volume of the grains. Within these mantles, photochemical reactions driven by UV photons are expected to generate a pure bulk ice chemistry devoid of significant interaction with the nature of the surface. In this chapter, we explore the validity of the assumption of a bulk ice chemistry on interstellar grains. So far, we have indeed considered the production of organic residues from interstellar/circumstellar ice analogs only on physically and chemically inert substrates, i.e. crystal windows made of MgF_2. Here, the use of more astrophysically relevant surfaces is questioned. We deposit our standard ice mixtures on amorphous silicate films in order to produce more realistic residues and to observe by in-situ

infrared spectroscopy the possible effects of the silicate surface on the nature of the organic residues. We perform a hot water extraction test on a silicate-based residue and discuss the problem of a key molecule, HMT. We also appreciate the spectral similarities between our more realistic samples and the natural pristine matter that can be found in the Paris meteorite.

6.1 Astronomical silicates

Astronomical silicates are compounds containing silicon (Si) and oxygen (O); elements such as magnesium (Mg), iron (Fe), calcium (Ca), aluminum (Al) etc. are also present, usually to a level that is imposed by the relative cosmic abundances of these elements. Iron is suspected to form iron sulfides (FeS) or even pure iron nanoparticles embedded in the silicates (Davoisne et al. 2006; Djouadi et al. 2007) but its presence in the silicate network as a ferro-silicate is highly debated and not observationally proven.

There are two chemical classes of crystalline silicates: olivines (Fe, Mg)SiO_4 and pyroxenes XY(Si, Al)$_2O_6$. Olivines include two endmembers of the solid solution series: forsterite (Mg-endmember, Mg_2SiO_4) and fayalite (Fe-endmember, Fe_2SiO_4). Similarly, pyroxenes include two endmembers that are enstatite (Mg-endmember, $MgSiO_3$) and ferrosilite (Fe-endmember, $FeSiO_3$).

In the ISM, silicate dust is observed to be largely or even totally amorphous rather than crystalline (Mathis 1990; Li & Draine 2001; Kemper et al. 2004). In the diffuse ISM, the crystalline fraction of the total silicate mass has an upper limit of 2% (Kemper et al. 2004; Min et al. 2007; Hanner & Zolensky 2010), and in dense molecular clouds silicates also appear purely amorphous (Watson et al. 2004). At the opposite, a significant crystalline component of dust can be observed in protoplanetary disks (Bouwman et al. 2001; van Boekel et al. 2004), in young stellar objects and in evolved stars (Waelkens et al. 2000) as well as in Solar System comets (Swamy et al. 1988; Crovisier et al. 1997; Harker et al. 2005). These observations suggest that dust has been thermally processed (Harker & Desch 2002) and imply extensive transport of dust from the hot inner regions to the outer parts of the disk and back (Bockelée-Morvan et al. 2002; Gail 2004). The main reason why silicates are amorphous in the ISM is probably the

amorphization of crystalline silicates by energetic particles such as fast protons (cosmic rays), as experimentally evidenced by Demyk et al. (2001; 2004).

6.2 Experiments and discussion

6.2.1 Laboratory make-up of icy silicate grain analogs

In order to investigate a possible interaction of the silicate surface on the formation and nature of organic residues, in the framework of the simulation experiments already described in this thesis, we have performed, in our group at IAS, original and more realistic experiments in which we simulate the global icy grain structure, including both the silicate surface and the icy mantle. This permits to mimic what may happen on interstellar grains where the silicate cores are covered by icy mantles. These experiments have been realized thanks to the collaboration with Dr. Z. Djouadi and Dr. S. Merouane, who, in our team, do specialize in the production of silicate analogs as described for example in Merouane's PhD thesis (2013).

We prepared two samples of silicate grain analogs of amorphous structure, one with enstatite composition (a pyroxene silicate mineral) and one with forsterite composition (an olivine silicate mineral). For these experiments we used two fragments of pure crystalline enstatite and pure crystalline forsterite silicates, respectively. As window supports, we used KBr windows because their frequency cut-off (350 cm^{-1}) allows observing vibrational Si-O modes from silicates located around 1000 cm^{-1} and 400 cm^{-1}. The windows were coated with a silicate film according to the following procedure. A KBr window was placed horizontally inside an evaporator evacuated to 10^{-6} mbar, secured in its upper part with two small screws on the edges, with the bottom surface facing the fragment of the crystalline silicate chosen, enstatite or forsterite, placed in a tungsten crucible in the bottom part of the evaporator (see Merouane 2013, PhD thesis). Each silicate fragment was sequentially vaporized by means of an electron beam from a heated tungsten filament. The vapors rose and slowly deposited onto the window which was maintained at a constant temperature of 300 K. On the window surface they formed a thin film with the same stoichiometric composition of the silicate fragment but with an amorphous structure. By this technique two different silicate films of about 150 nm in thickness were deposited onto the

surface of two distinct KBr windows. This procedure is described in papers from our group (see for example Djouadi et al. 2005, 2007) and has proven useful to discuss some spectroscopic aspects of silicate materials in various astrophysical environments (Demyk et al. 2000; Davoisne et al. 2006)

The two KBr windows coated with silicates have been then used as substrates for the preparation of organic residues following the standard MICMOC procedure in which icy mixtures of H_2O, CH_3OH, and NH_3 are deposited and simultaneously irradiated by UV photons. After irradiation (~48 hours for both samples) and following warm-up, two residues were obtained. The general scheme of the final samples (residue plus silicate film) on the KBr window is illustrated in Fig. 6.1.

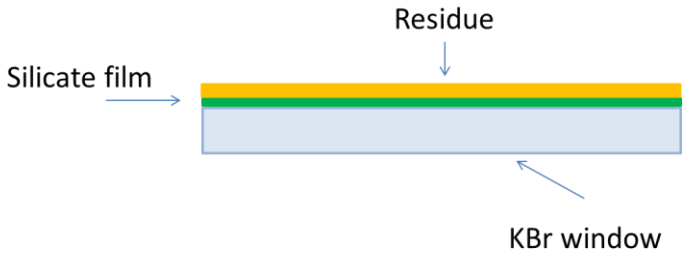

Figure 6.1 - Scheme of a sample constituted by an organic residue produced onto an amorphous silicate thin film (enstatite or forsterite) previously deposited on a KBr window.

The IR spectra of the samples (residue plus enstatite and residue plus forsterite) have been acquired at room temperature, directly in-situ on the MICMOC apparatus, and are shown in Fig. 6.2. The sample with enstatite is less abundant than that one with forsterite, as can be observed from the absolute absorbance of the bands. This difference is due to a partial loss of the ice film that occurred during the irradiation step of this sample, possibly due to a problem of adherence of the ice film to the enstatite film. However, the two spectra show the same bands and appear qualitatively similar.

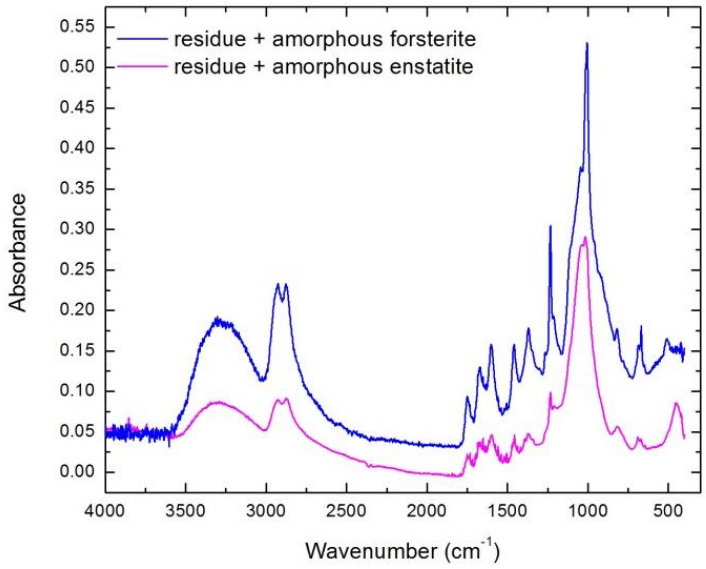

Figure 6.2 - Infrared spectra of the residue plus enstatite (magenta line) and the residue plus forsterite (blue line). The silicate contribution is visible in both spectra from the strong band around 1000 cm^{-1}.

In both spectra shown in Fig 6.2, the strong band centered around 1000 cm^{-1} receives the contribution of the Si-O stretch of the silicate film. This band appears dominant and in agreement with the spectra of the silicate films of pure amorphous forsterite and enstatite previously deposited on the KBr window, as shown in Fig. 6.3 *a* and *b*.

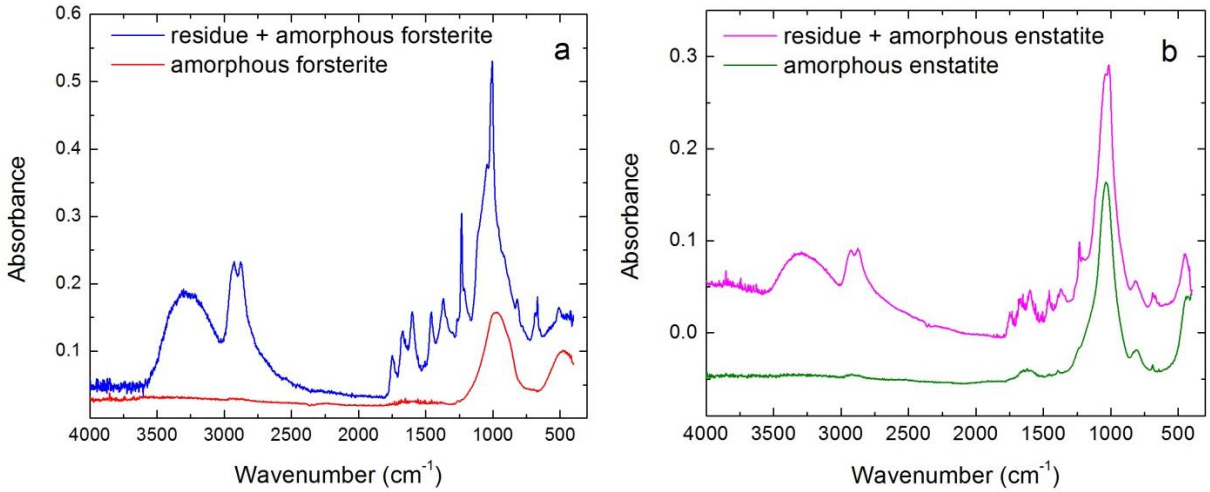

Figure 6.3 – Box a: Infrared spectra of the residue plus amorphous forsterite film (blue line) and amorphous forsterite film only (red line). Box b: Infrared spectra of the residue plus amorphous enstatite film (magenta line) and amorphous enstatite film only (olive line).

Compared to a standard residue produced without a silicate surface, both silicate-based residues do closely resemble the standard one produced directly on an inert MgF_2 window. This resemblance can be appreciated in Fig. 6.4 *a* and *b* where we show a comparison between the residue made on forsterite and a standard residue made on an MgF_2 inert window. For clarity reasons, the silicate features have been removed from the spectrum of the residue plus forsterite, so that the two spectra only pertain to the residues. It can be noted that all the bands present in the spectrum of the residue on forsterite are also observed almost at the same positions, shape and ratio in the spectrum of the standard residue.

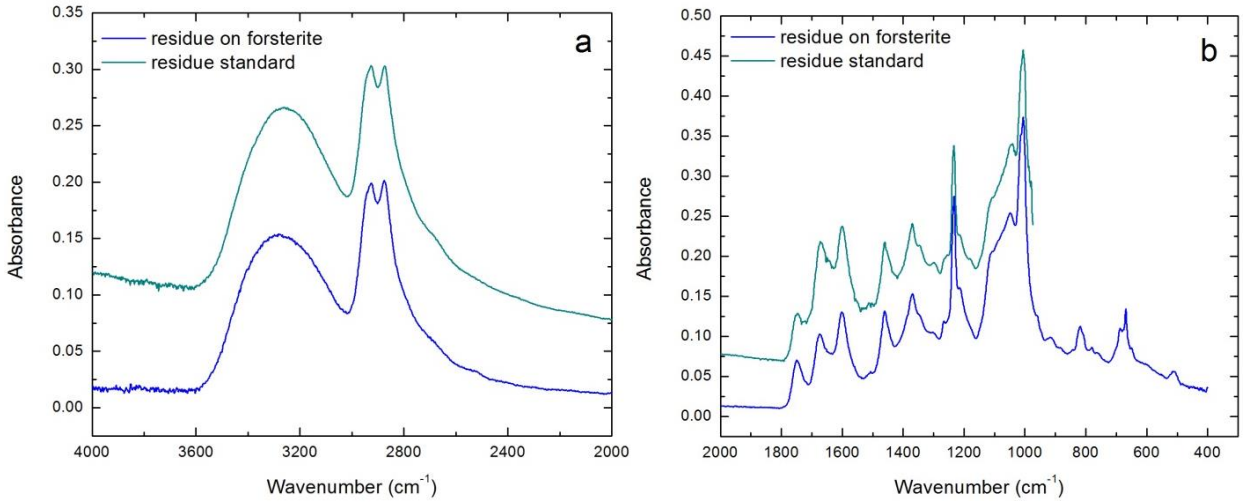

Figure 6.4 - IR spectra of a standard organic residue obtained on an MgF_2 window (cyan lines) and the residue obtained on the forsterite film but without the silicate contribution (blue lines) in the spectral regions 4000-2000 cm^{-1} (box a) and 2000-400 cm^{-1} (box b). From the comparison, these two spectra appear equivalent.

The same strong resemblance can be observed in the case of the residue made on enstatite, as shown in Fig. 6.5 *a* and *b,* even if in this case the quality of the spectrum is lower; for clarity reasons, in these figures the absorbance of enstatite has been multiplied by three. The possible small differences that can be noted from Fig. 6.4 and 6.5 could be ascribed to the slight variability among individual residue spectra. Therefore, we infer that the spectra made on silicates are equivalent to the spectra made on simple inert windows. This indicates that the presence and composition of silicates (forsterite or enstatite) does not play a significant role on

the nature of the organic residue produced by photo/thermo-chemistry of ices. From this we can also infer that our previous simulation studies, which do not involve any silicate surface, can be considered astrophysically pertinent as well. As indicated before, silicate surfaces in space do accrete ices so that volatiles and minerals remain separated and ices do not really react with the silicate surfaces. Naturally, it must be noted that the situation will change once icy grains are incorporated in meteoritic parent bodies such as comets and asteroids where, in particular, circulation of liquid water may occur.

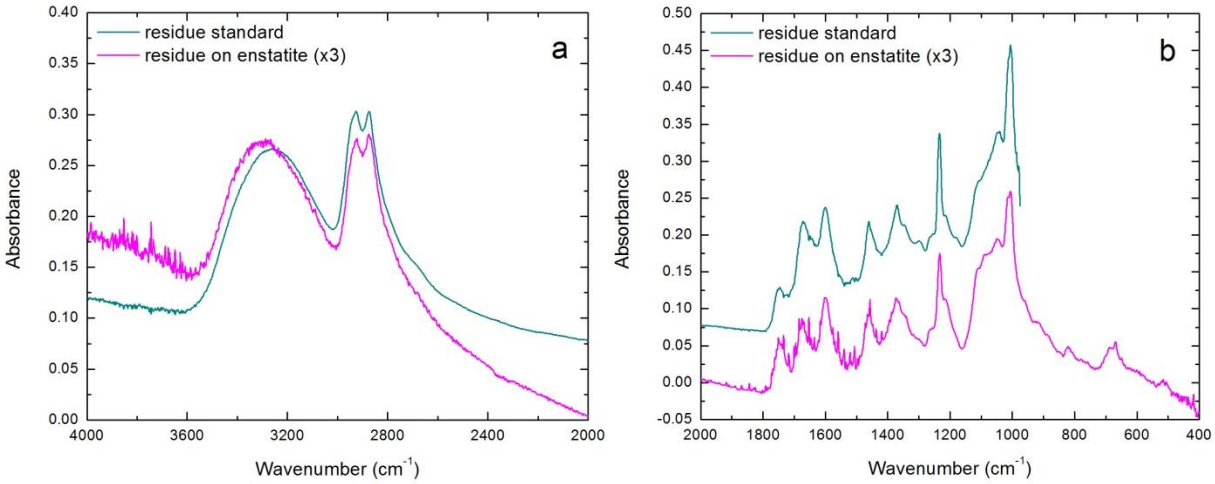

Figure 6.5 - IR spectra of a standard organic residue obtained on an MgF_2 window (cyan lines) and the residue obtained on the enstatite film but without the silicate contribution (magenta lines) in the spectral regions 4000-2000 cm^{-1} (box a) and 2000-400 cm^{-1} (box b). The absorbance of the enstatite spectrum has been multiplied by three for clarity. From the comparison, these two spectra appear equivalent.

6.2.2 Spectral comparison with the Paris meteorite

We wish now to go a step further, basing our deductions on the recent work of Merouane et al. (2012). In this work, four micron-sized fragments from the less altered lithology of the Paris meteorite showed peculiar micro IR spectra indicating a richer organic composition than the one of the main large fragment in which the micron-sized fragment were embedded. As previously described by Zanda et al. (2010), two lithologies are observed in Paris meteorite, one being less altered than the other. If the less altered lithology can be related to the most pristine matter in

the Paris meteorite, we can make the assumption that our laboratory organic residue may well be similar to the organic content of this less altered lithology. To substantiate this assumption, we compare in Fig. 6.6 the spectra of our residues and silicate films with one of the micron-sized fragments (fragment 2) examined by Merouane et al. (2012) since the four micron-sized fragments showed very similar spectra.

From Fig. 6.6, a global resemblance between this micron-sized fragment from the less altered lithology of the Paris meteorite and our residues and silicate films can be appreciated, mainly in the 3600-2500 cm^{-1} region and in the 1700-1200 cm^{-1} region. In particular, a good match can be noted between the features observed in the three spectra in the 2800-3000 cm^{-1} region, the well-known 3.4 μm band, which is attributed to the aliphatic hydrocarbon groups CH_2 and CH_3 in their vibrational stretching asymmetric and symmetric modes. Moreover, a general good resemblance can be noted in the 1200-800 cm^{-1} silicate band due to the Si-O stretch, mainly with the spectrum of the residue plus enstatite. In this region, the main difference is represented by the two bands at ~850 and ~900 cm^{-1} in the Paris meteorite spectrum which are due to the presence of crystalline structures in the meteoritic silicates; naturally, these bands cannot be found in our samples because of the totally amorphous structure of the laboratory silicate films. Finally, the lack of carbonates at 1400 cm^{-1} in the Paris meteorites spectrum (a further peculiarity of the micron-sized fragments with respect to the main fragment) allows the comparison also in the 1600-1250 cm^{-1} region. Here, additional bands can be observed in the three spectra such as the 1600 cm^{-1} COO- stretch, the 1460 cm^{-1} C-H deformation, and the 1369 cm^{-1} C-H bending mode, which are indicated by dot lines in Fig. 6.6.

We recall that, in Merouane et al (2012), the organic content of these peculiar tiny fragments do present similarities with the one observed with ISO in the molecular phase of the ISM toward the Galactic Center, in particular with GCS3. Thus, we can interpret our simulations as representative of a process occurring in the interstellar medium, where the complex photo/thermo-chemistry from the ices may later find its place in a piece of pristine meteoritic matter.

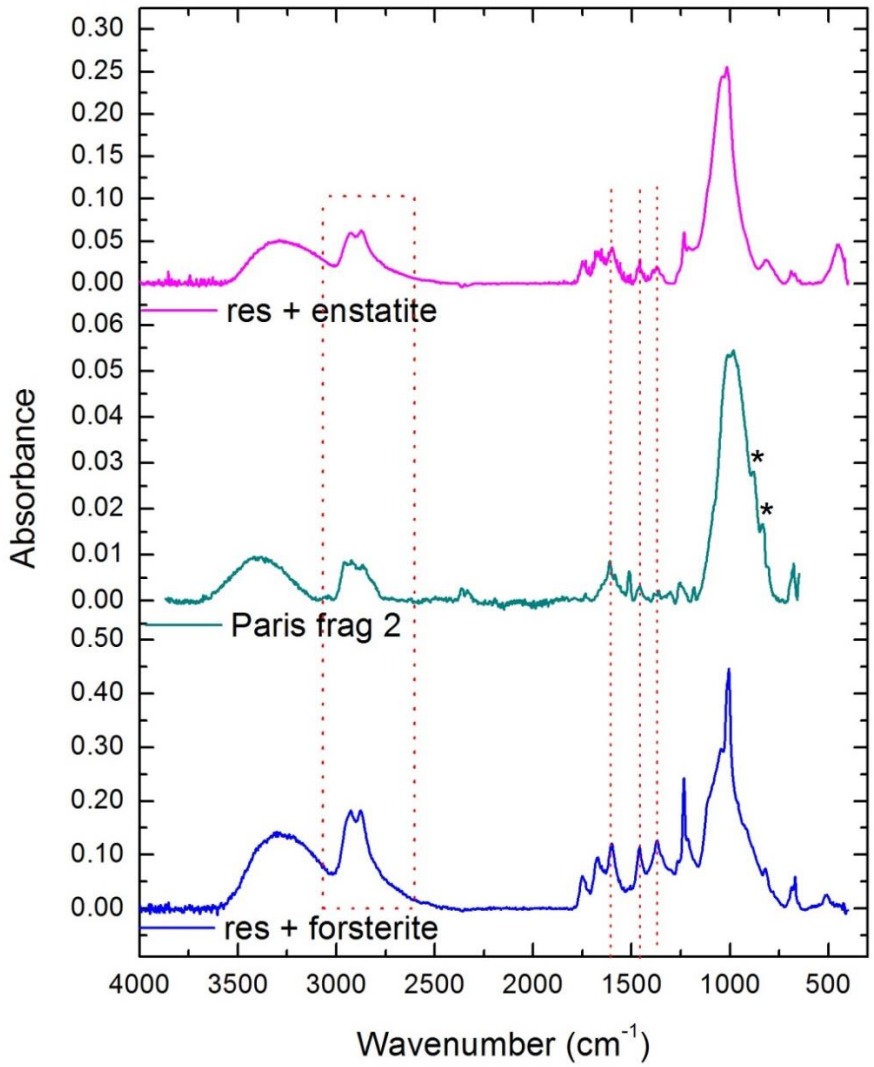

Figure 6.6 - Comparison between the infrared spectra of the residue plus enstatite sample (top), a micron-sized fragment of the Paris meteorite (middle, Merouane et al. 2012) and the residue plus forsterite sample (bottom). The main similarities are evidenced by the rectangle and the dot lines. The asterisks indicate crystalline structures in meteoritic silicates.

6.2.3 Hot water extraction test on laboratory samples

The classical extraction of the soluble organic matter (SOM) from the matrix of meteorites includes a first crucial step in which the meteoritic powder is put into a sealed ampoule with 1 ml of water and heated for 24 hours at 100 °C, as seen in Chapter 5. It is natural to wonder if this

procedure can affect the chemical nature of the original SOM, for example destroying the most labile molecules. In order to verify if and to what extent this procedure can modify the nature of the organic matter, we performed a simple experiment that imitates the hot water extraction of the SOM from meteorites according to a simplified procedure, feasible with the available equipment at IAS, and less aggressive than the classical protocol in terms of duration and temperature. This test was realized in a clean room, using all the right precautions to prevent ambient contaminations of the sample. We used one of our samples made of residue and silicate as an analog for the meteoritic original sample.

The residue plus enstatite film sample was chosen for this experiment. This sample was carefully scratched from its KBr window with a stainless steel spatula. A razor was used to remove the remaining part. Great care was taken, as far as possible, not to remove the KBr material in the scratching process. An image of the scratched sample is given in Fig. 6.7, viewed through a microscope X32.

Figure 6.7 – The residue and the enstatite film during the scratching process from the KBr window. On the left of the image, the surface of the sample is still unaltered; on the right, the signs of the scratching and the material removed are visible.

The scratched sample was then transferred into a glass vial with 1 ml of purified water. The solution was well mixed by means of an agitator, and then the vial was put into a thermoblock and heated at 80 °C for 10 hours. We chose to operate at these milder conditions (lower temperature and shorter time) because less aggressive then the classical protocol. During the heating phase, hot water was repeatedly added in order to replace the evaporated water. After 10 hours, the heating was stopped and the water was allowed final evaporation for additional 10 hours. The remaining solution (~0.3 ml) was recovered with a micropipette and re-deposited on the surface of a non-hygroscopic zinc selenide (ZnSe) window until dryness. Finally, a circular spot of extracts (residue and enstatite film fragments) of about 8 mm in diameter remained well visible on the surface of the window, as shown in Fig. 6.8.

Figure 6.8 - The re-deposited residue mixed with enstatite film fragments after hot water extraction, viewed through the microscope. The diameter of the circular spot is about 8 mm. The yellow color is due to the ZnSe window substrate.

After this procedure, an infrared spectrum of the hot water extracts of the re-deposited sample was taken in order to check for chemical modification of the initial sample. This spectrum is shown in Fig. 6.9, together with the spectrum of the same sample before hot water extraction at

80 °C; both spectra are shown without any baseline correction. Substantial differences can be observed between the two spectra, signs of deep chemical modifications occurred in presence of hot liquid water, as indeed expected. Firstly, the aliphatic features in the 2950-2850 cm^{-1} region completely disappear, then the carboxylic and amine bands in the 3500-3000 cm^{-1} region become broader and more structured, the band due to esters at 1750 cm^{-1} disappears, the two bands due to the amides in the 1670-1600 cm^{-1} region lose their structure. At the same time new bands appear, such as the broad band in the 1500-1250 cm^{-1} region and the sharp bands at 1191, 919, and 781 cm^{-1}.

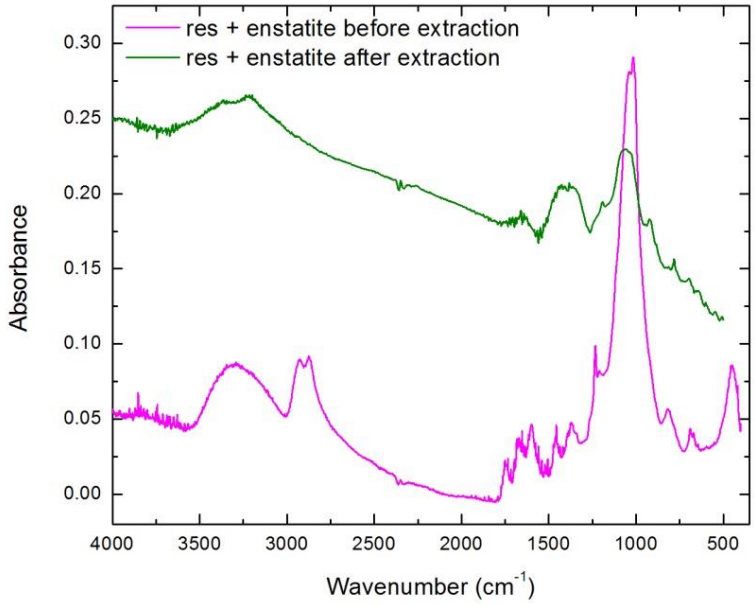

Figure 6.9 - Infrared spectra in the 4000-400 cm^{-1} region of the residue and enstatite film before (magenta line) and after (olive line) hot water extraction.

Among these changes we wish to emphasize, in particular, the disappearance of the bands of HMT. Six of the HMT bands fall in the 1600-400 cm^{-1} region and their presence can be observed in the spectrum of our residue before extraction in the enlargement shown in Fig. 6.10. In particular, the bands at 1370 cm^{-1} (C-H bending), 1236 cm^{-1} (C-N stretch), and 1007 cm^{-1} (C-N stretch) are ascribed to HMT only. If we look at the spectrum after hot water extraction, we can note that these bands are not present anymore. This is particularly evident for the sharp bands

at 1007 and 1236 cm^{-1}, and the weak band at 670 cm^{-1}, which totally disappear after hot water extraction, but it is also true, to a lesser extent, for the weak band at 813 cm^{-1}. The bands at 1370 and 1236 cm^{-1} also seem to disappear but the presence of a broad and strong band at the same position does not allow a firmer deduction. From the simple examination of these infrared spectra we can thus infer that the classical hot water extraction procedure of the SOM from meteoritic samples modifies the nature of the organics. Therefore, if labile molecules, such as HMT, were originally present in any meteoritic samples, they would be easily destroyed using this procedure and never detected.

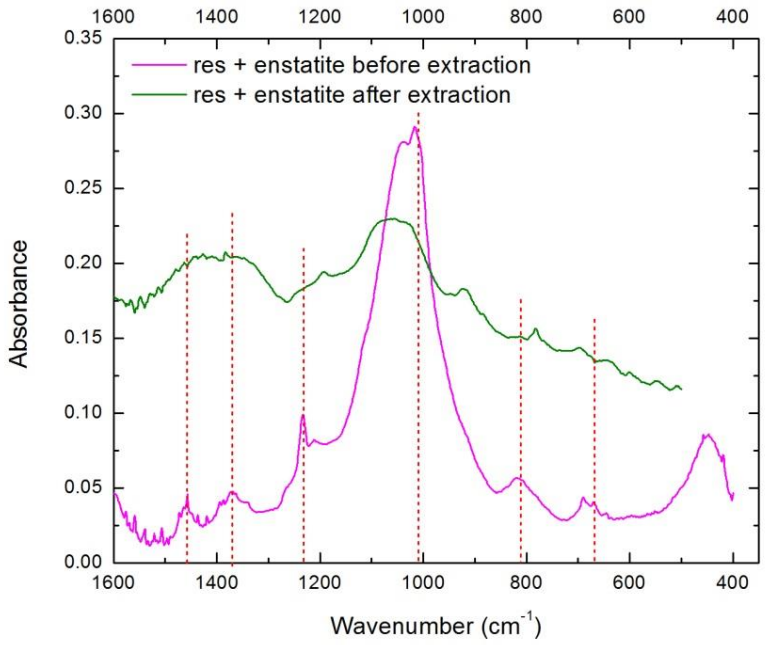

Figure 6.10 - Infrared spectra in the 1600-400 cm^{-1} region of the residue and enstatite film before (magenta line) and after (olive line) hot water extraction. The positions of the bands of HMT are evidenced by vertical dotted lines. After extractions, these bands are no more visible.

6.2.4 The search for HMT in the Paris meteorite

So far, using only the tool of infrared vibrational spectroscopy, the only molecule detected without any ambiguity in laboratory residues is the HMT molecule. HMT dominates the IR spectra of most of the residues, in particular those made out of H_2O, CH_3OH and NH_3 ices as in

our case. From that, we may infer that this molecule could also be present either on interstellar grains or, more importantly, in pristine meteorites. Note, however, that the direct observation of HMT by infrared spectroscopy of protostars in molecular clouds is a matter of debate because, exactly as in the laboratory case, the IR spectra of the residues are covered by bands from molecular ices that totally dominate the spectra (Muñoz Caro & Dartois 2009). HMT forms above 280 K (Vinogradoff et al. 2013), a temperature probably reached in the circumstellar disks during the accretional phase and the formation of planetesimals, when grains may have been heated and finally brought this molecule into meteoritic parent bodies (Ciesla & Sandford 2012).

Given the similarities already observed between our residues and the Paris meteorite (Chapter 5 and here above), we assume that HMT should be present inside very primitive meteorites, unless the presence of liquid water destroys it fast enough so that it escapes detection. In any case, HMT may represent a missing link between evolved ices in the final stages of molecular clouds and the original organic matter in our Solar System. HMT has been searched using GC-MS techniques in Murchison and Orgueil (Cottin et al. 2004) and in Orgueil, Acfer 094, and GRA 95229 (de Marcellus 2010, PhD Thesis). Unfortunately, negative results did not allow going further on this hypothesis that remains crucial in our scenario.

We have already evidenced the fact that the hot water extraction procedure clearly destroys HMT. Reconsidering the less altered lithology from four micron-sized fragments of the Paris meteorite, we checked for the possible presence of HMT in these fragments where *no previous chemical treatment* was employed. We used the data from Merouane et al. (2012) on fragment 1, obtained with the non-destructive method of IR micro spectroscopy. Naturally, since this fragment comprises rocky plus organic content with no selection of the SOM, we cannot expect to find intense HMT bands but only very weak ones. The micro IR spectrum of fragment 1 is shown in Fig. 6.11 where we checked for the main HMT bands. We can observe that, among the six checked bands, four very weak bands around 1458, 1236, 1007, and 811 cm^{-1} may be present, as evidenced by the arrows in Fig. 6.11. Of course, this identification needs to be further confirmed and should be regarded as only a tentative one.

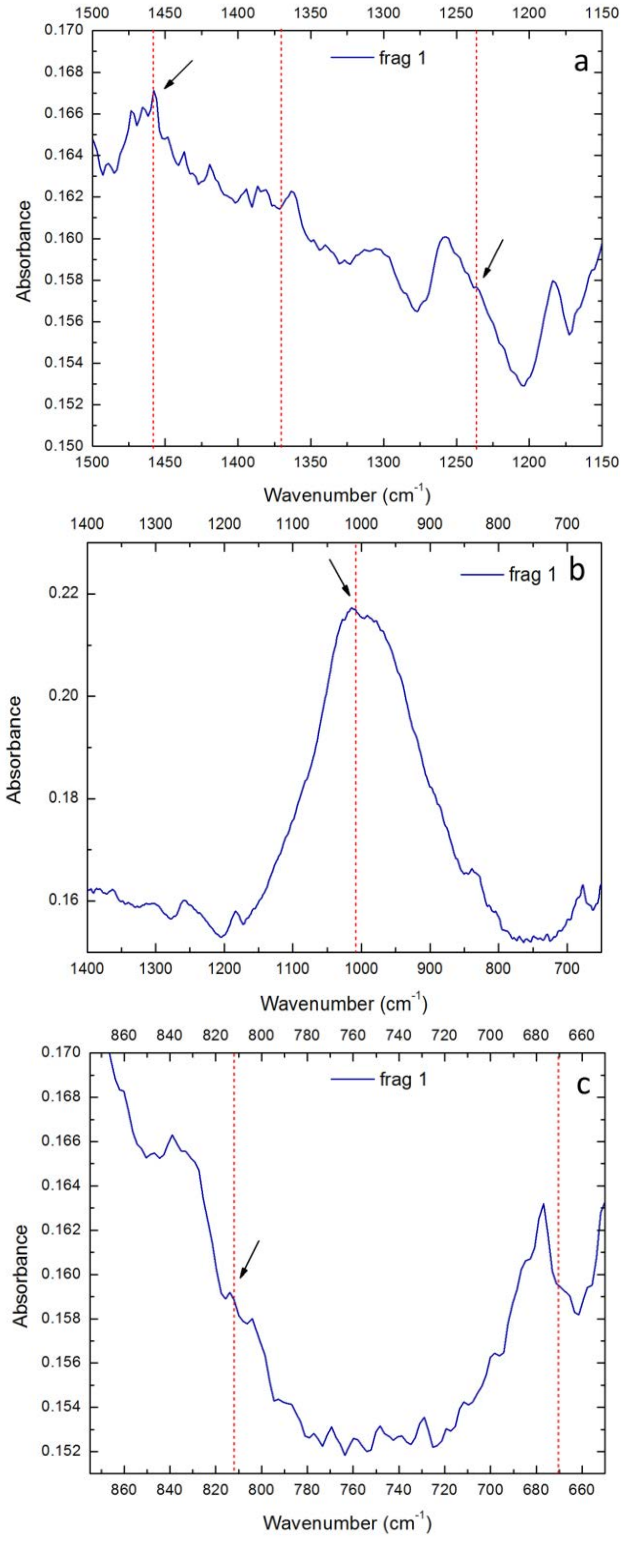

Figure 6.11 - Micro IR spectra of a fragment of Paris meteorite in the spectral regions 1500-1150 cm^{-1} (box a), 1400-650 cm^{-1} (box b), and 870-650 cm^{-1} (box c). Vertical dotted lines evidence the position expected for the HMT bands and arrows evidence the bands tentatively identified.

In support of the possible presence of HMT in pristine meteorites, a recent study on the thermal evolution of HMT in laboratory refractory residues suggests that HMT could be present in astrophysical environments in materials which have been slightly heated (Briani et al. 2013). More precisely, HMT could be present in the solid state in the small bodies of our Solar System such as comets and asteroids (the parent bodies of meteorites) in which the accreting materials have experienced temperatures between 280 K (the temperature at which the molecule starts to form) and 400 K (the temperature at which it sublimates), temperature conditions that certainly occurred in the nascent Solar System (Briani et al 2013). Although this temperature range is narrow, it is however possible that the most pristine carbonaceous chondrites contain some fractions of HMT. Since the Paris meteorite is reported having experienced only mild thermal metamorphism (Bourot-Denise et al. 2010; Zanda et al. 2010), this could well be the case.

Finally, an extraction method of the SOM without destroying its possible HMT content through hot water extraction is planned in our group and the detection of HMT could then be validated by a sensitive GC-MS technique.

6.3 Conclusions

We performed original experiments in which ice mixtures are deposited onto thin films of silicates and UV irradiated following the standard MICMOC procedure. This method allowed us proposing more realistic analogs of interstellar grains which include simultaneously the silicate (the core) and the ices (the mantle). We verified by IR spectroscopy that the organic residues formed on the silicate surface appear to be very similar in their chemical nature to the residues produced by the standard method on simple inert windows, thus validating our previous experimental approach. From the astrophysical point of view, these results imply that photo/thermo-chemistry on icy grains is performed in the bulk of the ices and that the silicate surface does not participate to the chemistry. Then, we compared favorably the IR spectrum of our analogs (organic residues plus silicate film) with the IR spectrum of a tiny fragment of the Paris meteorite selected within its less aqueously altered lithology. This suggests that part of the

organic matter present in very pristine meteorites may originate from interstellar/circumstellar ice chemistry prior to the formation of planetesimals.

In a further experiment, we showed that the classical method to extract the SOM from meteorites using hot liquid water can deeply influence the original SOM already at a temperature of 80 K. In particular, the key HMT molecule can be easily destroyed or react during this extraction. This could explain why HMT is at the present time not detected in the meteoritic SOM. Finally, a search for HMT in the micro-IR spectrum of a tiny fragment of the Paris meteorite not subjected to this extraction procedure, has revealed the presence of four weak bands that could tentatively be ascribed to HMT. Naturally, great care should be taken in this interpretation which awaits confirmation by more sensitive techniques.

Conclusions and perspectives

In this thesis we have shown that the photo/thermo-processes of simulated astrophysical ices prove to be efficient abiotic routes for the formation of complex organic compounds that may be relevant for prebiotic chemistry. We have based our work on laboratory simulations issued from non-directed experiments, a concept that was successfully initiated by Stanley Miller as far back as 1953. Non-directed experiments are those in which a system, starting from well-defined simple initial conditions, is freely let to evolve through complex multiple pathways until a final "arbitrary" status is reached. Only this final status represents the object of scientific interest for the study developed in this thesis, not the intermediate steps and pathways that led to it. This approach appears to be the most appropriate in experiments like ours where, starting from ice mixtures of only three simple components (water, methanol, and ammonia), the intrinsic complexity of the solid state chemistry evolves, through a very large set of reaction pathways, until the formation of the final products in the organic refractory residue. Undoubtedly, this residue contains organic materials of an extreme complex nature. In this sense, our experiments are similar to those of Miller concerning the primitive Earth's atmosphere and may be viewed as their generalization at the cosmic scale.

The use of these laboratory experiments for the production of organic refractory residues and their subsequent analysis has allowed obtaining several results in this thesis, as summarized below.

First, the polymeric and complex nature of the residues has been revealed by Fourier transform ion cyclotron resonance mass spectrometry (FT ICR MS). The observation of peaks at any nominal mass in the spectra shows the high compositional diversity of the molecules and the absence of chemical selectivity in their formation process, characteristics similar to what is observed in the SOM of meteorites. Several molecules have been detected, such as the HMT derivatives and, tentatively, also some amino acids. However, the potential of this technique is much higher than the detection of individual targeted molecules and can be extended to the

ensemble of molecules and family of molecules constituting the residue. Moreover, this technique could be successfully applied to the study of the SOM of pristine meteorites. These studies are planned in the next future in the frame of the already started TGE project.

In the course of this thesis, we had however the opportunity to study the SOM of a very pristine meteorite, the Paris CM chondrite. We analyzed its amino acid content and distribution by using the more classical method of GC MS. First, the primitiveness of Paris meteorite was confirmed by its high relative abundance of 4-carbon α-amino acids and very low ratio of β-alanine/glycine which can be correlated to a very low degree of aqueous alteration in the parent body of the meteorite. Then, this same analytical procedure was also used on our laboratory residues in order to obtain a coherent comparison of the results with the meteoritic ones. Indeed these results show that the amino acids distributions, and in particular the β-alanine/glycine ratio, perfectly match the meteoritic ones. These results first confirm the validity of our assumption according to which the laboratory residue represents the most primitive and non-altered material produced by photo/thermochemistry on cosmic grains; secondly they allow obtaining a sort of extension toward the “zero point” in the scale of aqueous alteration for different CM meteorites, where the residue represents an ideally and completely non-altered material. Our interpretation is that a relationship is possible between the amino acids present in very primitive meteorites and those produced in ices on grains prior to the formation of planetesimals.

We have also tested the validity of our experimental simulations by performing more realistic experiments in which we simulated the global icy grain structure, including the silicate surface. The presence of the silicates allowed obtaining infrared spectra that could be positively compared with that of a micron-sized rocky fragment from the less altered lithology of Paris. On the other hand, we show that the silicate surfaces do not play a significant role in the overall composition of the residues, probably because of the bulk nature of the ice photochemistry. We also propose a very tentative detection of HMT within one of these Paris fragments by micro-infrared spectroscopy. This detection should be confirmed by more appropriate GC MS methods and this experiment is underway. Since HMT is an abundant molecule in laboratory residues, this implies that, in the astrophysical context, HMT should be present in pristine meteorites and

be one of the main molecular targets for the Rosetta mission on comet 67P/ Churyumov-Gerasimenko.

Furthermore, we have studied the effects of the ultraviolet circularly polarized light (UV CPL) irradiation on cosmic ices to investigate the origin of the L-enantiomeric excesses observed in meteoritic amino acids. Using again our laboratory samples as analogs for cosmic ices, within the experimental framework of Chiral-MICMOC (thus using asymmetric UV irradiation), we detected 16 amino acids by GCxGC MS and the chiral ones were separated in the L and D enantiomers. These accurate separations allowed obtaining very precise measurements of the enantiomeric excesses induced in a total of five amino acids which clearly show a same helicity-dependent behavior at a fixed irradiation energy astrophysically relevant (10.2 eV). Similar experiments considering sugars (chiral biomolecules of D-handedness) are currently under development. The use of different parameters during our experimental campaigns allowed us obtaining an ample set of results that could be coherently interpreted and inserted in a plausible astrophysical scenario. The processes explored could explain the origin of the enantiomeric excesses observed in meteorites that may then lead to homochirality on the Earth. In this scenario, the ultraviolet photochemistry of ices for the formation of organic compounds is driven by UV CPL, also capable of inducing enantiomeric excesses in the chiral molecules. According to our scenario, asymmetric CPL of only one helicity from reflection nebulae associated with high mass YSOs irradiated our nascent Solar System. The asymmetrical photolysis of ices could induce slight enantiomeric excesses of the same form (for example L) in chiral amino acids or in their precursors. In the case in which ices were already sublimated (for example in the internal regions of the protoplanetary disc) these L-enantiomeric excesses could have been induced directly on the refractory organic residues themselves. Later, possibly after turbulent motions, the irradiated and enantioenriched materials may have been accreted into asteroids and comets, the parent bodies of meteorites. In these bodies aqueous alteration may have then increased the initial L values in some amino acids, such as in isovaline, as this seems to be the case in a series of meteorites with different degrees of alteration. The fact that in the Paris meteorite the isovaline ee_L value is not high (compatible with racemic) seems in line with its low degree of aqueous alteration, but unfortunately the error bars of our measurements obtained by classical

CG MS are too large for more conclusive results. In any case, the search for very small ee_L in the most pristine meteorites with sensitive equipment able to measure significant ee_L with small error bars is necessary and should be a top priority.

The fact that the Earth has indeed been seeded by organic compounds originating from extraterrestrial materials is quite certain, as attested by the analyses of primitive meteorites in which the presence of a rich and complex organic chemistry is clearly observed. However, due to the (yet) unknown nature of the laws governing the transition from the inert to the living and the unfortunate absence of preserved rocks and molecular “fossils” from this transition epoch, the hypothesis according to which life needed an exogenous supply of organic compounds to emerge is tempting but needs to be further explored. From this thesis and some general considerations on astrochemistry we may try to propose some positive arguments in favor of this hypothesis.

First, the richness of the ice chemistry, as well as its ubiquitous nature in molecular clouds are observational and experimental facts. Amino acids, the molecular bricks of life, are produced in the processes we simulate and they indeed could reach the surface of the Earth. The most important cosmic constraint here is the bulk chemistry of the ices that is clearly separated from the mineral chemistry, allowing for the build-up of a pure organic reservoir. This kind of chemistry can find its place only in environments where such separation takes place. This constraint is met in molecular clouds, while on the Earth the elements are clearly nor of cosmic abundances neither separated. In absence of this separation, an endogenous organometallic or mineral chemistry would possibly sequestrate all the CHNOPS in minerals, leaving not much room for an abundant organic chemistry.

Then, it is remarkable that the most pristine meteorites (Paris included) as well as our laboratory samples contain predominantly α-amino acids, the same class of amino acids involved in the making-up of proteins in living organisms. This argument may be considered a weak one, as due to pure coincidence, but it cannot be denied.

Finally, the production of different amino acids with enantiomeric excesses of the same form in our laboratory experiments could explain the L-enantiomeric excesses observed in meteorites. The presence of these meteoritic excesses may have directed the initial occurrence of the ee_L that further led to L-homochirality of amino acids on Earth. This constitutes a solid argument in favor of the hypothesis that life as we know it has indeed received a decisive extraterrestrial contribution to emerge.

However, a serious difficulty remains at this stage. The chemistry displayed in our laboratory residues, as well as in meteorites, shows an extreme complexity as well as clearly almost no molecular selectivity so that we may think that this awfully complicated organic mixture will never be able of any kind of auto-organization that is mandatory for life to emerge.

Keeping in mind difficulties and favorable arguments, the transition from the inert to the living, from a purely scientific point of view, must have been issued from deterministic processes governed by the laws of Nature. If, as scientists, we admit this proposition, then the next stage will be to be able to test it. This should be done step by step possibly following non-directed experiments, because there was obviously no prebiotic chemist on the early Earth with predetermined experiments on his mind. But clearly, this is definitely another idea that has to be developed in the future.

Appendix

Table 1 - Amino acid peak identification in the GC-MS chromatograms of the serpentine blank (hydrolyzed), and the Paris meteorite (hydrolyzed). Molecular ions used for quantification (first ion) and identification and are also displayed.

Peak #	Amino acid	Single ion (*m/z*)
1	α-AIB	154
2	L-Isovaline[a]	168
3	D-Isovaline[a]	168
4	D-Alanine	140/168
5	L-Alanine	140/168
6	D-α-ABA[b]	154
7	L-α-ABA[b]	154
8	D-Valine	168
9	L-Valine	168
10	Glycine	126/154
11	D,L-β-AIB[b,c]	182/153
12	D-Norvaline	168
13	L-Norvaline	168
14	β-Alanine	168/185
15	D-β-ABA[b]	140/182/153
16	L-β-ABA[b]	140/182/153
17	D-Leucine	140/182
18	L-Leucine	140/182
19	D-Norleucine	182/114
20	L-Norleucine	182/114
21	γ-ABA	182/154
22	D-Aspartic acid	184/212
23	L-Aspartic acid	184/212
24	EACA	210
25	D-Glutamic acid	180/198
26	L-Glutamic acid	180/198

[a] Isovaline enantiomers could not be separated using the Chirasil-L-Val column. Instead, D- and L-isovaline enantiomers were separated using the Chirasil-Dex CB column.

[b] Optically pure standard not available for enantiomeric identification. However, the order of elution of D-α-ABA and L-α-ABA was tentatively assigned, as the enantiomer of D-amino acids elutes first followed by the L-enantiomer when using the Chirasil-L-Val column.

[c] Enantiomers could not be separated under the chromatographic conditions.

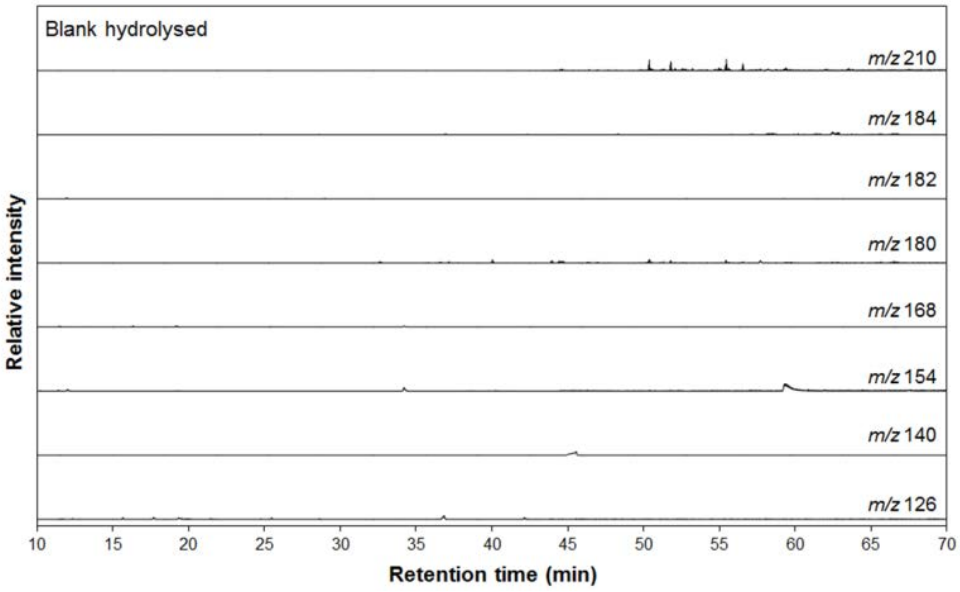

Figure 1 - The 10 to 70 min region of the single ion GC-MS traces of the derivatized and hydrolyzed serpentine blank for the meteoritic sample.

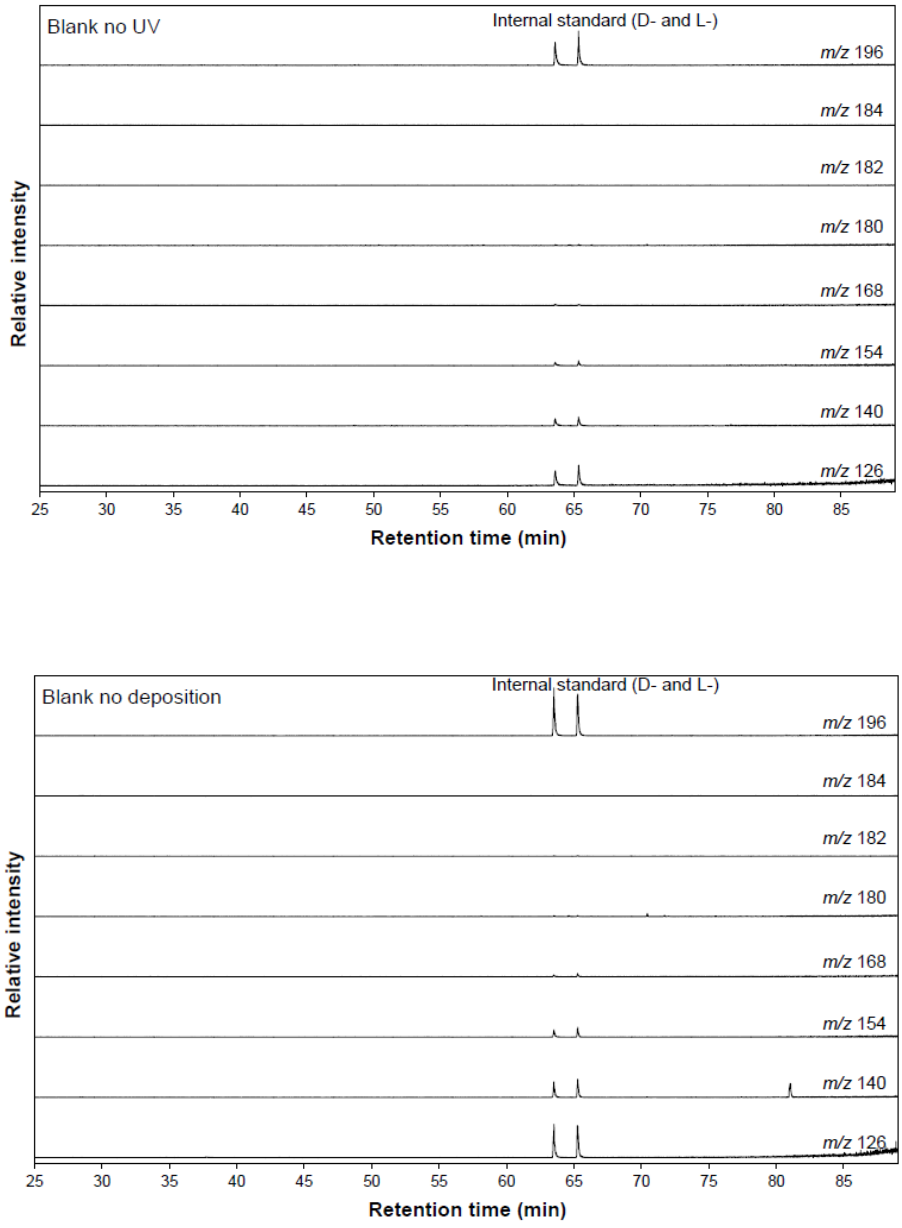

Figure 2 - Gas chromatograms in the 25-90 min region of the laboratory residue blanks obtained from deposition of the gas mixture without UV irradiation (top) and from UV irradiation without any deposition (bottom), respectively.

References

- Adams, W. S. 1941, Astrophys. J. 93, 11
- Agarwal, V. K., Schutte, W., Greenberg, J. M. et al. 1985, Origins of Life, 16, 21
- Allamandola, L. J., Sandford, S. A., Valero, G. J. 1988, Icarus, 76, 225
- Allamandola, L. J., Tielens, A. G. G. M., Barker, J. R. 1989, ApJ, 71, 733
- Allègre, C. J., Manhès, G., Göpel, C. 1995, Geochim. Cosmochim. Acta, 59, 1445
- Allen, M. & Robinson, G. W. 1977, ApJ, 212, 396
- Amster, I. J. 1996, J. Mass Spectrom. 31, 1325
- Backman, D. E., Werner, M. W., Rieke, G. H. et al. 1997, ASP Conference Series, Vol. 122, 1997, ed. Yvonne J. Pendleton; A. G. G. M. Tielens, p. 49
- Bailey, J. 2001, Orig. Life Evol. Biosph., 31, 167
- Bailey, J. 2006, Proceedings of the 6th Australian Space Science Conference, p 17
- Bailey, J., Chrysostomou, A., Hough, J. H. et al. 1998, Science, 281, 672
- Balavoine, G., Moradpour, A., Kagan, H. B. 1974, J. Am. Chem. Soc. 96, 5152
- Baratta, G. A., Leto, G., Palumbo, M. E. 2002, A&A, 384, 343
- Baratta, G. A., Spinella, F., Leto, G., Strazzulla, G., & Foti, G. 1991, A&A, 252, 421
- Barron, L. D. 1994, Science, 266, 1491
- Bell, M. B., Feldman, P. A., Travers, M. J. et al. 1997, ApJ, 483, L61
- Belloche, A., Menten, K. M. Comito, C., et al. 2008, A&A, 482, 179
- Belloche, A., Müller, H. S. P., Menten, K. M. et al. 2013, A&A, 559, A47
- Bennett, C. J., Chen, S.-H., Sun, B.-J. et al. 2007, ApJ, 660, 1588
- Bernstein, M. P., Dworkin, J. P., Sandford, S. A. et al. 2002, Nature, 416, 401
- Bernstein, M. P., Sandford, S. A., Allamandola, L. J. 2000, ApJ, 542, 894
- Bernstein, M. P., Sandford, S. A., Allamandola, L. J. et al. 1995, ApJ, 454, 327
- Blanchard, I., Gounelle, M., Bourot-Denise, et al. 2011, Meteoritics and Planetary Science Supplement, id.5322

- Bland, P. A., Cintala, M. J., Hörz, F. 2001, 32nd Annual Lunar and Planetary Science Conference, Houston, Texas, abstract no.1764
- Bland, P. A., Smith, T. B., Jull, A. J. T. 1996, MNRAS 283, 551
- Blank, J. L. 2001, Origins of Life and Evolution of the Biosphere, 31, 15
- Bockelée-Morvan, D., Crovisier, J., Mumma, M. J. et al. 2004, Comets II, M. C. Festou, H. U. Keller, and H. A. Weaver (eds.), University of Arizona Press, Tucson, 745, 391
- Bockelée-Morvan, D., Gautier, D., Hersant, F. Et al. 2002, Astron. Astrophys., 384, 1107
- Bockelée-Morvan, D., Lis, D. C., Wink, J. E. et al 2000, A&A, 353, 1101
- Bonner, W. A. & Rubenstein, E. 1987, Biosystems, 20, 99
- Bonner, W. A. 1991, Orig. Life Evol. Biosph., 21, 59
- Boogert, A. C. A., Pontoppidan, K. M., Knez, C. et al. 2008, ApJ, 678, 985
- Botta, O. & Bada, J. L. 2002, Extraterrestrial Organic Compounds in Meteorites, Surveys in Geophysics, 23, 411
- Botta, O., Glavin, D. P., Kminek, G., Bada, J. L. 2002, Origins of Life and Evolution of the Biosphere, 32, 143
- Botta, O., Martins, Z., Ehrenfreund, P. 2007, Meteoritics & Planetary Science 42, 81
- Bottinelli, S., Ceccarelli, C., Neri, R. et al. 2004b, ApJ, 617, L69
- Bottinelli, S., Ceccarelli, C., Williams, J. P. et al. 2007 A&A, 463, 601
- Bottinelli, S., Ceccarelli., Lefloch, B. et al. 2004a, ApJ, 615, 354
- Bourot-Denise, M., Zanda, B., Marrocchi, Y. et al. 2010, 41st Lunar and Planetary Science Conference #1533, p.1683
- Bouwman J., Meeus G., de Koter A. et al. 2001, Astron. Astrophys., 375, 950
- Bradley, J. P. 2003, Treatise on Geochemistry, 1, 689
- Brearley, A. J. 2005, Geochimica et Cosmochimica Acta Supplement, 69, A750
- Briani, G., Fray, N., Cottin, H. et al. 2013, Icarus, 226, 541
- Briggs, R., Ertem, G., Ferris, J. P. et al. 1992, Orig. Life Evol. Biosph., 22, 287
- Brown, P. D. & Charnley, S. B. 1990, MNRAS, 244, 432

- Brown, P. D., Charnley, S. B., Millar, T. J. 1988, MNRAS, 231, 409
- Browning, L. B., McSween, H. Y., Zolensky, M. E. 1996, Geochimica Cosmochimica Acta 60, 2621
- Brückner, H., Gams, W., Degenkolb T. 2009, Meteoritics and Planetary Science Supplement., p. 5052
- Buchardt, O. 1974, Angew. Chem. Int. Ed. 13, 179
- Burton, A. S., Stern, J. C., Elsila, J. E. et al. 2012, 41, 5459
- Buschermohle, M. & Whittet, D. C. B. 2005, ApJ, 624, 821
- Caillet Komorowski, C., Boudouma, O., Reynard, B., et al. 2011, Meteoritics and Planetary Science Supplement, id.5289
- Caravatti, P. & Allemann, M. 1991, Org. Mass Spectrom. 26, 514
- Cardelli, J. A. 1984, Astronomical Journal, 89, 1825
- Cardelli, J. A., Savage, B. D., Bruhweiler, F. C. et al. 1991, ApJ, 377, L57
- Cazaux, S., Tielens, A. G. G. M., Ceccarelli, C. et al. 2003, ApJ, 593, L51
- Ceccarelli, C. 2004, Star Formation in the Interstellar Medium, ASP Conference Proceedings, Vol. 323. Edited by D. Johnstone, F. C. Adams, D. N. C. Lin, D. A. Neufeld, and E. C. Ostriker. San Francisco: Astronomical Society of the Pacific, p.195
- Cerf, C. & Jorissen, A. 2000, Space Science Reviews, 92, 603
- Charnley, S. B., Kress, M. E., Tielens, A. G. G. M., & Millar, T. J. 1995, ApJ, 448, 232
- Charnley, S. B., Tielens, A. G. G. M., & Millar, T. J. 1992, ApJ, 399, L7
- Chen, Y.-J., Chuang, K.-J., Muñoz Caro, G. M. et al. 2014, ApJ, 781, 15
- Cheung, A. C., Rank, D. M., Townes, C. H. et al. 1968, Physical Review Letters, 21, 1701
- Chiar, J. E., Adamson, A. J., Pendleton, Y. J. et al. 2002, ApJ, 570, 198
- Chiar, J. E., Tielens, A. G. G. M., Whittet, D. C. B. et al. 2000, ApJ, 537, 749
- Chrysostomou, A., Gledhill, T. M. Menard, F. et al. 2000, MNRAS, 312, 103
- Chrysostomou, A., Lucas, P. W., Hough, J. H. 2007, Nature, 450, 71

- Chyba, C. & Sagan, C. 1992, Nature, 355, 125
- Chyba, C. F. 1990, Nature, 343, 129
- Ciesla, F. J. & Sandford, S. A. 2012, Science, 336, 452
- Clayton, R. N. & Mayeda, T. K. 1984, Earth Planet. Sci. Lett. 67,151
- Clayton, R. N. & Mayeda, T. K. 1996, Geochimica et Cosmochimica Acta, 60, 1999
- Clayton, R. N. & Mayeda, T. K. 1999, Geochimica et Cosmochimica Acta, 63, 2089
- Cody, G. D., Alexander, C. M. O'D. 2005, Geochimica et Cosmochimica Acta, 69, 1085
- Condon, E. U. 1937, Rev. Mod. Phys. 9, 432
- Cooper, G. W. & Cronin, J. R. 1995, Geochimica et Cosmochimica Acta 59: 1003
- Cooper, G. W., Onwo, W. M., Cronin, J. R. 1992, Geochimica et Cosmochimica Acta, 56, 4109
- Cottin, H., Engrand, C., d'Hendecourt, L. 2004, 35th COSPAR Scientific Assembly. Held 18 - 25 July 2004, in Paris, France., p. 2982
- Cottin, H., Gazeau, M. C., Raulin F. 1999, Planet. Space Sci., 47, 1141
- Cottin, H., Szopa, C., Moore, M. H. 2001, ApJ, 561, L139
- Cournède, C., Gattacceca, J., Zanda, B., Rochette, P. 2011, Meteoritics and Planetary Science Supplement, id.5252
- Cronin, J. R. & Chang, S. 1993, Organic matter in meteorites: molecular and isotopic analyses of the Murchison Meteorite, in The chemistry of life's origin, eds Greenberg, J. M., Mendoza-Gomez, C. X., Pirronello, V., Kluwer Academic Publishers, 209
- Cronin, J. R. & Pizzarello, S. 1983, Advs. Space Res., 3, 5
- Cronin, J. R. & Pizzarello, S. 1997, Science, 275, 951
- Cronin, J. R. & Pizzarello, S. 1999, Adv. Space Res., 23, 293
- Cronin, J. R. 1976, Origins of Life, 7, 337
- Cronin, J. R., Cooper, G. W., & Pizzarello, S. 1995, Adv. Space Res., 15, 91
- Cronin, J. R., Pizzarello, S., Cruikshank, D. P. et al. 1988, Organic matter in carbonaceous chondrites, planetary satellites, asteroids and comets, in Meteorites and the early solar system, eds Kerridhe, J. F. & Matthews, M. S., University of Arizona Press, p 819

- Crovisier, J., Leech, K., Bockelée- Morvan, D. et al. 1997, Science, 275, 1904
- Danger, G., Orthous-Daunay, F.-R., de Marcellus, P., Modica, P. et al. 2013, Geochim. Cosmochim. Acta, 118, 184
- Dartois, E. & Muñoz-Caro, G. M. 2007, A&A, 476, 1235
- Dartois, E. 1998, PhD thesis, Université Paris VI
- Dartois, E. 2005, Space Science Reviews, 119, 293
- Davoisne, C., Djouadi, Z., Leroux, H., et al. 2006, A&A, 448, L1-L4
- de Marcellus, P., Bertrand, M., Nuevo, M., et al. 2011b, Astrobiology, 11, 847
- de Marcellus, P., Meinert, C., Nuevo, M., et al. 2011a, ApJL, 727, 1
- de Marcellus, P., PhD thesis, Université Paris-Sud XI
- Delsemme, A. H. 1982, Icarus, 49, 438
- DeMeo, F. E., Binzel, R. P., Slivan, S. M. et al. 2009, Icarus, 202, 160
- Demyk, K., Carrez P., Leroux H. et al. 2001, Astron. Astrophys., 368, L38
- Demyk, K. 2000, PhD thesis, Université Paris-Sud XI
- Demyk, K., Dartois, E., d'Hendecourt, L. et al. 1998, A&A, 339, 553
- Demyk, K., Dartois, E., Wiesemeyer, H. et al. 2000, Composition of the Silicates around Evolved Stars and Protostars, in ISO Beyond the Peaks: The 2nd ISO Workshop on Analytical Spectroscopy, 456, 183
- Demyk, K., d'Hendecourt, L., Leroux, H. et al. 2004, A&A, 420, 233
- d'Hendecourt, L. B. & Jourdain de Muizon, M. 1989, A&A, 223, L5
- d'Hendecourt, L. B., Allamandola, L. J., Baas, F. et al. 1982, A&A, 109, L12
- d'Hendecourt, L. B., Allamandola, L. J., Greenberg, J. M. 1985, A&A, 152, 130
- d'Hendecourt, L. B., Allamandola, L. J., Grim, R. J. A., et al. 1986, A&A, 158, 119
- d'Hendecourt, L., & Dartois, E. 2001, Spectrochimica Acta Part A: Molecular and Biomolecular Spectroscopy, 57, 669
- d'Hendecourt, L., Jourdain de Muizon, M., Dartois, E. et al. 1996, A&A, 315, L365
- Djouadi, Z., d'Hendecourt, L., Leroux, H. et al. 2005, A&A, 440, 179
- Djouadi, Z., Gattacceca, J., d'Hendecourt, L. et al. 2007, A&A, 468, L9
- Douglas, A. E. & Herzberg, G. 1941, Astrophys. J. 94, 381

- Draine, B. T. 2003, Annual Review of Astronomy & Astrophysics, 41, 24
- Dunne, L., Eales, S., Ivison, R. 2003, Nature, 424, 285
- Ebel, D. S. 2000, J. Geophys. Res., 105, 10363
- Ehrenfreund, P. & Charnley, S. B. 2000, ARA&A, 38, 427
- Ehrenfreund, P. & Schutte, W. A. 2000 Advances in Space Research, 25, 2177
- Ehrenfreund, P., Bernstein, M. P., Dworkin, J. P. et al. 2001b., ApJ, 550, L95
- Ehrenfreund, P., Charnley, S. B., Botta, O. 2005, In: Astrophysics of life. Proceedings of the Space Telescope Science Institute Symposium, held in Baltimore, MD, USA, May 6-9, 2002, edited by M. Livio, I. N. Reid, W. B. Sparks. Space Telescope Science Institute symposium series, Vol. 16. Cambridge University Press, p. 1
- Ehrenfreund, P., Glavin, D. P., Botta, O. et al. 2001a, Proceedings of the National Academy of Sciences USA 98: 2138
- Elsila, J. E., Dworkin, J. P., Bernstein, M. P. et al. ApJ, 2007, 660, 911
- Elsila, J. E., Glavin, D. P., Dworkin, J. P. 2009, Meteoritics & Planetary Science, 44, 1323
- Engel, M. H., & Macko, S. A. 1997, Nature, 389, 265
- Engel, M. H., & Nagy, B. 1982, Nature, 296, 837
- Evans, A. C., Meinert, C., Bredehöft, J. H., et al. 2013, Top. Curr. Chem., 341, 271
- Evans, A. C., Meinert, C., Giri, C., Goesmann, F., Meierhenrich, U. J. 2012, Chem. Soc. Rev., 41, 5447
- Flores, J. J., Bonner, W. A., Massey, G. A. 1977, J. Am. Chem. Soc. 99, 3622
- Fomenkova, M. N., 1999, Space Science Reviews 90, 109
- Fukue, T., Tamura, M., Kandori, R. et al. 2009, ApJL, 692, L88
- Fukue, T., Tamura, M., Kandori, R. et al. 2010 Orig. Life Evol. Biosph., 40, 335
- Gail, H.-P. 2004, Astron. Astrophys., 413, 571
- Garrod, R. T. & Herbst, E. 2006, A&A, 457, 927
- Garrod, R. T., Weaver, S. L. W., Herbst, E. 2008, ApJ, 682, 283
- Geballe, T. R., Baas, F., Greenberg, J. M. et al. 1985, A&A, 146, L6
- Genzel, R. & Stutzki, J. 1989, ARA&A, 27, 41

- Geppert, W. D., Hamberg, M., Thomas, R. D., et al. 2006, Faraday Discussions, 133, 177
- Gerakines, P. A., Moore, M. H., Hudson, R. L. 2000, A&A, 357, 793
- Gerakines, P. A., Schutte, W. A., Greenberg, J. M. et al. 1995, A&A, 296, 810
- Gibb, E. L. & Whittet, D. C. B. 2002, ApJ, 566, L113
- Gibb, E. L., Whittet, D. C. B., Schutte, W. A. et al. 2000, ApJ, 536, 347
- Gillet, F. C. & Forrest, W. J. 1973, ApJ, 179, 483
- Gilmam, R. G. 1969, Astrophysical Journal, 155, L185
- Glavin, D. P., & Dworkin, J. P. 2009, PNAS, 106, 5487
- Glavin, D. P., Bada, J. L., Brinton K. L. F. et al. 1999, Proceedings of the National Academy of Sciences, 96, 8835
- Glavin, D. P., Callahan, M. P., Dworkin, J. P. et al. 2011, Meteoritics & Planetary Science 45, 1948
- Glavin, D. P., Callahan, M. P., Dworkin, J. P., Elsila, J. E. Meteorit. Planet. Sci. Suppl., 2010, id 5131
- Glavin, D. P., Dworkin, J. P., Aubrey, A. et al. 2006, Meteoritics, 41, 889
- Glavin, D. P., Elsila, J. E., Burton, A. S. et al. 2012, Meteoritic & Planetary Science, 47, 8, 1347
- Gledhill, T. M. & McCall, A. 2000, MNRAS, 314,123
- Goesmann, F., Rosenbauer, H., Roll, R., 2007 Space Science Reviews, 128, 257
- Gomes, R., Levison, H. F., Tsiganis, K. et al. 2005, Nature, 435, 466
- Gounelle, M. & Meynet, G. 2012, A&A, 545, A4
- Gradie, J. & Tedesco, E. 1982, Science, 216, 1405
- Greenberg, J. M. & Yencha, A. J. 1973, Interstellar Dust and Related Topics. IAU Symposium no. 52, held at the State University of New York at Albany, Albany, N.Y., U.S.A. Edited by Jerome Mayo Greenberg and Henrik Christoffel van de Hulst. International Astronomical Union. Symposium no. 52, Dordrecht, Boston, Reidel, p.369
- Greenberg, J. M. 1974, Astrophys. J. Lett., 189, L81
- Greenberg, J. M. 1986, Astrophysics and Space Science, 128, 17

- Greenberg, J. M. 2002, Surface Science, 500, 793
- Greenberg, J. M., Li, A., Mendoza-Gomez, C. X. et al. 1995, ApJL, 455, L177
- Greenberg, J. M., Yencha, A. J., Corbett, J. W. 1972, Ultraviolet effects on the chemical composition and optical properties of interstellar grains, in: Mem. Soc. Roy. des Sciences de Liege, 6e Serie, tome III, p. 425
- Greenberg, M. J, & Hage, J. I. 1990, ApJ, 361, 260
- Greenberg, M. J. 1973, Molecules in the Galactic Environment, Proceedings of a Symposium, held at the University of Virginia, November 4-7, 1971, Edited by M.A. Gordon, and Lewis E. Snyder. New York, NY: John Wiley and Sons, 1973, p. 93
- Greenberg, M. J. 1982, “Dust in dense clouds - One stage in a cycle” in Submillimeter Wave Astronomy, eds Beckman, J. E. & Phillips, J. P., 261
- Greenberg, M. J. 2002 "Cosmic dust and our origins". Surface Science 500, 793, 822
- Greenberg, M. J., Kouchi, A., Niessen, W. et al. 1994 J. Biol. Phys. 20, 61
- Grim, R. J. A., Baas, F., Greenberg, J. M. et al. 1991, A&A, 243, 473
- Gudipati, M. & Allamandola, L. 2003, ApJ, 596, L195
- Guillois, O., Ledoux, G., & Reynaud, C. 1999, ApJ, 521, L133
- Guss, K. M.-R. 2013, PhD thesis, Leiden University
- Haack, H., Grau, T., Bischoff, A. et al. 2012, Meteor. Planet. Sci. 47, 30
- Hagen, W., Allamandola, L. J. & Greenberg, J. M. 1979, Ap&SS, 65, 215
- Hahn, J. H., Zenobi, R., Bada, J. L. et al. 1988, Progress Toward a Cosmic Dust Collection Facility on Space Station. Edited by Ian D. R. Mackinnon and William C. Carey. LPI Technical Report 88-01, published by Lunar and Planetary Institute, 3303 NASA Road 1, Houston, TX 77058, 1988, p. 32
- Hall, J. S. 1949, Science, 109, 166
- Hanner, M. S. & Bradley, J. P 2004 “Composition and mineralogy of cometary dust” in Comets II, eds Festou, M. C., Keller, H. U., Weaver, H. A., 555
- Hanner, M. S. & Zolensky, M. E. 2010, in Lecture Notes in Physics, Berlin Springer Verlag, vol 815, ed T. Henning, 203
- Harker, D. E. & Desch, S. J. 2002, Astrophys. J., 565, L109

- Harker, D. E., Woodward, C. E., Wooden, D. H. 2005, Science, 310, 278
- Hasegawa, T. I., Herbst, E., Leung, C. M. 1992, ApJS, 82, 167
- Hendrickson, C. L. & Emmett, M. R. 1999, Annu. Rev. Phys. Chem. 50, 517
- Henning, T. 2003, Astromineralogy, Lecture Notes in Physics, eds Henning, T., Vol 609
- Herbst, E. & van Dishoeck, E. F. 2009, ARA&A, 47, 427
- Herbst, E. 1995, "Large Molecules in the Interstellar Medium", in "The Diffuse Interstellar Bands" eds. Tielens, A.G.G.M. & Snow, T. P. ASSL series, vol 202, 307
- Herbst, E., Green, S., Thaddeus, P., & Klemperer, W. 1977, ApJ, 215, 503
- Hester, J. J., Healy, K. R., Desch, S. J. 2004 American Astronomical Society Meeting 205, #105.01, Bulletin of the American Astronomical Society, Vol. 36, p.1516
- Hewins, R. H., Bourot-Denise, M., Zanda, B. et al. 2014 Geochimica et Cosmochimica Acta, 124
- Hillenbrand, L. A., 1997, Astron. J., 113, 1733
- Hiltner, W. A. 1949, Nature, 163, 283
- Hobbs, L. M., Welty, D. E., Morton, D. C., Spitzer, L. et al. 1993, ApJ, 411, 750
- Hollenbach, D. & Salpeter, E. E. 1970, J. Chem. Phys. 53, 79.
- Hollenbach, D. & Salpeter, E. E. 1971, ApJ, 163, 155
- Hollis, J. M., Jewell, P. R., Lovas, F. J., & Remijan, A. 2004, ApJ, 613, L45
- Hollis, J. M., Lovas, F. J., Jewell, P. R. 2000, ApJ, 540, L107
- Hollis, J. M., Lovas, F. J., Jewell, P. R. et al. 2002, ApJ, 571, L59
- Hollis, J. M., Lovas, F. J., Remijan, A. J. et al. 2006, ApJ, 643, L25
- Horn, A., Møllendal, H., Sekiguchi, O., et al. 2004, ApJ, 611, 605
- Hough, J. H., Bailey, J. A., Chrysostomou, A. 2001, Adv. Space Res., 27, 313
- Hudson, R. L. & Moore, M. H. 2000, Icarus, 145, 661
- Hudson, R. L., Moore, M. H., Gerakines, P. A. 2001, ApJ, 550, 1140
- Irvine, W. M. 1999, Space Science Reviews, 90, 203
- Irvine, W. M., Schloerb, F. P., Crovisier, J. et al. 2000, Protostars and Planets IV (Book - Tucson: University of Arizona Press; eds Mannings, V., Boss, A. P., Russell, S. S.), p. 1159

- Jenniskens, P., Baratta, G. A., Kouchi, A. et al. 1993, A&A, 273, 583
- Jones, A. P. 2001 Royal Society of London Philosophical Transactions Series A, 359, 1961
- Jungclaus, G., A., Yuen, G. U., Moore, C. B. et al. 1976, Meteoritics, 11, 231
- Kaneko, F., Yagi-Watanabe, K., Tanaka, M. et al. 2009, The physical Society of Japan, 78, 1
- Kasamatsu, T., Kaneko,T., Saito, T. et al. 1997, Bulletin of the Chemical society of Japan, 70, 1021
- Keane, J. V., Boogert, A. C. A., Tielens, A. G. G. M. et al. 2001, A&A, 375, L43
- Keil, R. G. & Kirchman, D. L. 1991, Marine Chemistry, 33, 243
- Keller, J. W., Baurick, K. B., Rutt, G. C. et al. 1990, J. Biol. Chem. 265, 5531
- Kemper, F., Molster, F. J., Jäger, C. et al. 2002, A&A. 394, 679
- Kemper, F., Vriend, W. J., Tielens, A. G. G. M. 2004, ApJ, 609, 826
- Kemper, F., Waters, L. B. F. M., de Koter, A. et al. 2001, A&A, 369, 132
- Kimura, M., Grossman, J. N., Weisberg, M. K. 2011, Meteoritics & Planetary Science 46, 431
- Kissel J. & Krueger F. R. 1987, Nature 326, 755
- Kotra, R. K., Shimoyama, A., Ponnamperuma, C. et al. 1979, Journal of Molecular Evolution 13, 179
- Kuan, Y., Charnley, S., B., Huang, H. et al. 2003, ApJ, 593, 848
- Kuan, Y., Huang, H., Charnley, S. B. et al. 2004, ApJ, 616, L27
- Kuhn, W. & Braun, E. 1929, Naturwissenschaften, 17, 227
- Kuhn, W. 1930, Trans. Faraday Soc., 26, 293
- Kvendvolden, K. A., Lawless, J., Pering, K. et al. 1970, Nature, 228, 923
- Kvenvolden, K. A., Lawless, J. G., Ponnamperuma, Cyril 1971, Proceedings of the National Academy of Sciences of the United States of America, Vol. 68, Issue 2, p. 486
- Kwok, S., 2009, Astrophys. Space Sci., 319, 5
- Kwon, J., Tamura, M., Lucas, P. W. et al. 2013, ApJL, 765, L6
- Lacy, J. H., Baas, F., Allamandola, L. J., et al. 1984, ApJ, 276, 533

- Lacy, J. H., Carr, J. S., Evans, II, N. J., et al. 1991, ApJ, 376, 556
- Lacy, J. H., Faraji, H., Sandford, S. A., et al. 1998, ApJ, 501, L105
- Lawless, J. G. & Yuen, G. U. 1979, Nature, 282, 396
- Léger, A., Klein, J., de Cheveigne, S., et al. 1979, A&A, 79, 256
- Léger, A., Puget, J. L. 1984, A&A, 137, L5
- Leto, G. & Baratta, G. A. 2003, A&A, 397, 7
- Li, A., & Draine, B.T. 2001, ApJ, 550, L213
- Love, S. G. & Brownlee, D. E. 1993, Science, 262, 550
- Lucas, P. W., Hough, J. H., Bailey, J. et al. 2005, Orig. Life Evol. Biosph., 79, 921
- Magnani, L. & Onello, J. S. 1995, ApJ, 443, 169
- Marshall, A. G. & Grosshans, P. B. 1991, Anal. Chem. 63, 215A
- Marshall, A. G., Hendrickson, C. L., Jackson, G. S. 1998, Mass Spectrom. Rev. 17, 1
- Martin, P. G. 1978, Cosmic Dust, its Impact on Astronomy (Oxford: Oxford Univ. Press)
- Martins, Z., Watson, J. S., Sephton, M. A. et al. 2006, Meteoritics & Planetary Science 41, 1073
- Martins, Z., Alexander, C. M. O' D., Orzechowska, G. E. et al. 2007, Meteoritics & Planetary Science 42, 2125
- Martins, Z., Modica, P., Sephton, M. A. et al. 2013, 76th Ann. MetSoc. Meet, 2013 Edmonton, Meteorit. Planet. Sci. Suppl. id.5115
- Martins, Z., Modica, P., Zanda, B. et al. 2015, MAPS, accepted
- Martins, Z., Price, M. C., Goldman, N., et al. 2013, Nature Geoscience 6, 1045
- Mathew, S. P., Iwamura, H., Blackmond, D. G. 2004, Angew. Chem. Int. Ed, 43, 3317
- Mathis J. S. 1990, Ann. Rev. Astron. Astrophys., 28, 37
- Mathis, J. S., Rumpl, W., Nordsieck, K. H. 1977, ApJ, 217, 425
- Maurette, M. 1998, Origins of Life and Evolution of the Biosphere, 28, 385
- McKee, C. F. & Ostriker, J. P. 1977, ApJ, 218, 148
- McKellar, A. 1940, PASP, 52, 187

- McSween, H. Y., Jr., Sears, D. W. G., Dodd, R. T. 1988, Thermal metamorphism, in Meteorites and the early solar system (A89-27476 10-91). Tucson, AZ, University of Arizona Press, 1988, p. 102
- Meierhenrich, U. J. 2008, Amino Acids and the Asymmetry of Life - Caught in the Act of Formation. Springer, Heidelberg
- Meierhenrich, U. J., Filippi, J.-J., Meinert, C., et al. 2010, Angew. Chem. Int. Ed. 49, 7799
- Meierhenrich, U. J., Muñoz Caro, G. M., Bredehöft, J.-H., et al. 2004, PNAS, 101, 9182
- Meierhenrich, U. J., Nahon, L., Alcaraz, C., et al. 2005, Angew. Chem.-Int. Ed., 44, 5630
- Meinert, C. & Meierhenrich, U. J. 2012, Angew. Chem.-Int. Ed., 51, 10460
- Meinert, C. & Meierhenrich, U. J. 2014, ChemPlusChem doi:10.1002/cplu.201300328
- Meinert, C., Bredehöft, J. H., Filippi, J.-J., et al. 2012b, Angew. Chem. Int. Ed., 51, 4484
- Meinert, C., Hoffmann, S. V., Cassam-Chenaï, P., et al. 2014 Angew. Chem. Int. Ed., 53, 210
- Meinert, C., J.-J. Filippi, de Marcellus, P. et al. 2012a ChemPlusChem, 77, 186
- Menard, F., Chrysostomu, A., Gledhill, T. et al. 2000, ASPC, 213, 355
- Mennella, V., Baratta, G. A., Esposito, A. et al. 2003, ApJ, 587, 727
- Mennella, V., Brucato, J. R., Colangeli, L., Palumbo, P. 2002, Adv. Space Res., 30, 1451
- Merouane, S. 2013, PhD thesis, Université Paris-Sud XI
- Merouane, S., Djouadi, Z., d'Hendecourt, L. et al. 2012, ApJ, 756, 154
- Millar, T. J. & Hatchell, J. 1998, Faraday Discussions, 109, 15
- Millar, T. J., Herbst, E., & Charnley, S. B. 1991, ApJ, 369, 147
- Miller, G. E., & Scalo, J. M. 1978, PASP, 90, 506
- Min, M., Waters, L. B. F. M., de Koter, A. et al. 2007, A&A, 462, 667
- Misharin, A. & Zubarev, R. 2012, Science & Engineering Services, Inc., US 8304715 B2
- Modica, P., de Marcellus, P., Baklouti, D. et al. 2012, ECLA - Edited by C. Stehlé, C. Joblin and L. d'Hendecourt. EAS Publications Series, Vol. 58, 2012, 343
- Modica, P. & Palumbo, M. E. 2010, A&A, 519, A22
- Modica, P., Meinert, C., de Marcellus, P. et al. 2014, ApJ, 788, 79

- Molster, F. J., Waters, L. B. F. M., Tielens, A. G. G. M. et al. 2002 A&A, 382, 222
- Morgan, H. L. & Edmunds, M. G. 2003, MNRAS, 343, 427
- Mostefaoui, S., Lugmair, G. W., Hoppe, P. 2005 ApJ, 625, 271
- Mumma, M. J. 1997, ASP Conference Series, Vol. 122, ed. Y. J. Pendleton, A. G. G. M. Tielens, p. 369
- Muñoz Caro, G. M. & Dartois, E. 2009, A&A, 494, 109
- Muñoz Caro, G. M. & Schutte, W. A. 2003, A&A, 412, 121
- Muñoz Caro, G. M., Meierhenrich, U. J., Schutte, W. A. et al. 2004, A&A, 413, 209
- Muñoz Caro, G. M., Meierhenrich, U. J., Schutte, W. A. et al. 2002, Nature, 416, 403
- Nahon, L., de Oliveira, N., Garcia, G. A., 2012, Journal of synchrotron radiation, 19, 508
- Norden, B. 1977, Nature, 266, 567
- Nuevo, M. 2005, PhD thesis, Université Paris-Sud XI
- Nuevo, M., Auger, G., Blanot, D. et al. 2008, Orig. Life Evol. Biosph., 38, 37
- Nuevo, M., Bredehöft, J. H., Meierhenrich, U. J. et al. 2010, Astrobiology, 10, 245
- Nuevo, M., Meierhenrich, U. J., d'Hendecourt, L., et al. 2007, Adv. Space Res., 39, 400
- Nuevo, M., Meierhenrich, U. J., Muñoz Caro, G. M. et al. 2006, A&A, 457, 741
- Nuevo, M., Milam, S. N., Sandford, S. A., Elsila, J. E. et al. 2009, Astrobiology, 9, 683
- Öberg, K. I. 2009, PhD thesis, Leiden University
- Öberg, K. I., Linnartz, H., Visser, R., & van Dishoeck, E. F. 2009, ApJ, 693, 1209
- Oka, T. 2006, PNAS ,103, 33
- Oort, J. H. & van de Hulst, H. C. 1946, Bull. Astron. Inst. Netherlands, 10, 187
- Oró, J. 1961, Nature, 190, 389
- Oró, J., Gibert, J., Lichtenstein, H. et al. 1971, Nature, 230,105
- Orthous-Daunay, F. R. 2011, PhD thesis, Université de Grenoble, Institut de Planétologie et d'Astrophysique
- Palmer, E. E. & Lauretta, D. S. 2011, Meteoritics & Planetary Science 46, 1587
- Palumbo, M. E., Strazzulla, G., Pendleton, Y. J. et al. 2000, ApJ, 534, 801
- Peltzer, E. T. & Bada, J. L. 1978, Nature, 272, 443
- Peltzer, E. T., Bada, J. L., Schlesinger, G., & Miller, S. L. 1984, Adv. Space Res., 4, 69

- Pendleton, Y. J. & Allamandola, L. J. 2002, ApJS, 138, 75
- Pendleton, Y. J., Sandford, S. A., Allamandola, L. J. et al.1994, ApJ, 437, 683
- Pendleton, Y. J., Tielens, A. G. G. M., Tokunaga, A. T. et al. 1999, ApJ, 513, 294
- Pering, K. L. & Ponnamperuma, C. 1971, Science, 173, 237
- Pierazzo, E. & Chyba, C. F. 1999, Meteoritics & Planetary Science, 34, 909
- Pizzarello, S., & Cronin J. R. 2000, Geochim. Cosmochim. Acta, 64, 329
- Pizzarello, S., & Huang, Y. 2005, Geochim. Cosmochim. Acta, 69, 599
- Pizzarello, S., Feng, X., Epstein, S., & Cronin, J. R. 1994, Geochim. Cosmochim. Acta, 58, 5579
- Pizzarello, S., Huang Y., Alexandre, M. R. 2008, Proceedings of the National Academy of Sciences, 105, 3700
- Pizzarello, S., Krishnamurthy, R. V., Epstein, S., & Cronin, J. R. 1991, Geochim. Cosmochim. Acta, 55, 905
- Pizzarello, S., Schrader, D. L., Monroe, A. A. 2012, Proceedings of the National Academy of Sciences, 109, 11949
- Pizzarello, S., Zolensky, M., Turk, K. A. 2003, Geochim. Cosmochim Acta, 67, 1589
- Planck Collaboration 2014, ArXiv e-prints 1405.0873
- Prasad, S. S. & Tarafdar, S. P. 1983, ApJ, 267, 603
- Puget, J. L. & Leger, A. 1989 In: Annual review of astronomy and astrophysics, 27, 161
- Rachford, B. L., Snow, T. P., Tumlinson, J. et al. 2002, ApJ, 577, 221
- Rau, H. 2004 Direct asymmetric photochemistry with circularly polarized light. In: Inoue Y., Ramamurthy V., (eds) Chiral photochemistry. Marcel Dekker, New York, 1
- Raunier, S., Chiavassa, T., Duvernay, F., et al. 2004, A&A, 416, 165
- Remijan, A., Snyder, L. E., Friedel, D. N. et al. 2003, ApJ, 590, 314
- Rietmeijer, F. 2002, Chemie der Erde / Geochemistry, 62, 1
- Ringwood, A. E. 1979, Origin of the earth and moon, Springer-Verlag, New York, 307
- Robitaille, T., Whitney, B. A. , Indebetouw, R. et al. 2006, ApJS, 167, 256
- Rubenstein, E., Bonner, W. A., Noyes, H. P. et al. 1983, Nature, 306, 118

- Rubin, A. E., Trigo-Rodríguez, J. M., Huber, H. et al. 2007, Geochimica et Cosmochimica Acta, 71, 2361
- Sandford, S. A. & Allamandola, L. J. 1993, ApJ, 417, 815
- Sandford, S. A., Allamandola, L. J., Tielens, A. G. G. M., et al. 1991, ApJ, 371, 607
- Savage, B. D. & Sembach, K. R. 1996, ASPC, 99, 315S
- Schidlowski, M. A. 1988, Nature, 333, 313
- Schmitt, B. 1994, Molecules and Grains in Space, 50th International Meeting of Physical Chemistry, Proceedings of the Conference held in Mont Sainte-Odile, France, September 1993. New York: American Institute of Physics Press. Edited by I. Nenner, AIP Conference Proceedings, Vol. 312, p. 735
- Schmitt-Kopplin, P., Gabelica, Z., Gougeon, R. D. et al. 2010, PNAS, 107, 2763
- Schramm, L. S., Brownlee, D. E., Wheelock, M. M. et al. 1989, Meteoritics, 24, 99
- Schutte, W. A. & Khanna, R. K. 2003, A&A, 398, 1049
- Schutte, W. A. 1999, Formation and Evolution of Solids in Space, Edited by J. Mayo Greenberg and Aigen Li. Kluwer Academic Publishers, p.177
- Schutte, W. A., Allamandola, L. J., Sandford, S. A. 1993, Icarus, 104, 118
- Schutte, W. A., Boogert, A. C. A., Tielens, A. G. G. M. et al. 1999, A&A, 343, 966
- Schutte, W. A., Gerakines, P. A., Geballe, T. R. et al. 1996, A&A, 309, 633
- Sephton, M. A, Pillinger, C. T., Gilmour, I., 1998, Geochimica et Cosmochimica Acta, 62, 1821
- Sephton, M. A. & Botta, O. Space. Sci. Rev 2008, 135, 25
- Sephton, M. A. 2002, Nat. Prod. Rep., 19, 292
- Shen, C. J., Greenberg, J. M., Schutte, W.A., & van Dishoeck, E. F., 2004, A&A, 415, 203
- Shibata, T., Yamamoto, J., Matsumoto, N. et al. 1998, J. Am. Chem. Soc., 120, 12157
- Shimoyama, A. & Ogasawara, R. 2002, Origins of Life and Evolution of the Biosphere, 32, 165
- Shimoyama, A., Harada, K., Yanai, K. 1985, Chemistry Letters, 1183
- Shimoyama, A., Ponnamperuma, C., Yanai, K. 1979a, Nature, 282, 394

- Shimoyama, A., Ponnamperuma, C., Yanai, K. 1979b, Memoirs National Institute of Polar Research 15, 196
- Snyder, L. E., Buhl, D., Zuckerman, B. et al. 1969, Physical Review Letters, 22, 679
- Snyder, L. E., Lovas, F. J., Mehringer, D. M. et al. 2002, ApJ, 578, 245
- Soai, K., Shibata, T., Morioka, H., et al. 1995, Nature, 378, 767
- Soifer, B. T., Puetter, R. C., Russell, R. W. et al. 1979, ApJ, 232, L53
- Spaans, M. & Ehrenfreund, P. 1999 "The Interstellar Medium-a general introduction" in: Laboratory Astrophysics and Space Research, eds. Ehrenfreund, P., Krafft, K., Kochan, H., Pirronello, V., Kluwer Academic Publisher, p. 1
- Spoon, H. W. W., Moorwood, A. F. M., Pontoppidan, K. M. et al. 2003, A&A, 402, 499
- Stoks, P.G., Schwartz, A. W. 1981, Geochimica et Cosmochimica Acta, 45, 563
- Strazzulla, G. 1997, Advances in Space Research, 19, 1077
- Swamy, K. K. S., Sandford, S. A., Allamandola, L. J. et al. 1988, Icarus, 75, 351
- Takano, Y., Ohashi, A., Kaneko, T., et al. 2004, Appl. Phys. Lett., 84, 1410
- Takano, Y., Takahashi, J.-I., Kaneko, T., 2007, Earth Planet. Sci. Lett., 254, 106
- Tanaka, M., Yagi-Watanabe, K., Kaneko, F. et al. 2010, Journal of Electron Spectroscopy and Related Phenomena doi:10.1016/J.elspec.2010.04.001
- Tegler, S. C., Weintraub, D. A., Allamandola, L. J. et al. 1993, ApJ, 411, 260
- Tegler, S. C., Weintraub, D. A., Rettig, T. W. 1995, ApJ, 439, 279
- Thiemann, W. H. -P. & Meierhenrich, U. J. 2001, Orig. Life Evol. Biosph. 31, 199
- Thiemann, W. H. -P., Rosenbauer, H. and Meierhenrich, U. J. 2001, Adv. Space Res., 27, 323
- Tia, M., de Miranda, B. C., Daly, S. et al. 2013 J. Phys. Chem. Lett., 4, 2698
- Tielens, A. G. G. M. & Allamandola, L. J., 1987, in Astrophysics and Space Science Library, vol. 134, Interstellar processes, ed. D. J. Hollenbach & H. A. Thronson Jr., 397-469
- Tielens, A. G. G. M. & Charnley, S. B. 1997, Origins of life and Evolution of the Biosphere, 27, 23
- Tielens, A. G. G. M. & Hagen, W. 1982, A&A, 114, 245

- Tielens, A. G. G. M. & Whittet, D. C. B. 1996, Molecules in astrophysics: probes & processes: abstract book, IAU symposium 178: 1-5 July, Leiden, The Netherlands. Edited by Ewine Fleur van Dishoeck, p. 45
- Tielens, A. G. G. M. 1989, Interstellar Dust: Proceedings of the 135th Symposium of the International Astronomical Union, Edited by L. J. Allamandola and A. G. G. M. Tielens. International Astronomical Union. Symposium no. 135, Kluwer Academic Publishers, Dordrecht, p. 239
- Tielens, A. G. G. M. 2008, Annual Review of Astronomy & Astrophysics, 46, 289
- Tielens, A. G. G. M., Allamandola, L. J., Bregman, J., et al. 1984, ApJ, 287, 697
- Tomeoka, K., Buseck, P. R. 1985, Geochimica et Cosmochimica Acta 49: 2149
- Tsugita, A., Uchida, T., Mewes, H. W., et al. 1987, Journal of Biochemistry, 102, 1593
- van Boekel, R., Min, M., Leinert, C. et al. 2004, Nature, 432, 479
- van Broekhuizen, F. A., Keane, J. V., Schutte, W. A. 2004, A&A, 415, 425
- Vinogradoff, V., Duvernay, F., Danger, G. et al. 2011, A&A, 530, 7
- Vinogradoff, V., Fray, N., Duvernay, F., Briani, G. et al. 2013, A&A, 551, 9
- Voshchinnikov, N. V., Il'in, V. B.; Henning, Th., Dubkova, D. N. 2006, A&A, 445, 167
- Waelkens, C., Malfait, K., & Waters, L. B. F. M. 2000, in Astrochemistry: From Molecular Clouds to Planetary Systems (IAU Symp. 197), ed. E. F. van Dishoeck, Dordrecht: Kluwer, 435
- Wakelam, V., Herbst, E., Le Bourlot, J. et al. 2010, A&A, 517, A21
- Watanabe, N., Shiraki, T., & Kouchi, A. 2003, ApJ, 588, L121
- Watson, D. M., Kemper, F., Calvet, N., et al. 2004, Astrophys. J. Suppl., 154, 391
- Welty, D. E., Hobbs, L. M., Lauroesch, J. T. et al. 1995 ApJL, 449, L135
- Westley, M. S., Baragiola, R. A., Johnson, R. E. et al. 1955, Nature, 373, 405
- Whittet, D. C. B. 1993, Dust and Chemistry in Astronomy, The Graduate Series in Astronomy Dust. eds T. J. Miller & D. A. Williams. Philadelphia, PA: Institute of Physics Publishing, p. 9
- Whittet, D. C. B., Gibb, E. L., Nummelin, A. 2001, Origins of Life and Evolution of the Biosphere, 31, 157

- Whittet, D. C. B., Pendleton, Y. J., Gibb, E. L. et al. 2001, ApJ, 550, 793
- Williams, D. A., Hartquist, T. W., Whittet, D. C. B. 1992, MNRAS, 258, 599
- Wittung, P., Nielsen, P. E., Buchardt, O. 1994, Nature 368, 6471
- Wooden, D. H., Harker, D. E., Woodward, C. E. et al. 1999, ApJ, 517, 1034
- Woon, D. E. 2002, ApJ, 571, L177
- Woon, D. E. 2008. The astrochymist. http://www.astrochymist.org
- Wynn-Williams, C. G., Genzel, R., Becklin, E. E. et al. 1984, ApJ, 281, 172
- York, D. G. 1980, in Astrophysics from Spacelab, ed. P. L. Bernacca & R. Ruffini (Dordrecht: Reidel), p. 609
- Yuen, G., Blair, N., Des Marais, D. j. et al. 1984, Nature, 307, 252
- Zanda, B., Bourot-Denise, M., Hewins, R. H. et al. 2010, Meteoritics and Planetary Science Supplement, id. 5312
- Zanda, B., Humayun, M., Barrat, J.-A., et al. 2011, 42nd Lunar and Planetary Science Conference #1608, p. 2040
- Zolensky, M. E., Mittlefehldt, D. W., Lipschutz, M. E. et al. 1997, Geochimica et Cosmochimica Acta, 61, 5099
- Zolensky, M., McSween, H.Y. 1988, Aqueous alteration. Meteorites and the early solar system, In Meteorites and the early solar system. eds Kerridge J. F., Matthews M. S. (University of Arizona Press, Tucson, AZ), p 114